Titre: Title:	Comparison of heat flux and wall temperature based methods for predicting post-dryout surface temperature in tubes
Auteur: Author:	Eve-Lyne Pelletier
Date:	2008
Type:	Mémoire ou thèse / Dissertation or Thesis
Référence: Citation:	Pelletier, E.-L. (2008). Comparison of heat flux and wall temperature based methods for predicting post-dryout surface temperature in tubes [Mémoire de maîtrise, École Polytechnique de Montréal]. PolyPublie. https://publications.polymtl.ca/8393/

UNIVERSITÉ DE MONTRÉAL

COMPARISON OF HEAT FLUX AND WALL TEMPERATURE BASED METHODS FOR PREDICTING POST-DRYOUT SURFACE TEMPERATURE IN TUBES

EVE-LYNE PELLETIER
DÉPARTEMENT DE GÉNIE PHYSIQUE
ÉCOLE POLYTECHNIQUE DE MONTRÉAL

MÉMOIRE PRÉSENTÉ EN VUE DE L'OBTENTION
DU DIPLÔME DE MAÎTRISE ÈS SCIENCES APPLIQUÉES
(GÉNIE ÉNERGÉTIQUE)
NOVEMBRE 2008

Your file Votre référence
ISBN: 978-0-494-47679-6
Our file Notre référence
ISBN: 978-0-494-47679-6

UNIVERSITÉ DE MONTRÉAL

ÉCOLE POLYTECHNIQUE DE MONTRÉAL

Ce mémoire intitulé:

COMPARISON OF HEAT FLUX AND WALL TEMPERATURE BASED METHODS FOR PREDICTING POST-DRYOUT SURFACE TEMPERATURE IN TUBES

présenté par: PELLETIER Eve-Lyne

en vue de l'obtention du diplôme de: Maîtrise ès sciences appliquées

a été dûment accepté par le jury d'examen constitué de:

M. MARLEAU Guy, Ph.D., président

M. TEYSSEDOU Alberto, Ph.D., membre et directeur de recherche

M. LEUNG Laurence, Ph.D., membre et codirecteur de recherche

M. GIRARD René, Ph.D., membre

ACKNOWLEDGMENTS

The author would like to thank Laurence K.H. Leung for providing technical guidance, Alberto Teyssedou, Rene Girard and Elisabeth Varin for their technical advice and comments on the document. Armando Nava Dominguez, Nihan Onder and Luke McSweeney review of the manuscripts and their useful suggestions are deeply appreciated. All about mentioned individual have contributed to the success of this work.

The author would also like to thank Hydro-Quebec and École Polytechnique de Montreal for their financial support for this study and the Atomic Energy of Canada Limited for providing invaluable resources during my attachment to Chalk River.

ABSTRACT

In nuclear reactors, the surface temperature of fuel bundles is relatively close to the coolant saturation temperature during normal operating conditions. During some postulated accidents, the heat flux of the fuel bundle could increase or the mass flow rate to the fuel channel could reduce resulting in local heat flux exceeding the critical heat flux. Under those scenarios, the surface temperature may increase relatively sharply beyond the saturation temperature. The corresponding heat transfer regime is referred as the film boiling. Due to the potential adverse consequence of fuel sheath failure due to high temperature, it is important to predict accurately the film boiling heat transfer coefficient for establishing the maximum surface temperature of fuel bundles in safety analysis.

Two methodologies in predicting film-boiling heat-transfer coefficient have been assessed against experimental wall-temperature measurements obtained under steady-state conditions with water flow inside vertical tubes. One of these methodologies employs heat flux as the independent parameter (referred as the heat-flux-based methodology) while the other applies wall-temperature as the independent parameter (referred as the wall-temperature-based, or simply temperature-based methodology). The film-boiling heat transfer is separated into the developing film boiling conditions and fully developed film boiling conditions regions. Film-boiling heat-transfer coefficients are predicted using the film boiling look-up tables for fully developed flow. A modification factor is applied for developing film-boiling heat-transfer coefficients.

The assessment shows that applying the heat-flux-based methodology predicts wall-temperature measurements in the fully developed region with an average error of -0.8% and a standard deviation of 8.6%, and the temperature-based methodology with an average error of 1.8% and a standard deviation of 6.4%. The maximum wall temperature along the channel is predicted with an error of -0.8% and a standard deviation of 8.6% us-

ing the heat-flux-based methodology. It is slightly overpredicted using the temperature-based methodology (with an average error of 3.4% and a standard deviation of 6.9%). Based on the assessment result, it is concluded that both methodologies are applicable for steady-state calculations. Also, the temperature-based methodology seems stable and the final temperature distribution does not depend on the initial wall temperature guess.

Similar to film-boiling look-up tables for fully developed flow, the developing film-boiling factors are expressed in terms of either heat flux or wall temperature. The assessment shows larger prediction uncertainty of surface temperature in the developing film-boiling region, as compared to results observed for the fully developed region. The average prediction error of surface-temperature measurements is -4.4% with a standard deviation of 14.3% for the heat-flux based methodology, and 8.6% and 10.7% respectively for the temperature-based methodology. In addition, predicted surface-temperature trends using the temperature-based methodology differ from experimental trends in the developing film boiling region. The predicted surface-temperature rise is much steeper than the experimental trend at low mass fluxes, but more gradual at high mass fluxes. Based on the assessment result, the modification factor used in the temperature-based methodology has been revised to improve the prediction accuracy.

An examination of the experimental surface-temperature measurements illustrates strong effects of mass flux and quality on developing film-boiling heat transfer. These effects have been included via the Reynolds number of the vapor phase in the revised modification factor of the temperature-based methodology. Coefficients in the revised factor were optimized using the tube heat-transfer database. An assessment of the revised factor has shown an improvement in prediction accuracy of the wall-temperature measurements in the developing film boiling region (with an average error of -1.9% and a standard deviation of 13.0%). In addition, the maximum wall temperature is predicted accurately with an average error of 0.9% and a standard deviation of 5.5%. Further validation of

the revised factor is recommended against a wider range of experimental data.

As a simplification, all assessments have been performed with the assumption that the radiative heat transfer is negligible. A sensitivity analysis has been carried out to confirm this assumption. Including the radiative heat-transfer model has no apparent impact to the prediction accuracy of wall-temperature measurements. Therefore, it is concluded that the assumption is valid for the current range of flow conditions covered in the experimental data.

Strictly speaking, these methodologies are applicable for steady-state analyses. A discussion on applying these methodologies to transient analyses has been provided. It was shown that thermal inertia and prediction uncertainties in CHF and film-boiling heat transfer coefficient in the transition boiling region and minimum film boiling temperature predictions do not affect the steady-state film-boiling temperature predictions. Nevertheless, validation of the temperature-based methodology under transient conditions is recommended against transient experimental data.

RÉSUMÉ

La température à la surface des gaines de combustible demeure relativement basse (i.e. près de la température de saturation) pour les conditions normales d'exploitation des réacteurs nucléaires. Cependant, advenant certains scénarios d'accidents, la puissance des grappes de combustible peut augmenter, alors que le débit et la pression du caloporteur peuvent être considérablement réduits. Dans ces conditions, le flux de chaleur est susceptible d'excéder la valeur du flux de chaleur critique. Le régime de transfert de chaleur correspondant à cette condition est défini comme étant l'ébullition par film et se caractérise par une rapide augmentation de la température de la paroi. Étant donné que ces températures élevées sont susceptibles d'entraîner des défaillances de gaines, il est important pour la sûreté des réacteurs de prédire adéquatement le coefficient de transfert de chaleur en conditions d'ébullition par film. Ce coefficient dictera la température maximale des grappes de combustibles atteinte durant le scénario d'accident étudié.

Ce travail présente une évaluation de méthodes de prédictions du coefficient de transfert de chaleur en post-assèchement. Cette évaluation s'effectue par des comparaisons avec des données expérimentales recueillies en conditions stationnaires d'écoulement dans des tubes verticaux. La première de ces méthodes utilise le flux de chaleur comme paramètre indépendant alors que la seconde se base sur la température de paroi. Le transfert de chaleur en ébullition par film est divisé en deux régimes : un régime où se développent les conditions d'ébullition par film et un régime où les conditions d'ébullition par film sont totalement établies. Le coefficient de transfert de chaleur pour des conditions d'ébullition par film totalement établies est prédit par interpolation dans des tableaux de valeurs en fonction de la pression, du flux massique, du titre thermodynamique et de la surchauffe de la paroi. Un facteur de modification est ensuite appliqué afin de prendre en compte l'effet du développement des conditions d'assèchement.

L'évaluation de ces méthodes montre que la température de paroi est prédite avec une erreur moyenne de -0.8% et une déviation standard de 14.3% lorsque l'on utilise une méthodologie basée sur le flux de chaleur. Cette erreur et déviation standard sont respectivement de 1.8% et 10.7% lorsqu'on utilise une méthodologie basée sur la température de paroi. La température maximale de paroi est quant-à-elle prédite avec une erreur moyenne de 0.8% et une déviation standard de 8.6% avec la méthodologie basée sur le flux de chaleur. Elle est légèrement surestimée avec la méthodologie basée sur la température de paroi (avec une erreur moyenne de 3.4% et une déviation standard de 6.9%). En somme, les deux méthodologies peuvent être implémentées avec de bons résultats dans des programmes informatiques de calculs d'états permanents.

Similairement aux tableaux de valeurs d'ébullition par film, le facteur de modification s'exprime en fonction du flux de chaleur ou de la température de la paroi, suivant la méthodologie employée. Les résultats de l'évaluation montrent une plus grande incertitude lorsque les conditions d'assèchement se développent que lorsqu'elles sont complètement établies. Les températures dans la région où les conditions d'ébullition par film sont en développement sont prédites avec une erreur de prédiction de -4.4% et une déviation standard de 14.3% pour la méthode basée sur le flux de chaleur et une erreur de 8.6% et une déviation standard de 10.7% pour la méthode basée sur la température de la paroi. Pour cette méthode, les prédictions n'épousent pas parfaitement la courbe expérimentale dans cette région. En effet, pour de faibles flux massiques, la température augmente trop rapidement lorsque se produit l'assèchement alors qu'elle n'augmente pas suffisamment rapidement pour des flux massiques plus importants. Le facteur de modification pour le développement de l'écoulement utilisé dans la méthodologie basée sur la température doit donc être révisé.

Ce travail montre que le flux massique et le titre du mélange ont un effet sur le développement des conditions de transfert de chaleur. Le nombre de Reynolds de la phase

vapeur a donc été inclus dans le facteur de modification. Les coefficients de la corrélation ont été optimisés en utilisant la même base de données de transfert de chaleur dans des tubes. Une validation de la corrélation révisée montre une amélioration des prédiction des températures dans la région de développement des conditions d'ébullition par film (avec une erreur moyenne de -1.9% et une déviation standard de 13.0%). De plus, la température maximale de paroi est prédite avec une erreur moyenne de 0.9% et une déviation standard 5.5%. La corrélation révisée, cependant, devrait être d'optimisée et validée en utilisant une plus vaste base de données.

Pour fins de simplifications, le transfert de chaleur par rayonnement a été négligé dans les prédictions. Cette approximation est vérifiée en effectuant une étude de sensibilité qui valide cette hypothèse pour les températures et conditions d'écoulement des données expérimentales.

Finalement, les méthodologies présentées dans ce travail sont applicables pour des analyses en conditions stationnaires. L'application des ces méthodes à des analyses en conditions transitoires est également discutée. Il est ainsi démontré que l'inertie thermique, l'incertitude sur le flux de chaleur critique, la température minimum d'ébullition par film et le coefficient de transfert entre ces deux états (i.e. CHF et T_{MIN}) ne modifient pas les prédictions finales d'ébullition par film en conditions stationnaires. Cependant, une validation complète de la méthodologie basée sur la température de paroi devrait cependant être effectuée sous des conditions transitoires et en utilisant des données expérimentales recueillies dans ces mêmes conditions.

CONDENSÉ

La température à la surface des grappes de combustible est relativement basse (i.e. près de la température de saturation) pour les conditions normales d'exploitation des réacteurs nucléaires. Cependant, certains scénarios d'accident, tels des pertes de caloporteur ou des pertes de débit, entraînent l'augmentation de la puissance des grappes de combustible alors que le débit et la pression du caloporteur peuvent être considérablement réduits.

Dans de telles conditions, le flux de chaleur est successible d'excéder le flux de chaleur critique. Débute alors localement l'assèchement des gaines qui se traduit par l'apparition d'une couche de vapeur qui réduit le transfert de chaleur entre les gaines et le caloporteur. Cet effet résulte en une rapide augmentation de la température de la paroi, ce qui nuit à l'intégralité des gaines du combustible et peut mener à des défauts de gaine et de combustible. Étant donné les effets négatifs d'une telle excursion de température, il est important en analyse de sûreté de prédire avec précision le coefficient de transfert de chaleur en régime de post-assèchement.

Les prédictions du coefficient de transfert de chaleur pour des grappes de combustibles ayant excédé le flux de chaleur critique sont calculées dans les programmes informatiques en utilisant tables de coefficients de transfert de chaleur combinées avec des corrélations optimisées pour des grappes de combustibles. Ces tables et corrélations peuvent être implantés en utilisant une méthode basée sur le flux de chaleur ou une méthode basée sur la température de paroi. Ce travail vise à comparer et valider la précision de ces deux méthodologies quant à la prédiction de la température de la paroi en régime de post-assèchement. Étant donné les droits de propriété intellectuelle des expériences et corrélations pour des grappes de combustible, une base de données de transfert de chaleur en post-assèchement dans des tubes a été élaborée. Les prédictions effectuées

suivant les deux méthodes sont ainsi comparées aux données expérimentales de cette base de données.

Survol Théorique: prédictions du transfert de chaleur en post-assèchement

Le coefficient de transfert de chaleur en conditions de post-assèchement est généralement calculé en utilisant des corrélations. Ces dernières sont cependant souvent limitées à des conditions d'écoulement restreintes. Ce coefficient peut également être prédit en utilisant des modèles théoriques qui sont quant à eux complexe, résultent en de longs temps de calculs et ne sont généralement valides que pour un seul régime de transfert de chaleur. Pour pallier à ce problème, des tables exprimant des valeurs expérimentales du coefficient transfert de chaleur en fonction des paramètres de l'écoulement ont été construites et implantées dans les programmes informatiques.

Les prédictions faites par ces tables fournissent des coefficients de transfert de chaleur pour des conditions d'ébullition par film totalement établies. Ainsi, en conditions stationnaires, un profil de température basé sur ces prédictions résultera en une augmentation instantanée et irréaliste de la température de la paroi. En effet, il est impossible de passer instantanément d'un mode de transfert de chaleur à un autre. De plus, une fois le flux de chaleur critique excédé, l'assèchement du film liquide en contact avec la paroi débute. Des gouttelettes peuvent cependant encore entrer en contact avec la paroi, ce qui augmente le transfert de chaleur et diminue la température de la paroi. Cet effet se définit comme étant l'établissement des conditions d'ébullition par film et est pris en compte dans un facteur séparé, le facteur de modification du développement des conditions d'ébullition par film. Ce facteur de modification multiplie le coefficient de transfert prédit par les tables de valeurs (i.e. pour des conditions d'ébullition par film totalement établies) et permet de prédire plus précisément le transfert de chaleur et la température

de la paroi. Cet effet a donc un impact direct sur la température maximale.

Les méthodes de prédiction du transfert de chaleur en post-assèchement sont implémentées dans les programmes informatiques de sûreté suivant deux méthodologie; la première est basée sur le flux de chaleur alors que la seconde est basée sur la température de la paroi. La méthodologie basée sur le flux de chaleur est optimale pour des codes en état stationnaires ne résolvant pas l'équation de conduction de la chaleur au travers de la paroi. En effet, dans ces conditions, le flux de chaleur est un paramètre connu qui est utilisé directement pour trouver le coefficient de transfert de chaleur, lequel permet finalement de calculer la température de la paroi (en utilisant la loi de Newton). Cette méthodologie est cependant difficile à implanter dans certains programmes informatiques en état transitoires où le flux de chaleur n'est pas connu avant que soit déterminée la température de la paroi. De plus, tel que le prévoit la courbe d'ébullition (voir figure 1.1), trois régimes de transfert de chaleur sont possibles pour un même flux de chaleur, ce qui complexifie davantage l'application de cette méthode en régime transitoire. La méthodologie basée sur la température de la paroi a donc été développée pour palier à ces problèmes. Cette méthodologie base le calcul du coefficient de transfert de chaleur et du flux de chaleur sur la température de la paroi.

Méthodologie

Ce travail présente une évaluation des méthodes basées sur le flux de chaleur et sur la température de la paroi. Cette évaluation s'effectue en implantant les deux méthodologies dans un code informatique en conditions stationnaire. Les prédictions de la température de la paroi en post-assèchement effectuées par le code sont ensuite comparées à la base de données expérimentales.

Les conditions de post-assèchement sont rencontrées une fois le flux de chaleur critique excédé. Ce paramètre (qui est également utilisé dans les prédicitions du coefficient de tansfert de chaleur en post-assèchement) est calculé avec une table de valeur. Une correction est ensuite apportée afin d'éviter que l'incertitude associée à ce paramètre n'influence les prédictions dans des conditions d'ébullition par film. La correction est calculée en utilisant la relation suivante:

$$C.F._{CHF} = \frac{q''_{EXP\ DO}}{q''_{pred\ DO}}, \tag{1}$$

Le coefficient de transfert de chaleur pour la méthodologie basée sur le flux de chaleur est calculé en utilisant une table de valeurs basée sur le flux de chaleur, le titre thermodynamique, le flux massique et la pression. Le coefficient de transfert de chaleur est ensuite multiplié par le facteur de modification de développement des conditions d'ébullition par film basé sur le flux de chaleur critique:

$$K_{developing} = 1 + \left(\frac{h_{nb}}{h_f d} - 1\right) \exp\left[a\left(\frac{x - x_{DO}}{(1 - x_{DO})Bo}\right)^b\right], \tag{2}$$

où H_{fg} est la chaleur latente de vaporisation et Bo is est l'index d'ébullition défini comme:

$$Bo = \frac{q''}{GH_{fg}}. \tag{3}$$

La méthodologie basée sur la température de la paroi utilise quant-à-elle des tables de valeurs basées sur la surchauffe de la parroi, le titre thermodynamique, le flux massique et la pression pour calculer le coefficient de transfert de chaleur. Le facteur de modifica-

tion utilisé dans cette méthodologie est défini par:

$$K_{developing} = \frac{h_{PDO}}{h_{fd}} = 1 + \left(\frac{h_{NB}}{h_{fd}} - 1\right) \exp\left[c\,(WSR - 1)^b\right], \tag{4}$$

avec:

$$WSR = \frac{T_w - T_{sat}}{T_{CHF} - T_{sat}}. \tag{5}$$

Les prédictions de la température de la paroi ainsi obtenues sont comparées aux expériences de Bennett et al. (Bennett, 1967). Ces expérences donne la disitribution axiale de la température interne de la paroi pour un tube vertical dont la surface externe est chauffée uniformément et la surface interne est refroidie par un écoulement d'eau circulant vers le haut.

Résultats de l'évaluation des méthodes

Évaluation de la méthodologie basée sur le flux de chaleur

L'évaluation de la méthodologie basée sur le flux de chaleur montre cette méthode prédit adéquatement la température de la paroi lorsque les conditions d'ébullition par film sont totalement établies. En effet, la température est prédite avec une erreur moyenne de 0.8% et une déviation standard de 8.6% dans cette région. De plus, la méthode prédit la température de la paroi avec une erreur de -4.4% et une déviation standard de 14.3% dans la région où les conditions d'ébullition par film sont en développement. La température maximale est quant-à-elle prédite avec une erreur moyenne de -0.8% et une déviation standard de 8.6%. Ainsi, il peut être conclu que cette méthode peut être utilisée avec précision dans les programmes informatiques en conditions stationnaires.

Évaluation de la méthodologie basée sur la température de paroi

L'évaluation de la méthodologie basée sur la température de la paroi montre que cette méthode prédit adéquatement la température de paroi lorsque les conditions d'ébullition par film sont totalement établies. En effet, la température est prédite avec une erreur moyenne de 1.8% et une déviation standard de 6.4% dans cette région. Cependant, la température de la paroi est légèrement surévaluée dans des conditions de développement de l'ébullition par film; une erreur moyenne de 8.3% et une déviation standard de 10.7% sont trouvées dans cette région. La température maximale est prédite avec une erreur moyenne de 3.4% et une déviation standard de 6.9%. De plus, l'étude de l'évolution de la température montre que cette dernière croît trop rapidement une fois le flux de chaleur critique excédé et ne suit pas adéquatement les données expérimentales. Ainsi, le facteur de modification de cette méthodologie n'apporte pas une correction suffisante et devrait être révisé.

Sensibilité au facteur de modification

Ce travail présente une étude de l'impact du facteur de modification sur la température de la paroi. Cette étude montre qu'une variation de $\pm 10\%$ du facteur de modification résulte en une variation d'environ 20% de l'erreur moyenne sur la prédiction de la température de la paroi lorsque l'on utilise la méthodologie basée sur la surchauffe de la paroi. Cette variation est inférieure à 10% pour la méthodologie basée sur le flux de chaleur. La variation du facteur de modification a donc un plus grand impact dans la méthodologie basée sur la surchauffe de la paroi. L'effet est similaire pour une variation de $\pm 10\%$ des coefficients a, b et c des équations 2 et 4. Dans ces cas, une variation de $\pm 10\%$ des coefficients a et c résulte en des variations de 4% de l'erreur moyenne pour méthode baseée sur le flux de chaleur et de 12% pour la méthode basée sur la surchauffe de la paroi. Similairement, une variation de $\pm 10\%$ des coefficients c résulte en une vari-

ation de 10% et 15% respectivement pour ces deux méthodes.

Amélioration de la méthodologie basée sur la température de paroi

L'évaluation des méthodes de prédiction en post-assèchement montre que les deux méthodologies peuvent être implantées dans les programmes informatiques en conditions stationnaires. Cependant, la méthodologie basée sur la surchauffe de la paroi surestime la température de la paroi en condition de développement de l'ébullition par film. Cette surestimation est imputable au facteur de modification. Ce dernier est donc réexaminé dans ce travail.

L'étude du facteur de modification effectué dans ce travail monte que le développement des conditions d'ébullition par film est influencé par le titre et le flux massique. La figure 1 montre clairement cette influence. Ces effets ont été pris en compte dans un nombre de Reynolds de la phase vapeur définit par:

$$Re_v = \frac{xGD}{\mu_v}. \tag{6}$$

Ce nombre a permis de définir une corrélation révisée du facteur de modification qui s'exprime par:

$$K_{developing} = \frac{h_{PDO}}{h_{fd}} = 1 + \left(\frac{h_{NB}}{h_{fd}} - 1\right) exp\left\{c^{**}\left[Re_v\left(WSR - 1\right)\right]^{b^{**}}\right\}. \tag{7}$$

Les coefficients de cette corrélation ont été optimisés avec la base de données pour des tubes en post-assèchement retenue pour ce travail. La corrélation révisée est ré-évaluée

en comparaison avec la base de données expérimentales et montre un meilleur comportement du facteur de modification. Cette évaluation montre que le facteur de modification révisé permet de prédire la température de paroi avec une erreur de -1.9% et une déviation standard de 13.0% dans des conditions de développement de l'ébullition par film. La température maximale est quant à elle prédite avec une erreur de 0.9% et une déviation standard de 5.5%. Cette corrélation révisée apporte donc une amélioration importante de la méthodologie basée sur la température de la paroi. Cependant, cette corrélation révisée devrait être optimisée en utilisant une plus vaste base de données.

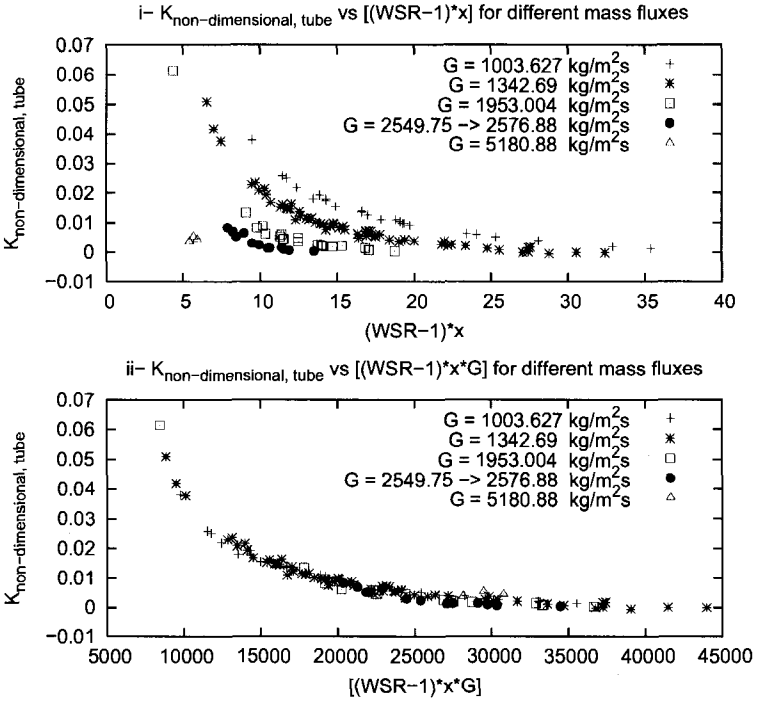

Figure 1 Experimental Developing-Flow Modification Factor vs $(WSR-1)x$ and vs $(WSR-1)xG$

Effet de la radiation thermique et influence de paramètres d'intérêts en conditions transitoires

L'évaluation des méthodes basées sur le flux de chaleur et sur la température de la paroi présentée dans ce travail s'effectue en conditions stationnaires et en négligeant le transfert de chaleur par rayonnement. L'impact de ces deux effets est étudié dans ce travail.

Radiation thermique

Un modèle de transfert de chaleur par radiation a été construit afin d'étudier l'impact de cet effet sur les températures de la paroi prédites dans le cadre de ce travail. Ce modèle suppose un échange thermique entre deux matériaux (la paroi du tube et l'eau) séparés par un milieu participatif (la vapeur d'eau) et assume un régime annulaire inversé.

Ce modèle de transfert de chaleur a par la suite été implanté dans le programme informatique effectuant les prédictions de températures afin de réévaluer les prédictions en les comparant avec les données expérimentales. Cette évaluation montre que le fait de prendre en compte le transfert de chaleur par radiation modifie très peu les prédictions. En effet, la valeur maximale du rapport du flux de chaleur par radiation et du flux de chaleur total est inférieur à 3%. La valeur moyenne de ce rapport pour des conditions d'ébullition par film est de l'ordre de 1.3% alors que la variation (due fait que soit négligée la radiation thermique) de l'erreur moyenne sur la température est de l'ordre de 0.2%. Il peut ainsi être conclu que le transfert de chaleur par radiation est négligeable dans les conditions de la base de données expérimentales recueillies par Bennett (Bennett, 1967).

Paramètres importants en transitoire

La méthodologie basée sur la température de paroi a été élaborée pour être implantée dans des programmes informatiques en conditions transitoires. Cependant, le programme informatique utilisé ne permet pas de valider cette méthodologie en conditions transitoires. Ainsi, un modèle CATHENA a été établi afin de simuler l'une des expériences de Bennett et al. (Bennett, 1967). De plus, les données expérimentales sont également en conditions stationnaires. L'approche utilisée est donc de vérifier la stabilité de la méthode en étudiant la convergence de la température de la paroi une fois un état stationnaire établi pour des coditions d'ébullition par film totalement établies. Cette étude s'effecute en faisant varier certains paramètres d'intérêt en conditions transitoires.

L'un des paramètres étudiés est l'inertie thermique (étudié en faisant varier l'épaisseur de la paroi et la vitesse de l'insertion de la puissance thermique). L'incertitude sur le flux de chaleur critique, sur la température minimale d'ébullition (T_{min}) et sur le coefficient de transfert de chaleur dans la région de transition entre ces deux valeurs sont également étudiés. La méthode utilisée pour prendre en compte l'effet du développement des conditions d'ébullition par film est un autre paramètre étudiée. Tout ces paramètres sont variés et la convergence obtenue sur la température de paroi en ébullition par film une fois ces conditions totalement établies sont comparées.

Dans tous les cas, bien que la variation de ces paramèetres entraîne une différence dans l'évolution du transitoire, la température finale en ébillition par film dans tous les cas demeure la même. Cependant, la validation de la méthodologie en comparaison avec des données expérimentales en état transitoire devrait être effectuée.

Conclusion

Ce travail présente une évaluation des méthodes de prédiction du transfert de chaleur en régime de post-assèchement. Cette évaluation montre que les deux méthodes (méthode basée sur le flux de chaleur et sur la surchauffe de la paroi) produisent des prédictions justes et sont applicables dans des programmes informatiques en conditions stationnaires. Il est également montré que la méthodologie basée sur la surchauffe de la paroi surestime la température de la paroi et la température maximale.

Une étude du développement des conditions d'ébullition par film effectuée dans ce travail montre que cet effet est influencé par le titre thermodynamique et le flux massique. Ces paramètres ont été inclus dans la corrélation utilisée pour prendre en comptre l'effet du développement des conditions d'ébullition par film.n L'évaluation de la méthodologie basée sur la surchauffe de la paroi incluant cette corrélation révisée montre un meilleur comportement par rapport aux données expérimentales et permet de prédire adéquatement la température de la paroi et la température maximale. Ceci représente donc une amélioration importante de cette méthodologie. La corrélation révisée devrait cependant être optimisée et validée avec une plus grande base de données expérimentales.

Cette évaluation est effectuée en négligeant le transfert de chaleur par radiation. Cet effet donc été implanté dans le code informatique, ce qui a permis de démontrer que la radiation thermique est négligeable dans les conditions de l'écoulement des données expérimentales utilisées dans ce travail.

La convergence de la température de paroi une fois les conditions d'ébullition par film totalement établies a été étudiée avec CATHENA en faisant varier des paramètres d'intérêt pour un code en état transitoire. Ces paramètres sont l'inertie thermique, l'incertitude sur le flux de chaleur critique, la température minimale d'ébullition par film, le coefficient

de transfert de chaleur dans la région de transition entre ces deux valeurs et la méthode de correction pour le développement des conditions d'ébullition par film. Dans tous ces cas, la température finale obtenue en conditions d'ébullition par film totalement établies converge vers la même valeur. La validation de la méthodologie en comparaison avec des données expérimentales en état transitoire devrait cependant être effectuée.

TABLE OF CONTENTS

LIST OF FIGURES

LIST OF TABLES

LIST OF APPENDICES

LIST OF NOTATIONS AND SYMBOLS

A	Area
Bo	Boiling Index
CHF	Critical Heat Flux
c_p	Specific Heat
c_{th}	Thermal Conductivity
D_e	Wetted Diameter
D_H	Heated Diameter
e	Power Density (Emissive Power)
F	View Factor
F_B	Heat Flux Splitting Factor
f_{cd}	Cumulative Droplet Deposition Factor
f_v	Friction Factor of the Vapor Phase
G	Mass Flux
h	Heat Transfert Coefficient
H_{fg} i	Latent Heat of Vaporization
J	Radiocivity
k	Thermal Conductivity
K	Modification factor
Nu	Nusselt Number
p	Pressure
PDO	Post Dryout
Q	Heat
q''	Heat Flux
q'''	Heat Generation rate
Pr	Prandtl Number

r	Radius
R	Equivalent Electric Circuit Resistance
Re	Reynolds Number
S	Suppression Factor
T	Temperature
T_{min}	Minimum Film Boiling Temperature
u_d	Droplet Deposition Velocity
V	Volume
WSR	Wall Superheat Ratio
x	Quality
α	Absorptivity
β	Reflectivity
ϵ	Void Fraction
ξ	emissivity
Γ	Irradiation
μ	Viscosity
ρ	Density
σ	Surface Tension
σ_{SB}	Stefan-Boltzmann's Constant
τ	Transmitivity
ΔT_e	Mean Superheat
ΔT_{sat}	Wall Superheat
Δp_e	Change Pressure Corresponding to ΔT_e
Δp_{sat}	Change of Pressure Corresponding to ΔT_{sat}

INDICES

a	Partial

b	Bulk
$actual$	Actual
$b.b.$	Black Body
DO	Dryout
e	Equivalent
$equil$	Equilibrium
ext	External
Exp	Experimental
f	Fluid
FB	Film Boiling
fc	Forced Convection
$film$	Film Boiling
$g.b.$	Gray Body
int	Internal
l	Liquid Phase
nb	Nucleate Boiling
OSV	Onset of Significant Void
rad	Radiation
sat	Saturation
Sim	Simulation
tot	Total
TB	Transition Boiling
tp	Two Phase
v	Vapor Phase
w	Wall

INTRODUCTION

The surface temperature of fuel bundles is relatively low (i.e., close to the coolant saturation temperature) during normal operating conditions of the nuclear reactor. Heat-transfer regimes encountered at these conditions are single-phase forced convection to liquid, nucleate boiling and forced convective evaporation. During some postulated accidents, such as Loss-of-Flow Accident (LOFA) or Loss-of-Regulation Accident (LORA), the local heat flux may be high enough at certain locations to prevent contacts between the coolant and the sheath, resulting in a drastic temperature increase. This point is referred as the critical heat flux (CHF) or dryout. Conditions encountered beyond dryout are referred as post-dryout (PDO) conditions. The sharp rise in sheath temperature may challenge the sheath, fuel, and fuel channel integrities. Therefore, it is important to establish accurately the maximum sheath temperature at these accident scenarios.

Safety analyses for the CANDU 6 nuclear reactors (such as the Gentilly-II and Point Lepreau CANDU reactors) are being carried out using the CATHENA computer code (Hanna, 1998). Maximum sheath temperature in the fuel channel is established with post-dryout heat-transfer correlations, derived using experimental data obtained from full-scale bundle tests at steady-state conditions. Two methodologies have been applied in the development of post-dryout heat-transfer correlations; one based on heat flux while the other based on wall temperature. Although both methodologies have been implemented into the CATHENA code, the temperature-based methodology is the default option due mainly to the cumbersome application of the heat-flux-based methodology (details to be provided in following sections). Outside the framework of CATHENA, prediction accuracy of heat-transfer coefficient for these methodologies has been established through assessments against experimental data used to develop the correlations at the local flow conditions (i.e., pressure, mass flux, and quality). A comparison of their prediction accuracy in sheath temperature is required for the same system conditions

(i.e., outlet pressure, mass flow rate, and inlet temperature).

Assessing bundle-data-based correlations against full-scale bundle data is not feasible due to the proprietary nature of these correlations and experimental data. A set of post-dryout surface-temperature data obtained with vertical upward water flow inside tubes has been assembled to assess the prediction accuracy of the two methodologies (i.e., heat-flux-based and temperature-based correlations). The assessment result would provide insight into the applicability of these methodologies in predicting the surface-temperature distribution and maximum surface temperature. If necessary, improvement will be recommended to extend the applicability and reduce the prediction uncertainty.

Objectives of this study are:

- To assess the heat-flux based and wall-temperature-based methodologies in predicting surface temperatures along a vertical heated tube at steady-state conditions.
- To improve the temperature-based methodology.
- To establish the impact of radiative heat transfer on film-boiling temperature predictions and examine various parameters of interest to transient calculations.

In the thesis, the theoretical concepts are presented first in Chapter 1. It is however assumed that the reader already has a heat transfer background. As a result, a general overview of heat transfer mechanisms can only be found in Appendix I while forced convection heat transfer, dryout and departure form nucleate boiling mechanisms and post-dryout conditions are the main topics presented in Chapter 1.

Chapter 2 presents a literature survey on experimental data and heat transfer prediction methods in post-dryout conditions. The look-up table technique in predicting film-boiling heat-transfer coefficient is also discussed in details in this chapter.

Chapter 3 describes the heat transfer models used in the assessment. The selection of the experiments, the description of the code and the simplifying hypothesis are also presented in the chapter.

The assessment results of the heat-flux based and wall-temperature-based methodologies are discussed in Chapter 4. An improved temperature-based methodology is presented. The assumption of negligible radiative heat transfer is closely examined and justified. This chapter also described a brief examination of the applicability of these methodologies in a transient calculation scheme.

Conclusions of this study and some relevant recommendations are provided at the end of this document.

CHAPTER 1

FORCED CONVECTIVE HEAT TRANSFER

Heat transfer can be generally categorized into natural and forced convective regimes. Boiling is encountered in each regime depending on the coolant temperature. The most common natural convective heat transfer is encountered under pool boiling. Various heat-transfer modes are encountered in these boiling heat transfer regimes; their relationship can be described via the boiling curve.

Dimensionless numbers are often used in heat transfer calculations. Thus, some of these numbers have to be defined before introducing heat transfer prediction methods. The Nusselt number, Nu, is defined as the ratio of the conductive heat transfer to the convective heat transfer and is expressed as:

$$Nu = \frac{D_H d}{k} \tag{1.1}$$

where D_H is the heated diameter and k is the thermal conductivity of the fluid. The Reynolds number is defined as the ratio of internal and viscous forces:

$$Re = \frac{D_e G}{\mu} \tag{1.2}$$

where D_e is the wetted diameter, G is the mass flux, and μ is the viscosity of the fluid. Finally, the Prandtl number is the ratio of momentum diffusivity (viscosity) and thermal diffusivity (conductivity):

$$Pr = \frac{c_p \mu}{k} \tag{1.3}$$

where c_p is the specific heat of the liquid.

1.1 The Boiling Curve

A classical boiling curve is shown in Figure 1.1 for a specific set of local flow conditions (i.e., pressure, mass flux, and quality). Single-phase liquid convective heat transfer is encountered at low wall temperatures and low heat fluxes. Once the saturation temperature is reached, nucleate boiling or forced convective evaporation regimes arise. These regimes are characterized with an efficient heat transfer mechanism. At sufficiently high heat fluxes, the wall temperature is too hot to permit contact between the liquid phase and the heated wall to take place, which results in a rapid decrease of the heat transfer rate. This phenomenon is referred as the critical heat flux (CHF), and is defined as Point B in Figure 1.1. Beyond the CHF point, the heat-flux variation with wall temperature follows two different paths depending on the controlling parameter in the system. In a wall-temperature controlled system, the heat flux decreases with increasing wall temperature and follows Path B-C to the minimum film boiling point (Point C), and subsequently increases following Path C-D and beyond corresponding to the stable film-boiling region. The stable film-boiling region is characterized with a stable vapor film covering the heated surface; there are no contacts between the heated wall and the liquid phase. In a heat-flux controlled system, the wall temperature increases sharply from Point B (i.e., CHF) to Point D (fully developed film-boiling regime) and the increasing trend follows the boiling curve beyond Point D with further increase in heat flux. The sharp increase in wall temperature from Point B to Point D is the main concern in safety analyses.

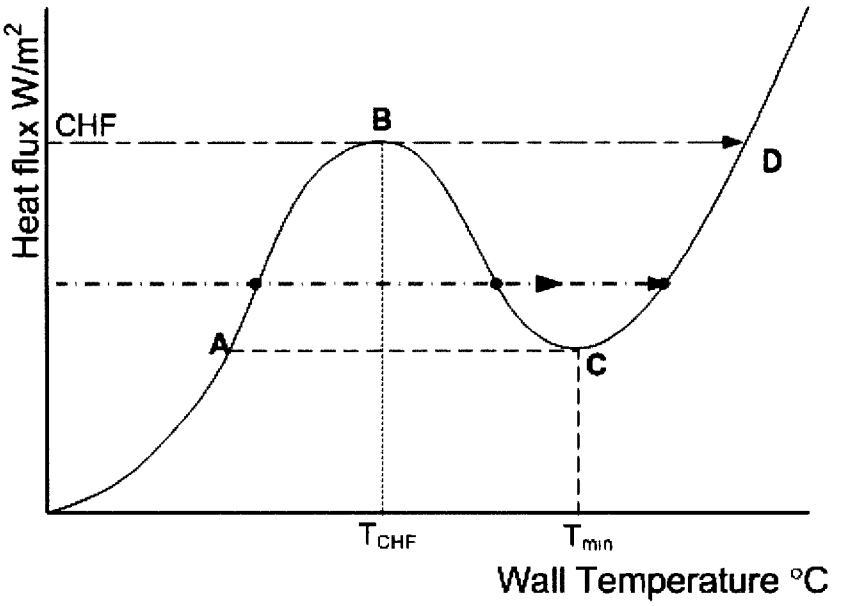

Figure 1.1 Idealized Boiling Curve

Heat flux based and its extrapolated temperature-based system boiling curves have been measured in tubes cooled by Freon-12 for several flow conditions by Groeneveld (Groeneveld, 1972). Figure 1.2 shows a typical trend observed in the flow boiling curves presented in this reference. Two behaviors can be observed from this Figure. First, comparing to pool boiling, a slight wall temperature reduction is observed just before CHF occurs. This temperature reduction is a consequence of the increasing velocity of the thin liquid film. Also, the transition from CHF to the stable film boiling is not a straight line, thus, a slight heat flux increase is necessary to reach a stable film boiling regime.

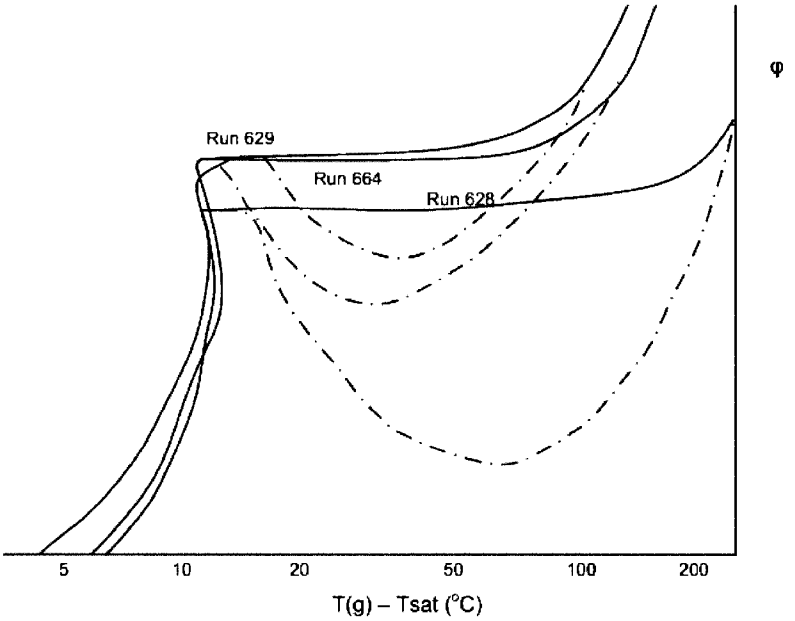

Figure 1.2 Examples of Temperature and Heat Flux Controlled Systems Boiling Curves in Freon-12 (Groeneveld, 1972)

Figure 1.3 illustrates heat transfer regimes, corresponding flow patterns, CHF mechanisms, and film-boiling regimes as a function of void fraction (not to scale). The boundaries (from (Tong, 1997) and (Kirillov)) are approximate and may vary significantly with the flow conditions, but provide the understanding of these general concepts. Figure 1.3 also introduces the topics presented in the current chapter; the numbers in parenthesis indicate the sections where the topics are presented.

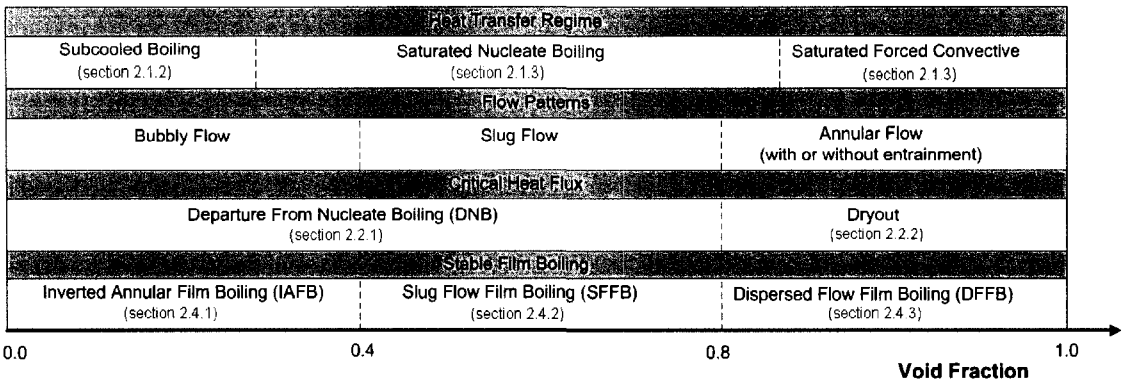

Figure 1.3 Heat Transfer Regimes and Organization of Chapter 2

1.1.1 Forced Convection to Liquid

For subcooled liquids with negligible viscous-dissipation effect, the heat transfer rate strongly depends on turbulences in the fluid. The Nusselt number depends on the Reynolds number, the Prandtl number, and the geometry factor L/D. For fully developed turbulent flows ($Re > 20000$), Dittus and Boelter (Dittus ans Boelter, 1930) suggested the following correlation:

$$Nu = 0.023 Re^{0.8} Pr^{0.3}. \tag{1.4}$$

In a heated channel where a large temperature gradient is encountered between the bulk fluid and near-wall fluid, Seider and Tate (Seider and Tate, 1936) introduced a modification factor to account for the heating effect:

$$Nu = 0.026 Re^{0.8} Pr^{1/3} \left(\frac{\mu_b}{\mu_w}\right)^{0.14}, \tag{1.5}$$

where μ_b is the viscosity evaluated at bulk temperature and μ_w, at wall temperature.

For laminar flows ($Re < 2100$), the Nusselt number is generally calculated as follows:

$$Nu = 1.86 \left(Re\ Pr\ \frac{D}{L} \right)^{1/3} \left(\frac{\mu_b}{\mu_w} \right)^{0.14}. \tag{1.6}$$

The heat transfer behavior between these two regions is complex and, usually, systems are designed in such a way that slightly turbulent flows are avoided.

1.1.2 Subcooled Boiling

Subcooled boiling is initiated at nucleation sites before the fluid reaches the saturation temperature. These sites are initially sparse and single-phase forced-convective heat transfer remains the main heat removal process. This region corresponds to the developing subcooled nucleate boiling regime. The activation of the nucleation sites increases and the heated wall is slowly covered with vapor bubbles. A fully developed subcooled boiling regime is then reached. Several heat transfer correlations have been developed for subcooled boiling; most of these correlations are based on the single-phase Dittus and Boelter type of equation. Groeneveld and Snoek (Groeneveld, 1986) recommended a correlation developed by Nixon (unpublished report) for water in tubes within the range of its database (Re ranging from 10000 to 327000 and Pr ranging from 1.9 to 10.5). The correlation expresses the Nusselt Number of the liquid, Nu_f , as:

$$Nu_f = 0.024 Re_f^{0.77} Pr_f^{0.057}. \tag{1.7}$$

Chen's correlation (see section 1.1.3) can also be extended to subcooled conditions and the amount of heat used in vapour generation is accounted by the Splitting Factor

(Beuthe, 2005). The heat flux Splitting Factor, F_B, is defined as the fraction of the wall-to-liquid heat flux that results in bulk liquid heating (i.e., sensible heat). The remainder, $1 - F_B$, results in vapour generation. This heat flux Splitting Factor is computed by:

$$F_B = \frac{q"_{OSV}}{q"_{tot}}, \tag{1.8}$$

where $q"_{tot}$ is the total heat flux computed using (for example) Chen's correlation (see section 1.1.3). $q"_{OSV}$ is the heat flux corresponding to the onset of significant void. When locally, this heat flux is exceeded, void generation is considered and the splitting factor is used to determine the amount of heat used in vapour generation and bulk liquid heating. $q"_{OSV}$is often fixed to $q"_{OSV} = max\left[q"_{OSV}, q"_{tot}\right]$ to avoid possible discontinuities.

Saha ans Zuber (Saha and Zuber, 1974) have derived correlations for the onset of significant void. These correlations are divided into two regions based on the flow conditions expressed trough the Peclet number, Pe.

For low flows ($Pe \leq 70000$) :

$$q"_{OSV} = 455.0\frac{K_f\left(T_f^{sat} - T_f\right)}{D_h}, \tag{1.9}$$

and for high flows ($Pe > 70000$) :

$$q"_{OSV} = 0.0065Gc_p\left(T_f^{sat} - T_f\right). \tag{1.10}$$

In this work, however, subcooled booling is neglected.

1.1.3 Saturated Nucleate Boiling and Forced Convective Evaporation

Once the saturation temperature is reached, bubbles remain in the liquid core and the void fraction starts rising. Thus, the fluid will undergo a succession of flow patterns. The increase in void fraction also corresponds to an increase in thermodynamic quality. Figure 1.4 shows the flow patterns for vertical upward flows. At low void fractions, the vapor phase can be found as a dispersion of bubbles within the liquid phase. With an increasing in void fraction, the vapor phase may form plugs within the liquid phase. This flow pattern is defined as slug flow. Still increasing the void fraction, the vapor plugs will deform leading to the formation of the churn flow. Increasing the amount of steam provokes a transition form churn to annular flow.

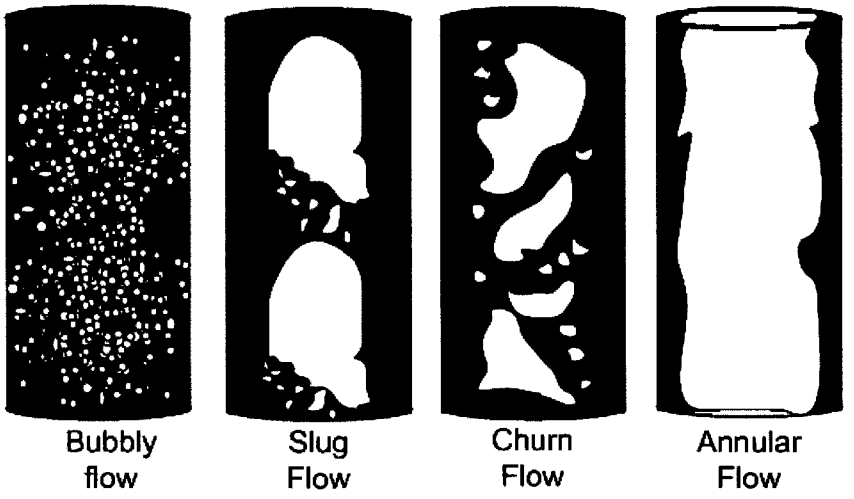

Figure 1.4 Flow Patterns for Upward Flows

In annular flow, a liquid annulus surrounds a vapor core containing (or not) entrained liquid droplets. At high mass fluxes, a rapid transition from bubbly flow to annular flow may occur. Initially, the heat transfer regime is defined as the saturated nucleate boiling. Increasing the quality, convective evaporation mechanism becomes progressively more

important leading to forced convective evaporation regime. In the transition region, both heat transfer regimes can coexist.

Chen (Chen, 1963) developed a correlation to cover the forced convective evaporation and nucleate boiling heat transfer regimes and the transition region. A single two-phase heat transfer coefficient, h_{tp}, is expressed as the sum of a nucleate boiling component, h_{nb}, and a forced convection component, h_{fc}, thus:

$$h_{tp} = h_{nb} + h_{fc}. \tag{1.11}$$

The forced convective component is calculated using a Dittus-Boelter type of correlation and is written as:

$$h_{fc} = 0.023 Re_{tp}^{0.8} Pr_{tp}^{0.4} \left(\frac{k_{tp}}{D} \right), \tag{1.12}$$

where the thermal conductivity, k, and Reynolds and Prandt numbers are calculated for the mixture. The nucleate boiling heat transfer coefficient component is calculated as follows:

$$h_{nb} = 0.00122 \left(\frac{k^{0.79} c_p^{0.45} \rho_l^{0.49}}{\sigma^{0.5} \mu_l^{0.29} H_{fg}^{0.24} \rho_v^{0.24}} \right) \Delta T_{sat}^{0.24} \Delta p_{sat}^{0.75} S, \tag{1.13}$$

where ρ_l is the density of the liquid phase, ρ_v is the density of the vapor phase, σ is the surface tension and H_{fg} the latent heat of evaporation. ΔT_{sat} is the wall superheat $(T_w - T_{sat})$, Δp_{sat} is the change of pressure corresponding to the temperature ΔT_{sat}. The suppression factor, S, is defined as:

$$S = \left[\frac{\Delta T_e}{\Delta T_{sat}}\right]^{0.99} = \left[\frac{\Delta T_e}{\Delta T_{sat}}\right]^{0.24} \left[\frac{\Delta p_e}{\Delta p_{sat}}\right]^{0.75}, \tag{1.14}$$

where ΔT_e is the mean superheat and Δp_e is the change of pressure corresponding to ΔT_e. The suppression factor has a value between 0 and 1. Its value approaches unity at low flow velocities and 0 at high flow velocities. Further details can be found in references (Chen, 1963) and (Collier, 1994).

1.1.4 Forced Convection to Vapor

This single-phase forced convection to vapor corresponds to the heat transfer mode at thermodynamic qualities greater than 1 (the vapor does not contain any droplets). At low wall superheats, correlations derived for single-phase forced convection to vapor are similar to those for single-phase forced convection to liquid (except with vapor properties). Modified correlations have been derived for heat transfer at high wall superheats. Groeneveld and Snoek (Groeneveld, 1986) recommend the Hadaller and Banerjee correlation (Hadaller and Banerjee, 1969) within the range of its database. The Hadaller and Banerjee correlation is expressed as

$$Nu = 0.0101 Re^{0.8774} Pr^{0.6112} \left(\frac{D}{L}\right)^{0.0328}. \tag{1.15}$$

Outside the database range of Hadaller and Banerjee, the Kutateladze and Borishanskii correlation (Kutateladze and Borishansky, 1953) is recommended (Groeneveld, 1986):

$$Nu = 0.027 Re^{0.8} Pr^{0.4} \left(\frac{T_v}{T_w}\right)^{0.55}, \tag{1.16}$$

where T_v is the vapor temperature in Kelvin and T_w is the wall temperature in Kelvin.

1.2 Critical Heat Flux

Critical heat flux is the transition point between nucleate boiling (or forced evaporative convection) and film boiling (or transition boiling). It is often referred as the departure from nucleate boiling (DNB) or dryout depending on the mechanism and flow conditions. The change in CHF mechanism would lead to differences in temperature rise. In general, a drastic temperature rise, impacting the sheath integrity, is observed for DNB while a gradual temperature rise, with no detrimental impact to the sheath, is encountered for dryout. Different CHF mechanisms and most common prediction methods are briefly presented in following sections. Details on CHF prediction methods can be found in Chapter 2.

1.2.1 Mechanisms Leading to DNB

Departure from nucleate boiling refers to the disruption of the liquid contact between the heated wall and the subcooled or saturated liquid. The DNB occurs at low void fractions and may result from one of the following mechanisms:

1. Surface Overheating at Nucleation Sites:

   A thin (micro) layer of liquid is present between the vapor bubble and the heat wall at the nucleation site. Evaporation of the liquid from the thin layer is continuously replenished with surrounding liquid. At sufficiently high heat fluxes, the evaporation rate increases drastically exceeding the replenishing rate. This has led to disruption of the liquid layer, exposing the heated surface to the vapour bubble directly. The wall temperature increases rapidly preventing wall rewetting and

compromising the integrity of the heated surface. This mechanism is shown in Figure 1.5-i.

2. Bubble Crowding and Vapor Blanketing:

   At medium and low subcoolings, the bubble density near the heated surface increases and the coalescence of adjacent bubbles may obstruct the thermal contact between the fluid and the wall (see Figure 1.5-ii). A rapid surface-temperature increase is observed and may prevent rewetting. With deteriorating heat-transfer characteristics, the dry patch may grow and spread quickly over the heated surface. This rapid temperature increase can seriously compromise the integrity of the heated surface.

3. Dryout of the Liquid Film Surrounding a Vapor Plug:

   In slug flows, the thin liquid film between the heated wall and the vapor plug may evaporate and form a dry patch that spreads over the heated surface (see Figure 1.5-iii). The low thermal conduction of the steam in contact with the surface will cause a local wall temperature increase.

i- Overheating at Nucleation Site

ii- Bubble Crowding

iii- Dryout of the Liquid Film Surrounding a Vapor Plug

Figure 1.5 Examples of DNB Mechanisms

1.2.2 Mechanisms Leading to Dryout

At high void fractions (about 80%) and lower wall superheating, CHF corresponds to the dryout phenomena, which refers to the complete evaporation of the liquid film in the annular flow regime. Again, different mechanisms explain the occurrence of this phenomenon:

1. Film Disruption due to Nucleate Boiling within the liquid Film:
   Nucleate boiling may still be present in the annular liquid film. Hence, bubble formation in the liquid film may produce the formation of dry spots. This process may not necessarily lead to film boiling conditions (if the bubble spreads and dryout the liquid film) or, as shown in Figure 1.6-i, to local DBN contiditions.

2. Liquid Film Breakdown due to Thermo-Capillary Effects:
   This dryout process is caused by the surfaces waves in the liquid film that causes a non-uniform heat transfer coefficient through the film. Under these conditions, the interfacial temperature changes provoke surface tension gradients that pumps out the liquid film from the hottest region. However, these dry patches may eventually disappear and the heated surface will rewet, thus this process does not necessarily lead to film boiling conditions. This CHF mechanism is shown in Figure 1.6-ii.

3. Liquid Film Dryout in Annular Flow:
   In annular flow, the liquid film thickness decreases with increasing quality. In this region, the heat transfer process is governed by droplet depositions, droplets entrainment and liquid film evaporation. If the droplet deposition rate does not balance the evaporation and droplets entrainment rate, dryout may occur. This mechanism is shown in Figure 1.6-iii and leads to dispersed annular flow film boiling characterized by a moderate wall temperature increase. A more detailed presentation of this heat transfer regime is discussed in this chapter since it is

studied in this work.

These mechanisms have been suggested in the literature and their classification is quite subjective. Experimental evidences of the occurrence of these mechanisms are, however, very limited.

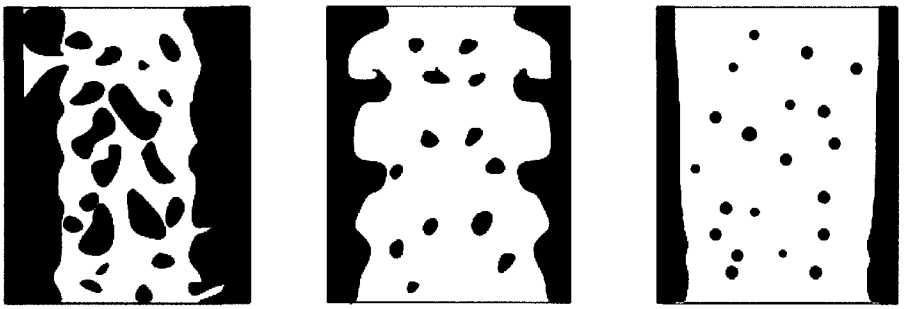

Figure 1.6 Examples of Dryout Mechanisms

1.3 Transition Boiling

Transition boiling is the heat transfer region between CHF and the minimum film boiling point (i.e., points B and C in Figure 1.1). This region is encountered mainly in temperature controlled systems and is a combination of unstable film boiling and unstable nucleate boiling taking place at the same location. For dryout occurring at low void fraction, the heated surface just in excess of the CHF temperature is partially covered with unstable vapor patches varying with space and time. Near the dryout location, the heated wall is almost entirely in contact with the coolant. The surface area in contact with the coolant decreases with increasing wall temperature.

Figure 1.7, from (Groeneveld, 1976), shows the microscopic behavior at the interface

between the heated wall and the fluid for pool boiling (column a), flow boiling where CHF is reached at low qualities (column b), and flow boiling where CHF is reached at high qualities (column c). In the figure, ϕ represents the heat flux and ΔT_w is the wall superheat. The behavior at the interface is shown at different steps of the boiling process; under nucleate boiling conditions (position I), at the CHF occurrence point (position II), under transition boiling conditions (positions III, IV and V) and at the minimum film boiling occurrence point (position VI).

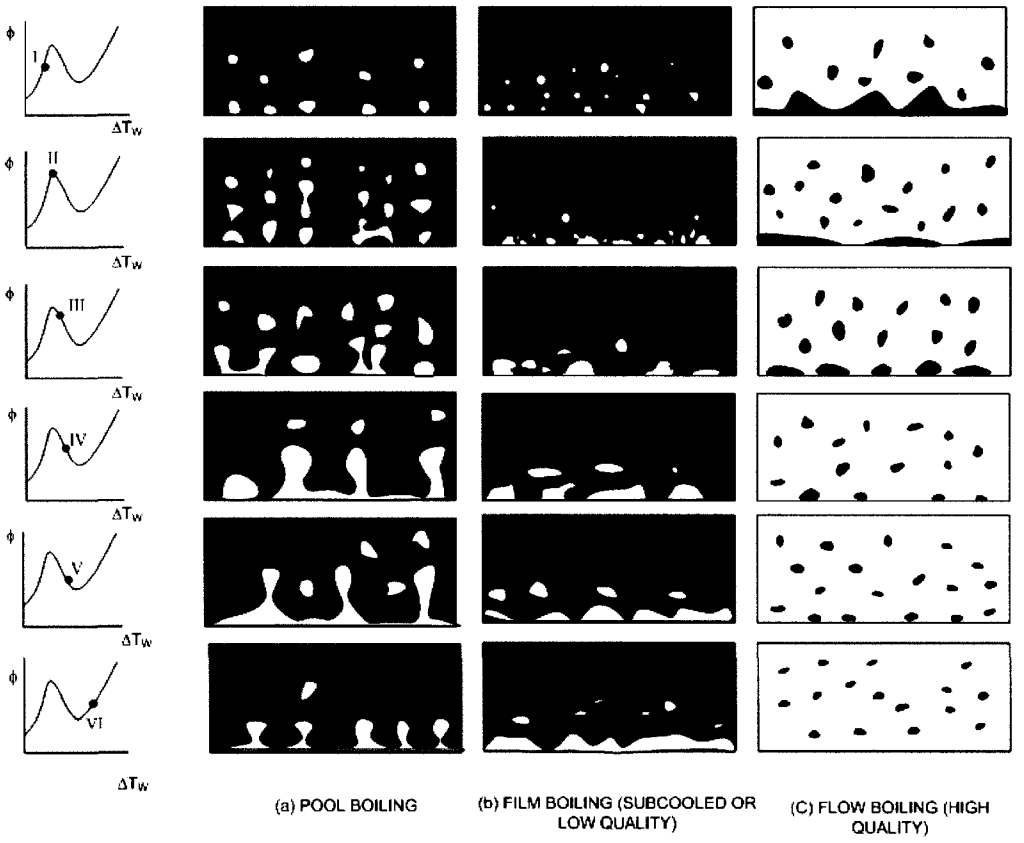

Figure 1.7 Microscopic Behavior of the Boiling Curve

Groeneveld and Fung (Groeneveld, 1976) stated that the boiling curve in temperature-controlled systems (i.e. the transition boiling and minimum film boiling temperature)

is affected by, among other variables, the mass flux, the thermodynamic quality, the local pressure and subcooling. In addition, there appears to be a strong effect of surface roughness on this boiling phenomenon.

1.4 Minimum Film-Boiling Temperature

The minimum film boiling temperature, T_{min} (point C on Figure 1.1)), is also referred as the Leidenfrost temperature. This temperature corresponds to the boundary that separates the transition boiling region from the stable film boiling region in a temperature controlled system. Once a stable film boiling regime is established, the rewetting process (described in Section 1.6.3) can be reached by decreasing the wall temperature. In this case, T_{min} bounds the beginning of this process. Hence, accurate T_{min} predictions are of great importance in safety analysis. Details on Minimum Film-Boiling Temperature prediction methods can be found in Chapter 2.

1.5 Stable Film Boiling

Stable film boiling regime is categorized into inverted annular flow film boiling, slug flow film boiling, and dispersed flow film boiling. The dispersed and inverted annular flow regimes are shown in Figure 1.8. Film boiling prediction methods will be presented Chapter 2.

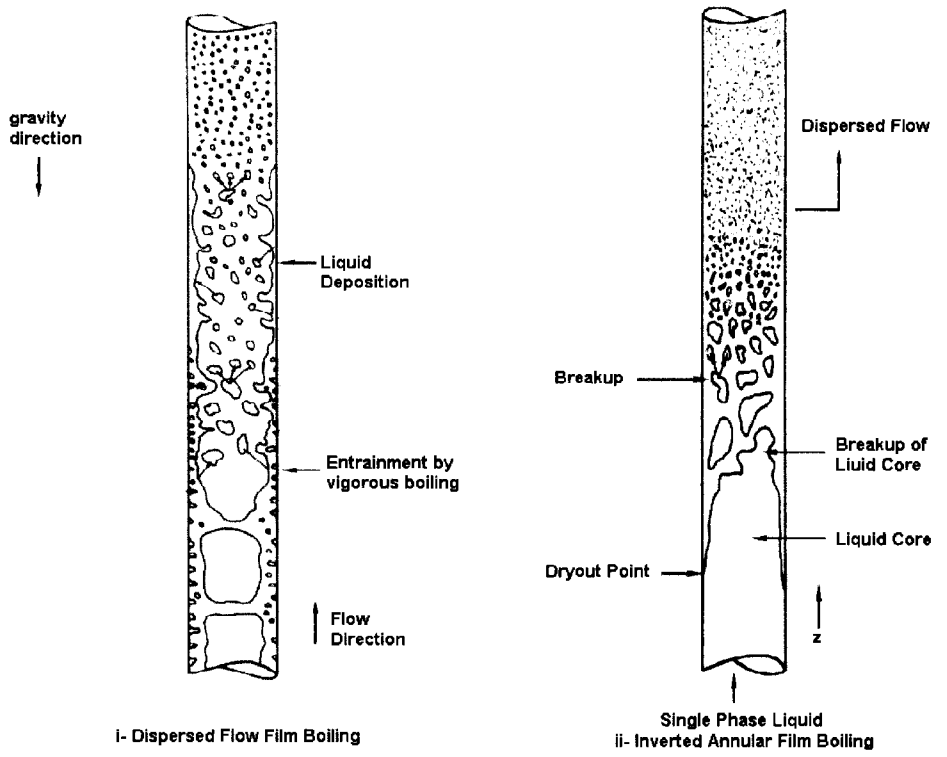

Figure 1.8 Illustration of (i) Dispersed Flow Film Boiling and (ii) Inverted Annular Film Boiling regimes

1.5.1 Inverted Annular Film Boiling (IAFB)

IAFB results from the Departure from Nucleate Boiling and occurs at void fractions lower than about 40%. Once the CHF is exceeded, vapor is generated rapidly near the wall, creating a vapor annulus that surrounds a liquid core which may contain entrained bubbles.

As the quality increase, the vapor accelerates faster than the liquid, causing instabilities in the liquid-vapour interface, which may breakup into droplets. The number of liquid droplets is not very high initially, and the droplet size is relatively large. These

droplets can eventually evaporate or break up into smaller droplets. IAFB may change to dispersed flow film boiling with increasing quality.

1.5.2 Slug Flow Film Boiling (SFFB)

This regime is usually encountered at low flow velocities and at void fractions that are too high to maintain inverted annular film boiling but too low to maintain the dispersed flow film boiling. As shown in Figure 1.8-(ii), this regime may be formed just downstream of the inverted annular flow regime, when the liquid core breaks up into slugs of liquid in a vapor matrix.

1.5.3 Dispersed Flow Film Boiling (DFFB)

Dispersed Flow Film Boiling (or liquid deficient region or mist flow) takes place after dryout had occurred. Since the void fraction under dryout conditions can be as high as 80%, the heat is transferred to a continuous vapor phase containing dispersed and fine liquid droplets; the diameter is approximately 50 to 1000 μm. The wall temperature at DFFB is a function of the heat transferred by forced convection from the wall to the vapor phase, convection from the vapor to droplets within the core, and radiation heat transfer from the wall to the vapor and droplets. The heat transfer rate is influenced by the droplets distribution and their behavior near the wall. Within the vapor core, the droplets initially tend to be large. These large droplets are deformable and spread considerably, and eventually breakup into many smaller droplets (see Figure 1.8). The reduction in droplet size increases the droplets-vapor interfacial area and improves the heat transfer between vapor and droplets.

1.6 Heat Transfer Regimes in Heated Channels

Heat transfer regimes encountered with an upward cooling flow in a uniformly heated tube are shown in Figure 1.9, from (Corradini). A subcooled fluid entering the tube encounters the single-phase forced convection to liquid, subcooled boiling, nucleate boiling, forced convective evaporation, film boiling, and single-phase forced convection to vapor. These regimes correspond closely to the boiling curve with a direct transition from nucleate boiling to film boiling at the CHF occurrence point (point B to point D on Figure 1.1).

The wall temperature increases sharply once the CHF is reached, as illustrated in Figure 1.9. This wall temperature increase is only possible if the heat flux from the heated wall to the fluid is temporarily reduced while the applied power remains constant. Under steady-state conditions (i.e. when the applied power, the wall temperature and flow conditions remain constant within the time in each position in the tube), these phenomena may be interpreted as the developing flow film boiling effect that will be presented in the following subsection.

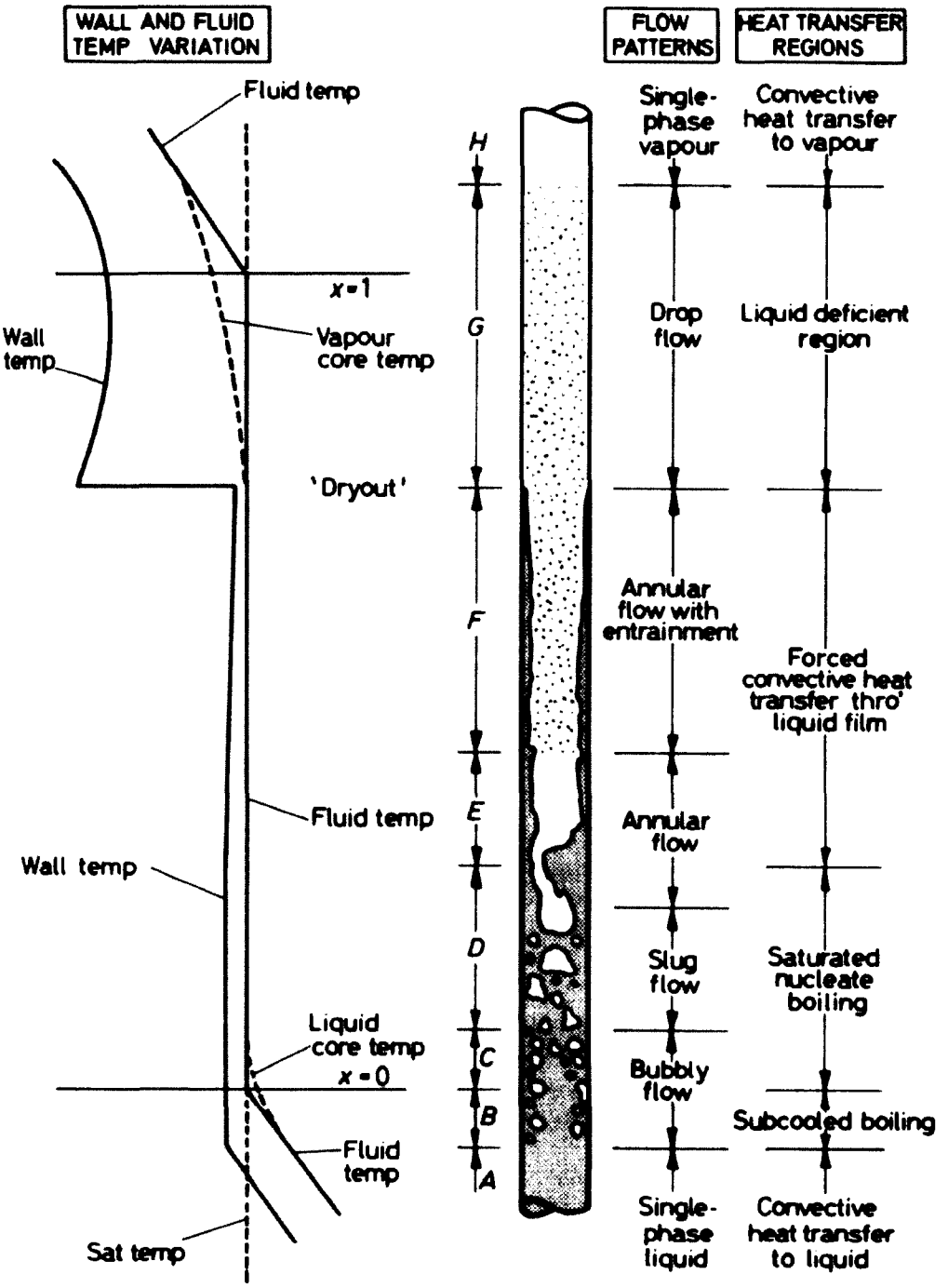

Figure 1.9 Forced Convective Boiling Curve

1.6.1 Developing Flow Film Boiling

The axial wall temperature distribution along the heated tube is shown in Figure 1.10, from (Guo, 1978), at steady-state high-flow conditions. An increase in wall temperature is illustrated at locations downstream of the CHF location, but the increasing trend is relatively gradual. Predicted wall temperatures for fully developed film boiling are also shown in the same figure for comparison, and are significantly higher than the observed wall temperatures beyond the CHF point. The region bounded between the dryout and maximum wall temperatures is referred as the developing film boiling region, and the region beyond the maximum wall temperature is identified as the fully developed film boiling region.

The gradual wall-temperature rise at the CHF location is attributed to the buildup of vapor superheat at high flow and high quality conditions (i.e., the flow would not be able to change from fully developed nucleate boiling heat transfer to fully developed film boiling heat transfer instantaneously at a specific axial location). Prior to CHF occurrence, droplets from the liquid core are repelled by vapor formed by the evaporation of the liquid film and having a velocity component toward the center of the channel. Once the dryout of the liquid film is completed, some of these droplets can impinge onto the heated wall increasing the heat transfer rate. The increasing in vapor superheat near the heated wall reduces the frequency of the droplet-surface interaction and the film boiling approaches fully developed conditions (at the maximum wall-temperature location). After reaching the maximum wall temperature, the droplet-wall interaction is completely inhibited and fully developed film boiling heat transfer is encountered.

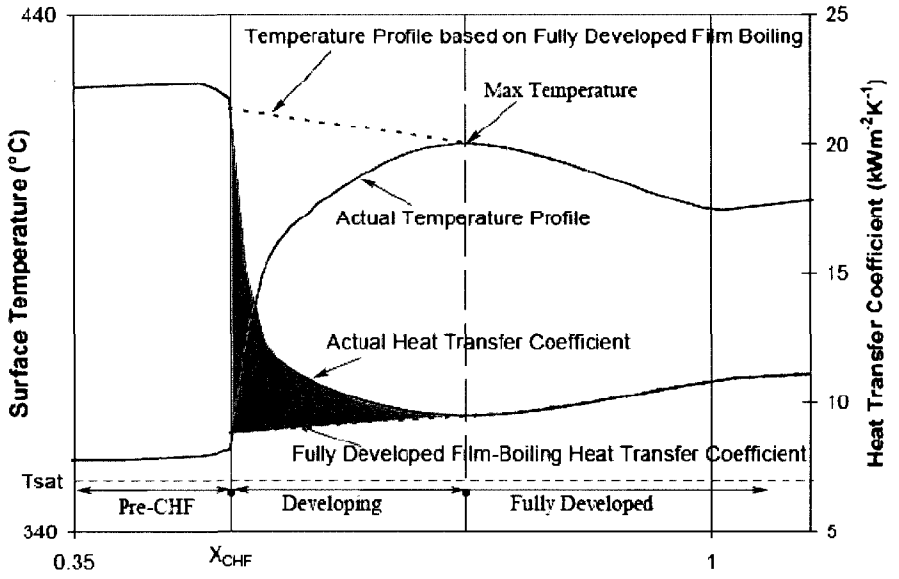

Figure 1.10 Heat Transfer Coefficient and Wall Temperature Evolution in Post-Dryout Conditions

1.6.2 Thermodynamic equilibrium in post-dryout conditions

Generally, flows with low dryout qualities and high mass fluxes show thermal equilibrium behaviors (i.e. the two phases are at saturation temperature) while flow with high dryout qualities and low mass fluxes show non-equilibrium behaviors. Typical wall temperature axial distribution and fluid and vapor temperatures are shown in 1.11 for a tube where post-dryout conditions are encountered. Consequently, the flow may not be under thermodynamic equilibrium under dispersed flow film boiling conditions and the quality (or void fraction) could be overestimated if thermal equilibrium is assumed.

Figure 1.12, from (Corradini), presents the equilibrium quality, x_{equil}, and the actual quality, x_{actual}. The figure shows that, before the dryout location, both phases are close to the saturation temperature. After CHF, the vapor-droplets heat transfer is small and

most of the heat goes to the vapor which provokes its superheating. The increase of the vapor temperature (i.e. superheated steam) then allows the heat transfer from the steam to the droplets to occur. Further downstream, the amount of heat transferred from the wall to the vapor may approximately balance the amount of heat absorbed by the droplets that starts evaporating.

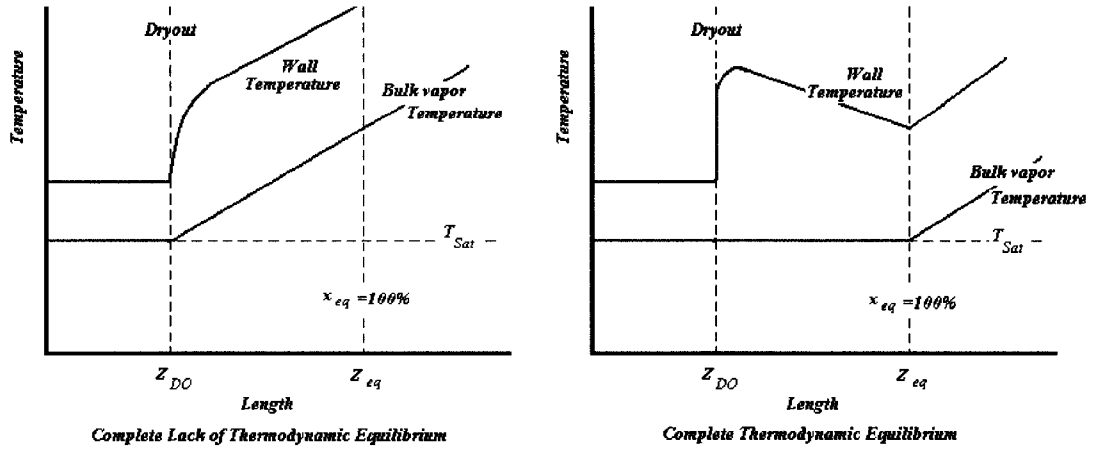

Figure 1.11 Impact of Thermal Equilibrium on the Post-Dryout Wall Temperature

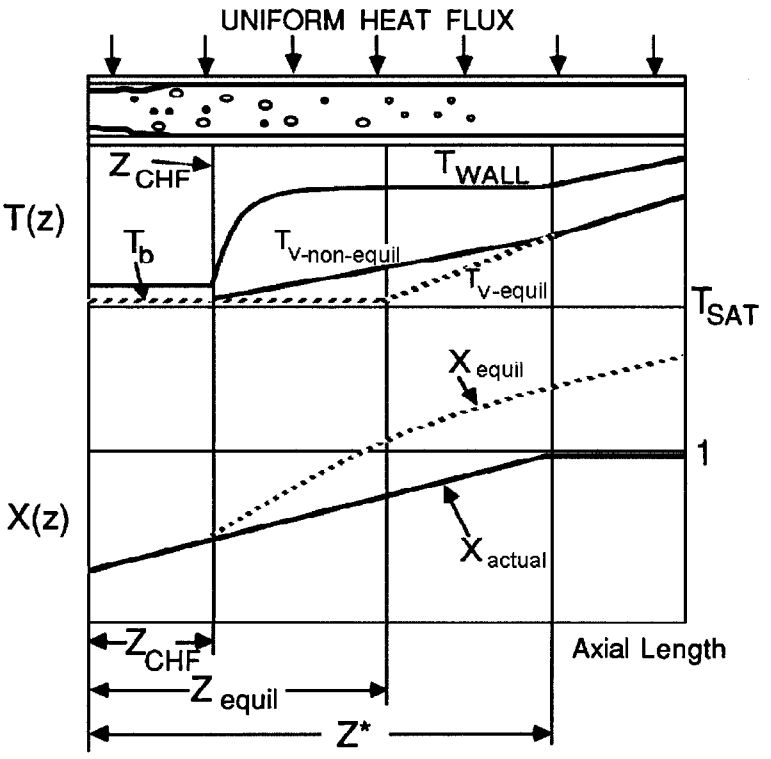

Figure 1.12 Equilibrium and Actual Qualities Distributions in Post-Dryout Conditions

1.6.3 Rewetting

If the applied heat flux is reduced once a stable film boiling regime is reached, the heat flux to the fluid will also be reduced and the film boiling region is observed until the minimum film boiling temperature is reached. At this point, a sudden transition to nucleate boiling then occurs (from point E to C of Figure 2.6). Dryout (increasing q'') and rewetting (decreasing q'') processes are shown on the boiling curve of Figure 1.13 for heat flux controlled systems.

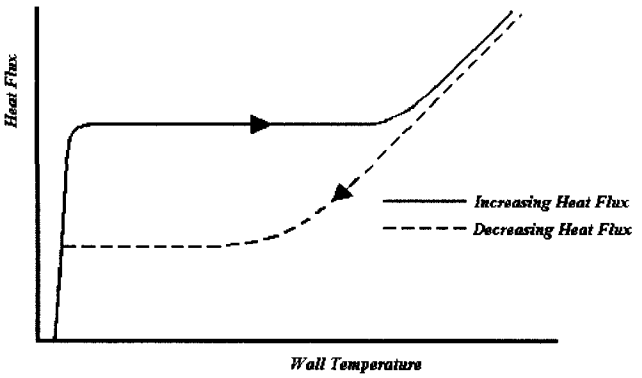

Figure 1.13 Post-Dryout and Rewetting Processes in Heat Flux Controlled Systems

CHAPTER 2

LITERATURE SURVEY ON POST-DRYOUT HEAT TRANSFER EXPERIMENTS AND PREDICTION METHODS

This chapter presents some relevant experiments related to post-dryout heat transfer and a detailed exposition of the data used in this work. It also presents a general overview of the critical heat flux and post-dryout heat transfer prediction methods available in the literature. Because of the exhaustive number of prediction methods available, only the most general and popular ones are presented. An alternative methodology, the look-up table, is used in the current assessment work. This method is also introduced in this chapter.

2.1 Post-Dryout Heat Transfer Experiments

A large number of post-dryout experiments have been performed for various test section geometries. Many of these experiments were carried out using cryogenics and refrigerants because of the high temperatures reached in such experiments. Also, most of the experimental data were obtained at steady-state conditions.

Kirillov and Groeneveld (Kirillov) tabulated a large number of film-boiling experimental data obtained in tubes. Additional data are available from Kastner et al. (Kastner, 1981), Kohler-Hein (Kohler and Hein, 1986), Konkov-Zuperman (Konkov and Zuperman, 1967), Leung (Leung, 1994), Nijhawan (Nijhawan, 1980), and Subbotin et al. (Subbotin, 1973). Among available experiments, data sets provided in Bennett et al. (Bennett, 1967) and Becker et al. (Becker, 1983) have been recognized as the most reliable and well documented. Both sets of data were obtained with upward water flow

inside vertical circular tubes. However, tubes used in the experiment of Bennett et al. (Bennett, 1967)] exhibited a uniform axial power profile, while those in Becker et al. (Becker, 1983) had non-uniform axial power profiles.

The experiment performed by Bennett et al. (Bennett, 1967) has been selected in this assessment of the two methodologies in predicting post-dryout heat-transfer coefficient. A brief description of the experiment is provided in this chapter. Details can be found in (Bennett, 1967).

2.1.1 Experiments of Bennett et all.

Bennett et al. (Bennett, 1967) measured directly the external surface temperatures to infer the internal surface temperature distribution in a vertical Nimonic-80a tube of 0.0127 m inside diameter. The tube was uniformly heated and cooled with an upward co-current flow of water at a pressure of 6893 kPa. Two heated lengths were used: 3.6576 m and 5.5626 m. It was not possible to obtain a 5.5626 m tubing in this material and the second test section was constructed of two pieces joined by a special quick-changing flange. This obviously affected the results; it was found (see (Bennett, 1967)) that it caused a depression of the heat flux over a short distance (approximately 3 cm). However, it was unlikely to have any significant effect on the critical heat flux and in no case the liquid deficient region propagated upstream of the flange. The experimental facility consisted of 27 thermocouples attached to the test section using one of the following two methods:

1. The bottom 12 thermocouples were made of standard chromel-alumel glass insulated wire. The junction was cemented to a piece of anodized aluminum which, in turn, was cemented to the test section outer wall. The attachment was very effective and resulted in a negligible temperature drop across the anodized aluminum insulator.

2. The top 15 thermocouples were sheathed type since the cement used to attach the anodized aluminum insulator type could not sustain the extremely high temperature found in the liquid deficient region. The thermocouples were bounded to the outer wall of the test section with wire and were electrically insulated from the test section by a mica layer.

Figure 2.1 shows the schematic diagram of the 5.5626-m heated length test section. Thermocouples locations are also shown in the figure.

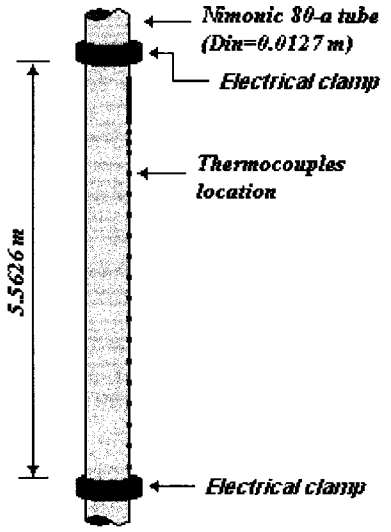

Figure 2.1 Schematic Diagram of the Bennett's Test Section

2.1.2 Test Procedures and Flow Conditions

The experiments were carried out as follows: the power was increased until the temperature measured at the last thermocouple began to increase rapidly. Then, the power was increased very slowly until both wall temperature and flow conditions remained constant. Once the steady-state flow conditions were reached, the outside wall temperature

distribution was recorded. These temperatures, and the applied power, are then used to infer the internal surface temperature distribution by solving heat conduction equation through the heated tube. The procedure was repeated for the next thermocouple until another steady-state conditions were reached, and so on. These operations were performed for each set of heat flux, inlet temperature and mass flux. Test conditions were remained between following boundaries:

$$p = 3.896\ MPa$$

$$380\ \tfrac{kg}{m^2 s} < G < 5235\ \tfrac{kg}{m^2 s}$$

$$80\ kW < P < 406\ kW$$

$$258\ ^{o}C < T_{in} < 277\ ^{o}C$$

Finally, there are no indications about the order of magnitude of experimental errors and uncertainties in the report (see (Bennett, 1967)).

2.2 Prediction Methods for Critical Heat Flux

A large number of CHF predictions methods have been developed and can be divided into three groups:

1. Local flow conditions correlations:

   These correlations express CHF in terms of local flow parameters (such as pressure, mass flux, and quality) and flow cross-sectional geometry (either diameter or area). An iterative approach is applied using the local CHF correlation and

the heat-balance equation to establish the dryout power and dryout location in a heated channel. Most local CHF correlations are derived for a specific geometry (e.g., tubes and annuli) with uniform axial and radial power profiles at steady-state conditions. Modification factors have been developed for separate effects, such as channel size, non-uniform axial and radial power profiles and transients. The commonly used local CHF correlations have been summarized in (Groeneveld, 1986).

2. Global conditions correlations:

   These correlations express CHF as functions of system-flow parameters (such as outlet pressure, mass flow rate or mass flux, and inlet enthalpy or inlet temperature), heated length, and flow cross-section geometry (either diameter or area). This type of correlations is valid for establishing average CHF (or critical power) for a specific geometry (i.e., length and diameter) only. It is not applicable to determine the local CHF value and CHF location in non-uniform heated channels.

3. Analytical model:

   Analytical models have been developed for bubble crowding CHF mechanism (e.g. Weisman and Pei (Weisman and Pei, 1983)) and annular film dryout mechanism (e.g., Hewitt (Hewitt, 1978). The bubble crowing model accounts for the bubble formation and coalescence, and considers the CHF occurrence at the near-wall void fraction of about 0.8. The annular-film dryout model accounts for the liquid-film depletion through evaporation and entrainment with the compensating effect of droplet deposition. These models, in principle, are valid for any channel geometries, steady state and transient flow conditions, and various axial and radial power profiles. However, each model is applicable for a specific CHF mechanism (or flow regime) and cannot be extended to others. In addition, there is no analytical model applicable to the transition regime further complicating their applicability.

Most empirical correlations and analytical models have a limited range of application. The look-up table approach was initiated to provide a general prediction method over a wide range of flow conditions. According to reference (Groeneveld, 2003 (1)), a standard CHF look-up table was developed in Russia with a relatively small amount of CHF data (about 5000). The table look-up approach was continued at the CENG (Centre Nucleaire de Grenoble) and the University of Ottawa using a more extensive database (Groeneveld, 1986). An international CHF look-up table was developed with databases contributed from various organizations (Groeneveld, 1996). It has been shown to have the best prediction accuracy over the widest range of flow conditions, among all correlations. A minor update has also been introduced recently (Groeneveld, 2007). The critical heat flux look-up table (CHF-LUT) presents discrete CHF values as a function of local pressure, mass flux and thermodynamic quality for vertical upward flow of water inside an 8-mm ID tube. The local CHF value at in-between flow conditions is calculated using interpolation of the tabulated CHF values at neighbouring flow conditions. Modification factors have been derived for various separate effects (such as tube diameters, geometry, axial power profile, and transient). Additional information about the CHF-LUT is presented in reference (Groeneveld, 1996).

2.3 Prediction Methods for Transition Boiling

A large number of correlations have been proposed for transition boiling, but often provide very different predictions. These correlations can be divided into three groups:

1. Empirical correlations: These correlations, although very simples, cannot generally be extrapolated outside the range of data on which they are based.

2. Correlations containing boiling and convective components: These correlations

are generally expressed as:

$$h_{TB} = h_{FB} + A \ \exp\left(-B \ (T_w - T_{sat})\right), \tag{2.1}$$

where h_{FB} is the film boiling heat transfer coefficient (or convective component) and the second term of the right hand side of the equation is the boiling component that becomes insignificant at high wall superheats.

3. Phenomenological Correlations: This set of correlations is based on physical models and on empirical correlations to overcome some inadequate physical understanding.

References (Groeneveld, 1986), (Groeneveld, 1976) and (Auracher, 1990) provide useful overviews on the current topic. In view of the deficiency of various prediction methods, Bjordard and Griffith (Bjornard, 1977) introduced a correlation to interpolate the heat flux at transition boiling between those at CHF and film boiling:

$$q'' = \lambda q''_{CHF} + (1 - \lambda)\, q''_{film}, \tag{2.2}$$

where q''_{CHF} is the critical heat flux, q''_{film} is the film boiling heat flux and λ given as:

$$\lambda = \frac{T_w - T_{min}}{T_{CHF} - T_{min}}. \tag{2.3}$$

Groeneveld and Snoek (Groeneveld, 1986) recommended an interpolation between the CHF and the minimum film-boiling points:

$$\frac{q"_{TB}}{q_{min}} = \left(\frac{CHF}{q_{min}}\right)^m, \tag{2.4}$$

where $q"_{TB}$ is the heat flux in the transition boiling region and $q"_{min}$ is the heat flux at the minimum film boiling temperature (see Figure 1.1). The coefficient m is calculated as follows:

$$m = \frac{ln\left(\frac{T_{min}-T_{sat}}{T_{TB}-T_{sat}}\right)}{ln\left(\frac{T_{min}-T_{sat}}{T_{CHF}-T_{sat}}\right)}, \tag{2.5}$$

where, T_{TB} is the temperature in the transition boiling region, T_{min} is the minimum film boiling temperature, T_{sat} is the saturation temperature and T_{CHF} is the critical heat flux temperature. The correlation of Groeneveld and Snoek (Groeneveld, 1986) exhibits a correct parametric trend of transition boiling.

2.4 Prediction Methods for Minimum Film Boiling Temperature

Several correlations are available to predict the minimum film boiling temperature. Many of them have been summarized in (Groeneveld, 1986); the reader is referred to this reference for further details. Groeneveld and Stewart correlation (Beuthe, 2005) has been widely used to predict the minimum film-boiling temperature:

for $x \leq 0$ and $p_f \leq 10^7\ Pa$

$$T_{min} = 284.7 + 44.11 \times 10^{-16} p_f - 3.72 \times 10^{-12} p_f^2 - 10^4 x / \left(2.819 + 1.219 \times 10^{-6} p_f\right). \tag{2.6}$$

For $x > 0$ and $p_f \leq 10^7\ Pa$

$$T_{min} = 284.7 + 44.11 \times 10^{-16} p_f - 3.72 \times 10^{-12} p_f^2. \tag{2.7}$$

For $p_f > 10^7\ Pa$

$$T_{min} = T_{sat} + \left(42.8 - min\left[x, 0.0\right]\frac{10^4}{15.01}\right) + \left(\frac{22.1 - p_f \times 10^{-6}}{12.1}\right), \qquad (2.8)$$

where p_f is the local pressure of the liquid phase.

2.5 Prediction Methods for Stable Film Boiling

In the stable film-boiling region, the predictions methods can be divided in the following three groups:

1. Empirical correlations that use functional relationships between the heat transfer coefficient and some independent parameters.
2. Phenomenological correlations that account for thermodynamic non-equilibrium in vapor actual quality and temperature.
3. Theoretical models developed by solving equations for various heat transfer processes.

2.5.1 Empirical Correlations

A large number of empirical correlations have been developed to predict film-boiling heat transfer (Kirillov). These correlations are expressed in modified form of the Dittus-Boelter equation. The simplest correlations were based on the assumption of thermalhydraulic equilibrium (e.g., Dougall-Rohsenow correlation (Dougall and Rohsenow, 1963),

Miropolskiy correlation (Mirololskiy, 1963), and Groeneveld correlation (Groeneveld, 1976)). All these equations have limited ranges of application and are valid only at high mass flow rates where non-equilibrium effects are relatively small.

The Groeneveld correlation was derived with experimental data obtained with tubes and annuli and is expressed as

$$Nu_v = a\left[Re_v\left\{x + \frac{\rho_v}{\rho_l}(1-x)\right\}\right]^b Pr_{g,w}^c Y^d, \tag{2.9}$$

where the Y factor is defined as:

$$Y = 1 - 0.1\left(\frac{\rho_v}{\rho_l} - 1\right)(1-x)^{0.4}. \tag{2.10}$$

Coefficients "a", "b", "c", and "d" were optimized using a large bank of selected data. Details on this correlation and the coefficients are given in (Groeneveld, 1973). A parametric comparison of post-dryout heat transfer correlations showed that the Groeneveld correlation produces artificially high heat transfer coefficients at low pressures (Kirillov). Slaughterback (Slaughterback, 1973) revised the Groeneveld correlation to improve the prediction accuracy.

2.5.2 Phenomenologicial Correlation

Phenomenological correlations represent the compromise approach between correlations and theoretical models. These correlations account for the degree of non-equilibrium between liquid and vapor phases. Examples of this type of correlation include those from Groeneveld and Delorme (Groeneveld, 1976), Plummer et al. (Plummer, 1976), Chen et al. (Chen, 1977) (Chen, 1979), Saha (Saha, 1980), Sergeev (Sergeev, 1985),

and Nishikawa (Nishikawa, 1986). Most of these correlations are a modified form of the Dittus-Boelter equation, expressed in terms of vapor Reynolds and Prandtl numbers. The Reynolds number in the phenomenological correlation is based on the actual quality, x', instead of the equilibrium quality, x_e (as in the empirical correlation).

The vapor non-equilibrium is accounted via the actual vapor quality. Plummer et al. (Plummer, 1976) expressed the actual vapor quality as a function of the mass flux (i.e., $\left(\left(x_{actual} - x_{DO}\right) / \left(x_{equil} - x_{DO}\right) = f\left(G\right)\right)$. Chen et al. (Chen, 1977) (Chen, 1979) presented the vapor quality in terms of pressure and wall temperature ($x_{actual}/x_{equilibrium} = f\left(p, T_w\right)$). Sergeev (Sergeev, 1985) defined the vapor quality using a differential equation (see reference (Kirillov) for further details). Groeneveld and Delorme (Groeneveld, 1976) expressed the vapor quality as:

$$\left[\frac{x_{actual}}{x_{equil}}\right] - max\left(1, x_{equil}\right) = \exp\left(-tan\left(\psi\right)\right), \tag{2.11}$$

where ψ is a function of $Re_{v,hom}, p, q, x_{equil}, x_{actual}$. (See (Groeneveld, 1976) for further details.)

2.5.3 Theoretical Models

Theoretical models for film-boiling heat transfer account for various heat transfer mechanisms that occur between the heated surface and the fluid. These models were based on mass, momentum and energy balance equations and included empirical closure relationships. Six different heat-transfer mechanisms have been identified:

1. Wet collisions: heat transferred from the surface to the liquid droplets that impact the wall.

2. Dry collisions: heat transferred from the surface to the liquid droplets that enter in

the thermal boundary layer but that do not wet the surface.

3. Forced convection heat transfer from the surface to the vapor.

4. Forced convection heat transfer from the vapor to the droplets.

5. Radiative heat transfer from the surface to the vapor.

6. Radiative heat transfer from the surface to the droplets.

A large number of analytical models have been developed and described in Kirillov and Groeneveld (Kirillov). These models are generally valid for a specific flow pattern.

According to reference (Wolverint), Garnic and Rohsenow proposed one of the early models for steady-state vertical upward flows in tubes. The total heat flux is considered as the sum of three contributions: wall-to-vapor convection, wall to droplet evaporation and radiation. An interesting aspect of this model is that a detailed analysis of the wall-to-droplet heat transfer mechanisms was attempted, although non-equilibrium effects were ignored. The heat flux due to the impinging droplets to the wall is expressed as:

$$q_L = u_d \left(1 - \epsilon\right) \rho_L h_{LG} f_{cd} \exp\left[1 - \left(\frac{T_w}{T_{sat}}\right)^2\right], \tag{2.12}$$

where f_{cd} is the cumulative deposition factor expressed as a function of the droplet size. The droplet deposition velocity u_d is calculated using:

$$u_d = 0.15 \frac{Gx}{\rho_l \epsilon} \sqrt{\frac{f_v}{2}}. \tag{2.13}$$

where f_v is the single-phase friction factor calculated at the effective Reynolds number of the vapor phase (i.e., $GxD/\epsilon\mu_v$).

According to reference (Wolverint), Yoder and Rhosenow improved the model of Garnic and Rohsenow and included the heat transferred from the wall to the vapor, from the wall to the droplets during droplet-wall collisions, and from the vapor to the entrained liquid droplets. Subsequently, Varone and Rohsenow (Varone, 1986) and (Varone, 1990) considered the average diameter of the droplets and their breaking up dynamics in their model, which provided improved prediction accuracy. Tong and Tang (Tong, 1997) recommended the model of Varone and Rohsenow for dispersed flow film boiling.

Theoretical models are highly complex and consist of empirical closure relationships that were based on limited range of experimental data. Despite of their apparent success (Varone, 1990), their applications remain limited particularly in transient analyses.

2.6 Film Boiling Look-Up Tables

A correlation or a theoretical model can be used to predict the heat transfer coefficient. However, the former is usually restricted to a limited range of flow conditions while the latter is rather complex and requires long computation times. To overcome these problems, the look-up table method was developed for predicting heat transfer coefficient in post-dryout conditions (Groeneveld, 1988). This look-up table consists of a set of tabulated stable film boiling heat transfer coefficients obtained from experimental values of wall temperatures. These coefficients are presented as a function of discrete values of mass flux, pressure, quality, and heat flux or wall superheat. The look-up technique is easy to implement in safety analysis computer codes and is currently the default post-dryout heat transfer prediction method in CATHENA (Hanna, 1998). In the present study, the look-up technique is used to predict the stable film boiling heat transfer coefficient.

According to reference (Groeneveld, 2003 (1)), the look-up tables have several advan-

tages: simple to use and implement, no iterative procedures required, wide range of applications, applicable to non-aqueous fluids using fluid-to-fluid modeling relationships, and provide accurate predictions. However, there are a few concerns with the latest look-up table, such as fluctuations in the film boiling heat transfer coefficients with flow parameters in some regions, sharp variations between adjacent tables entries, and data scarcity at some flow conditions. Further work is required to improve the table.

2.6.1 Description of the Film Boiling Look-up Tables

The Look-up Table (LUT) method was developed by Groeneveld and Leung and subsequently improved by Leung et al. (Groeneveld, 2003 (2)) at AECL and the University of Ottawa. The resulting 1996 look-up table is referred as the PDO-TW-96 and has been recommended in Kirillov et al. (Kirillov, 1996). The PDO-TW-96 table was based on 21525 data providing 14687 tabulated heat transfer predictions. It predicted wall temperature measurements in tubes with an average error of 1.2% and a root-mean-square (RMS) error of 6.73%. Vasic et al. (Vasic, 2001) introduced additional data and a smoothing process to the table.

The first LUT version was based on the heat flux, therefore, their implementation in transient calculations was cumbersome. Thus, subsequent versions were based on the wall superheat (rather than the heat flux) by using the same flow properties. The latest version of the look-up table (version 2003) has been based on 77 234 film-boiling data points obtained from 36 different sources.

The look-up table method provides fully developed film-boiling heat-transfer coefficients for upward flows in tubes of a given internal diameter. The heat transfer coefficient has to be corrected to take into account others effects, such as different tube diameters, bundle geometries, spacer devices, etc. The approach used to introduce these

corrections is to multiply the LUT heat transfer coefficient by a modification factor. The modification factor can be understood as follows; the Nusselt number can be expressed, at a specified location z, as:

$$Nu_z = Nu_0 \left(K_{geometry} \cdot K_{spacers} \cdot K_{developing} \cdot K_{ADF} \right), \tag{2.14}$$

where Nu_0 is the reference Nusselt number calculated at the same location and flow conditions for a clean tube. The coefficients K_i are the different modification factors that account for geometry, $K_{geometry}$, spacer devices, $K_{spacers}$, the development of the film boiling conditions, $K_{developing}$, axial heat flux distributions, K_{AFD}, and other negligible effects. Further details regarding the modification factor method can be found in reference (Leung, 2002). Equation (2.14) assumes that all the effects are totally independent of each other. However, this is not totally true but is a better assumption than ignoring these effects.

2.7 Developing Flow Modification Factor

Groeneveld and Leung (Leung, 2002) developed the heat-flux-based developing-flow modification factor for applications with the heat-flux-based film-boiling look-up table. The modification factor is expressed as:

$$K_{developing} = \frac{h_{PDO}}{h_{fd}} = 1 + \left(\frac{h_{nb}}{h_{fd}} - 1 \right) \exp \left[a \left(\frac{x - x_{DO}}{(1 - x_{DO})Bo} \right)^b \right], \tag{2.15}$$

where h_{PDO} is the post-dryout (or film boiling) heat transfer coefficient at the location of interest, h_{fd} is the fully developed film-boiling heat-transfer coefficient, and h_{nb} is the nucleate-boiling heat-transfer coefficient. The boiling number, Bo, is defined as:

$$Bo = \frac{q''}{GH_{fg}}. \tag{2.16}$$

where H_{fg} is the latent heat of vaporization. Coefficients "a" and "b" were optimized using 1222 points selected from the database of Becker et al. [4] under vertical upward steam-water flow condition in tubes. Reference (Leung, 2002) performed an assessment of this modification factor which indicated significant improvement in prediction accuracy; the average prediction error was 2.82% with the modification factor as compared to 11.86% without the modification factor (i.e., applying the fully developed film-boiling calculations).

Guo and Leung (Guo, 1978) developed a modification factor to be used in conjunction with the temperature-based look-up table. The temperature-based modification factor is expressed as:

$$K_{developing} = \frac{h_{PDO}}{h_{fd}} = 1 + \left(\frac{h_{nb}}{h_{fd}} - 1\right) \exp\left[c\,(WSR - 1)^b\right], \qquad (2.17)$$

where WSR is the Wall Superheat Ratio defined as:

$$WSR = (T_w - T_{sat}) \,/\, (T_{CHF} - T_{sat}) \qquad (2.18)$$

Coefficients "c" and "b" were optimized using a large experimental database (Guo, 1978). Applying this correlation in predicting the film-boiling heat-transfer coefficient resulted in an average error of -1.37% and a root-mean-square error of 13.03%.

A separate modification factor has been developed for low pressures (less than 2000 kPa) (Guo, 1978). It is expressed as:

$$H_{dev,lowP} = \frac{h_{pdo}}{h_{fd}} = 1 + \left(\frac{h_{NB}}{h_{fd}} - 1\right) \exp\left[-1.85 \left(\frac{\rho_l}{\rho_v}\right)^{-0.18} (WSR - 1)^{0.483}\right], \qquad (2.19)$$

where ρ_l and ρ_v are the liquid and gas densities. Applying this modification factor predicted the low-pressure heat-transfer coefficients with an average error of -0.07% and

a root-mean-square error of 5.98% for 554 data points.

CHAPTER 3

NUMERICAL MODELING

This section presents the numerical modeling used in the assessment of the proposed methods discussed in the previous chapter. The simulated temperatures are compared to the experimental data of Bennett et al. (Bennett, 1967). The modeling simplifications and hypothesis are presented. A brief description of the implemented post-dryout heat transfer models is presented in this chapter. Initially, the effect of radiation heat transfer is neglected. However, a model that takes into account this mechanism has been implemented in the assessment procedure to validate this initial assumption. The description of the approach used is presented at the end of this chapter.

3.1 Experiments Selection

The experimental set-up and procedures of Bennett et al. (Bennett, 1967) have been presented in Chapter 2. Pre-CHF and CHF runs in the experiment do not provide any post-dryout heat-transfer data and hence have been excluded in the assessment. Erroneous temperature measurements (e.g., sudden local temperature drop without justification) were also excluded from the database. This study focuses mainly on applications to the loss-of-flow and small-break loss-of-coolant accidents, where mass fluxes are generally higher than 1000 kg/m^2s. Therefore, experimental data obtained at low mass fluxes (i.e., less than 1000 kg/m^2s) have been excluded in the assessment.

As described in Chapter 2, the experimental data were collected from two test sections (3.66 m and 5.56 m heated lengths) in the experiment of Bennett et al. (Bennett, 1967). This study focuses only on data obtained with the 5.56 m tube, where distinctive post-

dryout sections have been observed (post-dryout data spread over a shorter length over the 3.66 m tube). The database includes 702 post-dryout temperature measurements from 104 runs, covering both developing and fully developed film boiling regimes. A classification in each region has been performed using the experimental maximum wall temperature. The final data set covers the following range of flow parameters:

$$p = 6.893\ MPa$$

$$1003\ \tfrac{kg}{m^2 s} < G < 5235\ \tfrac{kg}{m^2 s}$$

$$147\ kW < P < 277\ kW$$

$$259\ ^oC < T_{in} < 277\ ^oC$$

3.2 Simplifying Hypothesis

A few simplifying hypothesis have been introduced before performing the assessment of the model under steady-state conditions. These simplifications are discussed in the following paragraphs.

- Constant flow properties: Pressure-drop variations are neglected; the outlet pressure is assumed over the channel.
- Node position: The axial nodes coincide with the experimental locations of the thermocouples used to perform the experiments (see Section 2.1.1). Additional axial nodes could have been used when performing the simulations. However, the node distribution was considered satisfactory for temperature predictions.

- Heat losses: Heat losses are neglected since no such information is provided in the report of Bennett et al. (Bennett, 1967).

- Conduction heat transfer: Only the steady-state inside surface wall temperature distribution of the tube is simulated. Consequently, the conduction heat transfer equation through the heated wall is not solved. Appendix II attempts to study the impact of this assumption.

- Radiation heat transfer: The radiation heat transfer is neglected. This assumption results in an overestimation of the forced convection heat flux component and consequently can produce wall temperature errors. A validation exercise will be performed in order to confirm the validity of this assumption.

- CHF correction: The CHF value has an important impact on post-dryout heat transfer calculations. Prediction uncertainty in CHF would introduce a systematic bias in the post-dryout heat transfer coefficient. Since the CHF look-up table presents correct parametric trends and no significant fluctuations are observed in the table, the bias is anticipated to be systematic.

  To minimize bias in predicting the post-dryout temperature, all calculated CHF values under post-dryout conditions have been corrected using a correction factor evaluated at the experimental dryout location. This CHF correction may in turn introduce a small bias due to the separation of neighboring thermocouples (the correction can only be applied to the thermocouple location where CHF is observed despite the actual CHF location may be upstream). This bias is anticipated to be negligible. The correction factor is calculated as follows:

$$C.F._{CHF} = \frac{q''_{EXP\ DO}}{q''_{pred\ DO}}, \tag{3.1}$$

  where $q''_{EXP\ DO}$ is the experimental heat flux at the dryout location and $q''_{pred\ DO}$ is the predicted CHF at the dryout location. For a given experiment, the correction

factor multiplies all CHF predictions for the post-dryout region. In the heat-flux-based methodology, the CHF value is not required at the post-dryout region and hence the correction is not applied once the CHF occurrence point is correctly fixed. However, in the temperature-based methodology, the CHF correction is applied in evaluating T_{CHF} from the WSR ratio of the modification factor in the post-dryout region.

3.3 Post-Dryout Heat Transfer Methodologies

This study focuses on two methodologies implemented in the film boiling look-up table technique for safety-analysis computer codes. The heat-flux-based methodology refers to the calculation scheme applying the local heat flux to evaluate the heat transfer coefficient, while the wall-temperature-based methodology is the scheme applying the local wall temperature to evaluate the heat transfer coefficient. The descriptions and applications of these general calculation schemes are presented below.

3.3.1 Heat Flux Based Methodology

In this method, the heat transfer coefficient is evaluated using a known heat flux. The method is convenient for steady-state calculations where the heat flux applied to the coolant is known. The main calculations steps are:

1. Set the heat flux, q", equal to the applied heat flux
2. Calculate the heat transfer coefficient, h, as a function of the heat flux (using a heat flux based look-up table)
3. Calculate the wall temperature, T_w, from h = q"/(Tw - Tsat)

In some thermalhydraulic transient codes, however, the heat conduction equation within the wall is solved first. In these cases, the heat flux to the fluid is unknown until the heat transfer coefficient is found. Thus, a heat flux based methodology implementation is cumbersome and requires an iterative approach. Also, as shown in Figure 1.1, for the same heat flux, the boiling curve presents three different heat transfer modes. To overcome these problems, the wall temperature can be used to calculate the heat transfer coefficient.

3.3.2 Temperature-based Methodology

In this method, the heat transfer coefficient is calculated using the local wall temperature. The implementation of the temperature-based methodology in a transient code is faster and potentially more robust since no iterations are required. The simplified calculation steps are then:

1. Calculate Tw (for instance, by solving the heat conduction equation)
2. Calculate the heat transfer coefficient (using a temperature-based look-up table)
3. Calculate the heat flux $q"$ using Newton's heat transfer law ($q" = h(T_w - T_{sat})$)

3.4 Description of the Numerical Scheme

A simplified one-dimensional steady-state model is used to assess the heat-flux based and temperature-based methodologies. The code and associated properties were extracted from the Thermalhydraulics Evaluation Package presented in References (Leung, 1999) and (Guo, 2007). The source code of the main function is given in Appendix III.1. Slight modifications, however, have been made to simulate a tube geometry since the

code was originally treating the geometry of a bundle. The model was written in FORTRAN 77 and further modifications were applied to make it compatible with FORTAN 90/95. The numerical model uses the following modules:

- MODULE_DATA: Allocates, initializes and performs calculations on several variables.
- MODULE_PROP: Contains fluid property variables and their calculation functions.
- MODULE_FILES: Performs all the operations in the different files. It can modify data from MODULE_DATA.
- MODULE_CHF_LUT: Creates the CHF-LUT and performs interpolations to calculate the CHF.
- MODULE_LUT_Q_based: Creates the heat flux based film boiling LUT and performs interpolations to calculate the heat transfer coefficient.
- MODULE_LUT_T based: Creates the temperature-based film boiling LUT and performs interpolations to calculate the heat transfer coefficient.

These modules replace the common blocks that may be removed in further versions of FORTRAN compilers. The LUT data has been declared private and can only be accessed by the module's functions and cannot be mistakenly modified.

The temperature-based methodology is more appropriate for implementing transient calculations; it is faster and no iterations are required compared to the implementation of a heat flux based methodology. On the other hand, the current work performs an assessment under steady-state conditions. In this case, the heat flux methodology implementation is direct while the temperature-based methodology requires an iterative procedure.

The general heat transfer calculation scheme for both methodologies under steady-state conditions is shown in Figure 3.1.

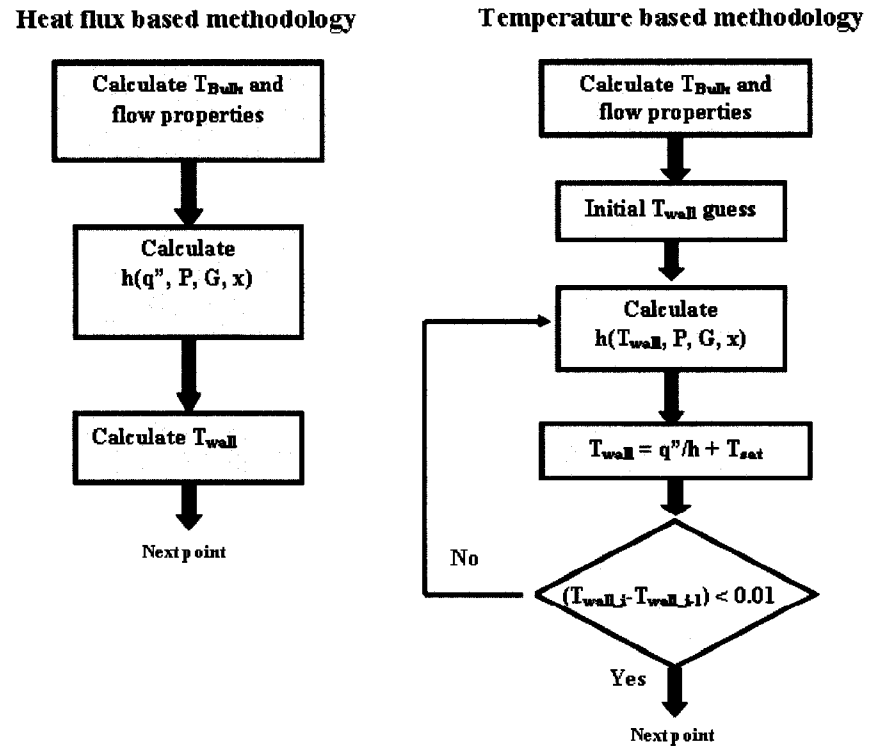

Figure 3.1 Heat Transfer General Calculation Scheme for the Heat Flux Based and Temperature Based Methodologies under Steady-State Conditions

3.5 Post-dryout Heat Transfer Coefficient Calculation Model

The current approach employs the film boiling look-up tables to predict the fully developed heat transfer coefficient. The developing-flow effect is then taken into account using a separate modification factor to the fully developed heat transfer coefficient.

Table 3.1 Flow Conditions and Grid Points for the Heat-Flux-Based Look-Up Table

	Flow range and grid points								
pressure	100	200	500	1000	2000	5000	7000	9000	10000
[kPa]	11000	13000	17000	20000					
Mass flux	0	50	100	200	500	1000	1500	2000	3000
$[\frac{kg}{m^2 s}]$	4000	5000	6000	7000					
quality	-0.20	-0.10	-0.05	0.00	0.05	0.10	0.20	0.40	0.60
	0.80	1.00	1.20						
heat flux	50	100	150	200	400	600	800	1000	2000
$[\frac{kW}{m^2}]$	3000								

3.5.1 Film Boiling Heat Transfer Coefficient

The look-up table technique is used in this work to predict the fully developed heat transfer coefficient (see Section 2.6.1).

3.5.1.1 Heat Flux Based Look-Up Table

The flow conditions of the heat flux based film boiling look-up table used in the present assessment are given in Table 3.1. Once obtained from the look-up table, the heat transfer coefficient has to be corrected for the internal diameter, D, since the tabulated values are normalized for tubes of a 9 mm internal diameter. The correction is made using the following relation (Groeneveld, 2003 (2)):

$$h = h_{table} \left(\frac{D}{0.009} \right)^{-0.2} . \tag{3.2}$$

Table 3.2 Flow Conditions and Grid Points for the Temperature-Based Look-Up Table

	Flow range and grid points							
pressure	100	200	500	1000	2000	5000	7000	9000
[kPa]	10000	11000	13000	17000	20000			
Mass flux	0	50	100	200	500	1000	1500	2000
$[\frac{kg}{m^2 s}]$	3000	4000	5000	6000	7000			
quality	-0.20	-0.10	-0.05	0.00	0.05	0.10	0.20	0.40
	0.60	0.80	1.00	1.20	1.40	1.60	1.80	2.00
wall superheat	5	50	100	200	300	400	500	600
[K]	750	900	1050	1200				

3.5.1.2 Temperature-based Look-Up Table

The temperature-based methodology uses a temperature-based look-up table. The discrete flow conditions used to tabulate the 32 448 heat transfer coefficients calculated from experimental data are given in Table 3.2. For this LUT, the heat transfer coefficients are normalized for a tube of a 8mm internal diameter. Therefore, the interpolated value has to be corrected as follows (Groeneveld, 2003 (2)):

$$h = h_{table} \left(\frac{D}{0.008} \right)^{-0.2} . \tag{3.3}$$

3.5.2 Developing-Flow Modification Factors

Developing flow modification factors have been presented Chapter 2. The correlations used in the current assessment are repeated here.

3.5.2.1 Heat Flux Based Correlations

The developing flow modification factor correlation used in this work has been developed in (Leung, 2002) and it is expressed as:

$$K_{developing} = 1 + \left(\frac{h_{nb}}{h_f d} - 1\right) \exp\left[a\left(\frac{x - x_{DO}}{(1 - x_{DO})Bo}\right)^b\right], \tag{3.4}$$

where H_{fg} is the latent heat of vaporization and Bo is the boiling index is given by Equation (2.16) i.e.:

$$Bo = \frac{q''}{GH_{fg}}. \tag{3.5}$$

3.5.2.2 Temperature-based Correlations

Leung and Guo (Guo, 1978) derived the developing flow modification factor correlation based on the wall temperature used in this work, that is:

$$K_{developing} = \frac{h_{PDO}}{h_{fd}} = 1 + \left(\frac{h_{NB}}{h_{fd}} - 1\right) \exp\left[c\,(WSR - 1)^b\right], \tag{3.6}$$

with:

$$WSR = \frac{T_w - T_{sat}}{T_{CHF} - T_{sat}}, \tag{3.7}$$

where T_{CHF} is defined as the wall temperature calculated using the CHF local value, the nucleate boiling heat transfer coefficient and the saturation temperature. The nucleate boiling heat transfer coefficient is calculated using the Chen correlation for forced convective boiling (correlation 1.11) where the local value of CHF is used for the heat

flux.

3.6 Radiation Heat Transfer Model

A radiation heat transfer module was implemented in the computational model in order to study the importance of this mechanism in the assessment procedure. Radiation between the heated wall and the liquid core and passing through a participating gas is assumed (i.e. inverted annular film flow). The model used for the validation is restricted to inverted annular film boiling but can be used for all post-dryout regime and can provide estimations for other conditions. Radiative exchange between three gray bodies is simulated and the following simplifications are assumed:

1. No entrainment of liquid droplets in the vapor film takes place.
2. Smooth liquid/vapor interface.
3. Radiation heat transfer in the axial direction is negligible.
4. Optically thin vapor film.
5. Uniformly heated wall and homogeneous liquid phase temperatures.

In order to calculate the radiative heat flux in the assessment code, the following calculations are performed:

1. Calculate the liquid core diameter (D_f).
2. Calculate the wall-to-fluid view factor (F_{w-f}).
3. Calculate the emissivity of the liquid core.
4. Calculate the emissivity the heated wall.

5. Calculate the emissivity of the vapor film.

6. Solve the system of equations.

7. Calculate the radiative heat flux.

The theory and details about this radiative heat transfer model are described in Appendix I.3, while the computer code for the radiative module is listed in Appendix III.2.

CHAPTER 4

RESULTS

Post-dryout heat transfer coefficient is calculated using either the heat-flux based or temperature-based methodology in safety analysis codes. The heat-flux-based methodology applies the known heat flux to calculate the heat transfer coefficient that is then used to calculate the wall temperature. The temperature-based methodology is applied when the heat flux is unknown and the heated wall temperature is used to calculate the heat transfer coefficient. The heat flux to the bulk fluid is then calculated.

This section presents the assessment result of the heat-flux based and wall-temperature-based methodologies (presented in Section 3.3) against experimental data obtained at steady-state conditions. The heat transfer coefficient for the fully developed flow is calculated using the corresponding film boiling look-up table (Groeneveld, 2003 (2)) and is corrected using the developing-flow modification factor. The corrected heat-transfer coefficient is applied to predict the internal wall temperature at each thermocouple position, which is compared against experimental data of Bennett et al. (Bennett, 1967). Prediction accuracy of each methodology is established from the bias and standard deviation.

An examination of the predicted wall-temperature trend has revealed deficiencies in the developing modification factor for the temperature-based methodology. A sensitivity analysis of the developing-flow factor has therefore been carried out. Improvements to the factor have been introduced to reduce the prediction accuracy and enhance the predicted trend. Prediction accuracy of the revised developing-flow modification factor has been assessed against the database.

The impact of several hypotheses has been examined on the applicability of a temperature-based methodology.

4.1 Assessment Results

Table IV.1 (for the heat flux based methodology) and Table IV.2 (for the temperature-based methodology) given in Appendix IV present detailed information about the experimental conditions and predictions for each experiment. These tables list flow properties, the CHF correction factor, experimental and predicted wall temperatures, and prediction errors on maximum wall temperature and local post-dryout wall temperature. The average prediction error and standard deviation are also presented. Appendix IV.3 compares the experimental and predicted wall-temperature distributions using the heat-flux based and temperature-based methodologies for all selected experiments.

To quantify the differences between the predicted and experimental temperatures, the relative error is calculated for each thermocouple position used to perform the experiment (Bennett, 1967). The local temperature prediction error is defined as:

$$\text{error}(i)[\%] = \frac{T_{Sim}(i) - T_{Exp}(i)}{T_{Exp}(i)} \times 100, \tag{4.1}$$

where T_{Sim} is the predicted local post-dryout temperature in ^oC and T_{Exp} is the experimental temperature in ^oC. The subscript i refers to the axial position of the thermocouple. The overall average error is expressed as:

$$\text{Error}[\%] = \frac{\sum_1^N error(i)}{N} \times 100 \tag{4.2}$$

and the standard deviation is:

$$STD[\%] = \sqrt{\frac{\sum_1^N [error(i) - Error]^2}{N-1}} \times 100\,. \tag{4.3}$$

where N is the total number of data points for all experiments, i.e. number of degree of freedom. The total error is calculated for both the fully developed and the developing film boiling regions.

The experiments (Bennett, 1967) present steady state inside wall temperature distributions of a tube where CHF has been exceeded at thermocouple locations near the outlet. As in Figure 1.10 (Guo, 1978), the steady-state temperature distribution shows an important temperature increase at the location where the heat flux corresponds to the local CHF value. Downstream of this point, post-dryout conditions are encountered and the temperature continues to increase, reaches a maximum temperature, and then decreases gradually. The experimental maximum temperature locates between the developing film boiling and the fully developed film boiling regions. Fully developed post-dryout temperature is considered at positions downstream of the maximum temperature, and developing post-dryout temperature at upstream positions but downstream of the dryout location. A total of 702 post-dryout data points have been assembled from the experiment; 441 points in the fully developed region and 261 in the developing flow region.

The heat transfer coefficient is corrected using a modification factor accounting for the developing flow effect. Consequently, the error in the developing flow region should be interpreted as the sum of the correlation error and the uncertainty of the look-up table.

Table 4.1 Wall Temperature Prediction Errors and Standard Deviations for the Heat-Flux-Based Methodology

	Value [%]	
	Average Error	**Standard Deviation**
Developing Flow Region	-4.4	14.3
Fully Developed Flow Region	0.8	8.6
All Regions	-2.1	11.2
Maximum Wall Temperature	-0.8	8.6

4.1.1 Heat Flux Based Methodology

Wall-temperature prediction errors using the heat-flux-based methodology are shown for various film-boiling regions in Table 4.1. The film boiling look-up table slightly overpredicts the fully developed wall temperature (or under predicts the fully developed heat transfer coefficient), with an average error of 0.8% and standard deviation of 8.6%.

Experimental wall-temperature data at the developing flow region are underpredicted with the heat-flux-based methodology (i.e., film-boiling look-up table and the developing-flow factor) with an average error of -4.4% and a standard deviation of 14.3%. However, the maximum wall temperature, often of interest in safety analyses, is predicted accurately with an average error of -0.8% and standard deviation of 8.6%. This assessment illustrates good prediction accuracy of the heat-flux-based methodology, which provides accurate wall temperature predictions for the current database (overall average error of -2.1% and standard deviation of 11.2% in wall-temperature predictions).

A detailed analysis is performed through comparing the predicted and experimental inside wall temperature distributions (Appendix IV.3). The predicted wall-temperature distributions follow closely the experimental trends in both developing flow and fully developed film boiling regions. Figure 4.1 compares wall-temperature profiles at mass fluxes greater than 1000 kg/m^2s for Runs 5249 and 5291.

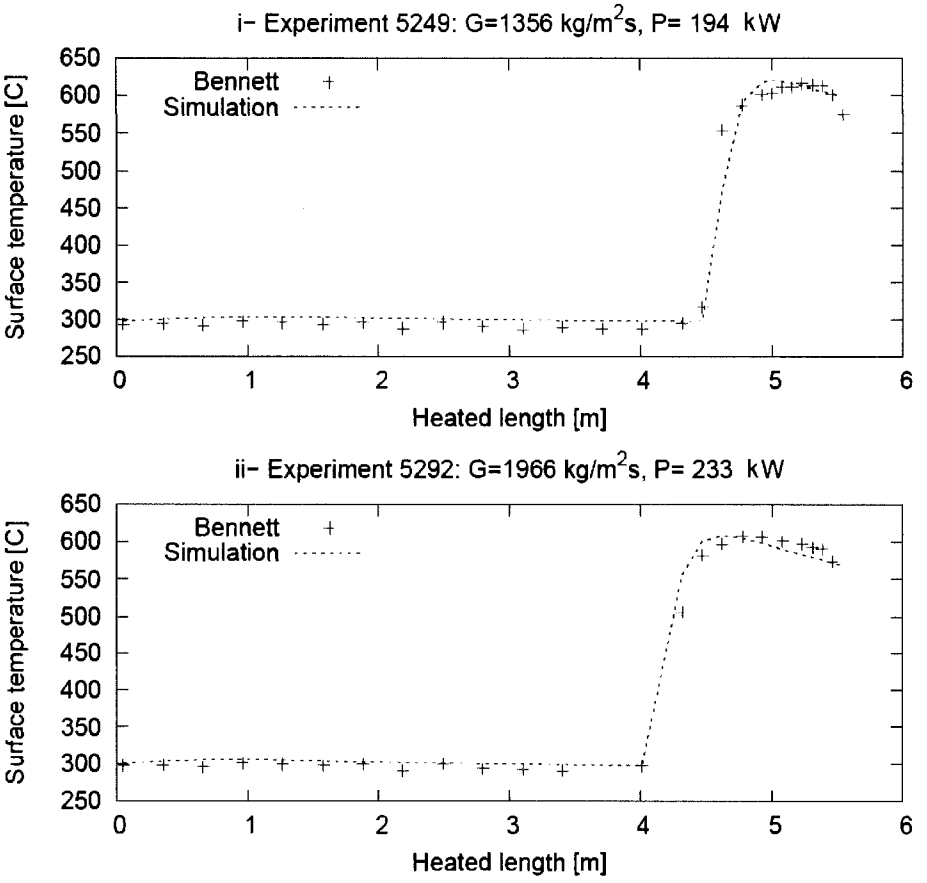

Figure 4.1 Wall Temperature Predictions Using a Heat Flux Based Methodology (Experiments 5249 and 5292)

Figure 4.2-i compares the temperature trends at the low mass flux ($G \approx 1000\ kg/m^2s$). The experimental inside wall temperatures are overpredicted at the developing-flow region, but approach the predicted values at the fully developed region. Since the local qualities are generally high at low mass fluxes, the developing-flow modification factor may not be applicable for low powers, where the degree of vapour superheating is low in the experimental conditions.

Figure 4.2-ii compares the temperature trends at the high mass flux (G > 2000 kg/m^2s).

The reversed trend has been observed with the experimental inside wall temperatures are underpredicted at the developed-flow region. This is attributed to possibly high degree of vapour superheating at high powers and low qualities, which has not been captured with the developing-flow factor. The look-up table predicts closely fully developed wall temperatures.

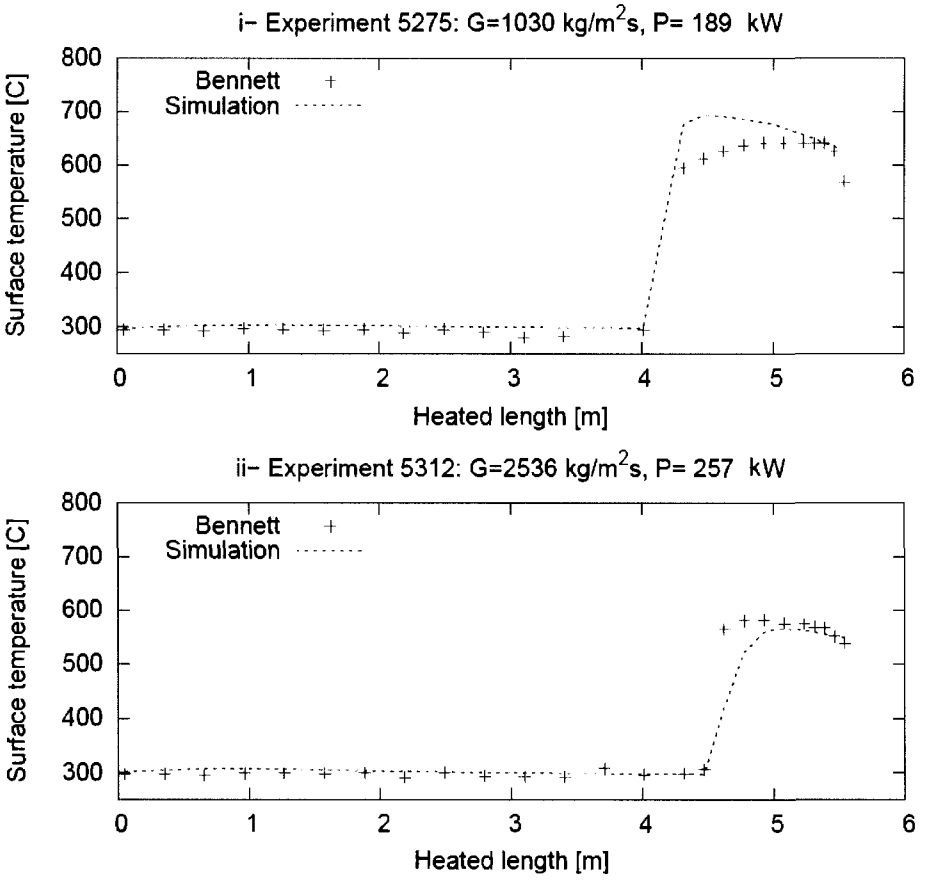

Figure 4.2 Wall-Temperature Predictions Using a Heat Flux Based Methodology (Experiments 5275 and 5312)

Other comparisons of predicted and experimental temperature trends are shown in Appendix IV.3. Overall, predictions obtained with the heat flux based methodology are in

Table 4.2 Wall Temperature Prediction Errors and Standard Deviations for the Temperature-Based Methodology

	Value [%]	
	Average Error	**Standard Deviation**
Developing Flow Region	8.3	10.7
Fully Developed Flow Region	1.8	6.4
All Regions	4.2	8.8
Maximum Wall Temperature	3.4	6.9

good agreement with the experimental data of Bennett et al. (Bennett, 1967). The prediction accuracy of the developing flow factor is better for mass fluxes ranging between 1300 and 2000 kg/m^2s than others.

4.1.2 Wall temperature-based Methodology

Similar simulations of wall temperatures are performed using a temperature-based method. Prediction errors and standard deviations are shown in Table 4.2. The fully developed post-dryout temperatures are predicted accurately with an average error of 1.8% and a standard deviation of 6.4%. Wall temperatures at the developing flow region, however, are overpredicted with an average error of 8.3% and a standard deviation of 10.7%. Hence, the developing flow modification factor has underpredicted the post-dryout heat transfer coefficient at this region. Maximum temperatures along the tube are predicted with an average error of 3.4% and a standard deviation of 6.9%. Combining developing and fully developed regions, the experimental wall temperatures are predicted with an overall average error of 4.2% and a standard deviation of 8.8%.

Figures presented in Appendix IV.3 (p.158) show that at low mass fluxes (G < 2000 kg/m^2) and powers ($P < 250kW$), the temperature increases drastically near the CHF location. This behavior is shown in Figure 4.3 and is common for the data set used in

this study. In many cases, however, (i.e., for $G > 2000\ kg/m^s$ and $P > 250\ kW$) the developing flow temperatures are predicted quite well as shown in Figure 4.3-ii).

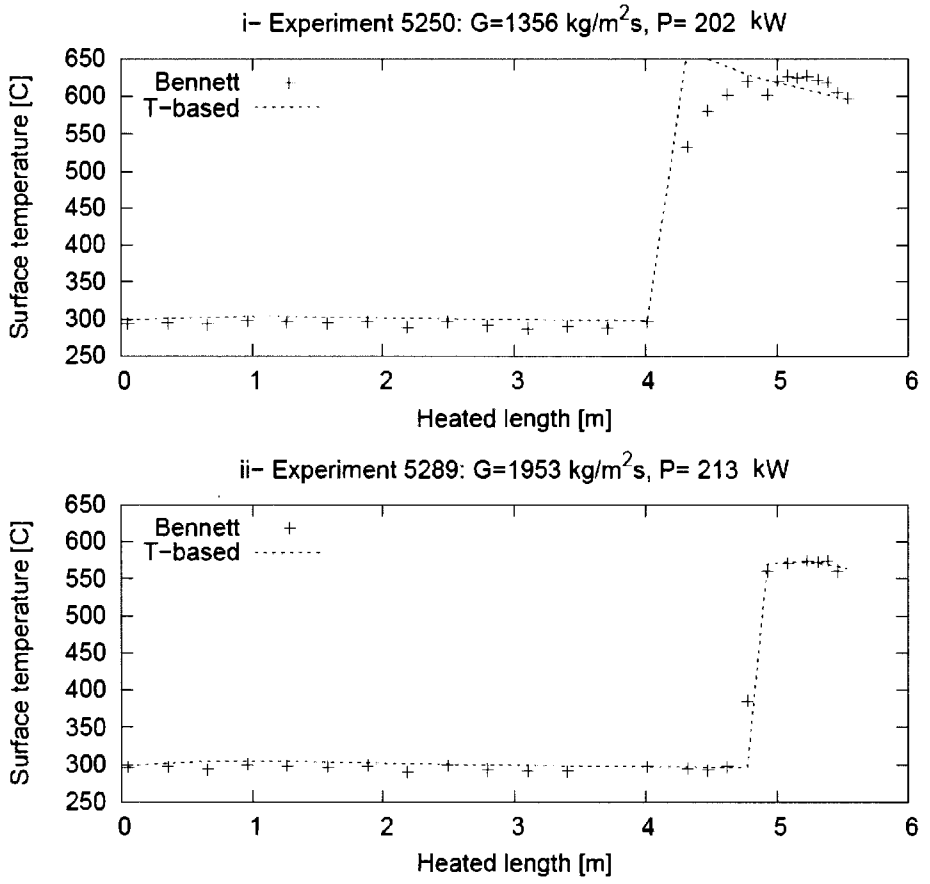

Figure 4.3 Experiments 5250 and 5289: Wall-Temperature Predictions Using a temperature-based Methodology

The steady-state algorithm uses the wall superheat to evaluate the heat transfer coefficient that is, in turn, used to calculate the wall temperature; an iterative procedure is therefore required. The wall temperature is initially guessed and updated until convergence is reached (i.e., typically better than 10^{-3}). To examine the impact of initial guess temperature on the prediction, several calculations are performed with different initial

values. No impact on the final results has been observed. This result is attributed to the smooth variation (i.e., the surface does not show any minimum points) of the heat transfer coefficient in the temperature-based look-up table (Groeneveld, 2003 (2)).

Guo et al. (Guo, 1978) derived two separate correlations (one for high pressures and the other for low pressures) for predicting the developing flow effect on film-boiling heat transfer. Based on the test conditions covered in the experiment of Bennett et al. (Bennett, 1967), the high-pressure correlation has been applied in the assessment. As a sensitivity study, the low-pressure correlation (Equation 2.19) has been assessed separately for its prediction accuracy. Applying the low-pressure correlation together with the film-boiling look-up table, the wall-temperature measurements are predicted with an overall average error of 1.7% and a standard deviation of 8.0%. The maximum temperatures are predicted with an average error of 0.3% and a standard deviation of 6.0%. The assessment result seems to suggest that the low-pressure correlation provides better prediction accuracy than the high-pressure correlation over the current database range. This improvement is attributed mainly to the database used in generating the correlation (which included a large number of low mass-flux data), which is representative to those of Bennett et al. (Bennett, 1967).

4.1.3 Sensitivity Analysis of the Developing-Flow Modification Factor

The accuracy of the post-dryout surface temperature prediction strongly depends on the developing-flow modification factor in both the heat-flux based and the wall-temperature-based methodologies. An underprediction of the surface temperature for the heat flux based methodology is attributed to the relatively smooth variation of the developing-flow modification factor after the occurrence of CHF. Conversely, the overprediction of the surface temperature for the wall temperature-based correlation is the result of a sharp change of the developing-flow factor. A sensitivity analysis of the developing-flow mod-

ification factor on the predicted wall temperature is therefore performed in this section.

4.1.3.1 Sensitivity of the Modification Factor

Figure 5.4-i shows the impact of $\pm 10\%$ change in developing-flow modification factors for the heat-flux based and temperature-based correlations. An increase in developing-flow modification factor tends to reduce the wall-temperature prediction error. The temperature prediction is very sensitive to the modification factor in the temperature-based methodology. A $\pm 10\%$ change in the developing-flow modification factor has led to about $\pm 20\%$ change in prediction error for the temperature-based methodology while the same variation has a smaller impact (less than $\pm 10\%$) for the heat flux based methodology.

The modification factor can be re-optimized to improve the prediction accuracy. An optimized value can be found graphically in Figure 4.4. Prediction uncertainties of these modification factors are attributed to the scatter among the developmental experimental database. In addition, these factors have been derived with reference to a specific LUT version (Groeneveld, 2003 (2)), which has since been updated/revised with additional data and improved smoothing process. This would lead to increased prediction uncertainty. Thus, further improvement of prediction accuracy is possible through re-optimization of correlation coefficients together with any new released version of the look-up table.

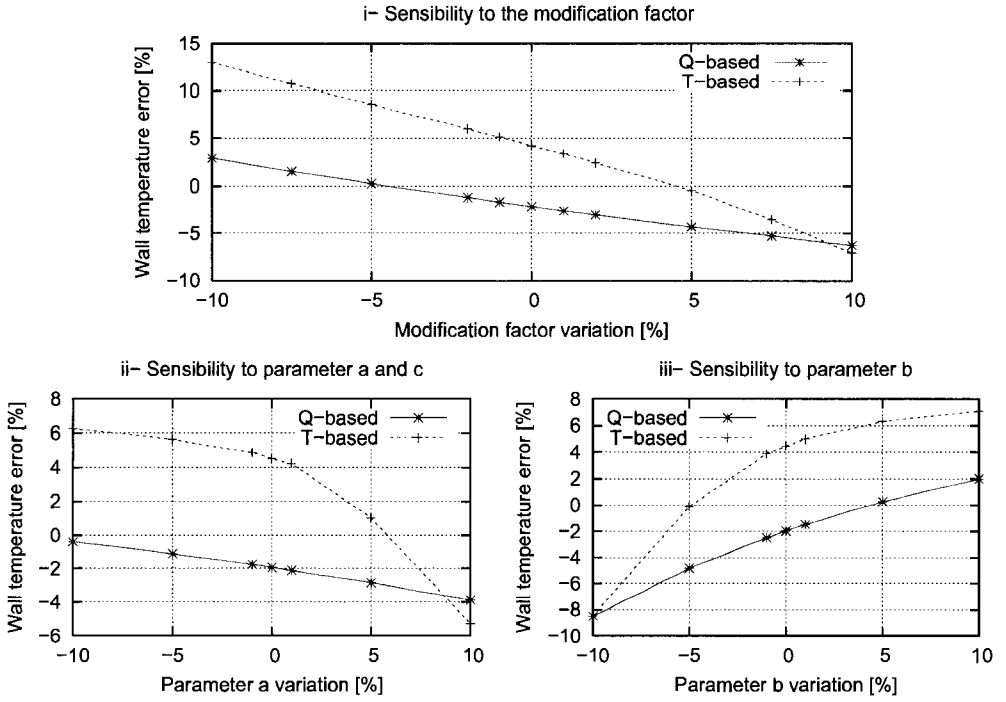

Figure 4.4 Wall Temperature Sensitivity to the Modification Factor and to Parameters a and b

4.1.3.2 Sensitivity of Coefficients a and c and Exponent b

The sensitivity of the coefficients and the exponent in developing-flow modification factors (i.e., Equations and) to film-boiling temperature predictions is examined.

$$K_{developing} = 1 + \left(\frac{h_{nb}}{h_f d} - 1\right) \exp\left[a\left(\frac{x_{th} - x_{DO}}{(1 - x_{DO})Bo}\right)^b\right], \tag{4.4}$$

$$K_{developing} = \frac{h_{PDO}}{h_{fd}} = 1 + \left(\frac{h_{NB}}{h_{fd}} - 1\right) \exp\left[c\,(WSR - 1)^b\right]. \qquad (4.5)$$

Figure 4.4-ii shows the impact of $\pm 10\%$ change in coefficients a and c on the prediction error of wall temperature. The impact of coefficient a variation in the heat-flux-based methodology on the prediction error is much smaller than that of coefficient c variation in the wall-temperature-based methodology. The overall variation in prediction error is only 4% with varying coefficient a as compared to 12% with varying coefficient c over for $\pm 10\%$.

Figure 4.4-iii shows the impact of $\pm 10\%$ change in the exponent b on the prediction error of wall temperature. The impact of varying exponent b on the prediction error is relatively similar for the heat- flux based and the wall-temperature-based methodologies. The overall variation in prediction error with varying exponent b is 10% for the heat-flux-based methodology as compared to 15% for the wall-temperature-based methodology.

Based on the sensitivity assessment, the prediction accuracy of wall temperature depends strongly on the optimization of coefficient c and exponent b in the wall-temperature-based modification factor. Therefore, the size of the database and their range of flow conditions would have a strong impact on the applicability of the wall-temperature-based methodology as compared to the heat-flux-based methodology.

4.1.4 Critical Heat Flux Correction Factor

As illustrated previously, the uncertainty of critical-heat-flux correlation has a strong impact on post-dryout wall-temperature predictions. The prediction accuracy of the CHF look-up table has been assessed against the current experimental database. The assess-

ment result is presented in Appendix IV. Tables IV.1 shows that the critical heat flux in the current database is generally overestimated using the CHF look-up table with an average error of 30.97% and a standard deviation of 34.66%. Improving the CHF look-up table prediction accuracy is beyond the scope of this study. An adjustment factor has been introduced to minimize the critical-heat-flux prediction uncertainty in the current assessment. Overall, an average adjustment factor of 0.825 has been applied to align the prediction from the CHF look-up table to the experimental point.

4.2 Improvements of the Temperature-Based Methodology

The assessment result has shown that the wall-temperature-based methodology overpredicts the experimental wall temperatures and does not follow the experimental trend of wall temperature at the developing-flow region. An improvement of the wall-temperature-based developing-flow factor is proposed to reduce the prediction uncertainty and represent the experimental wall-temperature trend.

Two separate approaches are introduced to improve the temperature-based developing flow modification factor. The simplest improvement is to re-optimize the coefficient c and exponent b in Equation 3.6 using data of Bennett et al. (Bennett, 1967). This would provide a better representation of the experimental film-boiling temperatures and allow the examination of the wall-temperature-based methodology with minimal film-boiling heat-transfer prediction uncertainty. The second approach takes into the account of the influence of mass flux and quality on post-dryout heat transfer in the developing-flow region. This would further minimize the film-boiling heat-transfer prediction uncertainty.

In this section, all the coefficients were optimized using the data collected by Bennett et al. (Bennett, 1967). The optimizations are performed by fitting the experimental value of the developing flow modification factor ($K_{non-dimensional} = \frac{h_{PDO}-h_{FD}}{h_{NB}-h_{FD}}$) as a function

Table 4.3 Values and Fitting Errors of the Optimized Coefficients c and b

Coefficient	Optimized value	Error [%]
c	-0.796432	3.312
b	0.561333	2.054

of the WSR ratio provided by the assessment code. Since the correlation presents an exponential trend, a nonlinear least square method has to be implemented in order to fit the coefficients and the GnuPlot's "fit" function was used to generate all the coefficients shown in this section. This function uses a nonlinear least-squares Marquandt-Levenberg's algorithm.

4.2.1 Optimization of Coefficients c and b

The coefficient c and exponent b in the temperature-based developing-flow factor (i.e., Equation 4.5) have been re-optimized using the database of Bennett et al (Bennett, 1967). The number of experimental data used in the re-optimization has been reduced to focus mainly on the developing flow temperatures. In addition, some data with high CHF prediction error have also been excluded to avoid propagation of the error to film-boiling prediction uncertainty. Overall, the database applied in the re-optimization contains 195 experimental points at developing flow conditions.

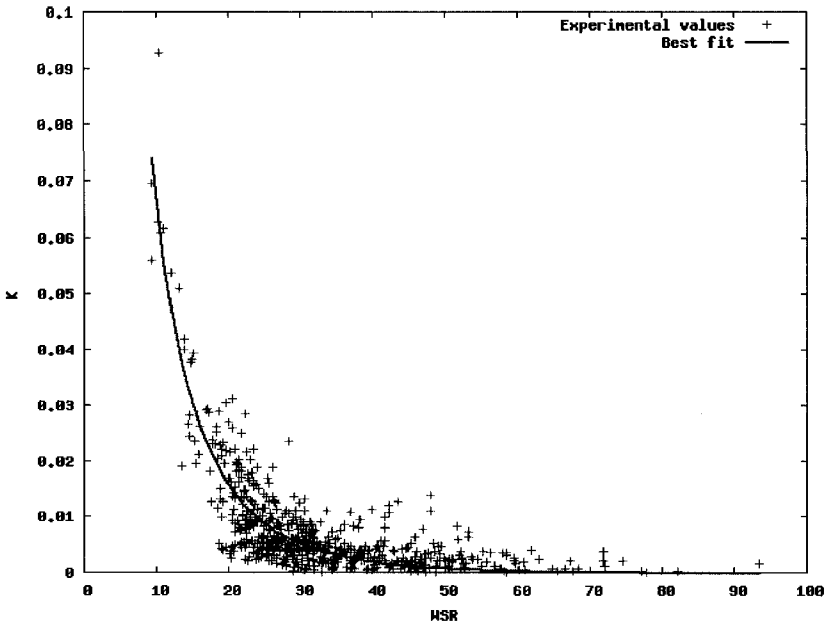

Figure 4.5 Best Fitting Function of the Experimental $K_{non-dimensional}$

Table 4.3 lists the re-optimized values and associated prediction errors. Figure 4.5 compares the re-optimized developing-flow factor against experimental values with respect to the wall-superheat ratio. An assessment of the re-optimized developing-flow factor is performed against the database. The post-dryout wall temperatures are predicted with an average error of -2.8% and a standard deviation of 12.6%. Despite the improvement in overall prediction accuracy, the revised developing flow factor remains deviating from the experimental wall-temperature trend at some conditions. The revised developing-flow factor provides improved prediction accuracy of wall temperatures at low mass fluxes but not at high mass fluxes. Figure 4.6 compares predicted wall temperatures using the revised developing-flow factor against experimental values for two sets of flow conditions. Therefore, additional parameters in the developing-flow factor may be needed to improve the prediction accuracy further.

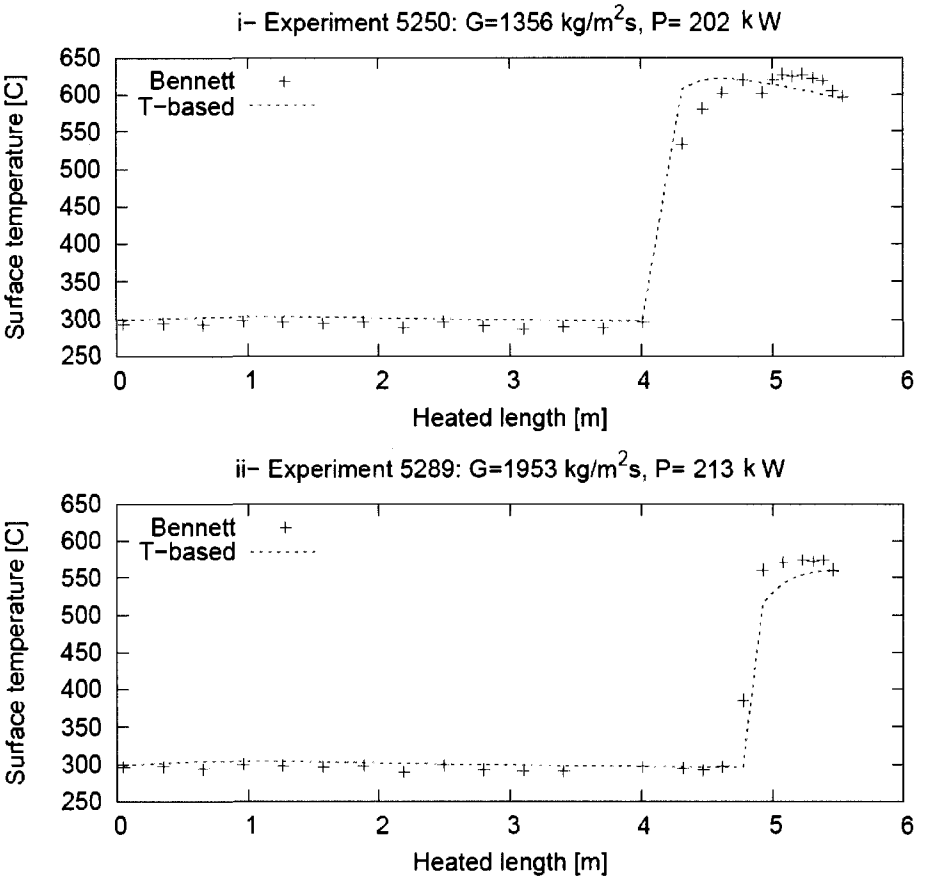

Figure 4.6 Wall Temperature Predictions Using a temperature-based Methodology with the Optimized c and b Coefficients (Experiments 5250 and 5289)

4.2.2 Mass Flux and Quality Effect and Optimized Developing Flow Modification Factor

The dependency of flow parameters in the developing flow effect is examined to improve the temperature-based developing flow factor. The examination focuses mainly on the mass flux and quality effects.

4.2.2.1 Mass Flux Effect

The assessment presented in Section 5.1 indicates a possible dependency in the developing-flow effect on mass flux. To study this potential dependency, the experimental Knon-dimensional (at developing-flow conditions) is examined in Figure 4.7 as a function of the WSR ratio for different mass fluxes. The impact of mass flux on the developing-flow factor is stronger at low mass fluxes than high mass fluxes. This is possibly attributed to the increase in lift force at high mass fluxes decreasing the interaction between the heated wall and entrained droplets (i.e., wet collisions). The heated wall temperature would increase more rapidly approaching fully developed film-boiling conditions. Therefore, the developing-flow factor tends to be small at higher mass fluxes, but large at low mass fluxes.

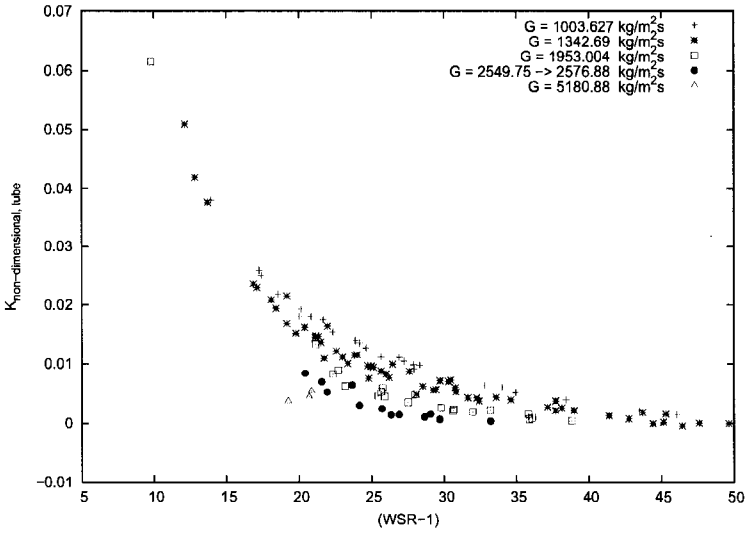

Figure 4.7 Experimental Developing-Flow Modification Factor vs (WSR-1)

4.2.2.2 Thermodynamic Quality Effect

The thermodynamic quality variation appears strong on the developing flow effect. As shown in Figure 4.8-i, the developing-flow factor varies systematically with the multiplication term of the over-wall-superheat ratio and thermodynamic quality (i.e., *(WSR-1) x*) at various mass fluxes. Further consolidation is observed in Figure 4.8-ii when the developing-flow factor is assessed against the multiplication term of the over-wall-superheat ratio, mass flux, and thermodynamic quality (i.e., $(WSR-1)\,xG$), which is a possible correlation parameter for the developing-flow effect, i.e.,

$$K_{non-dimensional} = exp\left\{c^{*}\left[Gx\,(WSR-1)\right]^{b^{*}}\right\}. \tag{4.6}$$

A dimensionless parameter is introduced to extend the application and the Reynolds number of the vapor is selected to represent effects of mass flux and quality.

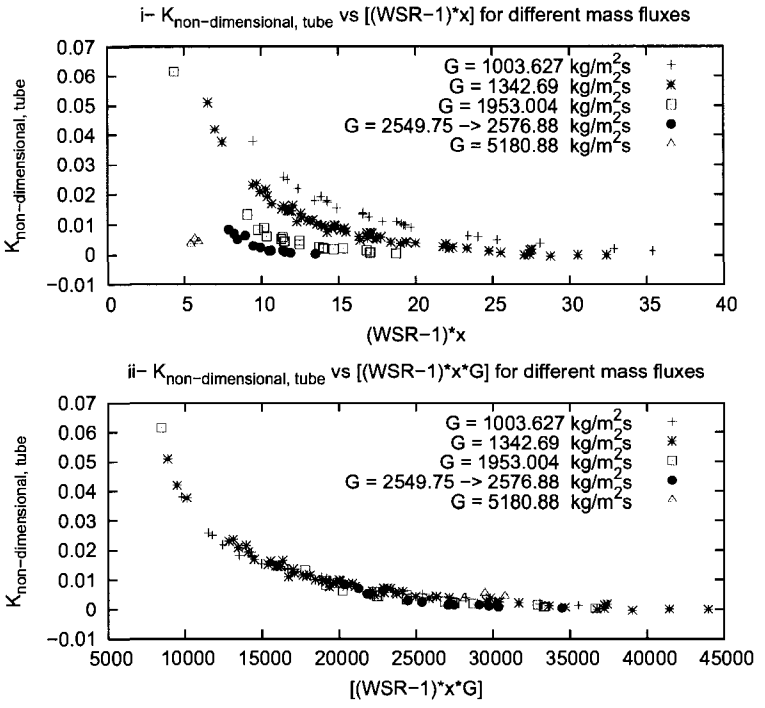

Figure 4.8 Experimental Developing-Flow Modification Factor vs $(WSR-1)x$ and vs $(WSR-1)xG$

4.2.2.3 Revised Correlation Based on the Reynolds number

The Reynolds number of the vapor phase is the ratio of inertia forces over viscous forces and, thus, may have an impact on the developing flow process. Also, it is expressed as a function of tube diameter and hence is applicable to tubes of different diameters. The Reynolds number of the vapor phase is defined as:

$$Re_v = \frac{G_v D}{\mu_v}, \tag{4.7}$$

where μ_v is the viscosity of the vapor (constant in the assessment code and calculated at saturation temperature) and D is the tube diameter. The mass flux of the vapor phase is expressed as $G_v = xG$ in a mixture model. The Reynolds number of the vapor phase is also written as:

$$Re_v = \frac{xGD}{\mu_v}. \tag{4.8}$$

A possible form of the developing-flow factor is:

$$K_{non-dimensional} = exp\left\{c^{**}\left[Re_v\left(WSR-1\right)\right]^{b^{**}}\right\}. \tag{4.9}$$

Some attempts have been made to include the Reynolds number in the coefficient c (or c^{**}). Figure 4.9 shows the relation between (i) $ln(K_{non-dimensional})$ vs $[(WSR-1)xG]$ and (ii) $\frac{1}{xG}ln(K_{non-dimensional})$ with the over-wall-superheat ratio (i.e., $WSR-1$). If the Reynolds number could be included in the coefficient c (or c**), the graph of $\frac{1}{xG}ln(K_{non-dimensional})$ vs $(WSR-1)$ would present a more linear trend than the graph of $ln(K_{non-dimensional})$ vs $[(WSR-1)xG]$. However, Figure 4.9 shows the opposite behavior. Therefore, a separate c^{**} coefficient is more appropriate than including it with the Reynolds number. A fit of the developing-flow factor with the term $(WSR-1)Re_v$ is performed using the database to optimize coefficients c^{**} and b^{**}. The optimized coefficients are presented in Table 4.4 with their fitting errors.

Table 4.4 Values and Fitting Errors of the Optimized Coefficients c^{**} and b^{**}

Coefficient	Optimized value	Error [%]
c^{**}	-0.000761511	18.10
b^{**}	0.531791	2.14

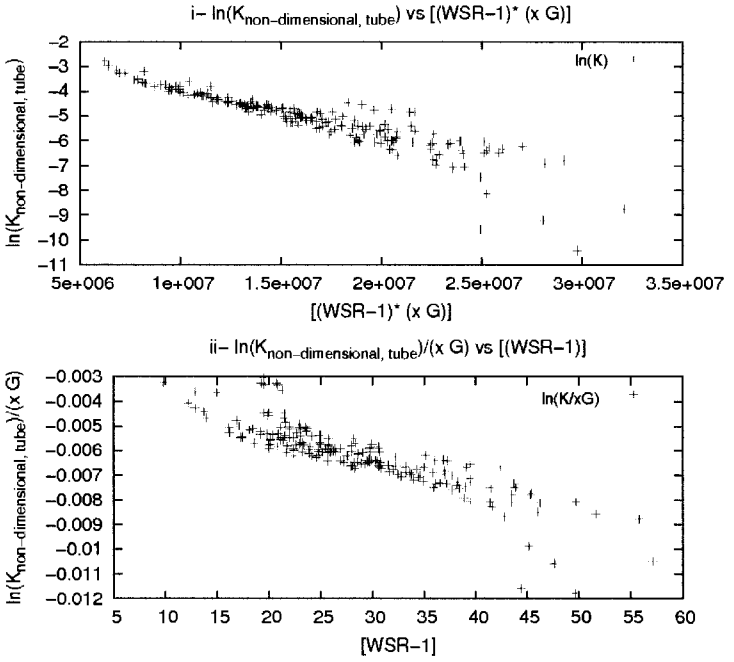

Figure 4.9 (i)- K vs (WSR-1)G and (ii)- K/(Gx) vs (WSR-1)

4.2.3 Revised Correlation Assessment

The revised developing-flow factor has been included in the code and assessed against all experimental data. Prediction errors and standard deviations are listed in Table 4.5. Comparisons of experimental and predicted temperature distributions are shown in Ap-

Table 4.5 Errors for the Revised Correlation

		Correlation parameter	
		$(WSR-1)$	$Re_g(WSR-1)$
Developing Flow Region	**Avg. Error [%]**	8.3	-1.9
	Std. Dev. [%]	10.7	13.0
Fully Developed Flow Region	**Avg. Error [%]**	1.8	1.9
	Std. Dev. [%]	6.4	5.1
All Regions	**Avg. Error [%]**	4.2	0.3
	Std. Dev. [%]	8.8	9.2
Maximum Wall Temperature	**Avg. Error [%]**	3.4	0.9
	Std. Dev. [%]	6.9	5.5

pendix V.2 for the two correlations.

The developing flow temperatures are predicted with an average error of -1.9% and a standard deviation of 13.0% using the revised developing-flow factor. This represents a significant improvement over the original developing-flow factor, which predicts the wall temperature with an average error of 8.3% and a standard deviation of 10.7%. An improvement has also been observed for the maximum wall temperature in the channel, which has been predicted with an average error of 3.4% and a standard deviation of 6.9% using the original developing-flow factor and is now predicted with an average error of 0.9% and a standard deviation of 5.5% using the revised factor. The change has been focusing on the developing-flow region and hence the prediction accuracy of wall temperature at the fully developed region has not been affected.

In addition to the improved overall prediction accuracy, the revised correlation provides a better agreement with temperature variations at the developing flow region than the original correlation for low and high mass fluxes. Figure 4.10 compares predicted temperatures using the revised correlation against experimental temperatures for two sets of flow conditions. Good agreement has been observed at both developing-flow and fully developed regions.

Despite the good prediction accuracy and improved parametric trend, further validation of the revised correlation is suggested, because the revised correlation has been developed using a small database covering only one tube diameter in a single source. Assessment against other databases would confirm the prediction accuracy and, if necessary, extend the application of the revised developing-flow factor.

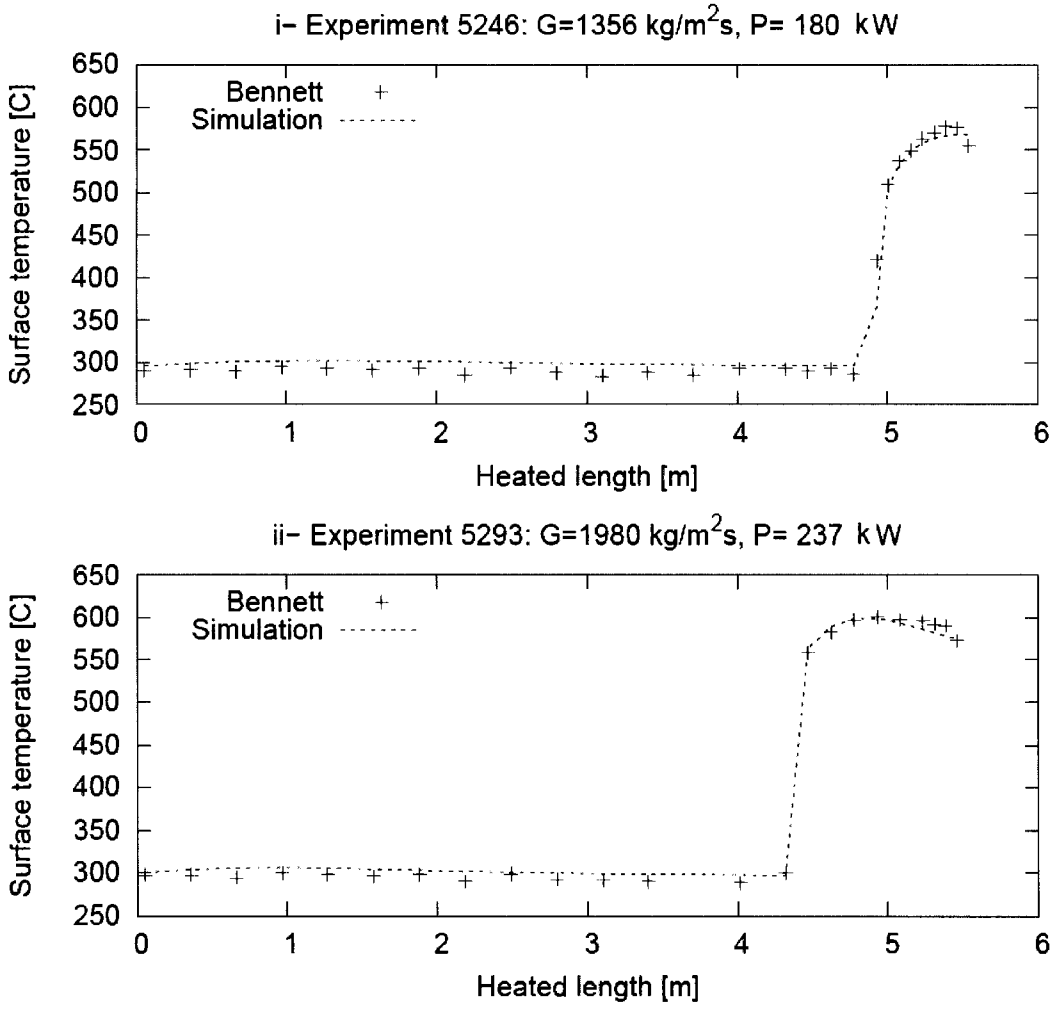

Figure 4.10 Wall Temperature Predictions Using the Revised Correlation (Experiments 5246 and 5293)

4.3 Validation of the Hypothesis

As mentioned in Chapter 3, the current assessment neglects the radiative heat transfer and heat conduction, and focuses only on steady-state applications. This section examines the impacts of these simplifying hypotheses.

4.3.1 Radiative Heat Transfer

In the steady state assessment code presented in Chapter 3, the total heat flux, rather than the convective heat flux, is used to determine the fully developed heat transfer coefficient from the look-up tables. The effect of this simplifying assumption is studied in this section. Before being implemented in the assessment computer code, the radiative heat transfer model (presented in Section 3.6) is tested first. Using this testing version, radiative heat flux can be computed for a typical value of the total heat flux for the data of Bennett et al. (Bennett, 1967). The ratio between the radiative heat flux and the total heat flux is shown in Figure 4.11 for different void fractions. The power of 214 kW is applied.

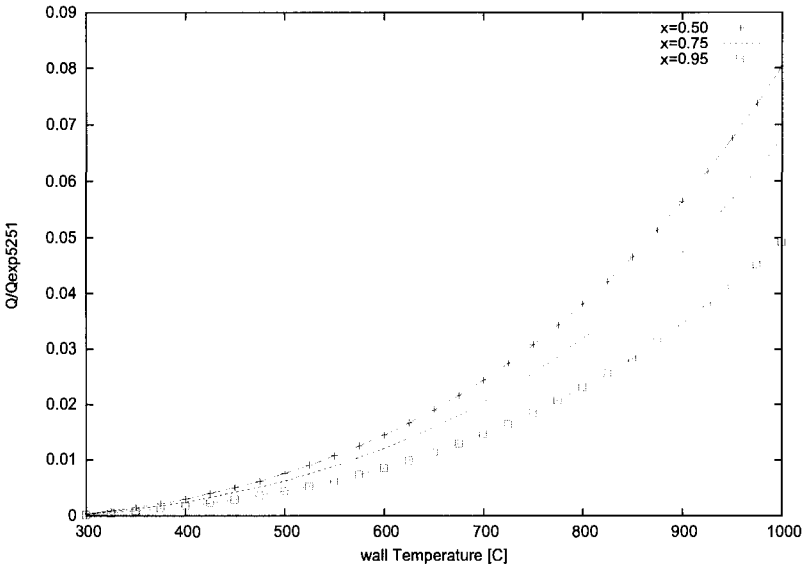

Figure 4.11 Radiation Heat Flux Ratio of for Different Void Fractions

Figure 4.11 shows that, for a typical wall temperature of 600^oC under post-dryout conditions and void fractions between 0.5 and 0.95, the ratio between the radiative heat transfer and the total heat transfer is less than 2%.

The radiative heat transfer model has been implemented in the assessment code presented in Chapter 3. Appendix III.2 presents the source code of this radiation heat transfer model. Some errors have been defined in order to study the impact of neglecting radiation heat transfer:

- · The average radiation heat flux ratio in post-dryout conditions is defined as:

$$\left\langle \frac{q_{rad}}{q_{tot}} \right\rangle_{PDO} = \frac{\sum_N^{i=1} \left(\frac{q_{rad}}{q_{tot}} \right)_i}{N}, \tag{4.10}$$

where N is the total number of experimental data points.

- The error on wall temperature resulting form neglecting radiation heat transfer is defined as:

$$ErrT_{wRad} = \frac{T_w - T_{wRad}}{T_{wRad}}, \tag{4.11}$$

where T_w the predicted wall temperature without radiative heat transfer while T_{wRad} TwRad is the predicted wall temperature including the radiative heat transfer.

- Finally, the average error in wall-temperature prediction with and without radiative heat transfer is calculated with:

$$\langle ErrT_{wRad} \rangle = \frac{1}{N} \sum_{N}^{i=1} \left[\frac{T_w - T_{wRad}}{T_{wRad}} \right]_i . \tag{4.12}$$

Table 4.6 lists prediction errors in wall temperatures with and without radiative heat transfer for both heat-flux based and temperature-based methodologies. These errors could be generalized as the impact of radiation heat transfer in post dryout conditions since they are restricted to the wall temperature predictions as computed by the assessment computer code presented in Chapter 3. Table 4.6 shows a small average error of 1.3% and maximum error of 3% while the $\langle ErrTW_{rad} \rangle$ errors are smaller than 0.2%. According to these results, the radiation heat transfer is negligible in the assessment within the flow conditions of its data base (i.e. Bennett et al. (Bennett, 1967)).

4.3.2 Conduction Heat Transfer and Transient Calculation Scheme

The temperature-based methodology was developed to be implemented in transient calculation schemes. Such calculations involve solving the heat conduction equation and going through the different heat transfer stages of the boiling curve (see Figure 1.1).

Table 4.6 Errors Resulting From Neglecting Radiative Heat Transfer

	Value [%]		
	$\left[\frac{q_{rad}}{q_{tot}}\right]_{max}$	$\left\langle \frac{q_{rad}}{q_{tot}} \right\rangle_{PDO}$	$\langle ErrT_{sRad} \rangle$
Q-based	3.0	1.27	0.09
T-based	3.0	1.25	0.20

For instance, a transient calculation scheme would simulate steady state experiments in tubes, such as Bennett experiments (Bennett, 1967), by applying a fixed power as the external surface boundary condition. Heat is generated through the tube (by Joules effect) and heat conduction would be computed. Finally, the remaining internal wall temperature would be used in the heat transfer coefficient calculation. The applicability of a temperature-based methodology could therefore depends on its sensitivity to thermal inertia, CHF predictions, heat transfer coefficient predictions in the transition boiling region, the minimum film boiling temperature prediction, etc. This concern is studied qualitatively in Appendix II where the results were obtained using the transient thermalhydraulics computer code CATHENA (Hanna, 1998). The reader is referred to this appendix for further details.

The results presented in Appendix II does not allow the applicability of a method based on the wall temperature in a transient calculation scheme to be validated; only an assessment of this method using transient experimental data could help in answering this concern. However, the sensitivity analysis presented in the appendix shows that, even if the evolution of the wall temperature during the transient is indeed affected by thermal inertia, the prediction of the heat transfer coefficient in the transition boiling region and the prediction of the T_{min} converges to almost the same final steady-state film boiling calculated value. It is also observed that the CHF uncertainty affects the maximum wall temperature but the film boiling predictions are unchanged. It remains unclear, how-

ever, when the developing flow conditions modification factor should be used to perform transient calculations since it could possibly induce non conservative or underpredicted wall temperatures. The axial heat transfer could also have a possible impact on the film boiling predictions.

CONCLUSION

This thesis presents the assessment result of film-boiling heat-transfer prediction methods (i.e., the heat-flux based and the wall-temperature-based methodologies) against experimental wall-temperature measurements at steady-state conditions. The assessment has shown that the wall temperature in the fully developed region is predicted accurately using both methodologies and that these two methodologies can be implemented in steady-state computer code calculations. It was also shown that the radiative heat transfer component can be neglected within the temperatures and flow conditions used to perform the assessment.

Despite the accurate fully developed film boiling predictions, the assessment has shown that the temperature-based methodology slightly overpredicts the maximum wall temperature and the wall temperature in the developing film boiling region. Furthermore, the predicted temperatures do not follow closely the experimental trend in the developing film boiling region.

Based on the assessment results, the temperature-based methodology has been revised to reduce the prediction uncertainty and improve the parametric trend. The experimental temperature increase has been examined in the developing film boiling region. The temperature rises drastically at the CHF point for low mass fluxes but gradually for high mass fluxes. In addition to the mass flux effect, the quality appears to have a strong effect on the developing film-boiling heat-transfer coefficient.

Consequently, the Reynolds number of the vapor phase has been included in the modification factor and the coefficients of the revised correlation are optimized using the data of Bennett et al. (Bennett, 1967). An assessment of the revised correlation against the database showed an improvement in surface-temperature prediction accuracy. Due to the limited database applied in this study, validation of the revised correlation is recom-

mended against experimental data covering a wider range of flow conditions.

A sensitivity analysis of the effect of thermal-inertia and other parameters of interest on steady-state film-boiling heat transfer has been performed. The effect has no apparent impact on the wall-temperature prediction. This alleviates one of the concerns to apply the proposed methodology, based on the steady-state data, in transient calculations. Nevertheless, further validation of the methodology against transient data is recommended.

REFERENCES

AURACHER, H., 1990, "Transition Boiling", *Proc. 9th Intertional Heat Transfer Conference*, Jerusalem, p.69-90.

BANKOFF, S.G., and MEHRA, V.S., 1962, "A Quenching Treory for Transition Boiling", *Ind. Eng. Chem. Fund.*, p.38-40.

BECKER, K.M., LING, C.H., HEELBERG, S., STRAND, G., 1983, "An experimental investigation of post-dryout heat transfer", *KTH-NEL-33*, Sweden.

BENNETT, A.W., HEWITT, G.F., KEARSEY, H.A., KEEYS, R.K.F., 1967, "Heat transfer to steam-water mixtures flowing in uniformly heated tubes in which the critical heat flux has been exceeded", *United Kingdom Atomic Energy Energy Authority, AERE-R-5373.*

BERGLES, E.A., COLLIER, J.G., DELHAYE, J.M., HEWITT, G.F., MAWINGER, F., 1981, "Two-Phase Flow and Heat Transfer in the Power and Process Industries", *Hemisphere Publishing Corporation.*

BJORNARD, T.A., GRIFFITH, P., 1977, "PWR blowdown heat transfer", *Proceedings ASME, Symposium on the Thermal Hydaulic Aspects of Nuclear Reactor Safety*, Atlanta Georgia, p.17-41.

BEUTHE, T.B., HANNA, B.N., 2005, "CATHENA MOD-3.5d Theory Manual", AECL document, 153-112020-STM-001, Revision 0.

CHEN, J.C., 1963, "A Correlation for Boiling Heat Transfer to Saturated Fluids in Convective Flow", *Paper ASME 63-HT-34*, p.267-272.

Chen, J.C., SUNDARAM, R.K., OZKAYANAK, F.T., 1977, "A Phenomenological Correlation for Post-CHF Heat Transfer", NUREG-0237.

Chen, J.C., OZKAYANAK, F.T., SUNDARAM, R.K., 1979, "Vapor Heat Transfer in Post-CHF Region Including the Effect of Thermodynamic Non-Equilibrium", *Nucl. Eng. Design*, volume 51, p.143-155.

COLLIER, J.G.,, "Heat Transfer in the Postburnout Region and During Quenching and Reflooding".

COLLIER, J.G., 1981, "Nuclear Reactor Safety Heat Transfer, Chapter 7: Single- and Two-phase Heat Transfer", *Ed. Owen C. Jones, Jr.*, Department of Nuclear Energy Brookhaven National Laboratory.

COLLIER, J.G., THOME, J.R., 1994, "Convective Boiling and Condensation, 3 ed.", *Oxford Science Publications*, Great Britain.

CORRADINI, M.L., "Fundamentals of Multiphase Flow", Department of Engineering Physics, University of Wisconsin, Madison WI 53706 (disponible online at: http://wins.engr.wisc.edu/teaching/mpfBook/main.html).

CUMO, M., FARELLO, G.E., 1967, "Heated Wall Droplet Interaction for Two Phase Flow Heat Transfer in Liquid Deficient Region", *Proceedings Symposium on Two Phase Flow dynamics*, Eindhoven, volume 2, p.1325-1357.

DENN, D., 1966, "An Outline of the Characteristics and Construction of the Data Acquisition System Used on the Harwell High Pressure Steam/Water Loop", *United Kingdom Atomic Energy Energy Authority, AERE-R-5128.*

DOUGALL, R.S., ROHSENOW, W.M., 1963, "Film Boiling on the Inside of Vertical Tubes with Upward Flow of Fluid at Low Qualities", MIT Report Number 9079 26, *Cambridge*, Massachusetts.

DITTUS, F.W., BOELTER, L.M.K., 1930, "Heat Transfer in Automobile Radiators of the Tubular Type", *University of California Publications*, vol. 2, No. 13, pp. 443-461.

GIRARD, R., and HANNA, B., LEUNG, L.K.H., 2004, "CATHENA New Post-Dryout Heat Transfer Methodology", *Proc. 6th Int. Conf. on Simulation Methods in Nuclear Engineering*, Montréal, Québec, Canada.

GUO, Y., and LEUNG, L.K.H., 2005, "Correlations for Developing Film Boiling Effect in Tubes", *Proc. 11th Topical Meeting on Nuclear Reactor Thermal-Hydraulics (NURETH-11)*, Avignon, France.

GUO, Y., LEUNG, L.K.H., VASIC, A., 2007, "An Update to The Multitasking Thermalhydraulics Evaluation Package", *Proceedings of the CNS 28th Annual Conference.*

GROENEVELD, D.C., 1972, "The Thermal Behavior of a Heated Surface and Beyond Dryout", Faculty of Graduate Studies of the University of Western Ontario, AECL-4309, Chalk River.

GROENEVELD, D.C., 1973, "Post-dryout heat transfer at reactor operating conditions", *AECL-4513, Nat. Topical Meeting on Water Reactor Safety*, ANS, Salt Lake City.

GROENEVELD, D.C., DELORME, G.G.J., 1976, "Prediction of Thermal Non-equilibrium in the Post-Dryout Regime", *Nuclear Engineering and design*, volume 36, p.17-26.

GROENEVELD, D.C., FUNG, K.K., 1976, "Forced Convective Transition Boiling - Review of Litterature and Comparison of Prediction Methods", AECL-5543.

GROENEVELD, D.C., SNOEK, C.W., 1986, "A Comprehensive Examination Heat Transfer Correlations Suitable for Reactor Safety Analysis", *Multiphase Science and Technology*, Hewitt, G.F. et al. eds., chapter 3, p.181-271.

GROENEVELD, D.C., 1988, "Recent Developments in Thermalhydraulic Prediction Methods", *International Topical Meeting on Thermalhydraulics and Nuclear Reactors*, Seoul, Rep. of Korea.

GROENEVELD, D.C., LEUNG, L.K.H., KIRILLOV, P.L., BOBKOV, V.P., SMOGALEV, I.P., VINOGRADOV, V.N., HUANG, X.C., ROYER, E., 1996, "The 1995 Look-Up Table for Critical Heat Flux in Tubes", *Nuclear Engineering and Design*, Volume 163, No. 1-2 p.1-23.

GROENEVELD, D.C., LEUNG, L.K.H., VASIC, A.Z., Guo, Y.J., Cheng, S.C., 2003, "A Look-up Table For Fully Developed Film-Boiling Heat Transfer", *Nuclear Engineering and Design*, volume 225, p.82-97.

GROENEVELD, D.C., LEUNG, L.K.H., Guo, Y.J, VASIC, A.Z.., El NAKLA, M., PENG, S.W., Cheng, S.C., 2003, "Look-Up Tables for Predicting CHF and Film-Boiling Heat Transfer: Past, Present and Future", *Proc. 10th Topical Meeting on Nuclear Reactor Thermal-Hydraulic*, Seoul, Korea.

GROENEVELD, D.C., SHAN, J.Q., VASIC, A.Z., LEUNG, L.K.H., DURMAYAZ, A., YANG, J., CHENG, S.C. and TANASE, A., "The 2006 CHF Look-Up Table",*Nuclear Engineering and Design*, Volume 237, No. 15-17, pp. 1909-1922.

HADALLER, G.I., BANERJEE, S., 1969, " Heat Transfer to Superheated Steam in Round Tubes", *AECL*, WDI-147.

HANNA, B., 1998, "CATHENA: A Thermalhydraulic Code for CANDU Analysis", *Nuclear Engineering and Desing*, p.113-131.

HEWITT, G.F., SHIRES, G.L., BOTT, T.R., 1994, "Process Heat Transfer", CRC Press LLC.

HEWITT, G.F., 1978, "Critical Heaf Flux in Flow Boiling", *Proc. 6th Int. Heat Transfer Conference*, Toronto, Canada, Vol 6. pp. 143-171.

KARLEKAR, B. V., DESMOND, R. M., 1985, "Transferencia de calor, 2da edición", traduced in spanish by A. G. Martínez, México D.F., México.

KASTNER, W., KOHLER, W., KRATZER, W., HEIN, D., 1981 "Wärmeübergang im Post Dryout-Bereich in Vertikalen und Horizontalen Rohren bei Gleichförmiger Beheizung ", *KWU-Abschlussbericht zum Förderungsvorhaben BMFT ET 1409 A.*

KIRILLOV, P.L., and GROENEVELD, D.C.,"General Film Boiling Heat Transfer Prediction Methods For Advanced Water Cooled Reactors", IPPE, Russia and AECL, Canada.

KIRILLOV, P.L., SMOGALEV, I.P., IVACSHKEVITCH, A.A., VINOGRADOV, V.N., SUDNITSINA, M.O., MITROFANOVA, T.V., 1996, "The Look-Up Table for Heat Transfer Coefficient in Post-Dryout Region forfater flowing in tubes (the 1996-version)", *Preprint FEI-2525*, Institute of Physics and Power Engineering, Obninsk, Russia.

KREITH, F. editor, 2000, "The CRC Handbook of Thermal Engineering", *CRC Press LLC.*

KOHLER, W., HEIN, D., 1986, "Influence of the Wetting State of a Heated Surface on Heat Transfer and Pressure Loss in an Evaporator Tube ", *Report NUREG/IA-0003.*

KOLEV, N., 2002, "Multiphase Flow Dynamics, Mechanical and Thermal Interactions", *Springer-Verlag*, Berlin Heidelberg, Germany.

KONKOV, A.S., ZUPERMAN, D.A., 1967, "Experimental study of heat transfer to wet steam"*Teploenergetika*, vol. 14, No. 3, pp. 54-56 (in Russian), Thermal Engineering, pp. 73-75 (English translation).

KUTATELADZE, S.S., BORISHANSKY, V.M., 1953 "Heat Transfer to Liquid Freely Flowing over a Surface Heated to a Temperature above the Boiling Point", *Problems of Heat Transfer during a Change of State: A collection of Articles*, AEC-tr-3405, p.109.

LECKNER, B., 1972, "Spectral and Total Emissivity of Water Vapor and Carbon Dioxide", *Combustion and Flame*, VOL.19, p.22-48.

LEUNG, L.K.H., 1994, "A Model for Predicting the Pressure Gradient Along a Heated Channel During Flow Boiling", Ph.D. thesis, *University of Ottawa*, Ottawa, Canada.

LEUNG, L.K.H., RUDZINSKI, K.F., VERMA, B., GROENEVELD, D.C., VASIC, A 1999, "Thermalhydraulics Evaluation Package (TEP V3.0) - A User-friendly Software Package for Evaluating Thermalhydraulics Parameters in Tubes and Bundles", *Proceedings of the 9th International Topical Meeting on Nuclear Reactor Thermal-Hydraulics (NURETH-9).*

LEUNG, L.K.H., GROENEVELD, D.C., CHENG, S.C., 2002, "Separate Effects on Film-Boiling Heat Transfer", *Proc. 12th Int. Heat Transfer Conference*, Grenoble, France.

LEUNG, L.K.H., GROENEVELD, D.C., ZHANG, J., 2005, "Prediction of the obstacle effect on film-boiling heat transfer", *Nuclear Engineering and Design*, volume 235, p.687-700.

MATTSON, R.J., and CONDIE, K.G., BENGSTON, S.J., OBENCHAIN, C.F., 1974, "Regression analysis of post-CHF flow boiling data", *Paper B3.8, 4, Proc. of 5th International Heat Transfer Conference*, Tokyo.

MCDONOUGH, J.B., and MILICH, W., KING, E.C, 1960, "AICHE Preprint no. 29", *4th US National Heat Transfer Conference.*

MIROPOLSKIY, Z.L. 1963, "Heat Transfer at Film Boiling Steam-Water Mixture in Tubes", *Keploenergetika*, volume 5, p.49-52.

NAKLA, E., CHENG, S.c., GROENEVELD, D.C., 2004, "Improvements of Prediction Accuracy. Parametric Trends and Smoothness of the Film Boiling Look-Up Tables at ACR Conditions of Interest", *Technical Report of University of Ottawa, UO-MCG-TH-2004-001.*

NIJHAWAN, S., 1980, "Experimental Investigation of Thermal Non-Equilibrium in Post-Dryout Steam-Water Flow ", Ph.D. Theses, *Lehigh University.*

NISHIKAWA, K., YOSHIDA, S., MORI, H., TAKAMATSU, H., 1986, "PDO Heat Transfer to Freon in a Vertical Tube at High Subcritical Pressure", *J. of heat Transfer*, volume 29, p.1245-1251.

PELLETIER, E.-L., LEUNG, L.K.H., GIRARD, R., TEYSSEDOU, A., VARIN, E., 2007, "Comparison of Heat-Flux and Wall-Temperature Based Correlations for Predicting Post-Dryout Surface Temperature in Tubes", *28th Annual Conference of the Canadian Nuclear Society*, Saint John, New Brunswick, Canada.

PLUMMER, D.N., GRIFFITH, P., ROHSENOW, W.M., 1976, "Post-Critical Heat Transfer to Flowing Liquid in a Vertical Tube", *16th National Heat Transfer Conference*, 76-CSME/CSCh-13, St-Louis.

RAMU, K., and WEISMAN, J., 1974, "A method for the correlation of transition boiling heat transfer data", *Paper B4.4, 4, Proc. of 5th International Heat Transfer Conference*, Tokyo.

SAHA,P., 1980, "A Non-equilibrium Heat Transfer Model for Dispersed Droplet Post Dryout Regime", *Int. J. Heat Mass Transfer*, volume 23, p.383-492.

SAHA, P. and N. ZUBER, 1974, "Point of Net Vapor Generation and Vapor Void Fraction in Subcooled Boiling", *Proc. Fifth International Heat Transfer Conference*, Tokyo, IV, p. 175-179.

SEIDER, E.N., TATE,E., 1936, "Heat Transfer and Pressure Drop of Liquids in Tubes", *Industrial Engineering Chemistry*, Volume 28: p. 1429.

SERGEEV, V.V., GALCHENKO, E.F., REMIZOV, O.V., 1985, "Engineering Method of Design PDO Heat Transfer", *Institute of Physics and Power Engineering*, Reprint FEI-1649, Obninsk, Russia.

SLAUGHTERBACK, D.C., and YBARRONDO, L.J., OBENCHAIN, C.F., 1973, "Flow film boiling heat transfer correlations - parametric stydy with data comparison", *ASME-AICHE Heat Transfer. Conference*, Atlanta

SUBBOTIN, V.I., REMIZOV, O.V., VOROBIEV, V.A., 1973, " Temperature Regimes and Heat Transfer in the Region of Degraded Heat Transfer", *IPPE Institute*, J., TVT, 11, 6, 73.

TONG, L.S., 1967, "Heat transfer in water-cooled nuclear reactors", *Nuclear Engineering and Design*, 6, 301.

TONG, L.S., and YOUNG, J.D., 1978, "A phenomenological transition and film boiling heat transfer correlation", *Paper B3.9, 4, Proc. of 5th International Heat Transfer Conference*, Tokyo.

TONG, L. S., and TANG, Y. S., 1997, "Boiling Heat Transfer and Two-Phase Flow, 2nd edition", *Taylor and Francis editions*, United States of America.

VARONE, Jr.A.F., ROHSENOW, W.M., 1986, "Post-Dryout Heat Transfer Predictions , *Nuclear Engineering Design*, p.315-317.

VARONE, Jr.A.F., RAHSENOW, W.M. 1990, "The Influence of the Dispersed Flow Film Boiling", Heat Transfer Lab, Massachusetts Institute of Technology, Cambridge, MIT Rep. 71999-106.

VASIC, A.Z., GROENEVELD, D.C., LEUNG, L.K.H., GUO, Y.J., CHENG, S.C., 2001, "Post-CHF heat transfer in water-cooled tubes: Compilation of world Data", *International Journal of Experimental Methods in Heat Transfer*, Thermodynamics and Fluid Mechanisms.

WEISMAN, J., PEI, B.S., 1983, "Prediction of critical heat flux in flow boiling at low qualities", *Int. J. Heat Mass Transfer* , Volume 26, pp. 1463-1477.

WINTERTON, R.S., "Transition Boiling", AEEW-R1567.

OTHER REFERENCES:

Commercial data. Available at: www.alloywire.com

Commercial data. Available at: www.espi-metals.com

Wolverint Tube, Inc., "Engineering Data Book III", (avaliable online)

APPENDIX I

INTRODUCTION TO HEAT TRANSFER MECHANISMS AND RADIATIVE HEAT TRANSFER

This appendix presents a short overview three different heat transfer mechanisms: conductive, convective and radiative heat transfer. Complements on radiative heat transfer are also introduced before presenting the radiative heat transfer model implemented in the assessment computer code.

I.1 General Heat Transfer Mechanisms

Descriptions of the three heat transfer modes are presented in this section. Specific equations useful for the assessment are also derived.

I.1.1 Conductive Heat Transfer

Conduction is the heat transfer propagation mode encountered mainely in solids. The velocity of the heat transfer is a function of the material and is expressed as a function of a macroscopic coefficient, the thermal conductivity, k.

The heat conduction equation can be expressed as:

$$\vec{\nabla} \cdot \vec{q''} + q''' = \rho c_{th} \frac{\partial T}{\partial t}. \tag{I.1}$$

where ρ is the density (in kg/m^3) of the material, c_{th}, its thermal conductivity (in $J/kg°C$) and T, the local temperature (in $°C$). The term q''' is the heat generation within

the material (in W/m^3) while the right hand side of Equation I.1 represents the heat accumulation within the material. Finally, $\vec{q''}$ is the heat flux (in W/m^2) defined as the heat, Q (in W), devided by the heated area, A (in m^2). This component can be related to the spatial temperature variation using Fourier's law defined as:

$$\vec{q''} = -k \vec{\nabla} T. \tag{I.2}$$

Substitution of Equation I.2 into Equation I.1 gives the general conduction equation based on the temperature:

$$-\vec{\nabla} \cdot \left(k \vec{\nabla} T \right) + q''' = \frac{\partial \left(\rho c_{th} T \right)}{\partial t}. \tag{I.3}$$

The above equation, used with the appropriate system of coordinates and boundary conditions, permits the temperature distribution in any conduction heat transfer problem to be calculated.

I.1.1.1 Conduction Through a Uniformly Heated Tube

The assessment work presented in this thesis studies temperature distributions in a uniformly heated tube under post-dryout conditions. Uniformly heated tubes are usually obtained by applying an electric potential along the heated length of the tube resulting in heat generation (q''' in Equations I.1 and I.3) through the tube by Joules effect. In such experiments, the external surface ($r = r_{ext}$) is isolated and the internal surface ($r = r_{int}$) is cooled by a fluid. Therefore, the boundary conditions are:

$$\left| \frac{\partial T}{\partial r} \right|_{r=r_{ext}} = 0 \tag{I.4}$$

and

$$\left|\frac{\partial T}{\partial r}\right|_{r=r_{int}} = h\left(T_w - T_{sat}\right). \tag{I.5}$$

In steady-state conditions, the conduction equation can be written as follows:

$$\vec{\nabla} \cdot \left(k\, \vec{\nabla}\, T\right) = -q'''. \tag{I.6}$$

In cylindrical coordinate with negligible conduction in the axial direction and having angular (θ direction) symmetry, the equation simplifies to:

$$k\frac{\partial^2 T}{\partial r^2} + \frac{k}{r}\frac{\partial T}{\partial r} = -q''', \tag{I.7}$$

where r is the radial direction.

The stady-state temperature distribution can be calculated using Fourier's Equation I.2 or Equation I.7. Once a stady-state temperature distribution is reached with an external thermally insulated boundary, the applied power is entirely transferred to the coolant. This property was used in the assessment code presented in Chapter 3 where the heat flux was constant and taken as the ratio between the applied power and the area presented to the fluid.

Transient conditions implies a more complex temperature distribution obtained by solving Equation I.3. This distribution is more conveniently solved numerically. For very thin tube thicknesses or materials with a very high thermal conductivity, however, the heat conduction trough the heated material seems instantaneous and thermal inertia can be neglected. This simplification could be made for Bennett's experiments (Bennett,

1967). It remains unclear, however, if transient heat conduction trough the heated material (or thermal inertia) could have an impact on the post-dryout predictions. This concern is studied in Appendix II.

I.1.2 Convective Heat Transfer

Heat convection defines the heat transfered from a body to a fluid. Natural convection is considered for nil or low fluid velocities. In these case, temperature gradients are formed within the fluid causing density changes. These changes of density are responsible for the relative motion between the liquid and the body. Natural convection is outside of the scope of this project and is not presented in this document. As the fluid velocity increases, the velocities due to density changes become insignificant. In these cases, forced convective heat transfer is considered and is presented in this section.

By extension to conduction heat transfer, Prandtl introduced the thermal boundary layer in the fluid (at the interface between the solid and the liquid) of a thickness δ and in which all the thermal resistance is localized. The thermal boundary layer concept is used to define the heat transfer coefficient. Defining the wall temperature as T_w and the bulk fluid temperature as T_b, the heat flux from the wall to the fluid can be estimated using Fourier's law:

$$q'' = \frac{-k}{\delta}(T_b - T_w) \tag{I.8}$$

Since δ cannot be estimated independently, it is combined with k in a single number, h, defined as the heat transfer coefficient. This coefficient gives the velocity of the heat transfer and is expressed in $W/°Cm^2$. The heat flux can then be calculated using Newton's law:

$$q'' = h\,(T_w - T_b) \tag{I.9}$$

I.1.3 Convective Heat Transfer

Heat convection defines the heat transfered from a body to a fluid. Natural convection is considered for nil or low fluid velocities. In these case, temperature gradients are formed within the fluid causing density changes. These changes of density are responsible for the relative motion between the liquid and the body. Natural convection is outside of the scope of this project and is not presented in this document. As the fluid velocity increases, the velocities due to density changes become insignificant. In these cases, forced convective heat transfer is considered and is presented in this section.

By extension to conduction heat transfer, Prandtl introduced the thermal boundary layer in the fluid (at the interface between the solid and the liquid) of a thickness δ and in which all the thermal resistance is localized. The thermal boundary layer concept is used to define the heat transfer coefficient. Defining the wall temperature as T_w and the bulk fluid temperature as T_b, the heat flux from the wall to the fluid can be estimated using Fourier's law:

$$q'' = \frac{-k}{\delta}\,(T_b - T_w) \tag{I.10}$$

Since δ cannot be estimated independently, it is combined with k in a single number, h, defined as the heat transfer coefficient. This coefficient gives the velocity of the heat transfer and is expressed in $W/°Cm^2$. The heat flux can then be calculated using Newton's law:

$$q'' = h\,(T_w - T_b) \tag{I.11}$$

I.1.4 Radiative Heat Transfer

Thermal radiation results from the emission of electromagnetic waves from a heated body to a colder one. Radiation heat transfer is usually negligible when compared to a direct interaction (i.e. conduction and convection) and is generally not taken into account in common heat transfer problems. However, in some high temperature applications and without contacts between the heated wall and the liquid phase (such as post-dryout conditions), radiation may be important. This section therefore presents some radiation concepts.

1. **Black-Body, Gray-Body and Stefan-Boltzmann's Law:** An ideal emitting body is defined as a black body and emits its energy according to Stefan-Boltzmann's law:

$$e_{b.b.} = (\sigma_{SB})T^4 \tag{I.12}$$

where $e_{b.b.}$ is the power density of the black body (the total energy emitted per units of area and time), σ_{SB} is the Stefan-Boltzmann's constant ($\sigma_{SB} = 5.66 \times 10^{-8} W/m^2K^4$) and T is the temperature of the black body (in K). A black body is characterized by the fact that at any given temperature, its power density is the maximum value of any body at the same temperature. The black body is an ideal concept and the power density of a real body at a given temperature is only a fraction of the power density of a black body at the same temperature. A fraction between these two powers is defined as the emissivity, ξ, which is function of the material and has a value between 0 and 1. The emissive power of a body is then

given by the following equation:

$$e_{g.b.} = \xi e_{b.b.} = \xi(\sigma_{SB})T^4 \tag{I.13}$$

2. **Form Factors:**

   The form factor, F_{i-j}, is defined as the fraction of the radiation energy emitted by a surface i that will reach the surface j. The form factors are based on geometric characteristics. Two relationships are of a great interest.

   The first, the *Sum Relation*, states that all the radiation emitted in a closed surface of N internal faces will be absorbed within it. We therefore have:

$$\sum_{n=1}^{N} F_{m-n} = 1; (m = 1, 2, ..., n) \tag{I.14}$$

   The second is the *Reciprocity Relation* and relates the form factor to the area with:

$$A_m F_{m-n} = A_n F_{n-m} \tag{I.15}$$

3. **Radiation Properties of a Surface**

   The most important radiation properties of a surface are:

   - **Irradiation**

     The irradiation, Γ, of a surface i is defined as the energy incident on the surface from any other surface. This irradiation will be absorbed, reflected or transmitted, hence:

$$\Gamma = \alpha\Gamma + \beta\Gamma + \tau\Gamma \tag{I.16}$$

were α is the absorptivity, β is the reflectivity and τ the transmitivity. These quantities are defined in such a way that:

$$\alpha + \beta + \tau = 1$$

The concept of the gray body supposes that all the energy going through the body is absorbed and entirely re-emitted.

- **Radiocivity**

  The radiocivity, J, of a surface is often considered uniform on the surface. It is defined as the outgoing energy form the surface and it is the sum of the reflected and emitted energies:

$$J = \beta\Gamma + e \tag{I.17}$$

- **Radiative Heat Loss**

  Finally, the difference between the radiocivity and the irradiation of a surface is defined as its radiative heat loss:

$$Q_{rad} = Aq_{rad} = A\left(J - \Gamma\right) \tag{I.18}$$

I.2 Complement on Radiative Heat Transfer

Before presenting the radiative heat transfer model implemented in the assessment code, a complement on this topic is presented in this section.

I.2.1 Radiative Exchange Between Two Gray Bodies

We consider a gray body (surface 1) surrounded by another gray body (surface 2) The two surfaces are separated by a non-participating gas. In this case, the net radiation can be written as:

$$Q_2 = A_2 F_{2-1} \left(J_2 - J_1 \right), \tag{I.19}$$

$$Q_1 = A_1 F_{1-2} \left(J_1 - J_2 \right) = -Q_2. \tag{I.20}$$

Using Equation (I.17) for surface 1, we have:

$$\Gamma_1 = \frac{J_1 - \xi_1 e_{b1}}{\beta_1}, \tag{I.21}$$

$$\frac{Q_1}{A_1} = J_1 - \Gamma_1 = J_1 - \frac{J_1 - \xi_1 e_{b1}}{\beta_1}. \tag{I.22}$$

.

Since $\beta_1 = 1 - \alpha_1 = 1 - \xi_1$ for an opaque gray body we can write:

$$Q_1 = \frac{e_{b1} - J_1}{\frac{1-\xi_1}{\xi_1 A_1}}, \tag{I.23}$$

$$Q_2 = \frac{e_{b2} - J_2}{\frac{1-\xi_2}{\xi_2 A_2}}. \tag{I.24}$$

Equation I.20 can therefore be re-written as:

$$\frac{e_{b1} - J_1}{\frac{1-\xi_1}{\xi_1 A_1}} = A_1 F_{1-2} \left(J_1 - J_2 \right) = -\frac{J_2 - e_{b2}}{\frac{1-\xi_2}{\xi_2 A_2}}. \tag{I.25}$$

This latest equation can be analyzed as follows:

- $(e_{b1} - J_1)$, $(J_1 - J_2)$ and $(J_2 - e_{b2})$ can be considered as equivalent electrical potentials,
- $\left(\frac{1-\xi_1}{\xi_1 A_1}\right)$, $\left(\frac{1}{A_1 F_{1-2}}\right)$ and $\left(\frac{1-\xi_2}{\xi_2 A_2}\right)$ can be considered as electrical resistances
- Q_1 and Q_2 can be considered as current passing through resistances 1 and 2

With these analogies, the heat-transfer system can be represented as the equivalent electric circuit illustrated in Figure I.1 where:

$$R_1 = \frac{1-\xi_1}{\xi_1 A_1},\ R_{1-2} = \frac{1}{A_1 F_{1-2}} \text{ and } R_2 = \frac{1-\xi_2}{\xi_2 A_2}\ .$$

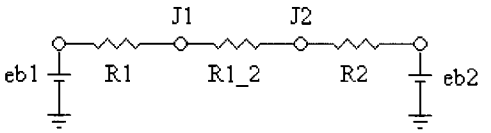

Figure I.1 Two Gray Bodies Equivalent Electric Circuit

Equation (I.25) can then be found from Kirchhoff's law applied to nodes J_1 and J_2.

I.2.2 Radiative Exchange Between Three Gray Bodies

The equivalent circuit is used to describe the thermal radiation exchange between three gray bodies (i.e. a cylinder 1 surrounded by a cylinder 2, both separated by a partic-

ipating gaz, represented as a surface 3). In this case, the equivalent electric circuit is represented in Figure I.2 where:

$$J_3 = e_{b1},\ R_3 = \frac{1}{A_1 F_{1-3}},\ R_4 = \frac{1}{A_2 F_{2-3}} \text{ and } R_5 = \frac{1-\xi_3}{\xi_3 A_3},$$

and others quantities have been presented previously.

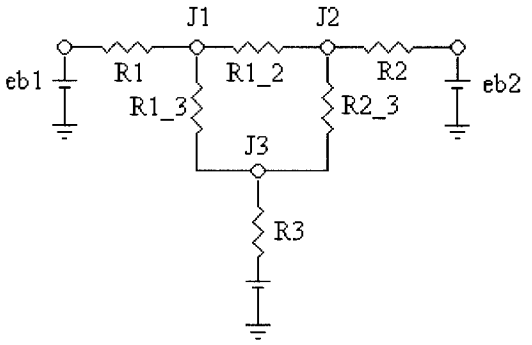

Figure I.2 Three Gray Bodies Equivalent Electric Circuit

Applying Kirchhoff's law at nodes J_1, J_2 and J_3, we easily find the following set of equations:

$$\frac{e_{b1} - J_1}{(1-\xi_1)/(\xi_1 A_1)} + \frac{J_2 - J_1}{1/(A_1 F_{1-2})} + \frac{J_3 - J_1}{1/(A_1 F_{1-3})} = 0 \tag{I.26}$$

$$\frac{e_{b2} - J_2}{(1-\xi_2)/(\xi_2 A_2)} + \frac{J_1 - J_2}{1/(A_1 F_{1-2})} + \frac{J_3 - J_2}{1/(A_2 F_{2-3})} = 0 \tag{I.27}$$

$$\frac{e_{b3} - J_3}{(1-\xi_3)/(\xi_1 A_3)} + \frac{J_1 - J_3}{1/(A_1 F_{1-3})} + \frac{J_2 - J_1}{1/(A_2 F_{2-3})} = 0 \tag{I.28}$$

These equations are used in this work to calculate the radiative heat transfer in post-dryout conditions.

I.2.3 Emissivity of the Vapor Film: Leckner's Method

The emissivity of the vapor film is calculated using the method presented by Leckner (Leckner, 1972). According to this work, the ratio between the emissivity of a gas (within a mixture of gases), ξ, and its emissivity at a reference pressure of 1 bar, ξ_0, is expressed as a function of a pressure correction function:

$$\frac{\xi}{\xi_0} = f\left(p_a L_b, p, T_g, p_e\right), \tag{I.29}$$

where L_b is the mean-beam length, T_g, the temperature of gas, p_a is the partial pressure of the absorbing gas, p is the total pressure and p_e is the gas equivalent pressure. p_e is calculated using:

$$p_e = \frac{p}{p_0}\left[1 + 4.9\left(\frac{p_a}{p}\right)\left(\frac{273}{T}\right)^{0.5}\right] \tag{I.30}$$

and the mean-bean length can be estimated by:

$$L_b \cong 0.9 L_o \cong 0.9 \frac{4V_v}{A_v}, \tag{I.31}$$

where V_v and A_v are the total vapor phase volume and area.

The ratio $\left(\frac{\xi}{\xi_0}\right)$ is limited by a maximum value of $\left(\frac{\xi}{\xi_0}\right)_{max}$. Equation I.29 can then be written as:

$$\frac{\xi}{\xi_0}\left(p_a L_b, p, T_g\right) = \left[1 + \left[\frac{\xi}{\xi_0} - 1\right]_{max} exp\left(-c\left[log_{10}\frac{(p_a L_b)_m}{p_a L_b}\right]^2\right)\right], \tag{I.32}$$

with

$$\left[\frac{\xi}{\xi_0} - 1\right]_{max} = -\frac{(a-1)(1-p_E)}{a+b-1+p_E}. \tag{I.33}$$

Finally, the emissivity at reference state, ξ_0, is calculated using the following correlation:

$$\xi_0\left(p_a L_b, P, T_g\right) = exp\left[\sum_{i=0}^{M}\sum_{j=0}^{N} c_{ji}\left(\frac{T_g}{T_0}\right)^j \left(log_{10}\frac{p_a L_b}{(p_a L_b)_0}\right)^i\right]. \tag{I.34}$$

Table I.1 Correlation Constants for Water Vapor Emissivity

Constant	Value	Restriction
T_0	1000 K	
p_0	1 bar	
t	T/T_0	
$(p_aL_b)_0$	1 bar cm	
$(p_aL_b)_m$ / $(p_aL_b)_0$	$13.2t^2$	
a	2.144	$t < 0.75$
	$1.88 - 2.053\ log_{10}t$	$t > 0.75$
b	$1.10/t^{1.4}$	
c	0.5	

Table I.2 Coefficients for Water Vapor Emissivity

Coefficient c_{ji}			**Value**		
c_{00}	$c_{1,0}$	$c_{2,0}$	-2.2118	-1.1987	0.035596
c_{01}	$c_{1,1}$	$c_{2,1}$	0.85667	0.93048	-0.14391
c_{03}	$c_{1,2}$	$c_{2,2}$	-0.10838	-0.17156	0.045915

The constants *a*, *b*, *c*, $(p_aL_b)_0$, $(p_aL_b)_0$ and T_0 required to evaluate Equations I.32, I.33 and I.34 are given for water vapor in Table I.1, while the coefficients c_{ji} are given in Table I.2.

I.3 Radiative Heat Transfer Model

A radiative heat transfer model was implemented in the assessment code. It is restricted to inverted annular film boiling but can be used for all the post-dryout regimes and can provide estimates for other conditions. Radiative exchange between three gray bodies is simulated and the following simplifying assumptions have been used:

- The entrainment of droplets by the vapor film are neglected.
- The interface between the liquid and its vapor is smooth.
- There is no radiation heat transfer in the axial direction.
- The vapor film is completely transparent to the whole electromagnetic spectra.
- The wall is uniformly heated and the liquid phase temperature is homogeneously distributed.

To develop the heat transfer model, Equations I.26 to I.28 are solved. The subscript 1 is replaced by *w* for the heated wall, subscript 2 by *f* for the fluid core and subscript 3 by *v* for the vapor film. We assume that there is no gain or attenuation of the energy within the vapor film. Hence, Q_v, vanishes and there is only two unknown currents (i.e. radiative heat transfer), Q_w and Q_f, thus:

$$\frac{J_w - e_{bw}}{\frac{1-\xi_w}{A_w \xi_w}} + \frac{J_w - J_f}{\frac{1}{A_w F_{w-f}(1-\xi_v)}} + \frac{J_w - e_{bv}}{\frac{1}{A_w \xi_v}} = 0 \tag{I.35}$$

$$\frac{J_f - e_b f}{\frac{1-\xi_f}{A_f \xi_f}} + \frac{J_f - J_w}{\frac{1}{A_f F_{f-w}(1-\xi_v)}} + \frac{J_f - e_{bv}}{\frac{1}{A_f \xi_v}} = 0. \tag{I.36}$$

These equations can be grouped in the following system:

$$\widetilde{A}\widetilde{J} = \widetilde{B} \tag{I.37}$$

where:

$$\widetilde{A} = \begin{bmatrix} -F_{f-w}\left(1-\xi_v\right)\left(1-\xi_f\right) - \xi_f - \xi_v\left(1-\xi_f\right) & F_{f-w}\left(1-\xi_v\right)\left(1-\xi_f\right) \\ F_{w-f}\left(1-\xi_v\right)\left(1-\xi_w\right) & -F_{w-f}\left(1-\xi_v\right)\left(1-\xi_w\right) - \xi_w - \xi_v\left(1-\xi_w\right) \end{bmatrix} \tag{I.38}$$

$$\widetilde{J} = \begin{bmatrix} J_f \\ J_w \end{bmatrix}. \tag{I.39}$$

$$\widetilde{B} = \begin{bmatrix} -\xi_v\left(1-\xi_f\right)e_{bv} - \xi_f e_{bf} \\ -\xi_v\left(1-\xi_w\right)e_{bv} - e_w E_{bw} \end{bmatrix} \tag{I.40}$$

The net heat transfer of the heated wall is finally given by:

$$Q_w = \frac{A\xi_w}{1-\xi_w}\left[e_{bw} - J_w\right], \tag{I.41}$$

where J_w calculated solving the system of equations I.37.

In order to calculate the radiative heat flux in the assessment code, the following calculation steps are performed:

1. Find the liquid core diameter considering an inverted annular flow, i.e., $D_f = D\sqrt{1-\epsilon}$.

2. Find the wall-to-fluid view factor as, $F_{w-f} = \frac{A_f}{A_w} = \frac{\pi D_f L}{\pi D L} = \frac{D\sqrt{1-\epsilon}}{D} = \sqrt{1-\epsilon}$.

3. Calculate the emissivity of the liquid core. The emissivity of the water ranges from 0.85 to 0.7 at temperatures beyond 260^oC a average value of 0.775 is taken.

4. Calculate the emissivity the heated wall. The emissivity of Inconel-600 is used to simulate the emissivity of Nimonic-80a, then:

$$\xi_w = 0.6275 + 0.000198\, T_w\ .$$

   This approximations is justified by the fact that both material compositions are similar. Chemical approximative composition of Nimonic-80a and Inconel-600 are shown in Table I.3 and are taken form (alloywire.com) (espi-metals.com).

5. Calculate the emissivity of the vapor film using Lencker's method presented in Section I.2.3.

6. Solve the system of equations (Equation I.37).

7. Calculate the radiative heat flux by solving Equation I.41.

The function implemented in the code can be found in Appendix III.2 p.145.

Table I.3 Approximative Chemical Composition of Inconel-600 and Nimonic-80A

element	Nominal Composition [%] Inconel-600	Nimonic-80A
Ni	72.00	76.00
Cr	15.50	20.00
Fe	8.00	
Si	0.50	
Mn	1.00	
C	0.150	
Cu	0.50	
S	0.015	
Al+Ti		4.00
Density $[g/cm^3]$	8.47	8.19

APPENDIX II

INFLUENCE OF THERMAL INERTIA AND TRANSIENT CALCULATIONS ON THE PREDICTION OF STEADY-STATE FILM BOILING

The Temperature-Based Methodology was developed to be implemented in transient calculation schemes. Such calculations involve heat conduction within the heated material. It simulates steady state experiments in tubes, such as Bennett experiments (Bennett, 1967), with a transient calculation scheme involving a fixed power. Heat generation within the tube wall and conduction through the tube is then computed and the remaining internal wall temperature is used in the heat transfer calculations. As the heat flux between the heated wall and the fluid increases, the fluid at a specific axial location will follow all the heat transfer regimes including transition boiling (if the local value of the CHF is exceeded).

The applicability of a Temperature-Based Methodology could therefore depend on the thermal inertia, CHF predictions, transition boiling predictions and minimum film boiling temperature predictions. The purpose of this appendix is to determine whether the final steady state film boiling predictions depend on these parameters. This study is performed using the transient thermalhydraulics computer code, CATHENA (Hanna, 1998) Version 3.5d rev. 2 using the thermalhydraulic parameters from experiment no. 5251. Since the objective is not to assess CATHENA's predictions, the results are only taken qualitatively and no comparison to experimental data is carried out.

II.1 Thermal Inertia

In transient calculations, an electrical power is applied and heat is generated within the tube (by Joules effect). Such calculations usually begin by solving the heat conduction equation within the material. The wall temperature and the fluid properties will then determine the heat transfer coefficient and consequently the heat flux between the heated wall and the fluid. This quantity is defined as the ratio between the power transferred from the heated wall to the fluid and the heated area presented to the fluid.

In order to study the evolution of the heat flux between the heated wall and the fluid during transient conditions, this quantity is depicted in Figure II.1-i for two axial positions; at thermocouple no. 10, where nucleate boiling conditions are found during the entire transient, and at thermocouple no.21, where post-dryout conditions are eventually reached during the transient. This figure shows that, initially, both axial positions are under nucleate boiling conditions. Under these conditions, the heat fluxes increases with the applied power. Once the CHF is reached at thermocouple no. 21 (at approximatively 47 seconds), the heat transfer coefficient between the heated wall and the fluid suddenly decreases at that position, resulting in a rapid wall temperature excursion. During the next few seconds, the fluid undergoes transition boiling and reaches the minimum film boiling temperature and film boiling conditions. Since the heat flux is a calculated parameter, the velocity of this transition can not be controlled. Finally, fully developed heat transfer conditions are reached. When the applied power stops increasing, the heat flux between the heated wall and the fluid remains constant (some numerical oscillations can however be observed in post-dryout conditions but their study is beyond the scope of this appendix).

The heat flux is also shown as a function of the wall temperature in Figure II.1-ii. This figure shows the computed boiling curve at the location of thermocouple no. 21.

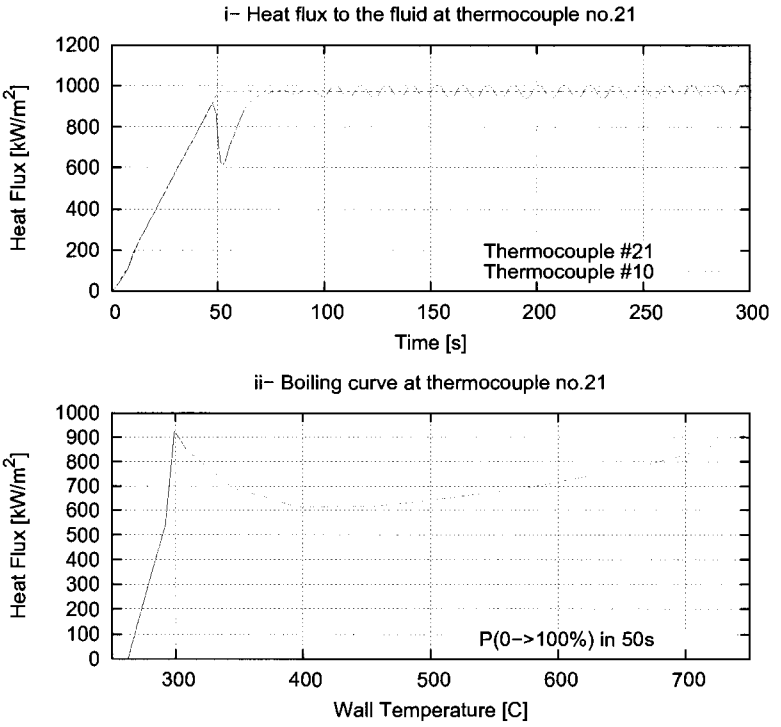

Figure II.1 Heat Flux to the Fluid Evolution as a Function of Time and Wall Temperature

The heat conduction through the tube would indeed influence the wall temperature evolution during transient calculations. However, it remains unclear whether this parameter can influence the final post-dryout steady state temperature distribution; a possible energy accumulation within the heated material could occur during the heat flux reduction (corresponding to the transition boiling region and the beginning of the film boiling conditions) and artificially overestimate the final wall temperature. This concern was in-

vestigated by simulating the same experiment with three different power insertion rates: the power was applied form 0% to 100% in 1s, 50 s and 500 s.

Figure II.2-i shows the temperature evolution at thermocouple no. 21 (i.e at 5.1308 m) for the three different power application rates and Figure II.2-i shows the internal axial temperature distribution for these cases. These figures show that the transient temperature evolution is affected by the applied power variation rate but, in all the cases studied, the final temperature distribution is independent of the rate of change in power. This suggests that thermal inertia does not affect the final wall temperature distribution.

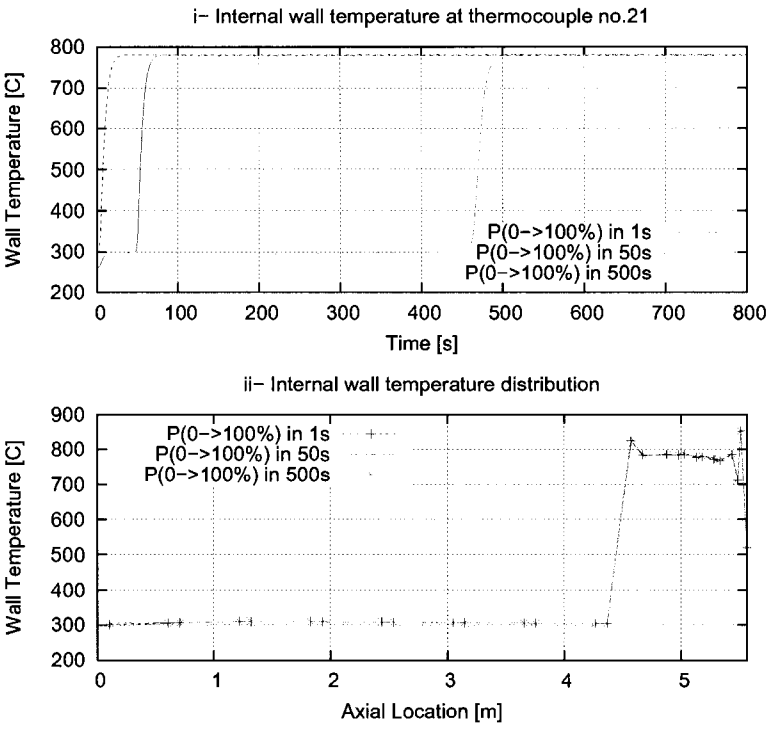

Figure II.2 Effect due to Power Variation Rate

The impact of thermal inertia was also investigated by modifying the thickness of the tube (the external radius was doubled while maintaining constant the internal radius). The internal wall temperature evolution at thermocouple no. 21 and the internal axial temperature distribution are shown in Figure II.3. Similarily to the power application rate, the internal wall temperature evolution are different for the two radius and results form the thermal inertia through the tube. The final temperature and internal axial temperature distribution are again similar for both wall thicknesses. Finally, with an increased wall thickness (which increases thermal inertia), the external surface wall temperature converges to higher temperatures as shown in Figure II.4

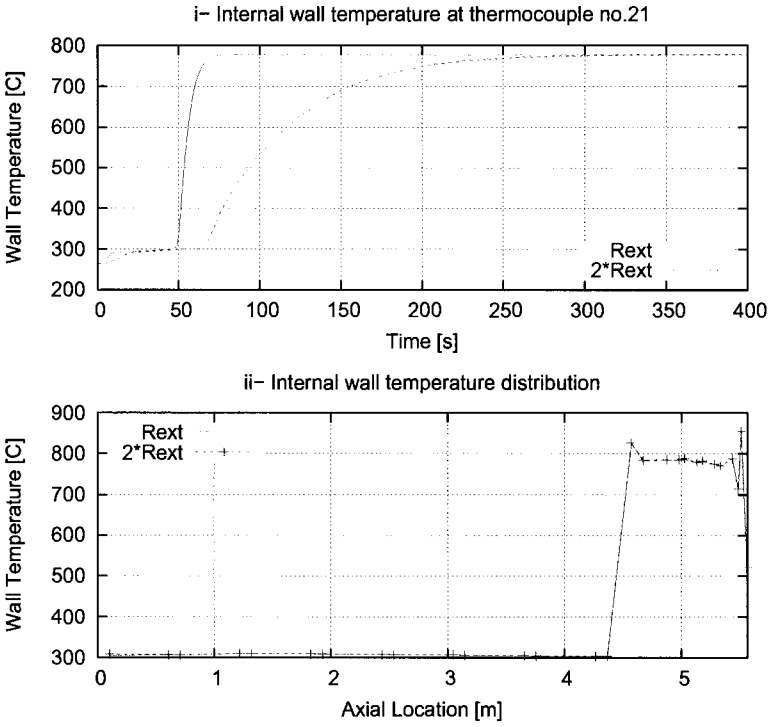

Figure II.3 Wall Thickness Effect

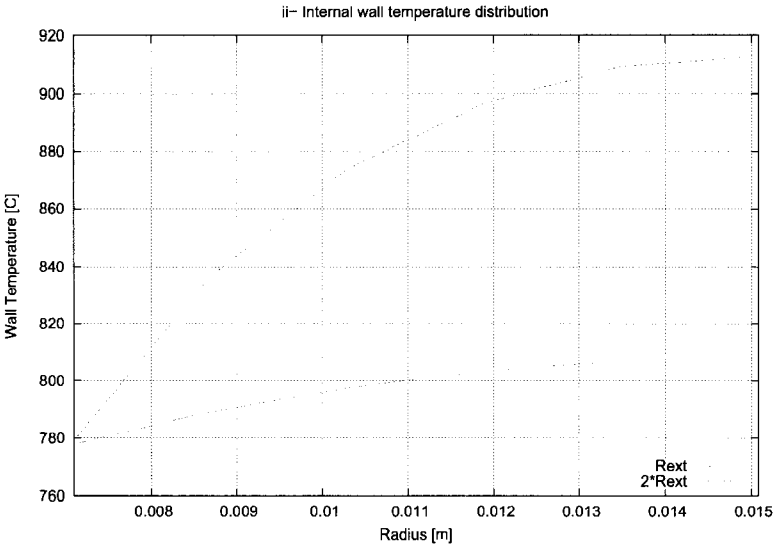

Figure II.4 Radial Wall Temperature Distribution for Different Wall Thicknesses

II.2 Critical Heat Flux

Under steady state conditions, the uncertainties of critical heat flux have a significant impact on the maximum temperature and on the predicted temperature during the developing flow conditions, while predictions of the fully developed film boiling are not affected by this parameter. Similarly to thermal inertia, the uncertainties of CHF could possibly have an impact on the wall temperature evolution when a transient calculation scheme is used. Consequently, the CHF uncertainties impact on the post-dryout predictions was studied by performing a sensitivity analysis with CATHENA (Hanna, 1998); the simulations were performed using the default CHF and using this default CHF multiplied by 0.3, 0.5 and 0.75 (a greater multiplication factor was also used but the fully developed conditions were not reached and the results were not included in this analysis).

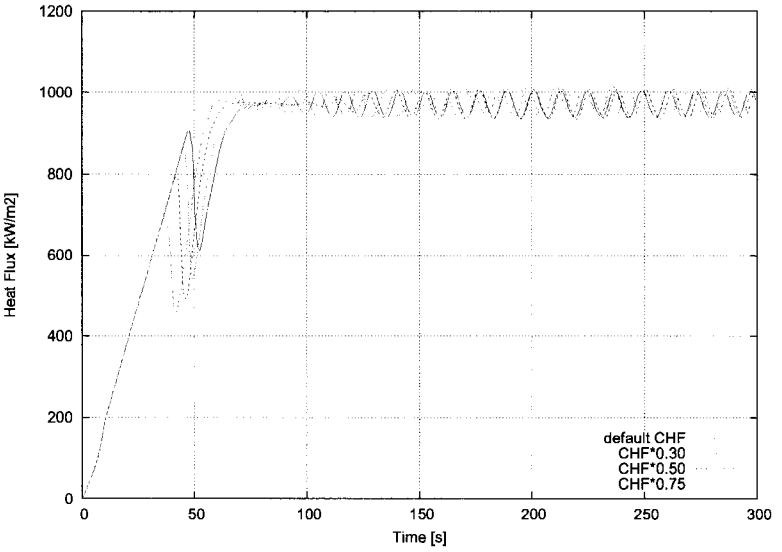

Figure II.5 Heat Flux to the Fluid for Several CHF Predictions

Figure II.5 shows the evolution of the heat flux between the heated wall and the fluid for different CHF predictions. As expected, the lower the CHF prediction, the sooner the dryout conditions are reached. All the simulations converge to the same final heat flux (some numerical oscillations are however again observed). Since the heat fluxes converge to the same final value, the final wall temperatures are also equal, as shown in Figure II.6-i. For some CHF predictions, however, slight final temperature differences can observed since film boiling conditions are not totally reached at this axial position. Figure II.6-ii shows that for these cases, the final fully-developped film boiling temperatures, encountered further downstream, are the same.

Figure II.6-ii shows the final axial temperature distribution for these simulations, i.e.

a similar parametric trend is observed in the fully developed region. In this case, the behaviour is similar to the one observed experimentally under steady-state conditions. As a result, CHF errors will have a significant impact the post-dryout predictions until steady state fully developed film boiling conditions are reached. Once fully developed film boiling conditions reached, no impact is observed on temperature predictions.

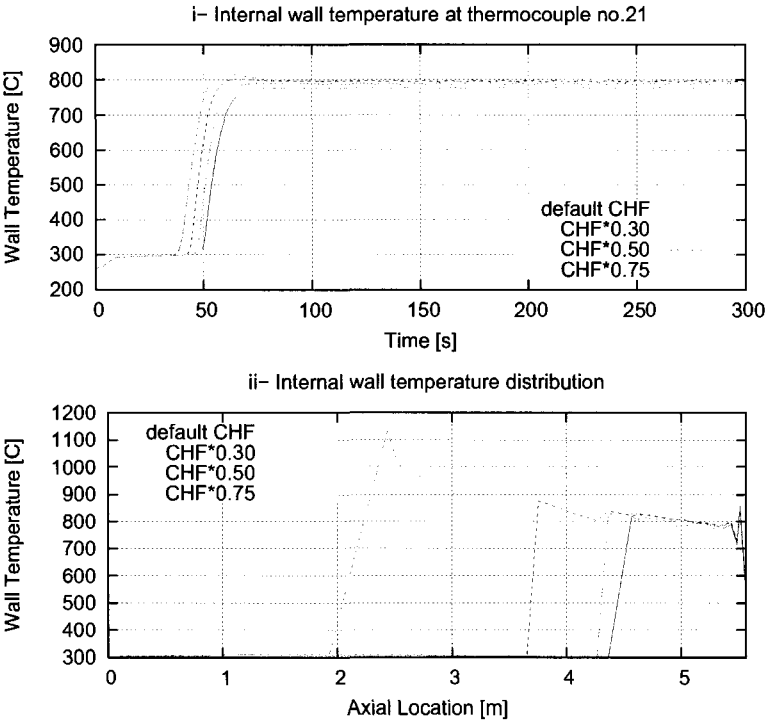

Figure II.6 Effects due to uncertainties in CHF

II.3 Transition Boiling

This section studies the possible effect of the uncertainty in the transition boiling region on the final steady state film boiling temperature. CATHENA (Hanna, 1998) uses by default the Bjornard and Griffith's correlation which computes the transition boiling heat flux as a transition function of the critical heat flux and stable film boiling heat flux. The code does not allow the transition boiling heat flux to be directly modified but only the relative importance of the critical and the film boiling heat fluxes can be actualized during the calculations. For this case, the approach used was therefore to compare the default transition boiling heat flux to the cases where this heat flux was computed based only on the critical heat flux and on only the film boiling heat fluxes. It should also be noted that these simulations were performed without including the developing post-dryout modification factor. The temperature evolution at thermocouple no.21 and the final axial wall temperature distribution for theses cases are are shown in Figure II.7-i and II.7-ii.

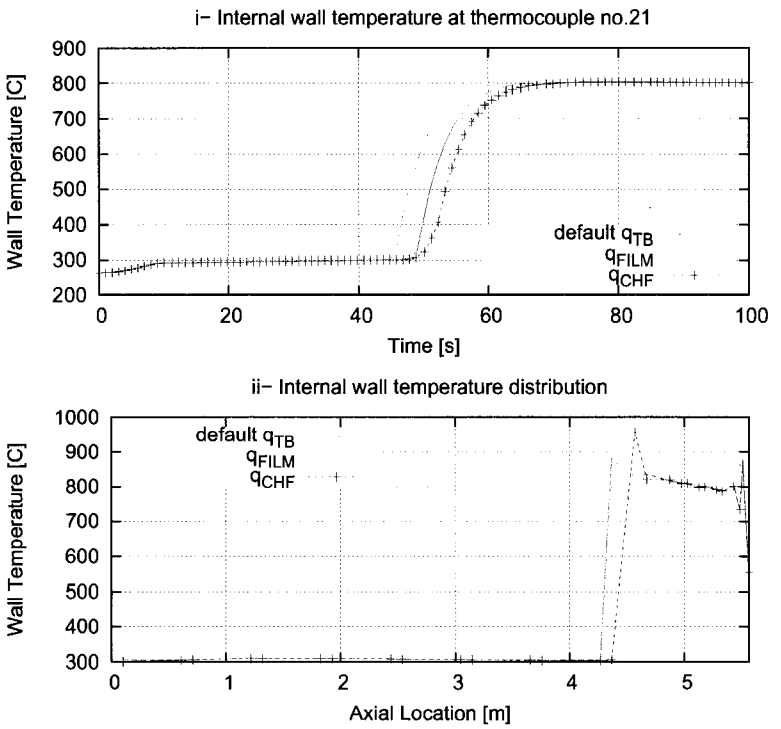

Figure II.7 Transition Boiling Uncertainty Effect on the Internal Wall Temperature

These results show that a heat flux uncertainty in the transition boiling region will indeed modify the temperature evolution but the temperatures will soon converge to the same steady state value in the film boiling region. Hence, the transition boiling region does not have a significant impact on the final steady state film boiling temperatures.

II.4 Prediction of the Minimum Film Boiling Temperature

Since the minimum film boiling temperature separates the transition boiling region (where the heat flux is reduced) from the film boiling region (where the heat flux begins to rise again), its underprediction (or overprediction) could possibly influence the final steady state temperature. This question was assessed by studying the temperature distribution for a minimum film boiling temperature calculated using the default technique in CATHENA (Hanna, 1998), with a forced transition from nucleate boiling to film boiling (i.e. by setting $T_{min} = T_{CHF} + 5$) and with the minimum film boiling temperature computed using Rajan's correlation.

Figure II.8 shows the temperature evolution as a function of time at thermocouple no.21 (Figure II.8-i) and the final internal wall temperature distribution (Figure II.8-ii). The figure shows that the prediction of the minimum film boiling temperature only has a slight influence on the wall temperature evolution while the final temperature distribution is unchanged. This results from the fact that T_{min} only bounds the beginning of the film boiling conditions. Once these conditions are reached, the predictions remain the same as depicted in the boiling curve computed for these T_{min} predictions (i.e. Figure II.9).

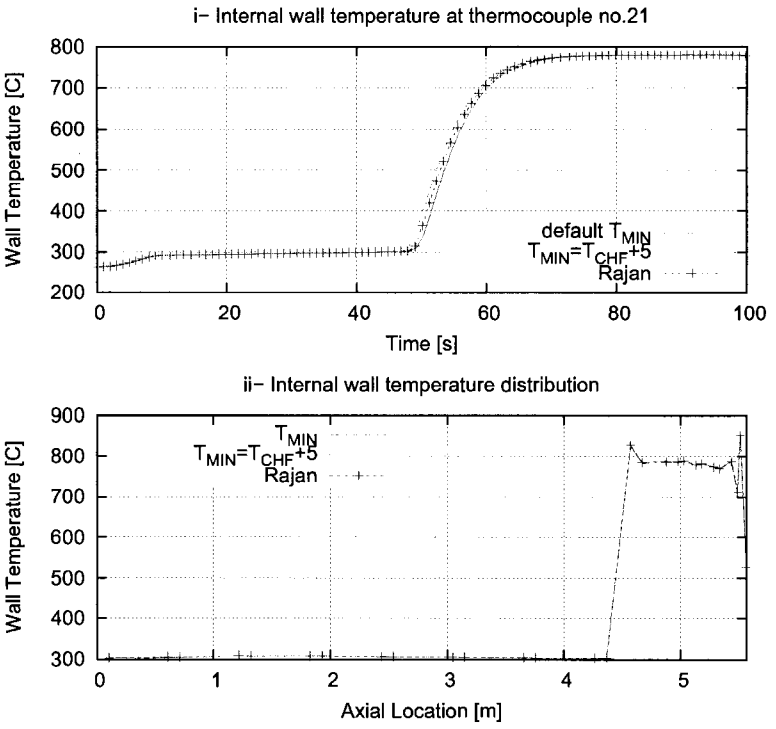

Figure II.8 Influence of the Uncertainty of the Minimum Film Boiling Temperature on the Internal Wall Temperature

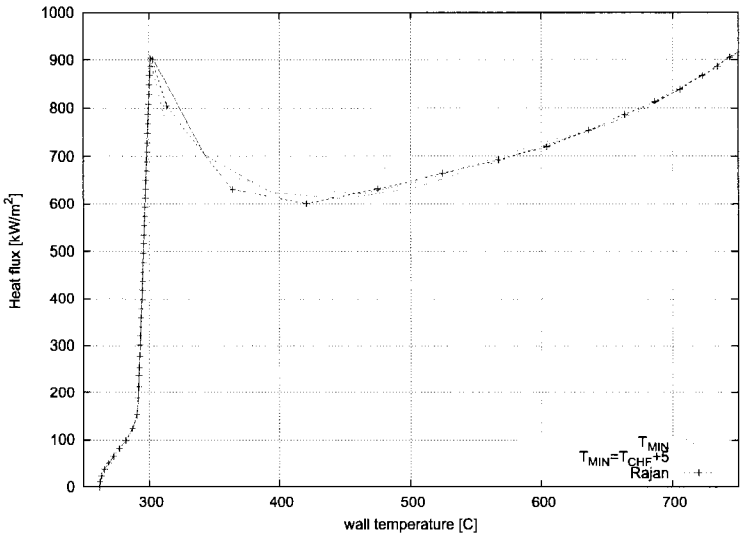

Figure II.9 Influence of the Minimum Film Boiling Temperature on the Boiling Curve

II.5 Developing Flow Film Boiling Conditions

The impact of including a correction factor that accounts for the developing PDO is studied in this section. The reference case was therefore simulated using a correction (slightly different that the one assessed in this thesis and assessed in section 4.1) without using any correction. The internal temperature distribution for these simulations is depicted in Figure II.10. The figure shows that the developing flow correction may be overestimated since it has an impact on a too large axial region when compared to the experiment and has no impact only at the lasts points. The study of the developing PDO uncertainty, however, is not the purpose of this section.

Figure II.11 presents the heat flux evolution as a function of time (Figure II.11-i) and

as a function of the internal wall temperature (Figure II.11-ii) for the same simulations. These heat flux evolutions are taken at thermocouple no.27 since the correction factor has no impact at that position at the end of the transient. The figure shows that the correction factor is applied for all heat transfer regions beyond CHF. However, the final steady-state heat flux converges to the same value and the same final temperature is reached which validates the applicability of the correction factor for steady-state predictions (using a transient calculation scheme). It is however difficult to determine whether the correction should be applied during transient calculations. Experimental data under transient conditions should be used to assess that concern.

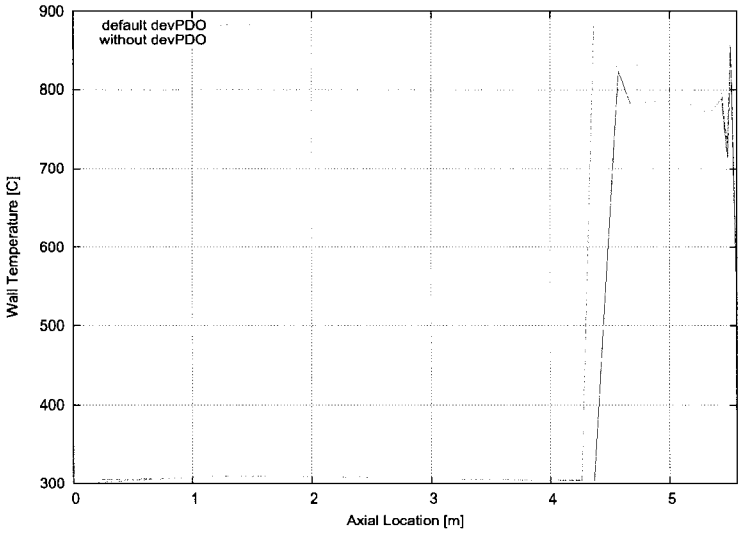

Figure II.10 Impact of the Developing PDO on Internal Wall Temperature Distributions

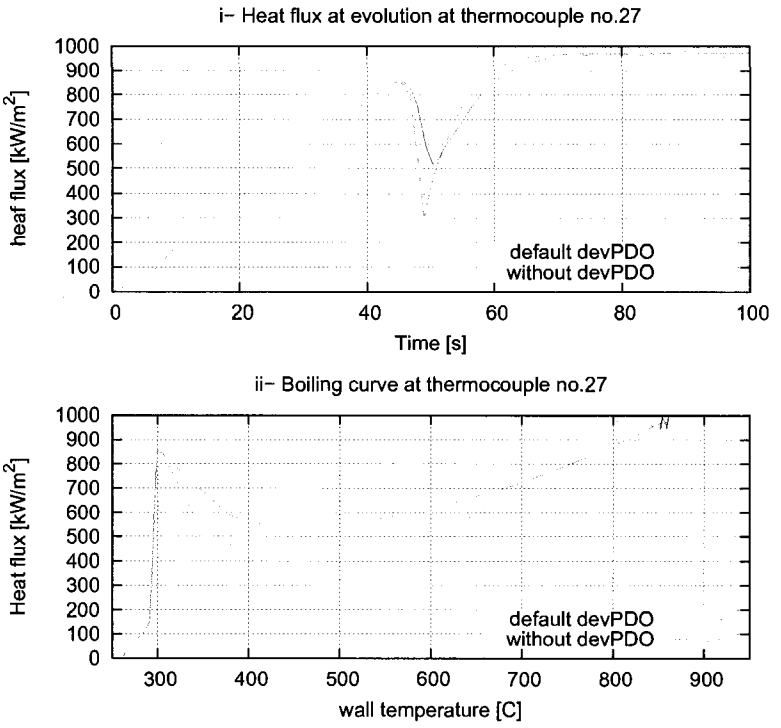

Figure II.11 Impact of the Developing PDO Effect on the Heat Flux Evolution

II.6 Film Boiling Predictions

The purpose of this chapter is to study the applicability of a Temperature-Based Methodology in a transient calculation scheme such as the one used by CATHENA (Hanna, 1998). Therefore, the predictions obtained using this methodology should be compared to the ones obtained using other methodologies.

The Figure II.12 compares the internal wall temperature predictions computed using the default T-Based LUT, the Q-Based LUT and Groneveld-Delorme's correlation (Groen-

eveld, 1988). For this case, a 50^oC temperature difference can be observed between the T-Based LUT and the Q-Based LUT predictions while the T-Based LUT and the Groenevled-Delorme correlation provide similar temperature predictions. Even if this result can not be generalized (an assessment using a wide range of experimental data would have to be performed to confirm the uncertainty of these predictions), it can be stated that the temperature distributions and evolution in the three methodologies (and therefore their applicability) in the current simulations are similar. The applicability of the temperature based methodology however, can not be totally validated (or invalidated) only based on these simulations. A complete assessment of this methodology using transient experimental data could eventually answer this concern.

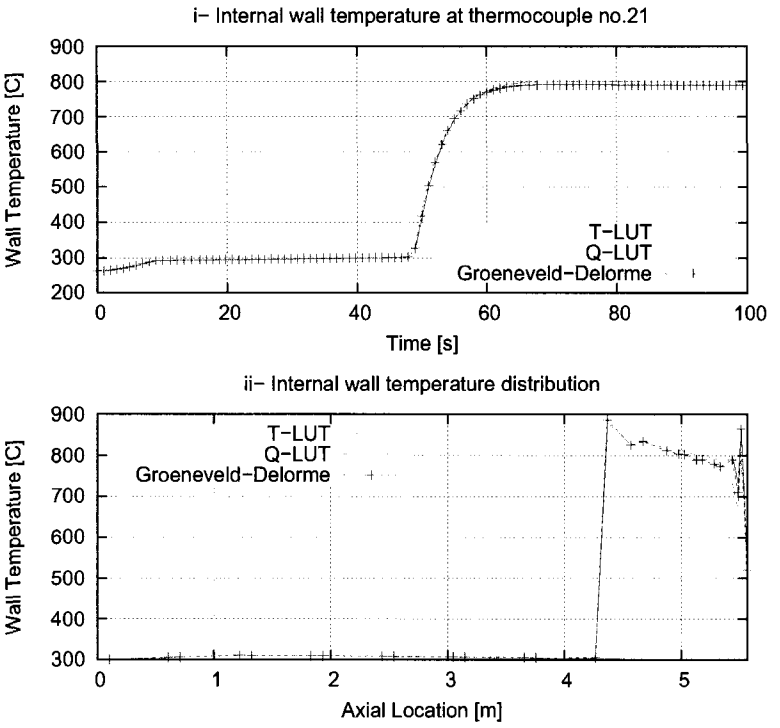

Figure II.12 Impact of the LUT Technique on the Internal Wall Temperature

II.7 Conclusions

This appendix studies the applicability of the Temperature-Based Methodology in a transient calculation scheme such as that used in the CATHENA code. It is found that thermal inertia, critical heat flux predictions, heat flux uncertainties under transition boiling conditions and minimum film boiling temperature have no impact on the final steady state wall temperature in the fully developed region. These results are essential to a methodology used in transient calculations. It is also shown that when the modification

factor that accounts for the developing PDO has no impact on the final steady state wall temperature in the fully developed region even if it is applied to the entire boiling curve (beyond CHF). However, it remains unclear whether this modification factor should be used to simulate transient effects.

The results of this appendix are based on experimental data collected under steady-state conditions (i.e. Bennett's experiments (Bennett, 1967)). Therefore, the transient heat fluxes, temperatures and heat transfer coefficients can not be validated. As a result, even if this study shows a similar applicability of the three deferent methods, the applicability of the Temperature-Based Methodology in a transient calculation scheme could only be determined by validating it using experimental data collected under transient conditions.

II.8 CATHENA Input File

```
'ELP Bennett experiment',
'insertion en 50s'/

'CONTROL GROUP'/

'SOLUTION CONTROL'/
0.0,1000.0,,0.001,0.001,0.50/

'PRINT CONTROL'/
1.0,1.0,1.0,,,,.TRUE.,'A'/

'RESTART CONTROL'/
,'bennett.rst',100.0,,.FALSE.,'C','C',0/

'NUMERICS OPTION'/
/
'PROCESSING OPTION'/
```

```
'RUN'/
'TIME STEP CONTROL'/
/
'END'/



'PIPING NETWORK'/
'RESIN'/
'PIPEBEN',  5.5626,  5.5626, 0.000124689, 0.0126, 0.0, 0.0,'CIRC', ,'H2O', , , /
0.1016, 0.5080, 0.1016, 0.5080, 0.1016, 0.5080, 0.1016, 0.5080, 0.1016, 0.5080,
0.1016, 0.5080, 0.1016, 0.5080, 0.1016, 0.2032, 0.1016, 0.2032, 0.1016,
0.0508, 0.1016, 0.0508, 0.1016, 0.0508, 0.1016, 0.0508, 0.0254, 0.0508/
'RESOUT'/
'END'/


'COMPONENT CONNECTIONS'/
'RESIN','L-PIPEBEN'/
'R-PIPEBEN', 'RESOUT'/
'END'/


'BOUNDARY CONDITIONS'/

'RESERVOIR B.C.','INCOND'/
'RESIN'/
6.893E+06, ,262.26,0.0000,'HG-BY-SAT','HF-BY-TEMP'/

'RESERVOIR B.C.','OUTCOND'/
'RESOUT'/
6.893E+06, ,,0.9,'HG-BY-SAT','HF-BY-SAT'/

'FLOW B.C.,'FLOWCON'/
'RESIN ','L-PIPEBEN'/
0.16911/

'END'/


'SYSTEM MODELS'/
'END'/
```

```
'SYSTEM CONTROL MODELS'/

'OUTPUT','GNUTEMP'/
1,'TEMPW.OUT','(F10.2,1X,2(1X, F10.3))',,1.0,,,'GNUPLOT'/
'TWALL:TUBE_B(21,1,1,1)'/
/

'OUTPUT','TDISIN'/
10,'DISTWI.OUT','(F10.2,1X,10(F10.3))',,1000.0,,,'GNUPLOT'/
'TWALL:TUBE_B(1,1,1,1)'/1
/
'TWALL:TUBE_B(2,1,1,1)'/2
/
'TWALL:TUBE_B(3,1,1,1)'/3
/
'TWALL:TUBE_B(4,1,1,1)'/4
/
'TWALL:TUBE_B(5,1,1,1)'/5
/
'TWALL:TUBE_B(6,1,1,1)'/6
/
'TWALL:TUBE_B(7,1,1,1)'/7
/
'TWALL:TUBE_B(8,1,1,1)'/8
/
'TWALL:TUBE_B(9,1,1,1)'/9
/
'TWALL:TUBE_B(10,1,1,1)'/10
/

'OUTPUT','TDISIN2'/
10,'DISTWI2.OUT','(F10.2,1X,10(F10.3))',,1000.0,,,'GNUPLOT'/
'TWALL:TUBE_B(11,1,1,1)'/1
/
'TWALL:TUBE_B(12,1,1,1)'/2
/
'TWALL:TUBE_B(13,1,1,1)'/3
/
'TWALL:TUBE_B(14,1,1,1)'/4
/
```

```
'TWALL:TUBE_B(15,1,1,1)'/5
/
'TWALL:TUBE_B(16,1,1,1)'/6
/
'TWALL:TUBE_B(17,1,1,1)'/7
/
'TWALL:TUBE_B(18,1,1,1)'/8
/
'TWALL:TUBE_B(19,1,1,1)'/9
/
'TWALL:TUBE_B(20,1,1,1)'/10
/


'OUTPUT','TDISIN3'/
8,'DISTWI3.OUT','(F10.2,1X,8(F10.3))',,1000.0,,,'GNUPLOT'/
'TWALL:TUBE_B(21,1,1,1)'/1
/
'TWALL:TUBE_B(22,1,1,1)'/2
/
'TWALL:TUBE_B(23,1,1,1)'/3
/
'TWALL:TUBE_B(24,1,1,1)'/4
/
'TWALL:TUBE_B(25,1,1,1)'/5
/
'TWALL:TUBE_B(26,1,1,1)'/6
/
'TWALL:TUBE_B(27,1,1,1)'/7
/
'TWALL:TUBE_B(28,1,1,1)'/8
/

'OUTPUT','TDISR21'/
6,'DISTRAD21.OUT','(F10.2,1X,6(F10.3))',,1000.0,,,'GNUPLOT'/
'TWALL:TUBE_B(21,1,1,1)'/1
/
'TWALL:TUBE_B(21,2,1,1)'/2
/
'TWALL:TUBE_B(21,3,1,1)'/3
/
'TWALL:TUBE_B(21,4,1,1)'/4
```

```
/
'TWALL:TUBE_B(21,5,1,1)'/5
/
'TWALL:TUBE_B(21,6,1,1)'/6
/

'OUTPUT','TDISR5'/
6,'DISTRAD5.OUT','(F10.2,1X,6(F10.3))',,1000.0,,,'GNUPLOT'/
'TWALL:TUBE_B(5,1,1,1)'/1
/
'TWALL:TUBE_B(5,2,1,1)'/2
/
'TWALL:TUBE_B(5,3,1,1)'/3
/
'TWALL:TUBE_B(5,4,1,1)'/4
/
'TWALL:TUBE_B(5,5,1,1)'/5
/
'TWALL:TUBE_B(5,6,1,1)'/6
/

'OUTPUT','PWRT'/
8,'PWRT.OUT','(F10.2,1X,8(F15.3))',,1.0,,,'GNUPLOT'/
'TOT_FLUX:TUBE_B(1-28,6,1,1)'/tot applied flux
/
'TOT_FLUX:TUBE_B(21-21,6,1,1)'/applied flux to therc #26
/
'TOT_FLUX:TUBE_B(10-10,6,1,1)'/applied flux to therc #10
/
'TOT_FLUX:TUBE_B(1-28,1,1,1)'/total flux to fluid
/
'BC_FLUX:TUBE_B(21-21,1,1,1)'/flux to fluid in thermoc. #26
/
'BC_FLUX:TUBE_B(10-10,1,1,1)'/flux to fluid in thermoc. #10
/
'BC_FLUX:TUBE_B(1-28,1,1,1)'/average heat flux to fluid
/
'BC_HTC:TUBE_B(21-21,1,1,1)'/average heat flux to fluid
/

'END'/
```

```
'HEAT TRANSFER PACKAGE'/

'MODEL:(TUBE_B)'/
'RADIAL:(1,0.0063, 6, 0.00794)', 'AXIAL:(5.5626, 28)-USER-BOUNDARY'/
0.1016,0.6096, 0.7112, 1.2192, 1.3208, 1.8288, 1.9304, 2.4384, 2.5400, 3.0480, 3.1496,
3.6576, 3.7592, 4.2672, 4.3688, 4.5720, 4.6736, 4.8768, 4.9784, 5.0292, 5.1308, 5.1816,
5.2832, 5.3340, 5.4356, 5.4864, 5.5118, 5.5626/
'BOUNDARY CONDITIONS:(1,1)'/
'INSIDE HYDRAULIC:(PIPEBEN)'/
'TUBE-CIR','HT-CRIT-DEFAULT','HT-CORR-DEFAULT',,,,,,,,,'DEV-PDO-5:()'/
'OUTSIDE PRESCRIBED:(TAG)',,,,,'SURFACE OPTION:(1)'/
'SURF-FLUX:(0.0)'/
'INCONEL'/
'HQ-TIME:(214000.,3)'/
/
0.0, 0.0,
50.0, 1.0,
2000.0, 1.0/
'TEMP-0D:(262.26)'/
'PRINT:(43111)'/

'END'/


'INITIAL CONDITIONS'/

'PIPEBEN','BY-ENDS','HG-BY-TEMP','HF-BY-TEMP'/
6.893E+06, , 262.26, 0.00000E+00,0.16911/
6.893E+06, , 262.26, 0.00000E+00,0.16911/

'RESIN ','L-PIPEBEN'/
0.16911/

'R-PIPEBEN', 'RESOUT'/
0.16911/

'END'/
```

APPENDIX III

ALGORITHM OF THE ASSESSMENT CODE

III.1 Main Function

```
      PROGRAM slpdo


USE MODULE_FILES !(contains and modify MODULE_DATA)
USE MODULE_DATA
USE MODULE_LUT_T_based
USE MODULE_LUT_Q_based
USE MODULE_CHF_LUT
  USE MODULE_PROP

CHARACTER*60 FicOutGraph
CHARACTER*4  NoRunChar

CALL DATA_SET_GEOM
CALL DATA_ASK_METHODOLOGY_AND_CORRELATION

IF(METHODOLOGY=='T') THEN
CALL GEN_HTABLE_T
ELSE
CALL GEN_HTABLE_Q
ENDIF

CALL CHF_INPUT_TABLE

DO 500 noLen=1,1

CALL DATA_SET_INPUT_DATA !Define some init parameters
CALL FILE_SET_INPUT_FILES !Define inp and out files
CALL FILE_INIT_FILES !Open and initialize inp and out files
CALL DATA_ALLOCATE_MEM_TUBE

c **********begin Loop for the nb of experiments in the fic***********c
```

```
   DO 12 IK = 1,idat

CALL FILE_GET_BENNETTexpi_VALUE

  ptDO=100  ! begin of DO (after the end of the tube)
  twloc=0
  x=0
  pow = ipow*1000.
  pin = pout
  flow=Gloc*AF
  corrCHF=0

  call proper(pin, 0.)
  if (tin .lt. tsat) then
 CALL PROPER(PIN,TIN)
 hin = hl
 XIN = (HL - HF) / HFG
 tbulk = tin
 amu = UL; rho = rhol; cp = cpl
  else
 hin = hf; xin = 0.; tbulk = tsat
 amu = uf; rho = rhof; cp = cpf
  end if
  rhoin = rho
  dhini = (hf-hin)/1000.
  X(1) = xin; xa = 0.; POW1 = POW
  do ij=1,(ntc+1)
 ploc(ij) = pout
  end do

   qavg = pow1/ah
   twmax = 0.
   imax = 1
   qratioRad(1,1)=0

c **********begin of Loop for the nb of pts in the tube************c
   DO 60 II = 2,(ntc)

QKW=qavg/1000
qratioRad(1,ii)=0
  CALL PROPER(Ploc(II),0.0) !TIN)
  HRISE   = POW1 * zlong(ii) /thl/ flow
```

```
 X(II) = (HIN + HRISE - HF) / HFG
 if (x(ii) .lt. 0.) then
tbulk = tsat - (hf - (hrise+hin))/((cp+cpf)/2)
call proper (ploc(ii),tbulk)
amu = ul; rho = rhol; cp = cpl
 else
tbulk = tsat; amu = uf; rho = rhof; cp = cpf
 end if

c           find q_CHF in the look-up table
  CALL CALCHF(ploc(ii),Gloc,de,X(ii),CHF1(ii))

c           calculate h_nb with chen correlation
  call CHENNB(Ploc(ii),Gloc,De,x(ii),qavg,tbulk,TWnb,HTCnb)
  htcnb = qavg/(twnb-tbulk)
  qratio = qavg/chf1(ii)-1
     if (ii<=nCHF) then !DO not reached (in the experimental data)
twloc(ii) = twnb
       TwlocFD(ii) = twnb
correction=qavg/chf1(ii)
Xdo = x(ii)
    if (Xdo >= 1.) then; Xdo=0.99; endif
Tchf = twloc(ii)
Tchf=Tsat+CHF1(ii)/htcnb
if (ii==nCHF) then
call ALPi(gloc,de,qavg,X(ii),alpha,xa, Re, Bo, slip, slip2)
alphaDO=alpha
corrCHF=correction
endif

           else
         chf1(ii)=chf1(ii)*correction; ! modify chf with the cst correct.
         qratio = qavg/chf1(ii)-1
call CHENNB(Ploc(ii),Gloc,De,x(ii),chf1(ii),tbulk,TWnb,HTCnb)
         Tchf=Tsat+CHF1(ii)/htcnb

 if(Methodology == 'Q') then
 temp=0
c******************Q based correlations************************
         DO while(abs(QKW-temp) >0.001)
temp=QKW
c           calculate h_PDO fully developped
```

```
c             (using look-up table or Groeneveld correlation)
 call CALPDO(Ploc(ii),gloc,De,X(ii),QKW,HTC) !!look-up table

c           calculate the correction factor and h_pdo developping film boiling
         Bo=qavg/(gloc*Hfg)  !boiling number for the modification factor
 htccor=1+(htcnb/htc-1)*exp(-0.2158*((x(ii)-Xdo)
     & /Bo/(1-Xdo))**0.6) !!latest correlation from COG-98-193
 htcbun = htc *htccor !!apply the correction factor
 twloc(ii) = qavg/htcbun+tsat !!Tw_loc corrected for developping
         TwlocFD(ii)=qavg/htc+tsat  !!Tw_loc assuming fully developped film boinilg

if(corRad=='Y') then !correct for radiation
!calculate void fraction(alpha)
call ALP1(gloc,de,qavg,x(ii),alpha,xa,Re, Bo, slip, slip2)
Qrad=RADIATION(ploc(ii),Tsat,twloc(ii),alpha,de,thl)!calculate q radiation
Qconv=qavg-Qrad
qratioRad(1,ii)=Qrad/Qavg
QKW=Qconv/1000
endif
enddo
c*************** end Q based correlations*********************

 elseif(Methodology == 'T') then
c******************T based correlations************************
!      Find the Fully developped wall tempertature
      Twguess(:)=1200
      TwlocFD(ii)=0;  test=0

call ALP1(gloc,de,qavg,X(ii),alpha,xa, Re, Bo, slip, slip2)
call PROPER(ploc(ii),Tsat)
ReynoldsG=de*gloc*x(ii)/ug


      DO while(abs(Twguess(ii)-TwlocFD(ii)) >0.001)
 delTwsat=Twguess(ii)-Tsat
 TwlocFD(ii)=Twguess(ii)

         call TableHT(Ploc(ii),gloc,De,X(ii),delTwsat,HTC)
Qconv=qavg
if(corRad=='Y') then !correct for radiation
!calculate void fraction(alpha)
call ALP1(gloc,de,qavg,x(ii),alpha,xa,Re, Bo, slip, slip2)
```

```
Qrad=RADIATION(ploc(ii),Tsat,twloc(ii),alpha,de,thl)!calculate q radiation
Qconv=qavg-Qrad
qratioRad(l,ii)=Qrad/Qavg
endif
 Twguess(ii) = Qconv/htc+tsat
         test=test+l
         if  (test>100) then;  go to 556;     endif
      END DO
  TwlocFD(ii)=qavg/htc+tsat

!      Find the developping film boiling wall Temperature
      Twguess(:)=300
      Twloc(ii)=0;  test=0
      DO while(abs(Twguess(ii)-Twloc(ii)) >0.001 .and. test<500 )
 delTwsat=Twguess(ii)-Tsat
 Twloc(ii)=Twguess(ii)
         call TableHT(Ploc(ii),gloc,De,X(ii),delTwsat,HTC)
 WSR=(Twguess(ii)-Tsat)/(Tchf-Tsat)
 if (WSR<1.) then; WSR =l; endif
if(correlation=='G')then

a=-0.8  !initial value
b=0.6   !initial value
htccor = l +(htcnb/htc-1)*exp(a*(WSR-1)**b)


! a               = -0.000761511  !   +/- 0.0001378    (18.1%)
! b               = 0.531791      !   +/- 0.01138      (2.14%)
! htccor = l +(htcnb/htc-1)*exp(a*((WSR-1)*ReynoldsG)**b)


elseif(correlation=='L')then
    htccor = l +(htcnb/htc-1)*
     &         exp(((RHOF/RHOG)**-0.18)*-1.85*(WSR-1)**0.483)
endif
         htcbun = htc*htccor
 Qconv=qavg
if(corRad=='Y') then !correct for radiation
!calculate void fraction(alpha)
call ALP1(gloc,de,qavg,x(ii),alpha,xa,Re, Bo, slip, slip2)
Qrad=RADIATION(ploc(ii),Tsat,twloc(ii),alpha,de,thl)!calculate q radiation
Qconv=qavg-Qrad
```

```
qratioRad(1,ii)=Qrad/Qavg
endif
 Twguess(ii) = Qconv/htcbun+tsat
         test=test+1
         if  (test>500) then
    test=test+1
 endif
      END DO
      Twloc(ii)=qavg/htcbun+tsat
c***************end T based correlations************************
 endif

c***************Output for PDO region************************
call PROPER(ploc(ii),Tsat)

END IF
if (twloc(ii) .gt. twmax) then !!find the max temperature
 imax = ii !position of the Max temperature
 twmax = twloc(ii)
    end if


IF ((ii>nchf) .and. (TwBEN(ii-1)>300.).and.(Tchf>286.))then
!Tchf=TwBEN(nchf)
IF (METHODOLOGY=='T') THEN
call TableHT(Ploc(ii),gloc,De,X(ii),delTwsat, hfdBen)
else
call CALPDO(Ploc(ii),gloc,De,X(ii),qavg, hfdBen)
end if
call ALP1(gloc,de,qavg,x(ii),alpha,xa,Re, Bo, slip, slip2)
tempHnb=HTCnb
tempTwBEN=TwBEN(ii-1)
  call CHENNB(Ploc(ii),Gloc,De,x(ii),qavg,tsat,tempTwBEN,tempHnb)
CALL FILE_WRITE_TEMP_OUTPUT(ii)
call WRITE_PDO_OUTPUTS(ii,htccor,htcbun,twloc(ii), TwBEN(ii-1),
     &          qratioRad(1,ii))

ENDIF

 60     CONTINUE
c **********end of Loop for the nb of pts in the tube***********c
  DO i=1,ntc            !for the outputs fic
```

```
 twbuf(1,i)=twloc(i)
 xbuf(1,i)=x(i)
  end do

CALL WRITE_FINAL_OUTPUTS

 12 CONTINUE !end Loop for the nb of experiments in the fic
 121 CONTINUE

CALL DATA_DEALLOCATE_MEM_TUBE
CALL FILE_CLOSE_FILES

IF(METHODOLOGY=='T') THEN
CALL DELETE_HTABLE_T
!ELSE

ENDIF

IF(METHODOLOGY=='Q') THEN
CALL analyse(Methodology,'fic/FD_SLPDO_RESULT_Q'
     &              ,noLen,correlation)
ELSE
CALL analyse(Methodology,'fic/FD_SLPDO_RESULT_T'
     &              ,noLen,correlation)
ENDIF

 500  END DO

CALL genGraphLen4(noLen)

 556  STOP
      END PROGRAM slpdo
```

III.2 Radiation Heat Transfer Model

```
C*****************************************************************
c radiation.for
c
c Calculates the q radiation
```

```
c assuming: - an inverted annular flow
c - circular tube
c  - vapor T = (Tsat+Tw)/2
c - no pressures loss
c - fixed void fraction
c - fluid = water
c - gas = water vapor
c - wall material = Inconel-60 (or Ni-Cr alloy)
c autor: E-L Pelletier
c date: 15/11/06
c
c*****************************************************************
REAL FUNCTION RADIATION(P,Tsat,Tw,void,dia,L)

c********* Data from main ************************************
c P= scalar, local pressure (kPa)
c Tsat= scalar, local sat temperature (C)
c Tw= scalar, local wall temperature (C)
c void=void fraction
c dia=tube inner diameter (m)
c L= nube lengh (m)

c********* Data declared in the function ***********************
c pa localpartial pressure of the participing gas
c     po reference pressure (1bar)
c Tf fluid temperature (assumed as = Tsat)
c Tvap vapor phase temperature (mean value Tw Tsat)
c StefBol:Stefan-Boltzmann cst
c emissF: emissivity of the fluid (water)
c emissW: emissivity of the wall (Inconel-60 or Ni-Cr alloy)
c emissV: emissivity of (water) the vapor film
c Ew: Black body emissive power at Tw
c Ef: Black body emissive power at Tf
c Evap: Black body emissive power at Tvap
c Fwf: View factor (wall to fluid core)
c Ffw: View factor ( fluid core to wall)
c Pe: Equivalent pressure of the gas
c a, b, c: correlations constants FOR WATER
c Cij: cij correlation constants FOR WATER
c tau: ratio Tvap/T(reference)
c Lmb: mean optical beam path
c frac: (ev/eo -1)/(ev/e0 -1)_max
```

```
c maxV: (ev/e0 -1)_max
c frac1: ev/e0
c maxfrac:(ev/e0)_max
C A, B, J:  matrix for system resolution
c RADIATION: radiation heat flux

c********* Variables declaration ********************************
REAL P, pa, po, Tsat, Tw, Tf, Tvap, void, dia
REAL StefBol, emissF, emissW, emissV, Ew, Ef, Evap
REAL Fwf, Ffw, Pe, tau, a, b, c, Cij(3,3), Lmb
REAL frac, maxV, frac1, maxfrac
REAL tempm k, w, pi
REAL Am(2,2), Bm(2), Jm(2)

c********* Initialize variables *********************************

c********** parameters from COG-90-86 example (validation)
c P=9500
c Tsat=307.2
c Tw=750
c Tvap=(Tf+Tw)/2
c void=0.2
c dia=0.009
c L=219*0.0254 !in->m
c emissF=0.775
c emissW=0.6275+0.000198*Tw !were Tw is in deg C
c*****************************************

pi = 3.1415926
!flow properties
pa=P
po=100 !kPa
Tf=Tsat
Tvap=(Tf+Tw)/2

c Geometry and material ppt
StefBol=5.67/(10**(8)) !W*m^2*K^4
emissF=0.775;!if (fluid=='water')
!if (wall_material=='Inconel-60') then !(or Ni-Cr alloy)
emissW=0.6275+0.000198*Tw !were Tw is in deg C
!else; !calculate emissW
!endif
```

```
c Convert temperatures in K
Tsat=Tsat+273.15
Tw=Tw+273.15
Tf=Tf+273.15
Tvap=Tvap+273.15

c Black Body emissive powers
Ew=StefBol*Tw**4
Ef=StefBol*Tf**4
Evap=StefBol*Tvap**4


c Calculate form factors
Fwf=(1-void)**0.5
Ffw=1

c Calculate correlation constants and variables
tau=Tvap/1000
Lmb=0.9*dia*void/(1+(1-void)**0.5)
Pe=(P/po)*(1+4.9*(pa/P)*(273/Tvap)**0.5)
c=0.5
a=1.888-2.053*log10(tau)
if (tau < 0.75) then; a=2.144; endif
b=1.10*tau**-1.4
Cij(:,1)= [-2.118, 0.85667, -0.10838]
Cij(:,2)= [-1.1987, 0.93048, -0.17156]
Cij(:,3)= [0.035596, -0.14391, 0.048915]

c Calculate the vapor film emissivity
frac=exp(-c*(log10(13.2*tau**2)-log10(Lmb*P))**2)
maxV=log10(Pe)*(1.149-0.412*tau)
frac1=1+maxV*frac
maxfrac=(a*Pe+b)/(Pe+a+b-1)
if(frac1>maxfrac) then
frac1=maxfrac
endif
emissV=0
c Calculate eo
temp=log10(P*Lmb)
Do k=1,3
Do w=1,3
```

```
emissV=emissV+Cij(k,w)*((tau)**(w-1))*(temp**(k-1))
enddo
enddo
emissV=exp(emissV)
emissV=fracl*emissV

c Solve the system
!Calculate the A matrix
Am(1,1)=-Ffw*(1-emissV)*(1-emissF)-emissF-emissV*(1-emissF)
Am(1,2)=Ffw*(1-emissV)*(1-emissF)
Am(2,1)=Fwf*(1-emissV)*(1-emissW)
Am(2,2)=-Fwf*(1-emissV)*(1-emissW)-emissW-emissV*(1-emissW)
!Calculate the B matrix
Bm(1)=-emissV*(1-emissF)*Evap-emissF*Ef
Bm(2)=-emissV*(1-emissW)*Evap-emissW*Ew
!Solve the system
temp=(Am(1,1)*Am(2,2)-Am(1,2)*Am(2,1))
Jm(1)=(Bm(1)*Am(2,2)-Bm(2)*Am(1,2))/temp
Jm(2)=(Bm(2)*Am(1,1)-Bm(1)*Am(2,1))/temp
RADIATION=emissW*(Ew-Jm(2))/(1-emissW)
if(RADIATION<0) then
RADIATION=0
endif

Tsat=Tsat-273.15
Tw=Tw-273.15 !in order to return the same value
RETURN

END FUNCTION RADIATION
```

APPENDIX IV

ASSESSMENT RESULTS

IV.1 Heat-Flux-Based-Methodology

IV.1.1 Errors and Maximum Temperatures

Table IV.1: Errors and Maximum Temperatures for the 5.56 m Test Section Using a Heat-Flux-Based Methodology

Run#	G	Tin	Pwr	CHF_{cor}	T_{MaxExp}	$T_{maxCode}$	$ErrT_{max}$	Err_{PDO}	STD
	$\left[\frac{kg}{m^2 s}\right]$	$[^oC]$	$[kW]$		$[^oC]$	$[^oC]$	[%]	[%]	[%]
5239	1356.	260.	166	0.5780	485.8	450.6	-7.25	-14.19	6.94
5240	1356.	260.	167	0.5948	492.6	452.4	-8.15	-16.23	8.07
5241	1370.	261.	168	0.5797	507.4	511.6	0.84	-11.65	10.78
5242	1356.	261.	170	0.5620	527.9	565.4	7.10	-2.24	8.33
5243	1356.	263.	174	0.6519	549.3	570.0	3.78	-7.51	12.18
5244	1356.	262.	174	0.5722	554.5	581.1	4.80	-1.13	7.94
5245	1356.	263.	177	0.5963	566.3	585.2	3.33	-1.96	9.76
5246	1356.	260.	180	0.5437	577.5	595.4	3.10	5.16	1.81
5247	1356.	259.	186	0.5579	596.1	606.5	1.74	2.43	3.56
5248	1261.	261.	189	0.7188	604.2	618.2	2.32	1.96	4.45
5249	1356.	260.	194	0.6080	616.3	619.2	0.46	-0.54	4.68
5250	1356.	263.	202	0.5428	627.2	641.5	2.27	2.29	4.65
5251	1356.	262.	214	0.5452	650.8	667.7	2.60	1.24	5.48
5252	1356.	263.	209	0.6205	638.2	648.0	1.54	0.63	1.89
5253	1356.	265.	199	0.6542	610.7	624.2	2.22	0.09	4.64
5254	1343.	267.	185	0.6318	579.6	600.6	3.62	3.80	4.15
5255	1356.	269.	176	0.6509	552.7	578.5	4.68	-0.82	10.12

...continued on next page.

Run#	G	Tin	Pwr	CHF_{cor}	T_{MaxExp}	$T_{MaxCode}$	$ErrT_{max}$	Err_{PDO}	STD
5256	1356.	270.	172	0.6756	533.0	568.5	6.66	-2.42	11.83
5257	1356.	271.	169	0.6706	512.5	559.3	9.13	-1.28	11.08
5258	1370.	271.	163	0.6925	453.9	368.6	-18.79	-18.79	0.00
5260	1044.	260.	147	0.5959	454.9	393.8	-13.43	-13.43	0.00
5261	1044.	260.	150	0.5705	498.6	581.6	16.65	4.02	12.53
5262	1044.	261.	150	0.6008	492.7	559.2	13.50	-0.11	13.63
5263	1004.	261.	152	0.6308	520.4	604.9	16.23	7.10	12.22
5264	1017.	258.	153	0.6065	519.0	603.9	16.35	6.89	12.76
5265	1004.	260.	155	0.6158	546.9	614.8	12.41	8.48	10.96
5266	1004.	261.	155	0.6249	548.9	614.1	11.88	7.71	11.59
5267	1004.	260.	157	0.6471	558.4	618.2	10.71	6.41	11.97
5268	1004.	261.	160	0.6095	582.8	628.9	7.91	8.51	4.10
5269	1004.	262.	164	0.5111	601.0	647.6	7.75	12.11	7.79
5270	1004.	262.	168	0.6152	611.3	650.7	6.44	6.99	3.38
5271	1004.	261.	176	0.5333	631.0	678.6	7.54	9.12	6.82
5272	1004.	262.	184	0.5023	645.9	702.0	8.68	11.04	18.54
5273	1017.	260.	203	0.5421	669.6	740.3	10.56	5.29	9.45
5274	1031.	264.	215	0.9306	688.4	738.9	7.34	0.07	5.36
5275	1031.	261.	189	0.6748	641.6	691.5	7.77	6.24	4.74
5276	1017.	261.	175	0.6995	613.4	659.2	7.46	8.10	4.04
5277	1031.	260.	155	0.6758	507.3	595.3	17.34	9.52	12.65
5278	1017.	262.	153	0.6735	503.4	595.4	18.27	9.28	14.44
5279	1044.	261.	152	0.6360	494.3	564.3	14.15	3.15	16.27
5282	1939.	268.	190	0.6284	581.7	464.6	-20.13	-27.95	12.16
5283	1939.	268.	193	0.6472	517.3	502.3	-2.91	-19.90	8.55
5285	1953.	265.	197	0.6500	514.4	506.5	-1.54	-12.69	4.35
5286	1953.	264.	203	0.6900	547.6	533.0	-2.67	-18.47	10.79
5287	1953.	264.	206	0.6662	558.5	552.3	-1.10	-11.22	11.81
5288	1953.	264.	209	0.6144	566.3	563.6	-0.47	-3.79	6.46
5289	1953.	265.	213	0.6741	574.1	564.8	-1.61	-6.05	8.39
5290	1953.	265.	218	0.6776	582.3	573.7	-1.47	-5.37	7.91

...continued on next page.

Run#	G	Tin	Pwr	CHF_{cor}	T_{MaxExp}	$T_{MaxCode}$	$ErrT_{max}$	Err_{PDO}	STD
5291	1953.	263.	229	0.7180	602.7	588.3	-2.38	-5.63	7.36
5292	1967.	266.	233	0.6061	607.9	608.5	0.11	0.36	3.66
5293	1980.	265.	237	0.7471	601.0	595.2	-0.96	-3.93	6.26
5294	1953.	266.	242	0.6852	618.6	612.7	-0.96	-2.02	1.74
5295	1980.	264.	230	0.8062	586.3	579.8	-1.11	-4.87	7.60
5296	1994.	265.	219	0.7318	566.7	566.8	0.02	-3.88	7.57
5297	1994.	266.	213	0.7879	552.2	552.2	0.00	-9.90	11.93
5298	1980.	261.	210	0.7353	535.3	539.3	0.75	-12.13	6.52
5302	2577.	266.	223	0.7966	494.7	399.3	-19.28	-24.41	5.12
5303	2577.	268.	219	0.7819	492.0	397.1	-19.29	-24.72	5.71
5304	2563.	267.	226	0.8033	511.8	487.4	-4.77	-14.66	7.95
5305	2577.	267.	229	0.8323	517.2	488.6	-5.53	-17.15	10.39
5306	2577.	267.	231	0.8325	531.5	510.8	-3.90	-15.81	11.52
5307	2509.	266.	232	0.8677	538.4	515.2	-4.30	-15.99	12.24
5308	2577.	264.	241	0.8419	546.7	537.0	-1.77	-9.90	12.05
5309	2550.	265.	243	0.9061	554.2	537.3	-3.05	-10.76	12.63
5310	2550.	266.	249	0.7925	565.2	554.8	-1.83	-4.75	7.96
5311	2550.	263.	250	0.8427	567.6	551.7	-2.80	-5.87	9.09
5312	2536.	265.	257	0.8122	581.9	565.0	-2.91	-5.17	8.01
5313	2536.	265.	265	0.8186	595.1	575.4	-3.32	-5.26	7.67
5314	2550.	267.	259	0.7834	579.2	569.6	-1.65	-4.08	6.98
5315	2523.	264.	246	0.8228	557.0	550.1	-1.24	-4.08	8.51
5316	2523.	265.	239	0.8707	573.4	536.5	-6.43	-10.17	14.18
5317	2523.	266.	230	0.8686	519.2	492.2	-5.20	-16.79	10.88
5318	2523.	264.	229	0.8526	501.7	456.6	-8.98	-12.99	4.77
5319	2563.	267.	229	0.9400	494.1	403.0	-18.43	-24.12	5.69
5367	3852.	274.	281	1.1698	424.3	337.8	-20.38	-20.38	0.00
5368	3852.	273.	287	1.1105	493.6	460.2	-6.76	-17.18	11.61
5369	3852.	271.	290	1.0616	495.3	482.6	-2.56	-9.03	8.84
5370	3852.	273.	298	1.2303	509.6	484.5	-4.92	-14.12	12.72
5371	3852.	274.	300	1.1730	515.5	503.3	-2.36	-8.12	11.85

...continued on next page.

Run#	G	Tin	Pwr	CHF_{cor}	T_{MaxExp}	$T_{MaxCode}$	$ErrT_{max}$	Err_{PDO}	STD
5372	3852.	274.	307	1.1281	521.7	514.5	-1.38	-3.32	9.52
5373	3852.	273.	309	1.1418	526.9	515.8	-2.12	-3.85	9.87
5374	3852.	274.	323	1.1437	545.9	529.3	-3.04	-1.83	10.86
5375	3838.	274.	322	1.0631	545.6	533.8	-2.16	-0.65	4.24
5376	3852.	271.	341	1.0329	555.9	554.8	-0.21	0.69	2.31
5377	3811.	270.	344	1.0522	571.8	559.1	-2.22	-1.07	4.18
5378	3811.	272.	348	0.9797	584.6	571.0	-2.32	1.52	3.88
5379	3798.	274.	377	1.0862	644.1	594.6	-7.68	-0.47	5.92
5380	3852.	273.	373	1.1782	614.5	577.9	-5.96	-0.19	5.33
5381	3825.	277.	344	1.1935	567.6	548.9	-3.29	-0.39	4.36
5382	3852.	271.	322	1.1653	536.0	527.2	-1.64	-3.64	8.53
5383	3906.	271.	316	1.3102	522.2	509.9	-2.36	-8.71	12.41
5384	3892.	274.	305	1.3514	508.8	485.3	-4.62	-13.97	12.60
5385	3906.	271.	300	1.2710	498.3	433.9	-12.93	-19.27	9.23
5386	3892.	271.	291	1.2351	428.9	339.2	-20.91	-20.91	0.00
5388	5181.	270.	359	1.3156	427.1	337.4	-21.00	-21.00	0.00
5389	5181.	270.	358	1.2048	482.4	444.1	-7.94	-9.77	7.53
5390	5167.	271.	368	1.3011	494.9	463.3	-6.39	-12.41	12.83
5391	5181.	270.	366	1.2394	500.0	463.7	-7.25	-13.48	12.64
5392	5154.	274.	367	1.1918	498.8	483.6	-3.05	-2.44	7.14
5393	5140.	270.	374	1.1673	509.2	491.9	-3.39	-4.32	8.92
5394	5181.	271.	388	1.1405	524.2	502.5	-4.14	-4.23	8.80
5395	5181.	271.	394	1.1219	529.4	509.3	-3.79	-1.50	4.76
5396	5235.	267.	404	1.1024	537.8	515.4	-4.16	-1.52	10.34
5397	5181.	270.	406	1.0745	543.4	524.9	-3.40	-2.00	4.46

IV.2 Temperature-Based-Methodology

IV.2.1 Errors and Maximum Temperatures

Table IV.2: Errors and Maximum Temperatures for the 5.56 m Test Section Using a Temperature-Based Methodology

Run#	G	Tin	Pwr	CHF_{cor}	T_{MaxExp}	$T_{maxCode}$	$ErrT_{max}$	Err_{PDO}	STD
	$\left[\frac{kg}{m^2 s}\right]$	$[^oC]$	$[kW]$		$[^oC]$	$[^oC]$	[%]	[%]	[%]
5239	1356	260	166	0.5780	485.8	552.1	13.64	15.97	2.33
5240	1356	260	167	0.5948	492.6	552.3	12.12	12.70	0.58
5241	1370	261	168	0.5797	507.4	554.9	9.35	10.66	1.61
5242	1356	261	170	0.5620	527.9	565.0	7.03	13.83	9.36
5243	1356	263	174	0.6519	549.3	563.8	2.64	4.96	1.93
5244	1356	262	174	0.5722	554.5	573.7	3.46	10.06	9.01
5245	1356	263	177	0.5963	566.3	577.7	2.01	6.85	5.31
5246	1356	260	180	0.5437	577.5	596.1	3.22	9.98	12.23
5247	1356	259	186	0.5579	596.1	610.9	2.49	4.96	6.76
5248	1261	261	189	0.7188	604.2	616.6	2.06	3.45	3.43
5249	1356	260	194	0.6080	616.3	624.0	1.25	1.25	4.34
5250	1356	263	202	0.5428	627.2	660.2	5.26	2.48	7.40
5251	1356	262	214	0.5452	650.8	697.0	7.10	1.83	9.06
5252	1356	263	209	0.6205	638.2	661.5	3.66	0.72	3.39
5253	1356	265	199	0.6542	610.7	629.8	3.12	2.01	4.18
5254	1343	267	185	0.6318	579.6	596.7	2.96	5.32	4.66
5255	1356	269	176	0.6509	552.7	568.5	2.86	6.79	4.20
5256	1356	270	172	0.6756	533.0	557.2	4.54	7.23	2.41
5257	1356	271	169	0.6706	512.5	551.0	7.51	10.95	3.83
5258	1370	271	163	0.6925	453.9	527.0	16.10	16.10	0.00
5260	1044	260	147	0.5959	454.9	575.2	26.45	26.45	0.00
5261	1044	260	150	0.5705	498.6	587.9	17.90	20.97	3.69
5262	1044	261	150	0.6008	492.7	583.8	18.50	20.16	1.24

...continued on next page.

Run#	G	Tin	Pwr	CHF_{cor}	T_{MaxExp}	$T_{MaxCode}$	$ErrT_{max}$	Err_{PDO}	STD
5263	1004	261	152	0.6308	520.4	598.3	14.96	18.51	3.73
5264	1017	258	153	0.6065	519.0	599.9	15.59	19.44	3.49
5265	1004	260	155	0.6158	546.9	608.9	11.34	15.28	5.50
5266	1004	261	155	0.6249	548.9	607.6	10.70	14.07	4.43
5267	1004	260	157	0.6471	558.4	610.5	9.32	12.24	3.69
5268	1004	261	160	0.6095	582.8	624.7	7.19	9.36	4.29
5269	1004	262	164	0.5111	601.0	659.9	9.80	10.66	10.18
5270	1004	262	168	0.6152	611.3	648.7	6.11	6.87	6.38
5271	1004	261	176	0.5333	631.0	686.7	8.83	6.99	9.35
5272	1004	262	184	0.5023	645.9	717.6	11.10	9.60	22.32
5273	1017	260	203	0.5421	669.6	759.9	13.49	5.12	11.43
5274	1031	264	215	0.9306	688.4	721.1	4.75	-6.89	15.02
5275	1031	261	189	0.6748	641.6	688.1	7.24	4.19	5.63
5276	1017	261	175	0.6995	613.4	651.3	6.18	7.17	6.04
5277	1031	260	155	0.6758	507.3	593.3	16.96	24.30	6.55
5278	1017	262	153	0.6735	503.4	592.0	17.60	23.13	4.37
5279	1044	261	152	0.6360	494.3	585.3	18.41	22.67	3.92
5282	1939	268	190	0.6284	581.7	530.7	-8.77	-0.89	8.98
5283	1939	268	193	0.6472	517.3	536.7	3.74	3.96	1.06
5285	1953	265	197	0.6500	514.4	542.7	5.50	15.55	14.51
5286	1953	264	203	0.6900	547.6	551.7	0.75	1.39	0.67
5287	1953	264	206	0.6662	558.5	559.2	0.12	1.65	1.49
5288	1953	264	209	0.6144	566.3	570.5	0.74	3.06	3.73
5289	1953	265	213	0.6741	574.1	572.2	-0.34	0.18	0.90
5290	1953	265	218	0.6776	582.3	582.0	-0.04	0.10	1.30
5291	1953	263	229	0.7180	602.7	601.2	-0.26	-0.42	1.94
5292	1967	266	233	0.6061	607.9	626.7	3.09	2.59	7.58
5293	1980	265	237	0.7471	601.0	611.7	1.78	1.31	3.48
5294	1953	266	242	0.6852	618.6	635.3	2.71	0.16	2.61
5295	1980	264	230	0.8062	586.3	591.9	0.95	0.73	1.65
5296	1994	265	219	0.7318	566.7	574.5	1.38	2.55	1.93

...continued on next page.

Run#	G	Tin	Pwr	CHF_{cor}	T_{MaxExp}	$T_{MaxCode}$	$ErrT_{max}$	Err_{PDO}	STD
5297	1994	266	213	0.7879	552.2	559.9	1.39	2.70	1.26
5298	1980	261	210	0.7353	535.3	558.9	4.41	10.87	9.94
5302	2577	266	223	0.7966	494.7	504.5	1.98	2.39	0.40
5303	2577	268	219	0.7819	492.0	499.2	1.47	1.25	0.58
5304	2563	267	226	0.8033	511.8	514.8	0.59	4.09	5.80
5305	2577	267	229	0.8323	517.2	516.3	-0.17	0.51	1.18
5306	2577	267	231	0.8325	531.5	521.0	-1.97	-1.38	1.49
5307	2509	266	232	0.8677	538.4	528.4	-1.86	-1.37	2.01
5308	2577	264	241	0.8419	546.7	536.8	-1.81	-0.38	1.83
5309	2550	265	243	0.9061	554.2	539.4	-2.67	-1.46	2.10
5310	2550	266	249	0.7925	565.2	559.1	-1.08	-0.23	1.70
5311	2550	263	250	0.8427	567.6	554.5	-2.32	-0.97	1.61
5312	2536	265	257	0.8122	581.9	574.7	-1.24	-0.55	1.55
5313	2536	265	265	0.8186	595.1	590.4	-0.80	-0.49	1.74
5314	2550	267	259	0.7834	579.2	584.0	0.83	0.49	2.40
5315	2523	264	246	0.8228	557.0	552.6	-0.80	0.94	1.56
5316	2523	265	239	0.8707	573.4	538.2	-6.13	-1.10	3.66
5317	2523	266	230	0.8686	519.2	521.9	0.52	1.02	1.53
5318	2523	264	229	0.8526	501.7	518.2	3.30	12.33	12.53
5319	2563	267	229	0.9400	494.1	503.9	1.99	1.48	0.51
5367	3852	274	281	1.1698	424.3	449.1	5.84	5.84	0.00
5368	3852	273	287	1.1105	493.6	500.5	1.39	3.63	2.87
5369	3852	271	290	1.0616	495.3	510.4	3.04	10.23	9.68
5370	3852	273	298	1.2303	509.6	505.5	-0.81	1.44	3.71
5371	3852	274	300	1.1730	515.5	513.3	-0.43	3.04	2.99
5372	3852	274	307	1.1281	521.7	528.7	1.34	3.50	2.75
5373	3852	273	309	1.1418	526.9	530.3	0.64	2.93	2.95
5374	3852	274	323	1.1437	545.9	552.8	1.26	4.62	5.23
5375	3838	274	322	1.0631	545.6	564.3	3.42	6.96	9.68
5376	3852	271	341	1.0329	555.9	597.5	7.49	5.89	5.28
5377	3811	270	344	1.0522	571.8	600.5	5.02	3.72	2.79

...continued on next page.

Run#	G	Tin	Pwr	CHF_{cor}	T_{MaxExp}	$T_{MaxCode}$	$ErrT_{max}$	Err_{PDO}	STD
5378	3811	272	348	0.9797	584.6	616.0	5.37	6.43	8.52
5379	3798	274	377	1.0862	644.1	636.8	-1.14	3.34	3.14
5380	3852	273	373	1.1782	614.5	617.7	0.53	3.77	2.61
5381	3825	277	344	1.1935	567.6	585.4	3.13	3.41	2.31
5382	3852	271	322	1.1653	536.0	548.6	2.35	3.29	1.67
5383	3906	271	316	1.3102	522.2	520.0	-0.42	2.34	3.03
5384	3892	274	305	1.3514	508.8	502.8	-1.18	0.59	3.79
5385	3906	271	300	1.2710	498.3	498.5	0.03	2.75	3.12
5386	3892	271	291	1.2351	428.9	468.7	9.28	9.28	0.00
5388	5181	270	359	1.3156	427.1	320.8	-24.90	-24.90	0.00
5389	5181	270	358	1.2048	482.4	453.6	-5.98	-5.43	7.38
5390	5167	271	368	1.3011	494.9	462.6	-6.52	-9.18	13.78
5391	5181	270	366	1.2394	500.0	463.8	-7.23	-9.75	13.45
5392	5154	274	367	1.1918	498.8	482.1	-3.35	-0.19	4.54
5393	5140	270	374	1.1673	509.2	491.5	-3.47	-1.66	4.16
5394	5181	271	388	1.1405	524.2	505.5	-3.58	-0.69	5.17
5395	5181	271	394	1.1219	529.4	514.1	-2.89	3.12	8.21
5396	5235	267	404	1.1024	537.8	524.7	-2.44	3.39	7.50
5397	5181	270	406	1.0745	543.4	535.2	-1.50	1.49	4.10

IV.3 Figures

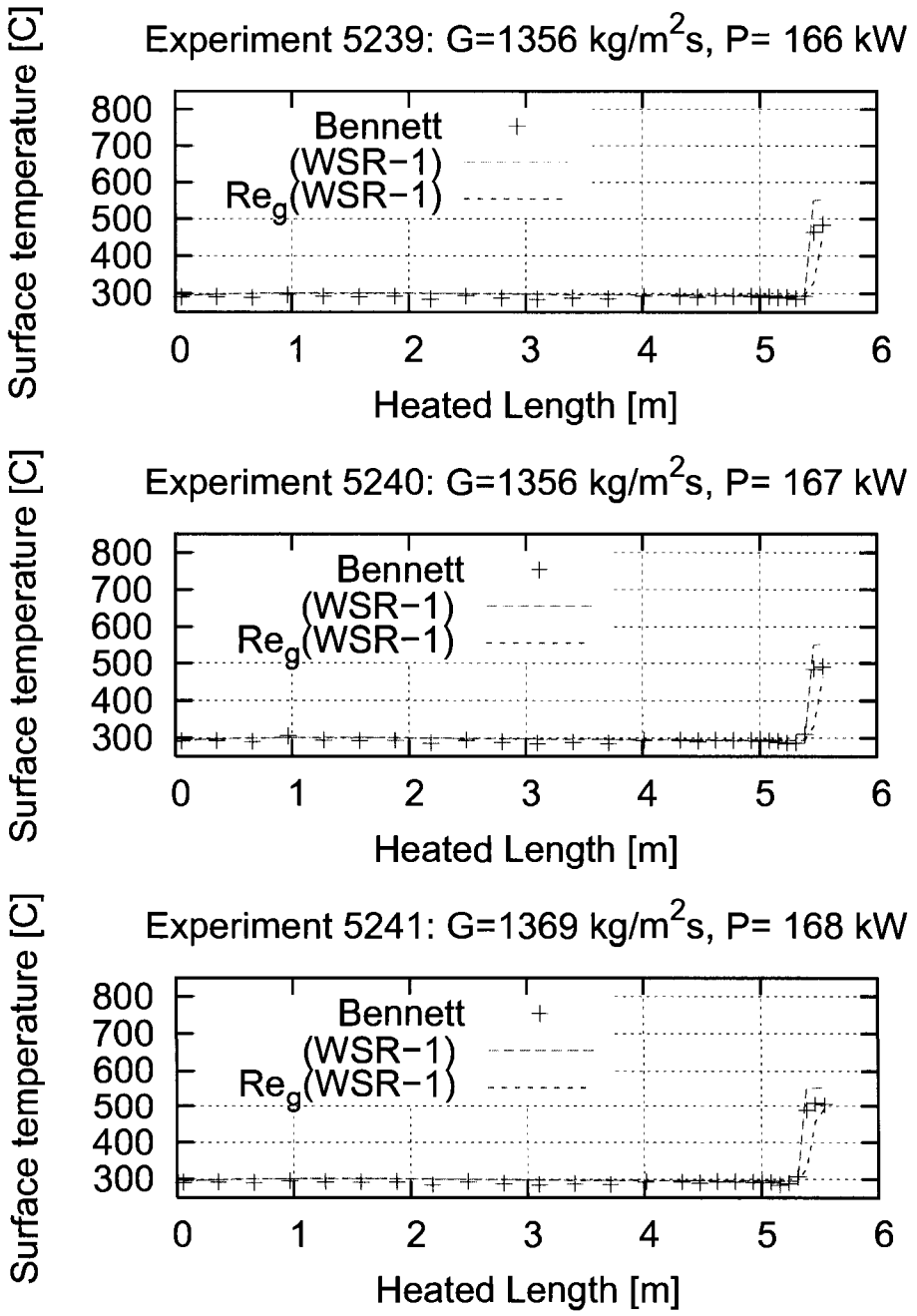

Figure IV.1 Experiments 5239, 5240 and 5241

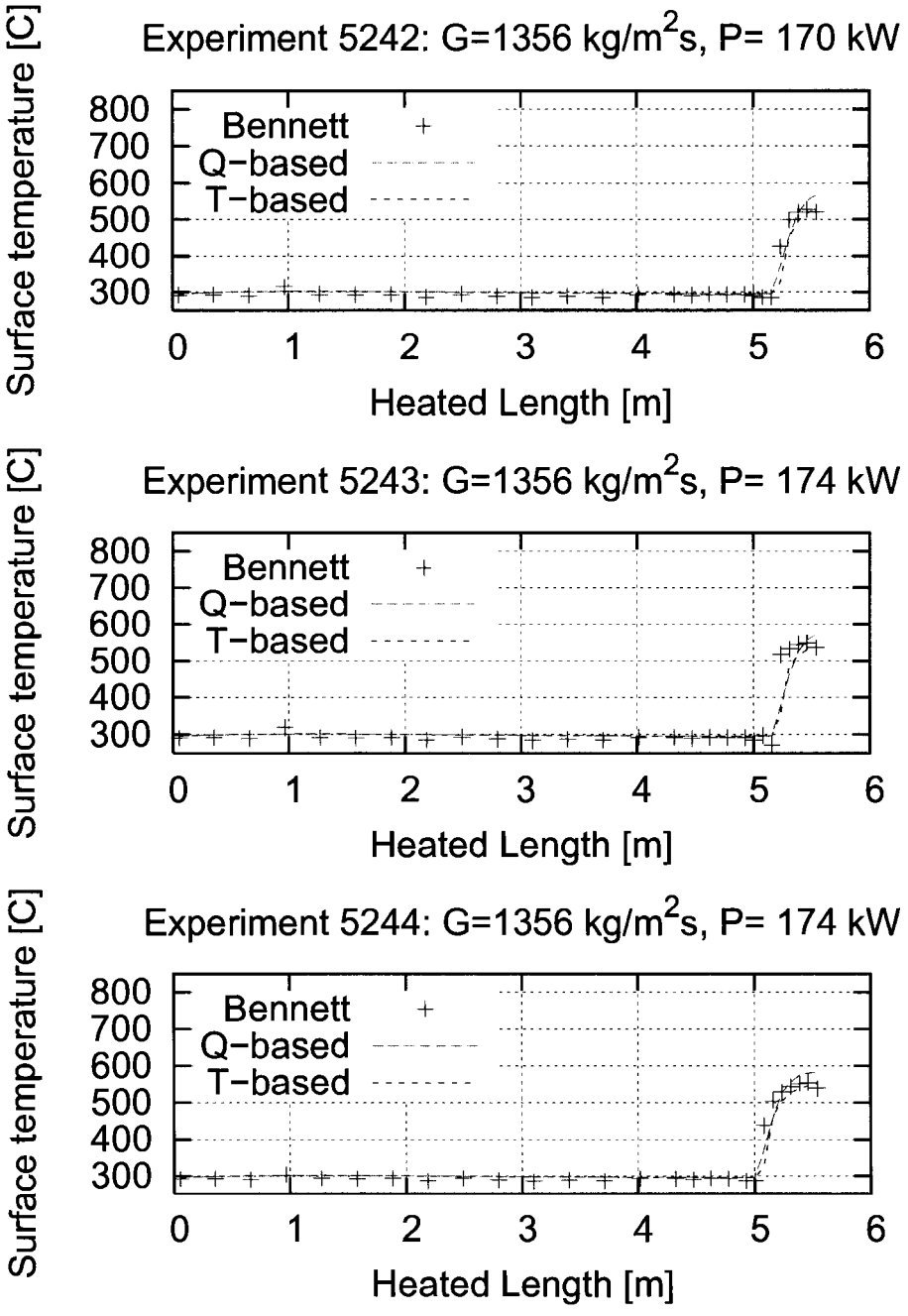

Figure IV.2 Experiments 5242, 5243 and 5244

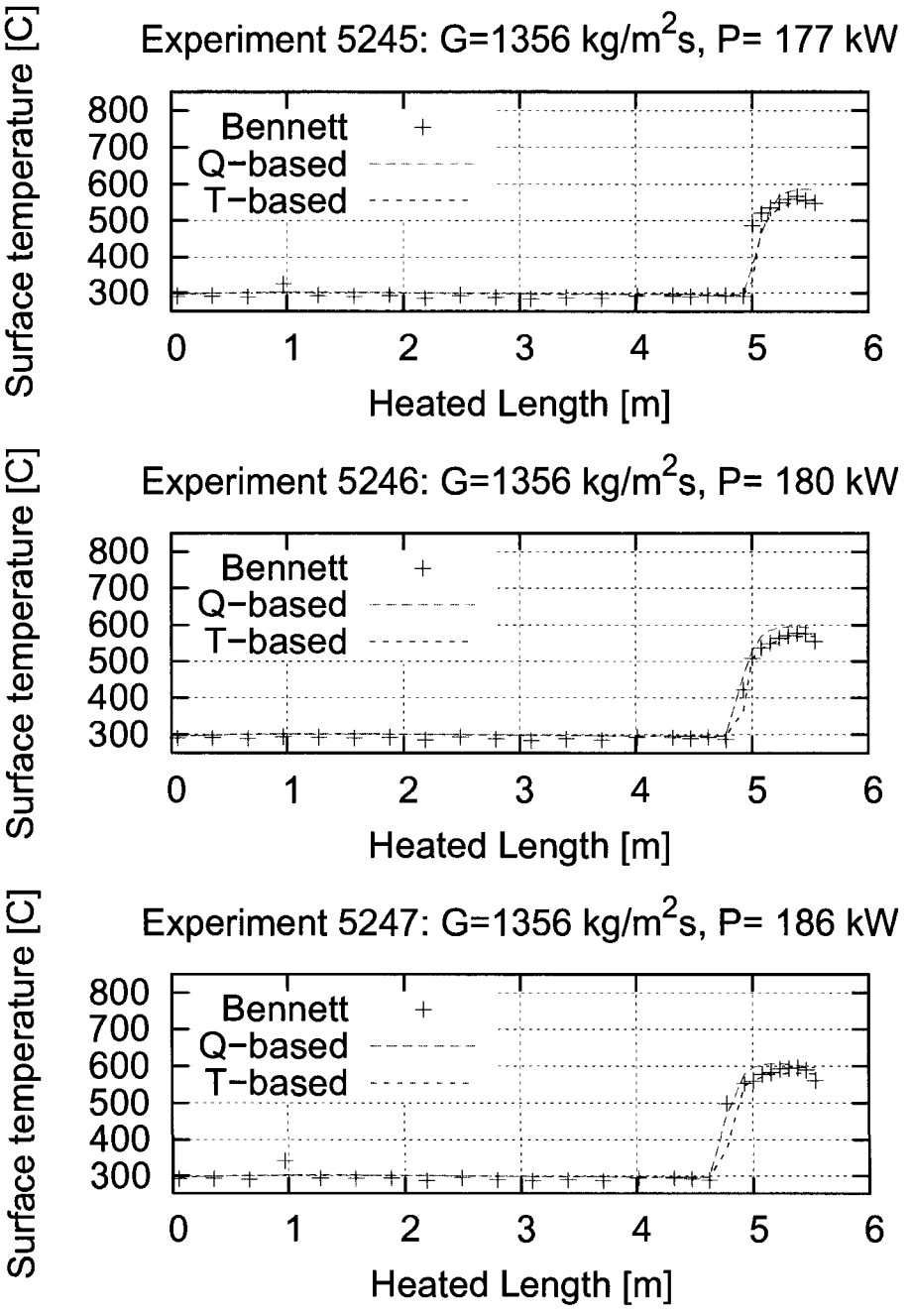

Figure IV.3 Experiments 5245, 5246 and 5247

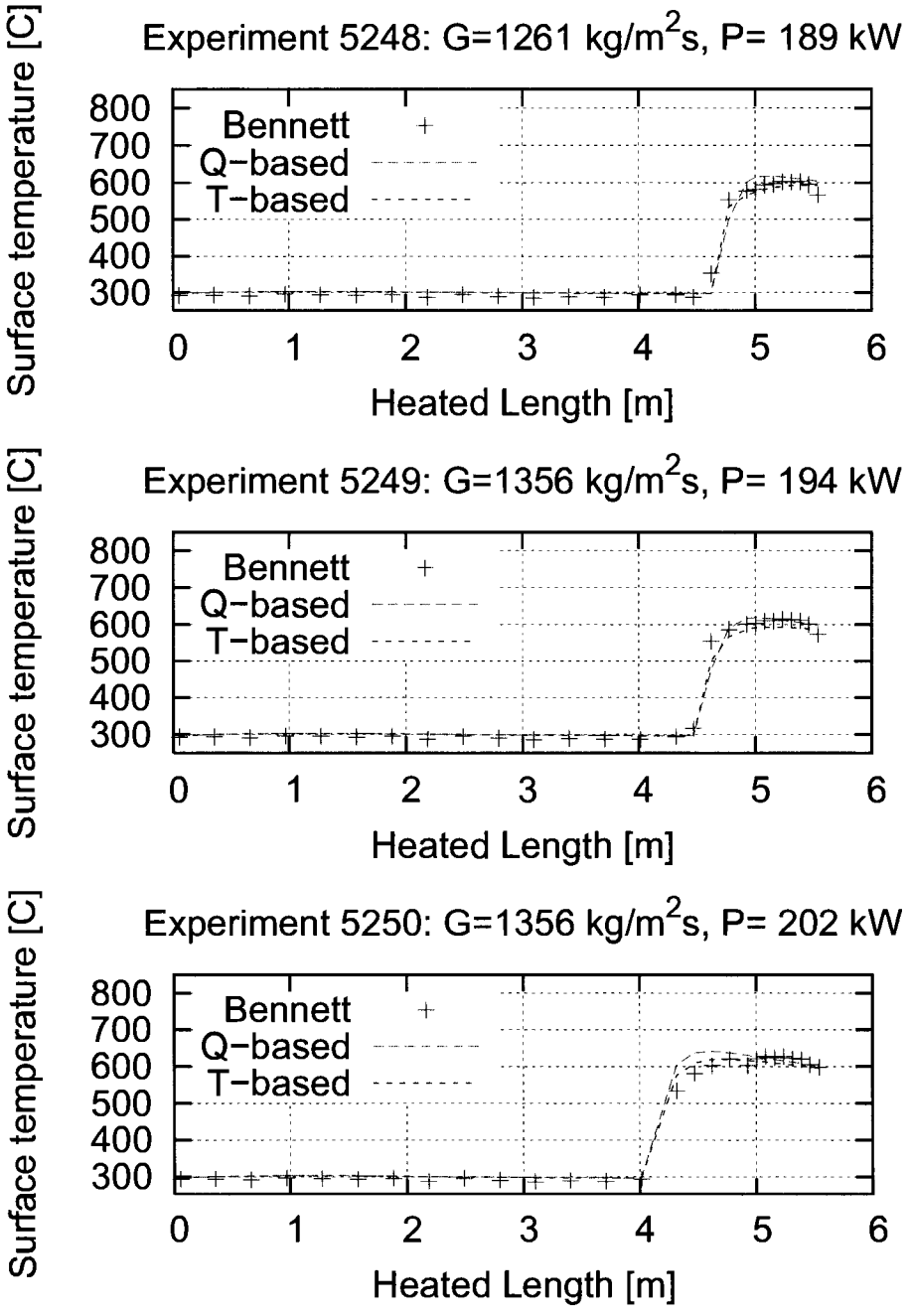

Figure IV.4 Experiments 5278, 5249 and 5250

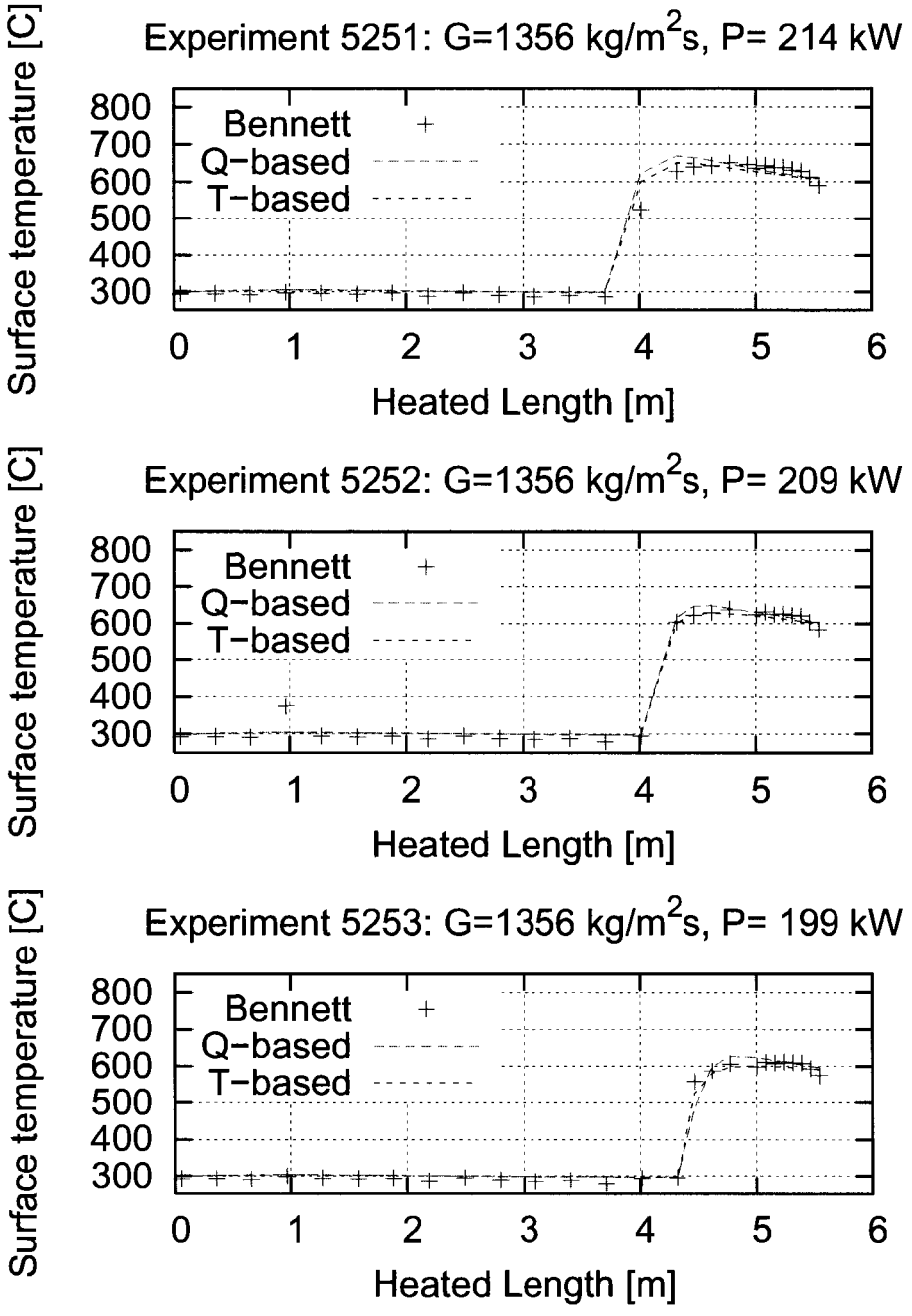

Figure IV.5 Experiments 5251, 5252 and 5253

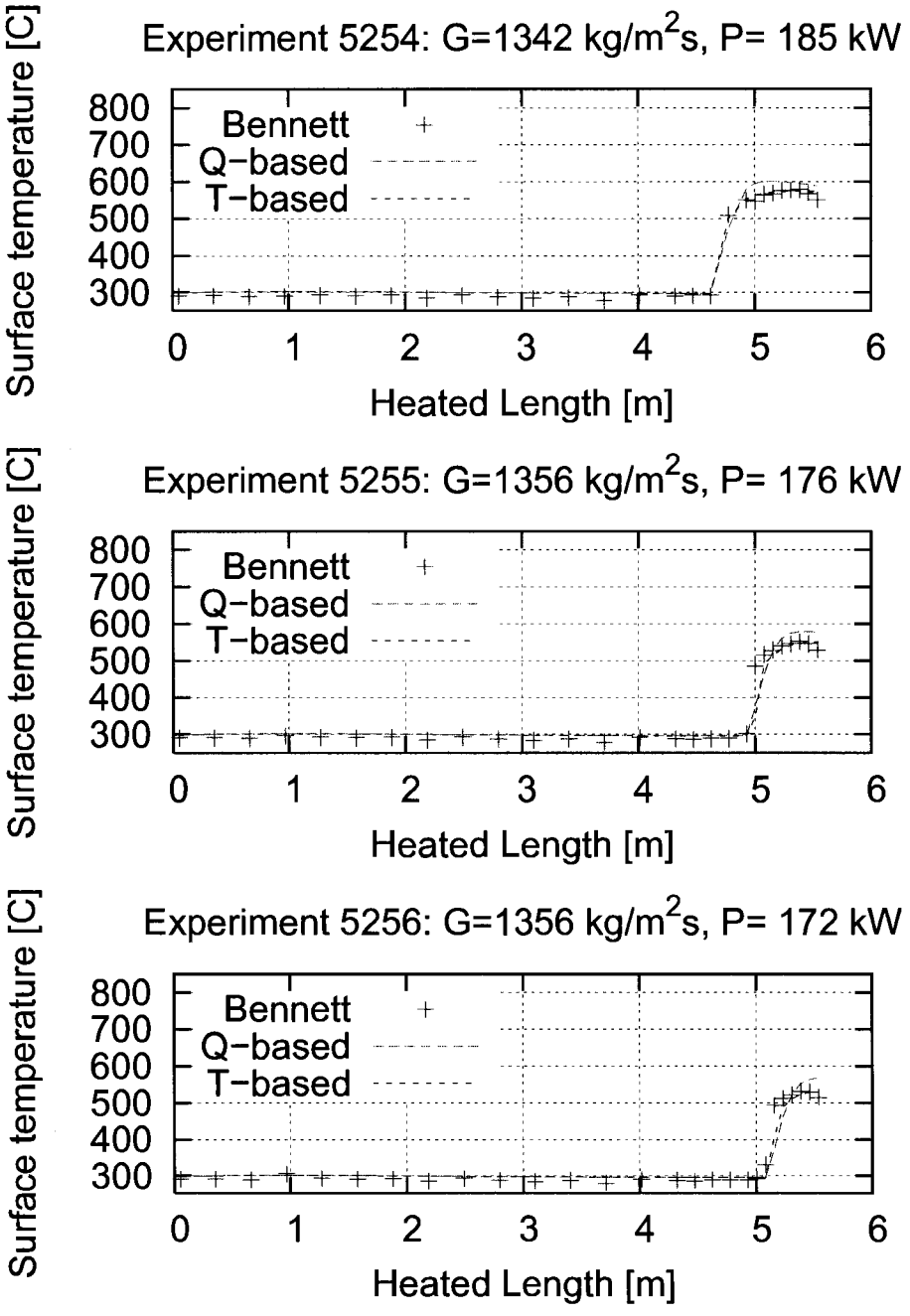

Figure IV.6 Experiments 5254, 5255 and 5256

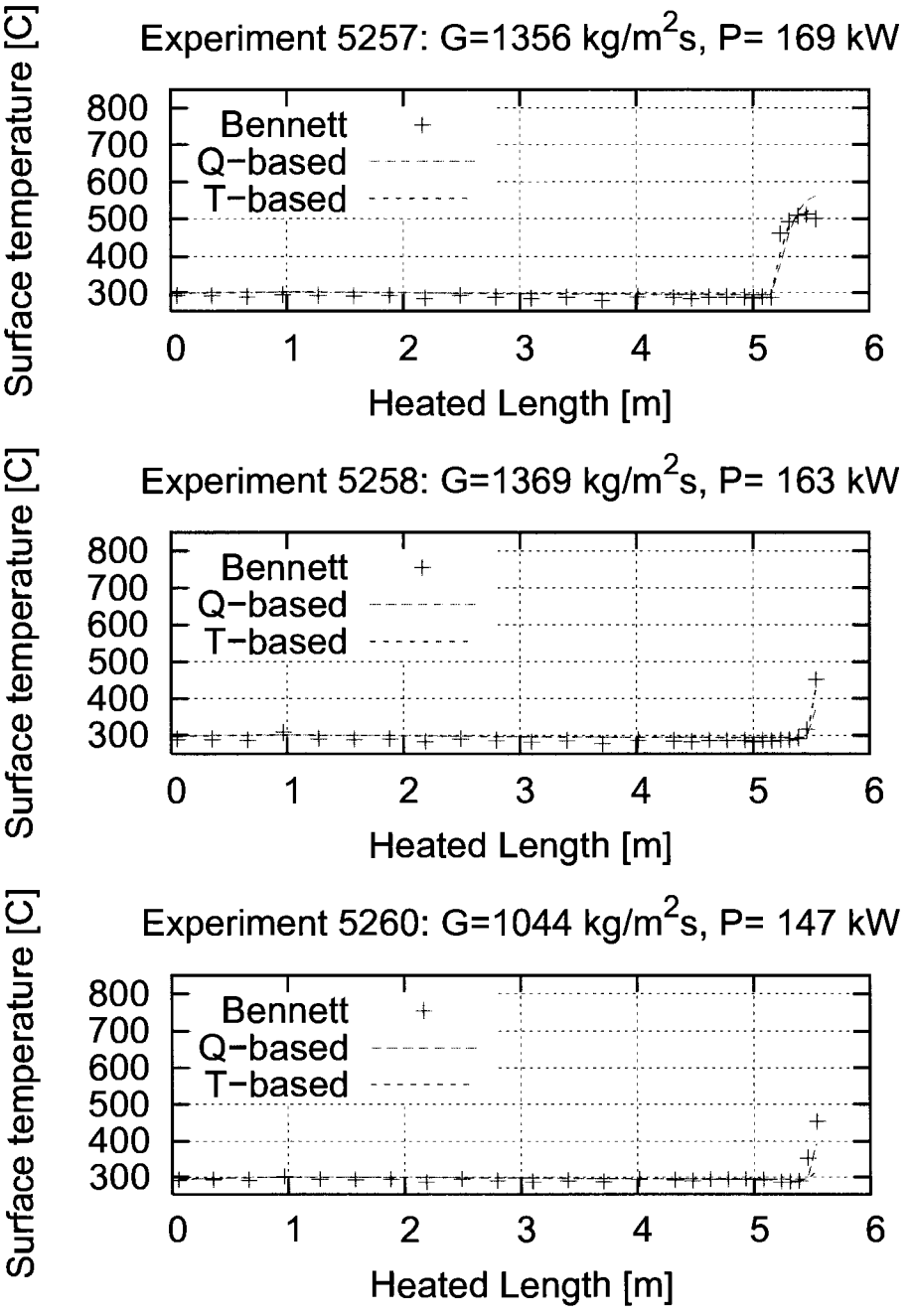

Figure IV.7 Experiments 5257, 5258 and 5260

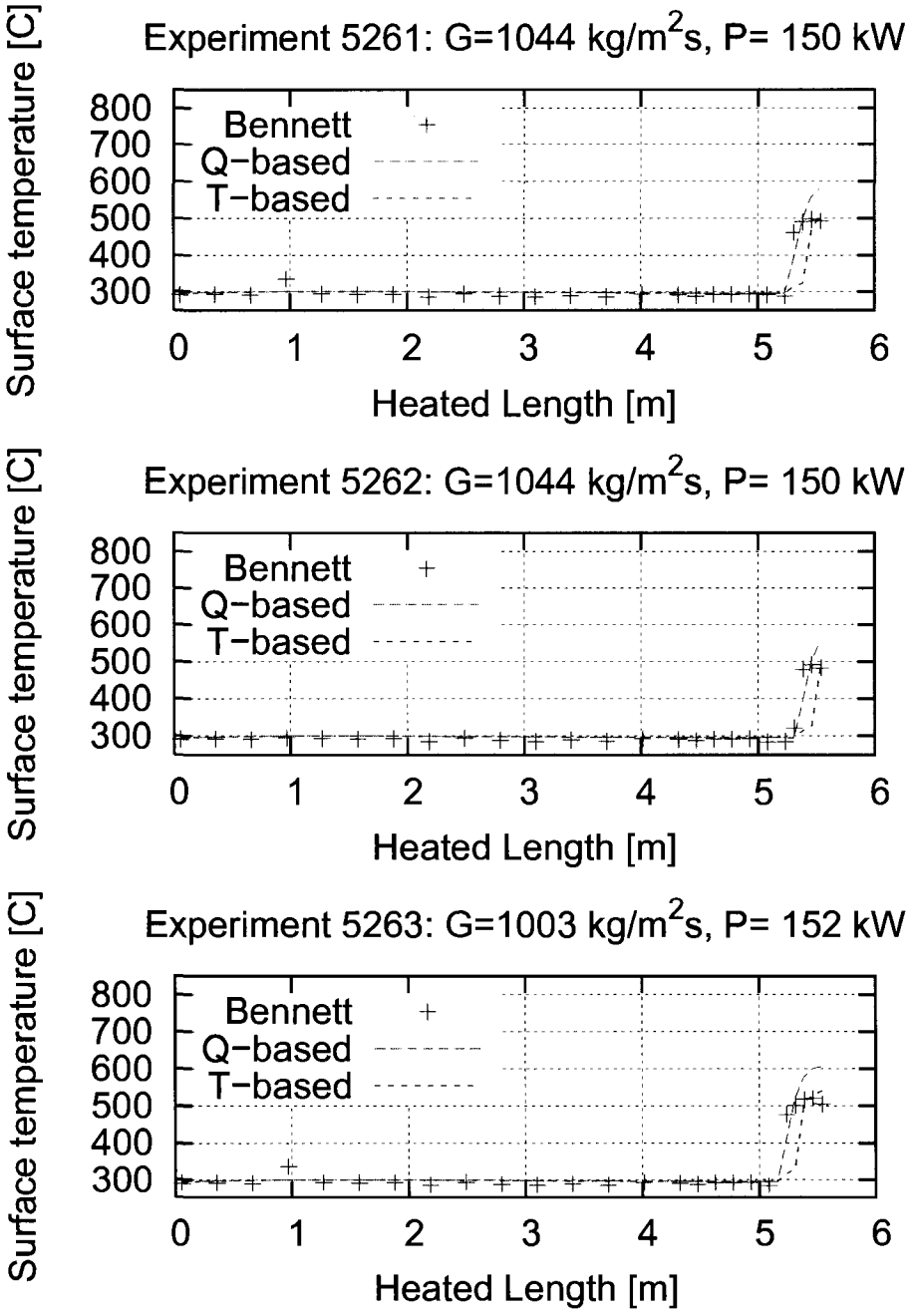

Figure IV.8 Experiments 5261, 5262 and 5263

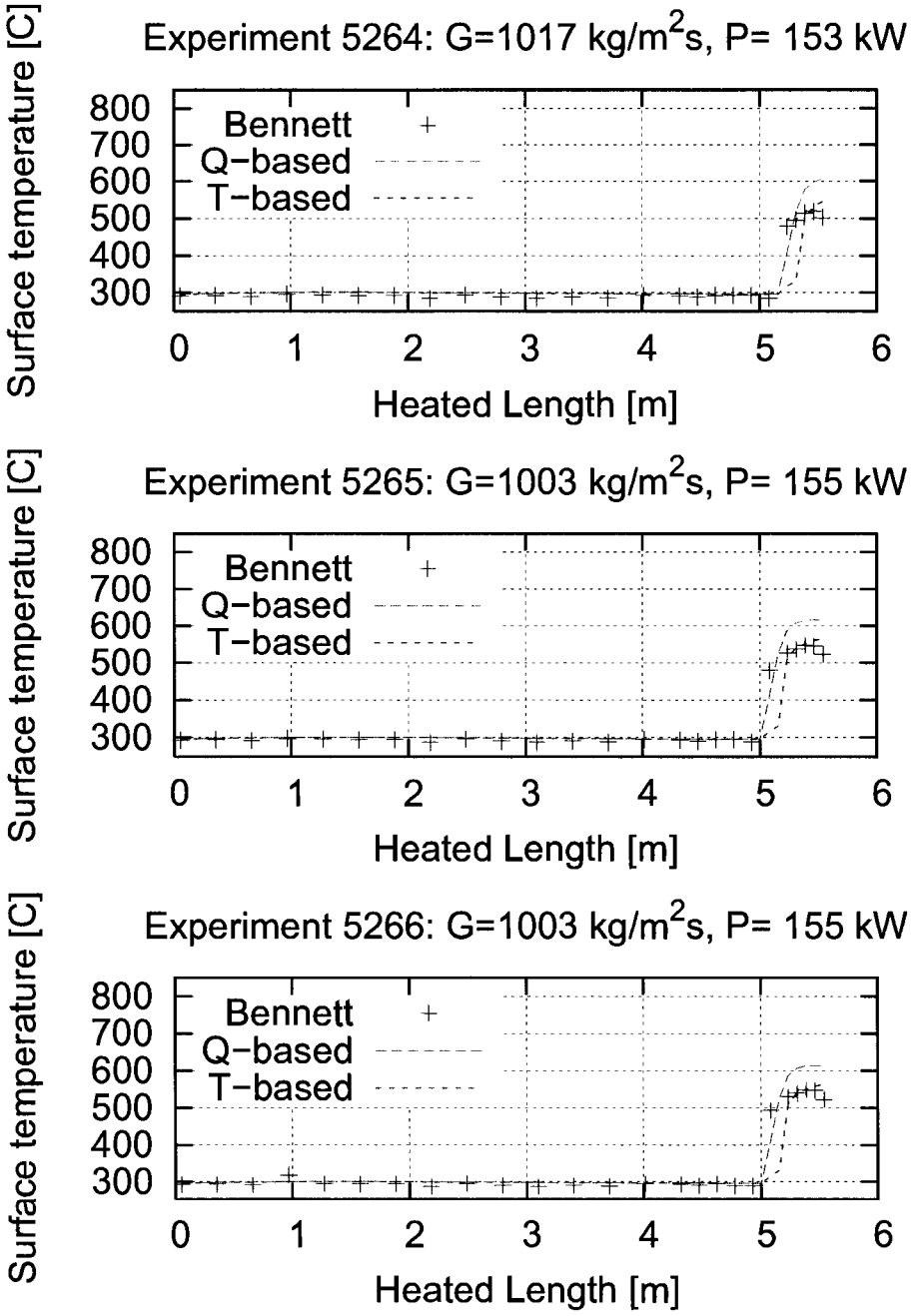

Figure IV.9 Experiments 5264, 5265 and 5266

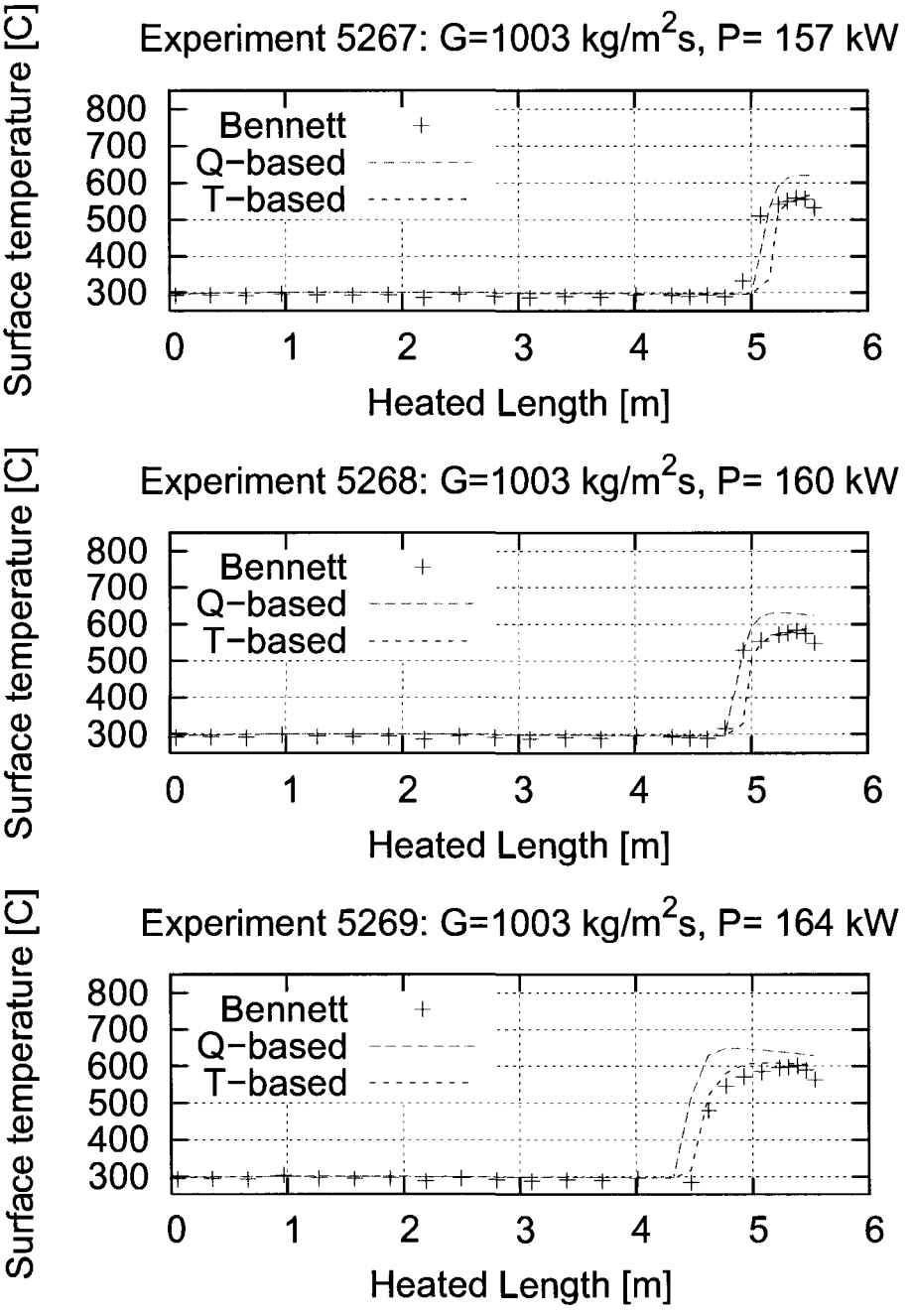

Figure IV.10 Experiments 5267, 5268 and 5269

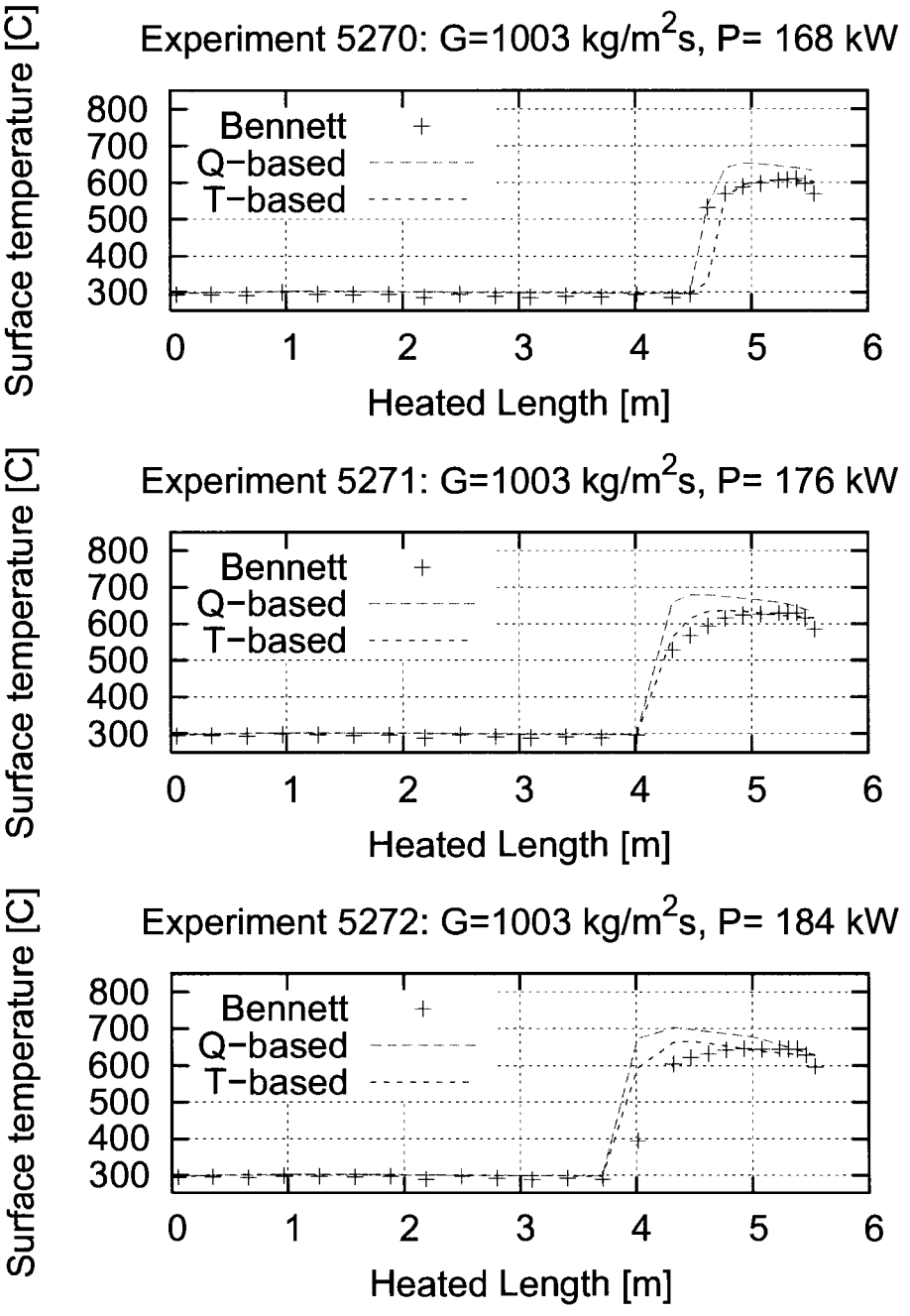

Figure IV.11 Experiments 5270, 5271 and 5272

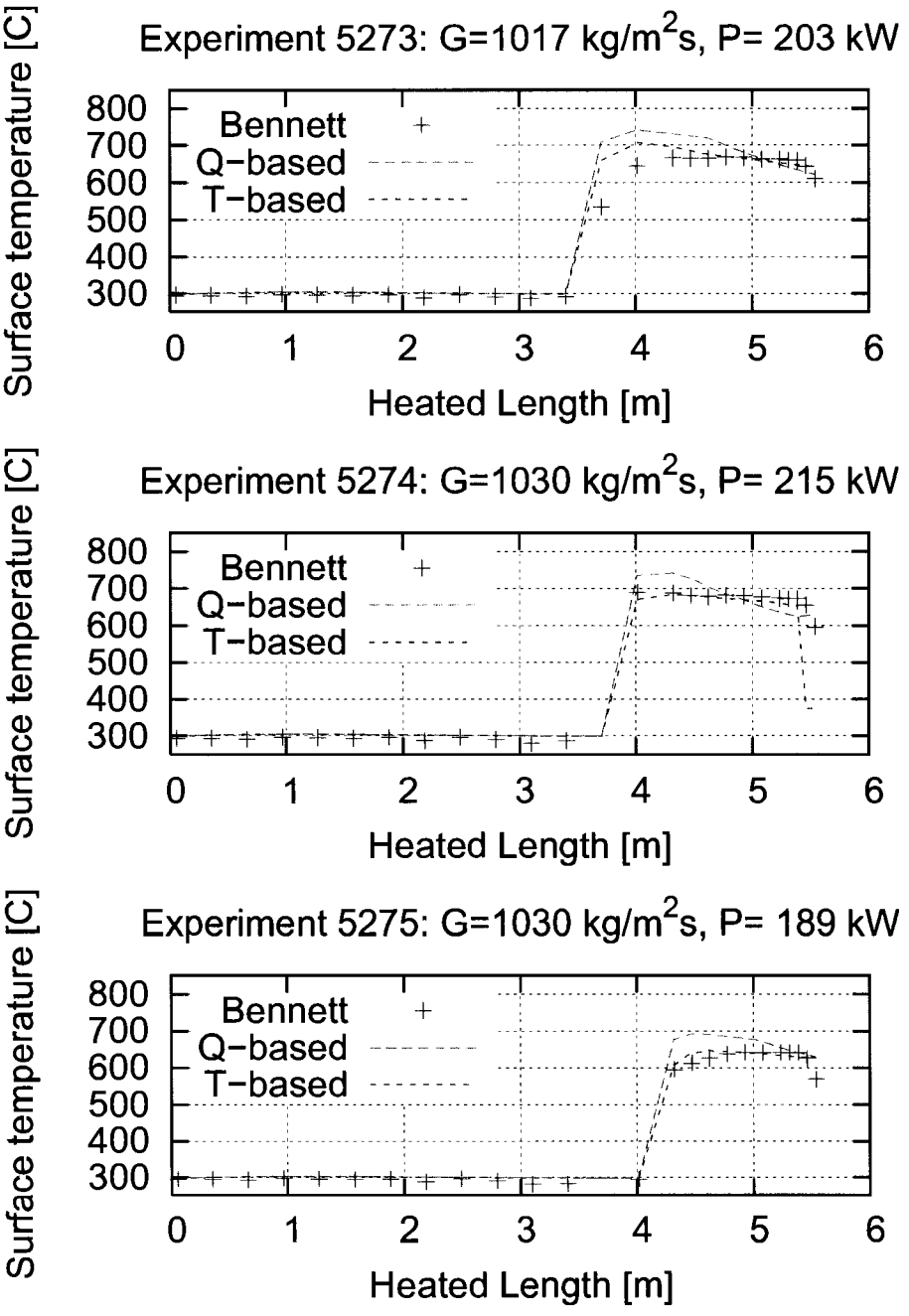

Figure IV.12 Experiments 5273, 5274 and 5275

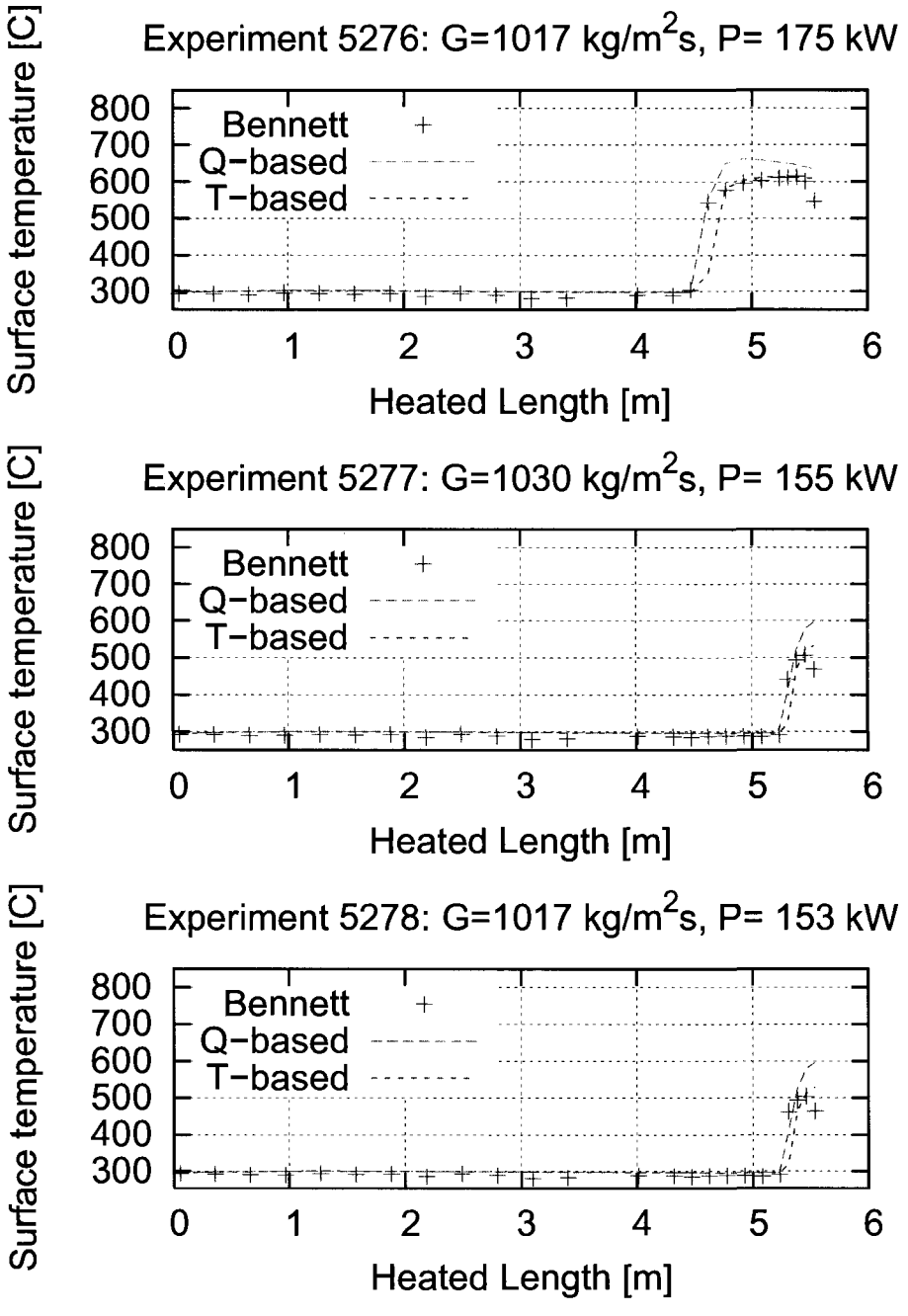

Figure IV.13 Experiments 5276, 5277 and 5278

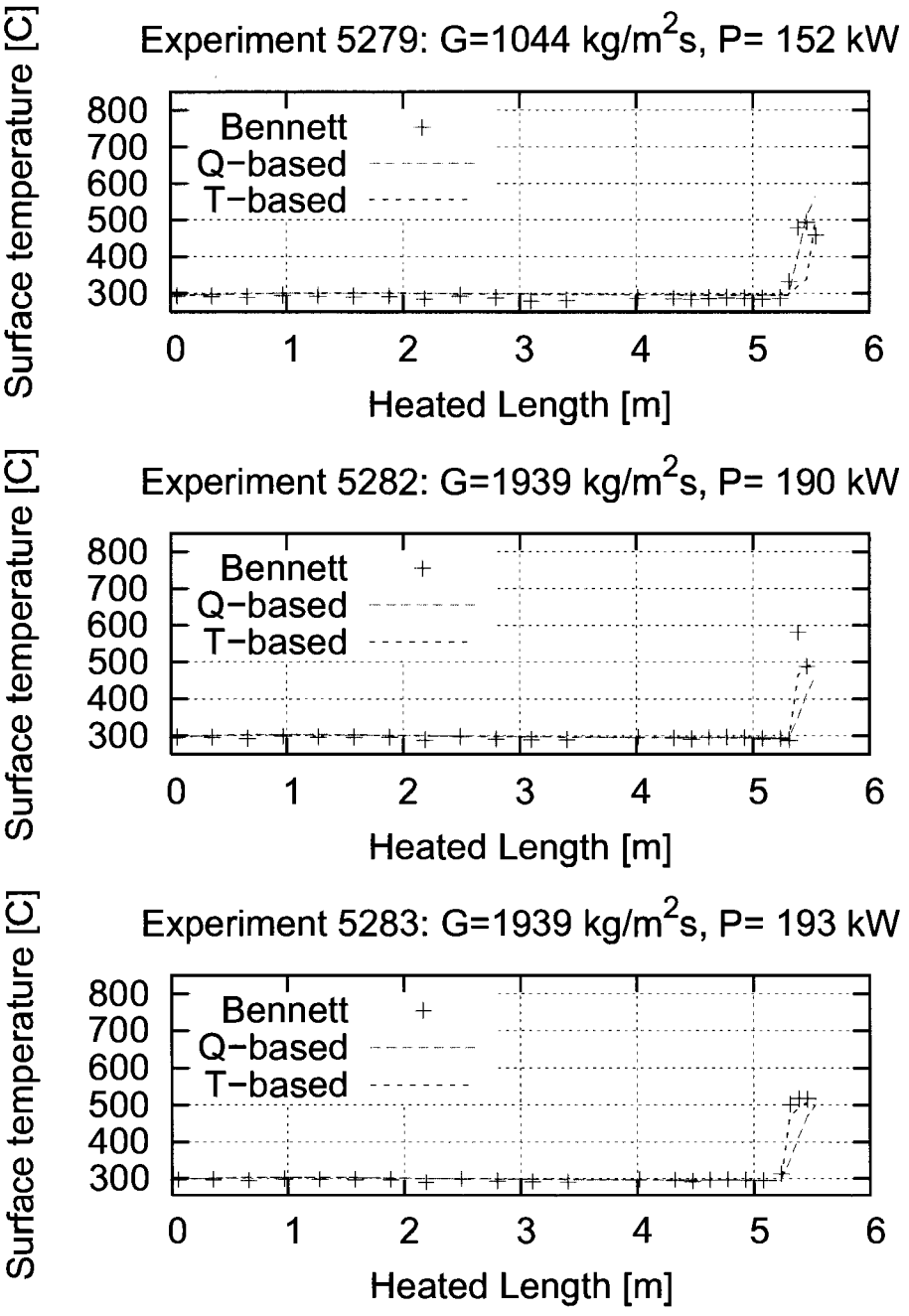

Figure IV.14 Experiments 5279, 5282 and 5283

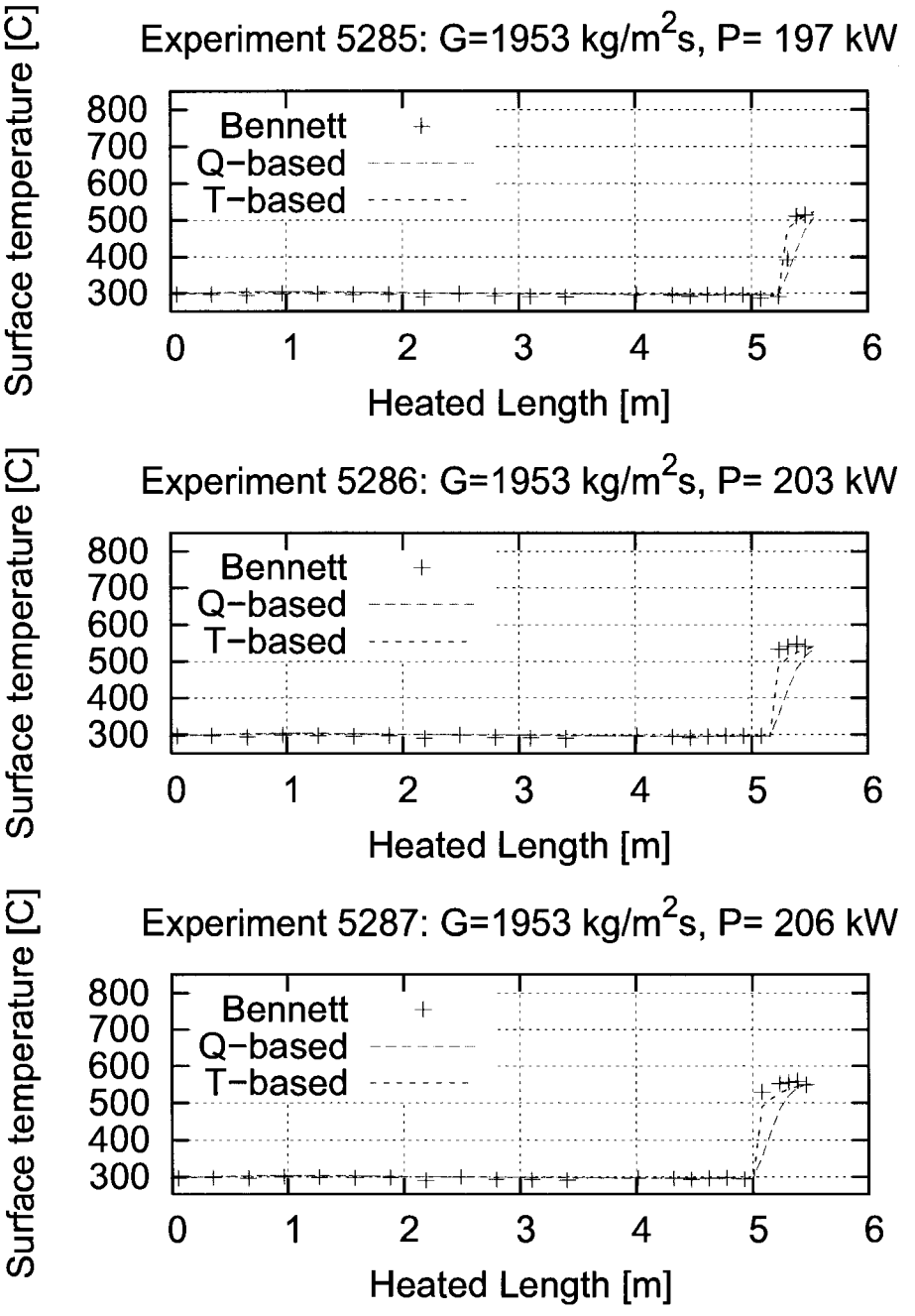

Figure IV.15 Experiments 5285, 5286 and 5287

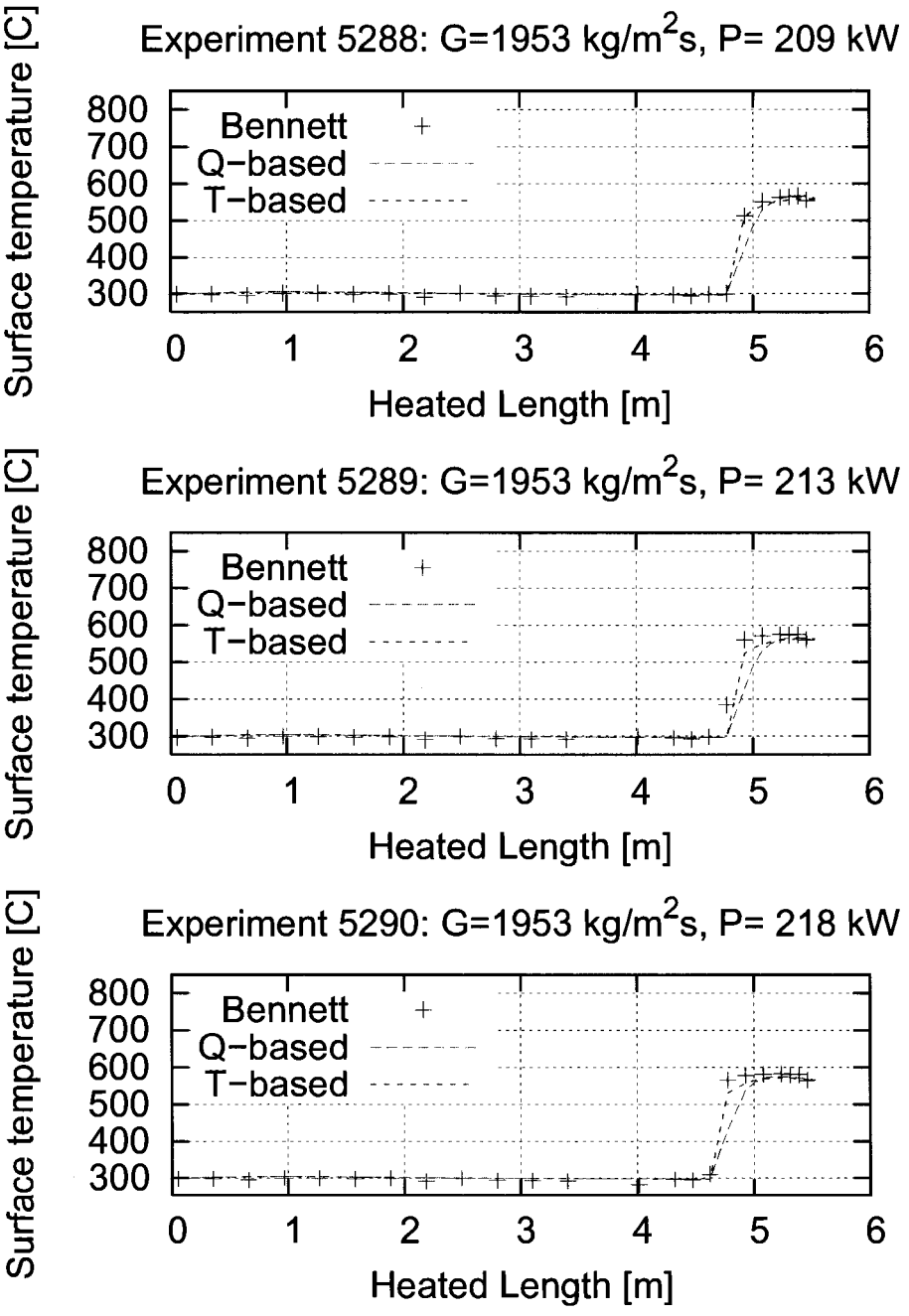

Figure IV.16 Experiments 5288, 5289 and 5290

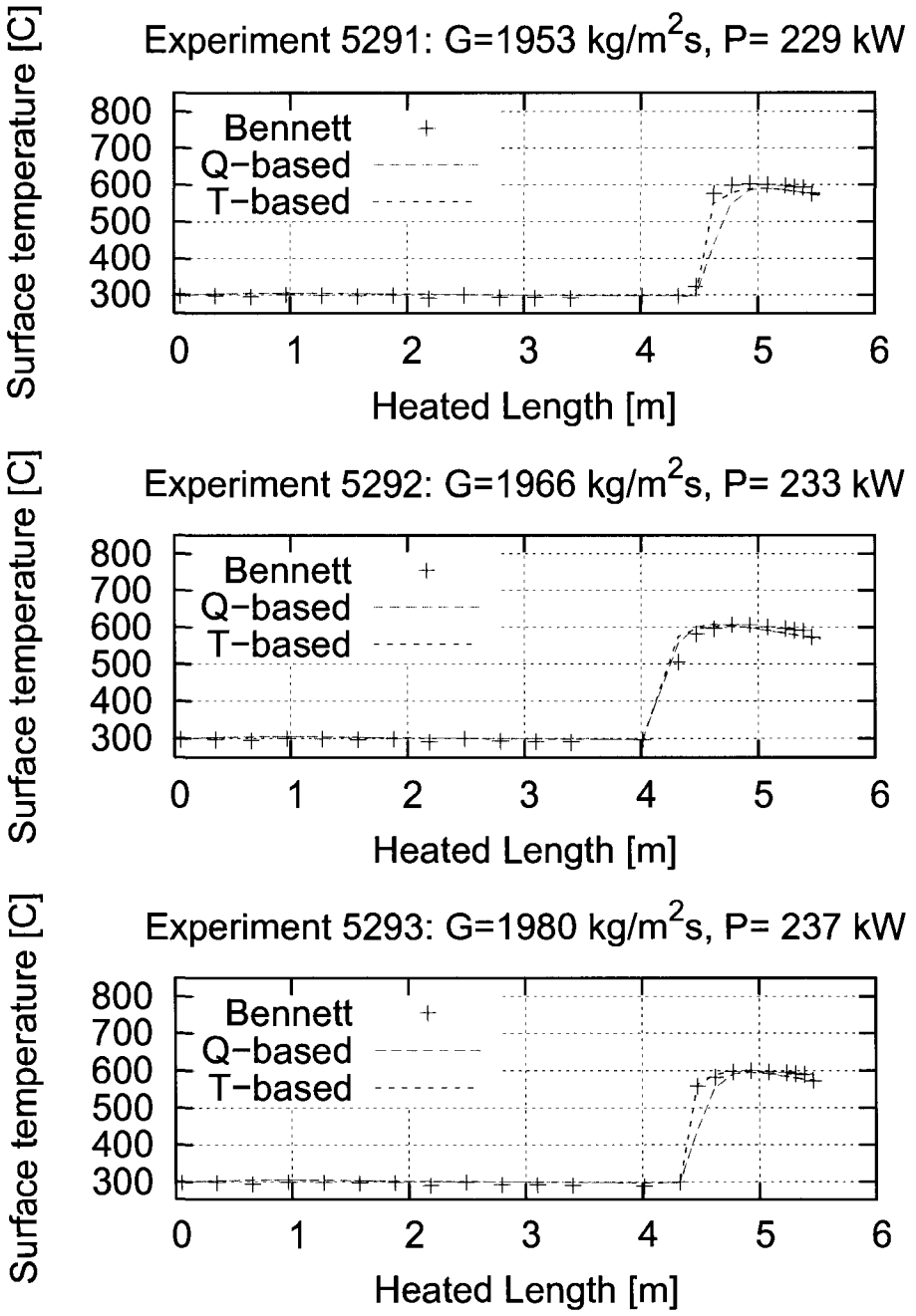

Figure IV.17 Experiments 5291, 5292 and 5293

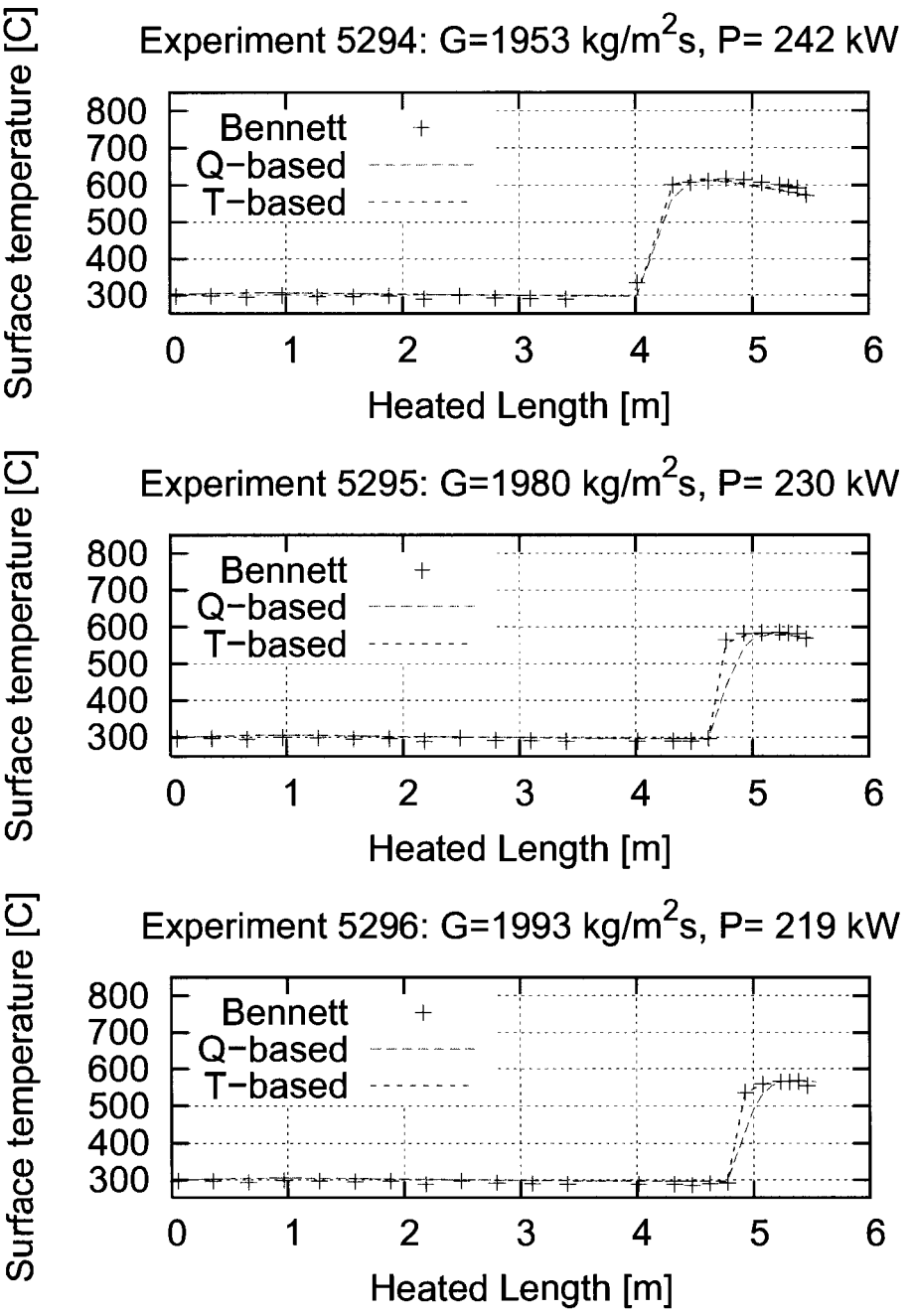

Figure IV.18 Experiments 5294, 5295 and 5296

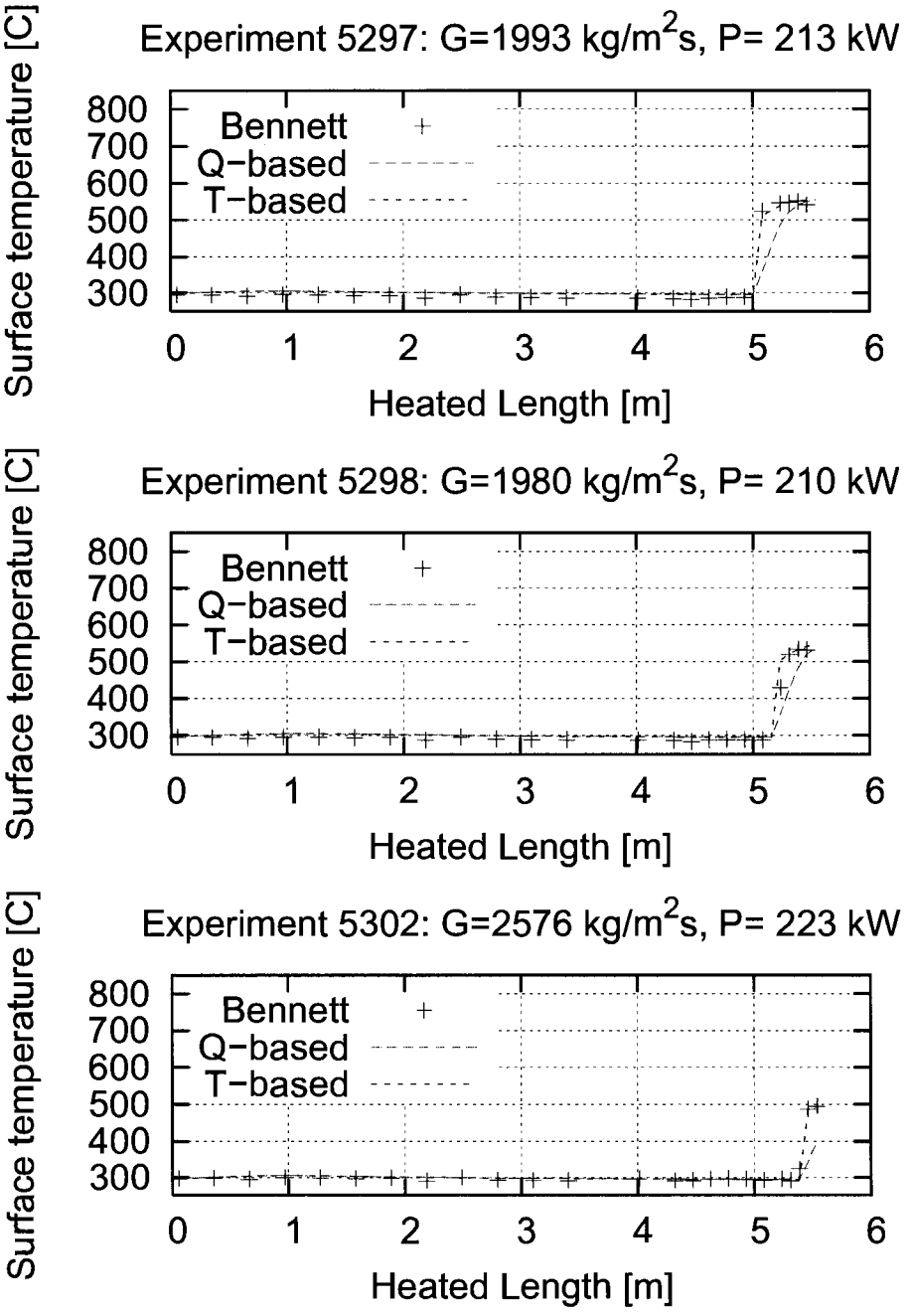

Figure IV.19 Experiments 5297, 5298 and 5302

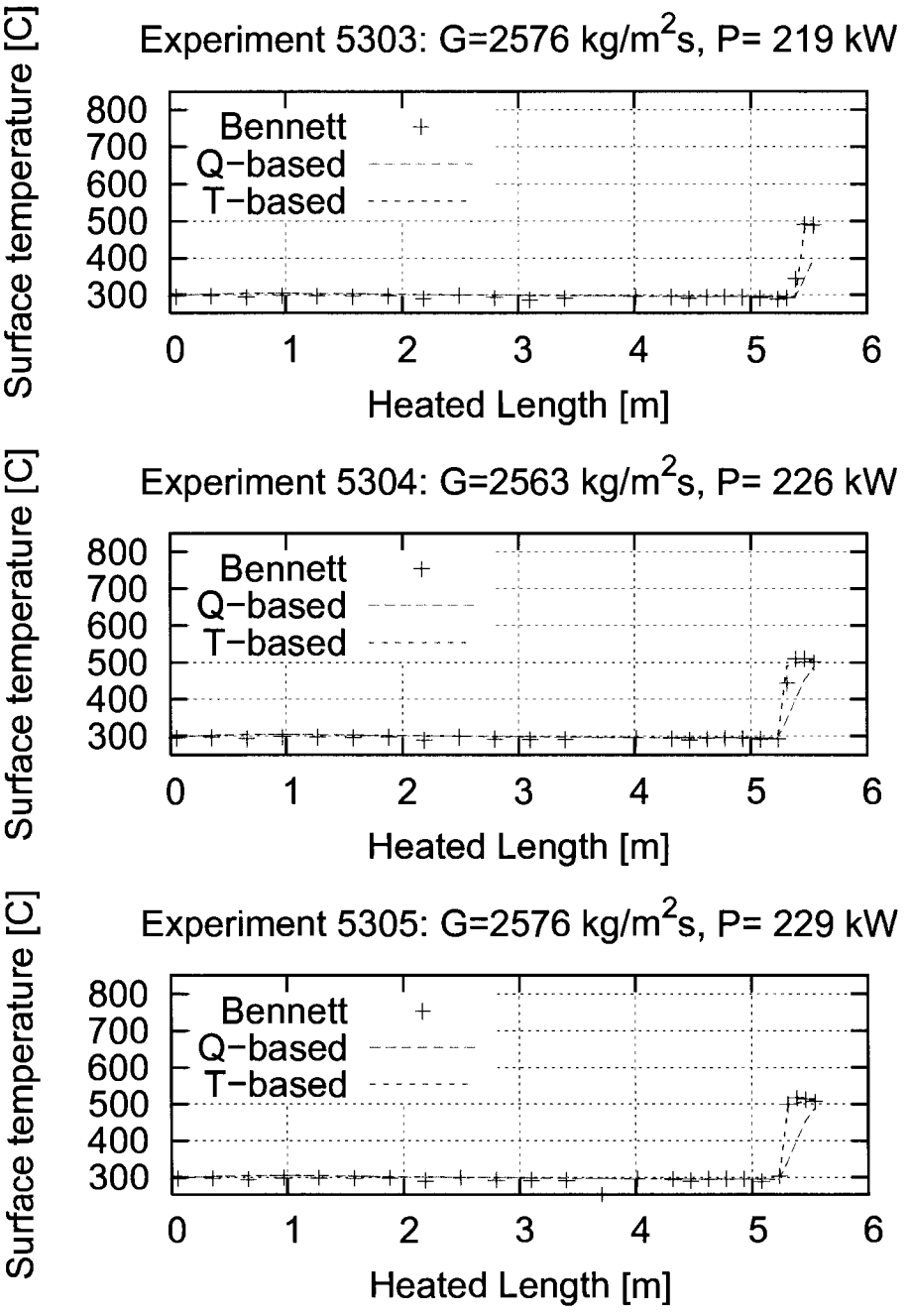

Figure IV.20 Experiments 5303, 5304 and 5305

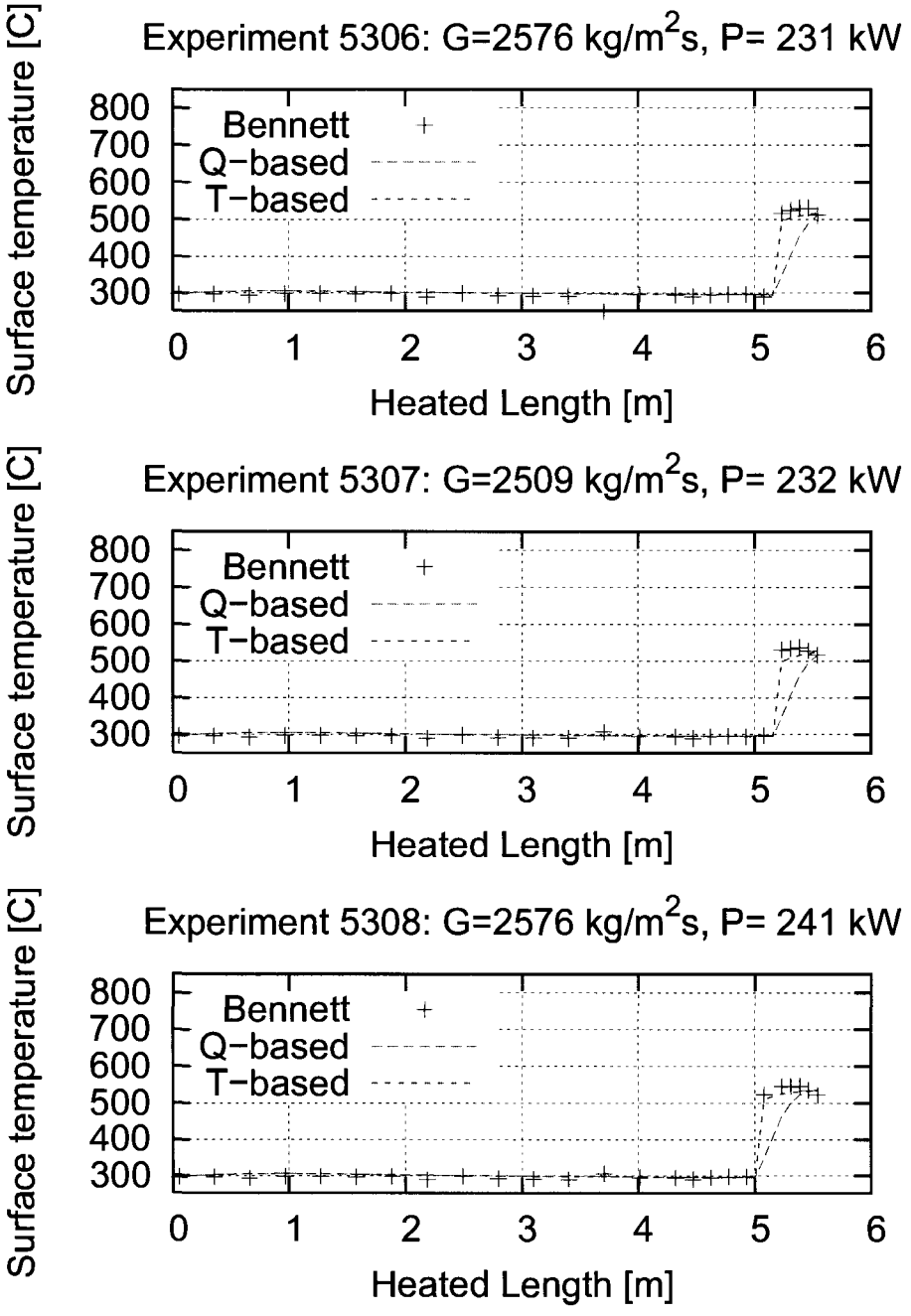

Figure IV.21 Experiments 5306, 5307 and 5308

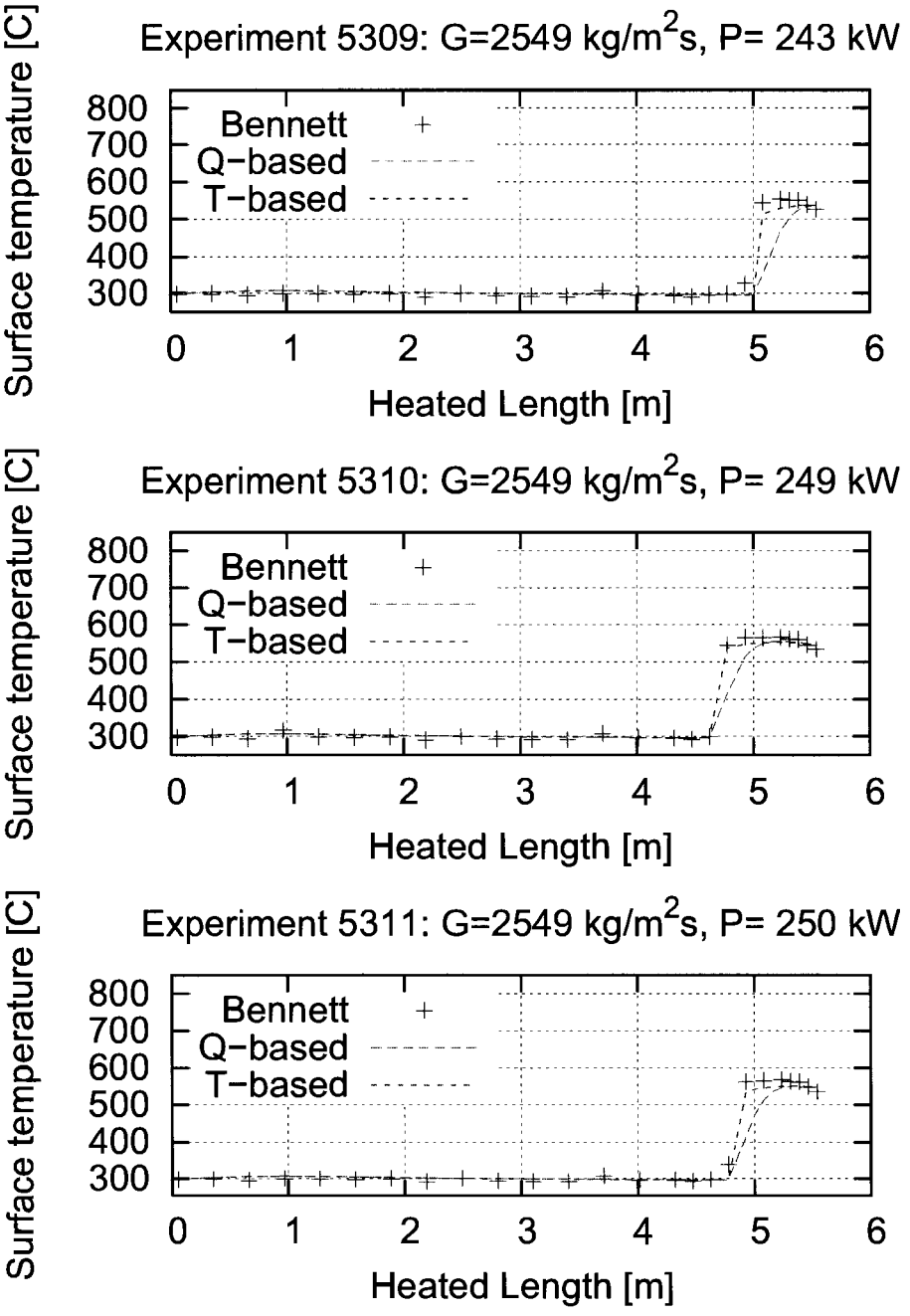

Figure IV.22 Experiments 5309, 5310 and 5311

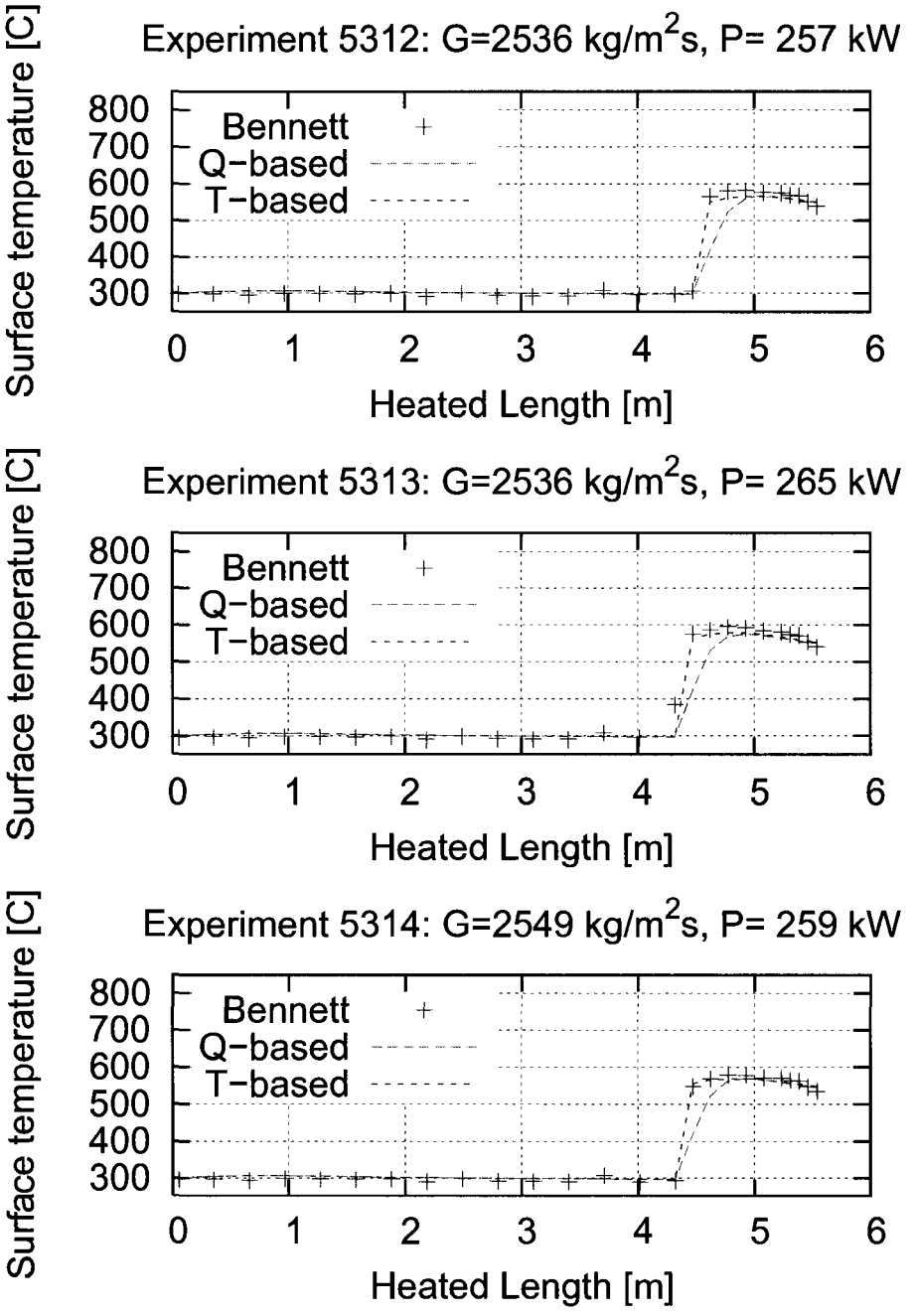

Figure IV.23 Experiments 5312, 5313 and 5314

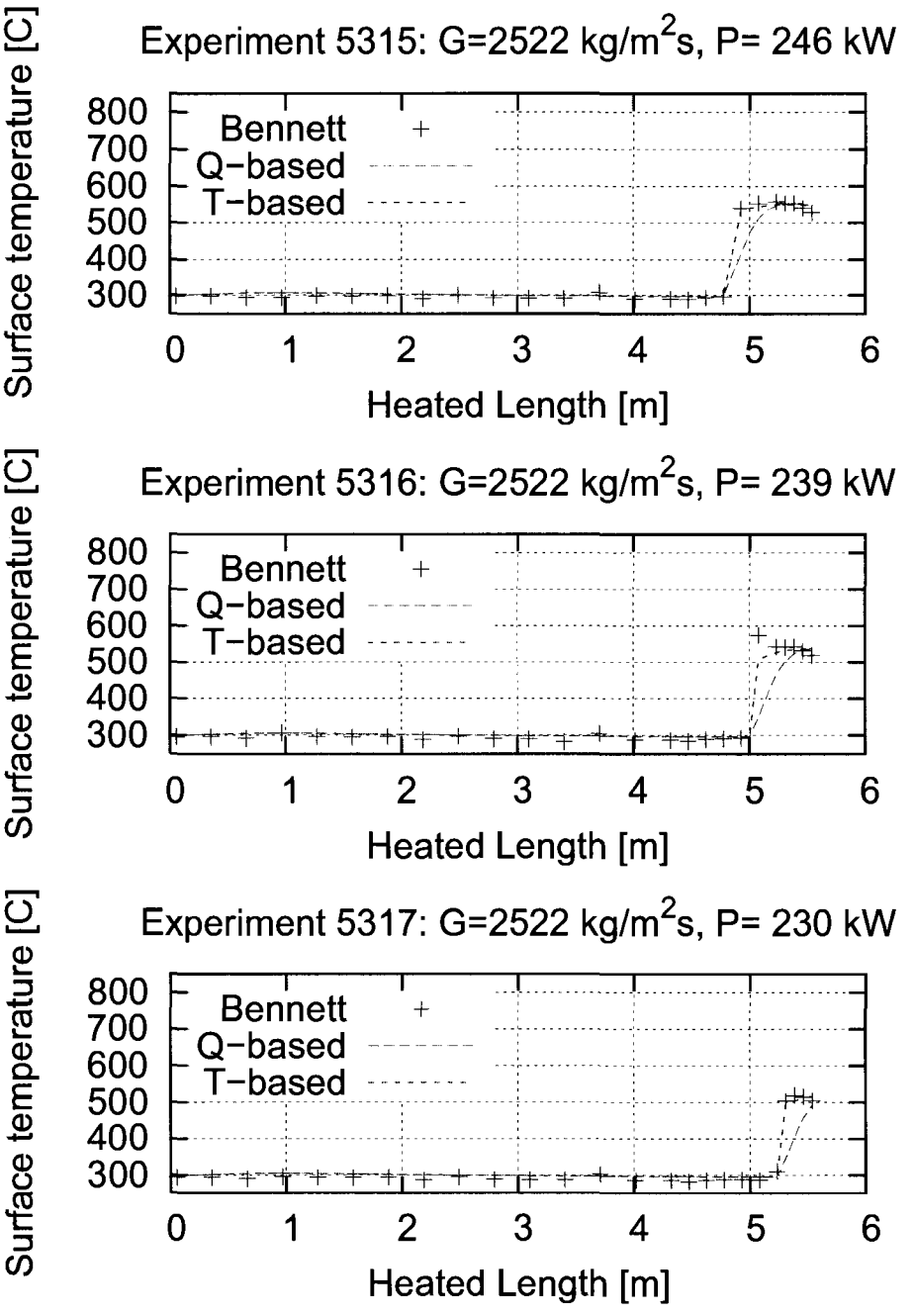

Figure IV.24 Experiments 5315, 5316 and 5317

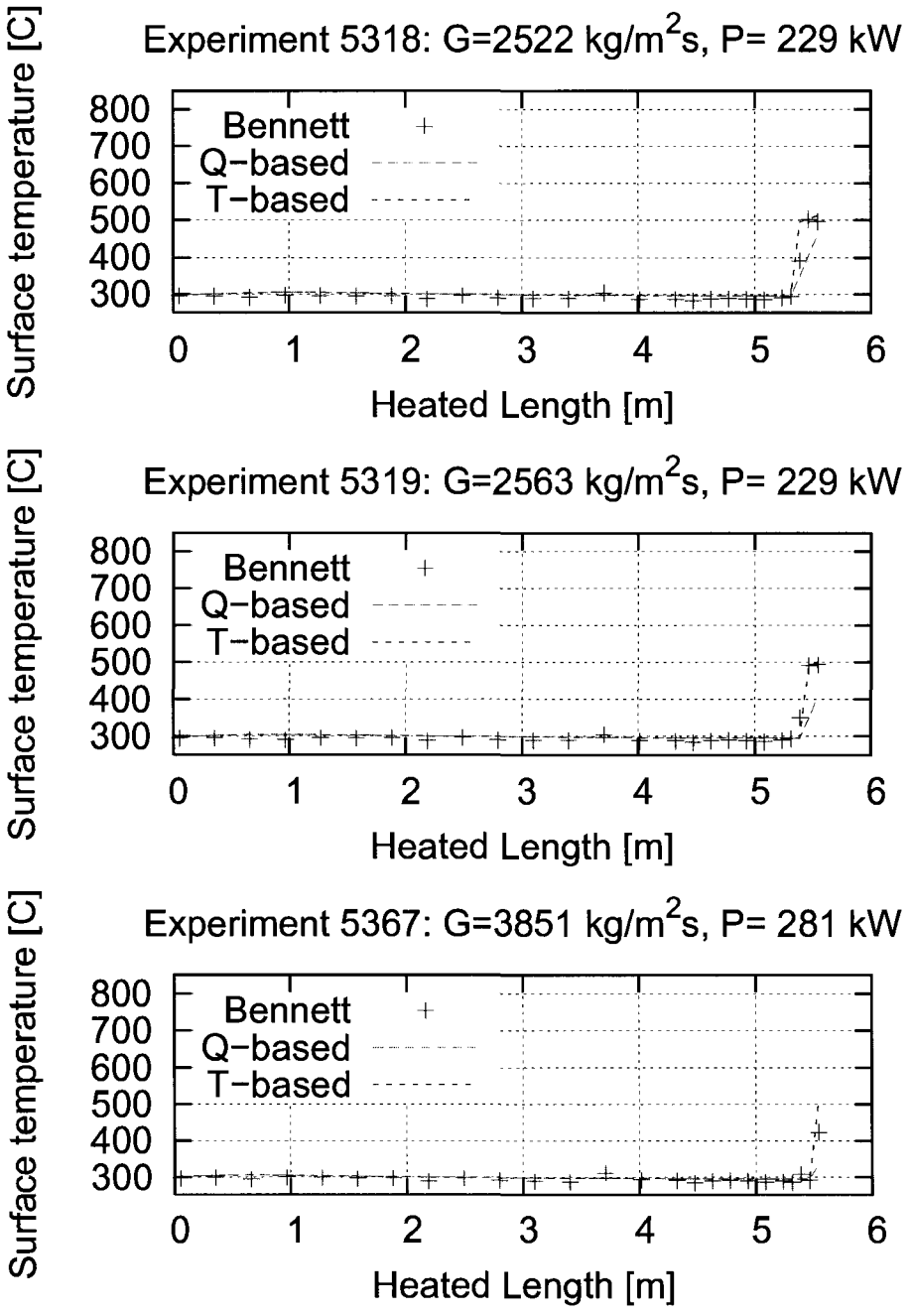

Figure IV.25 Experiments 5318, 5319 and 5367

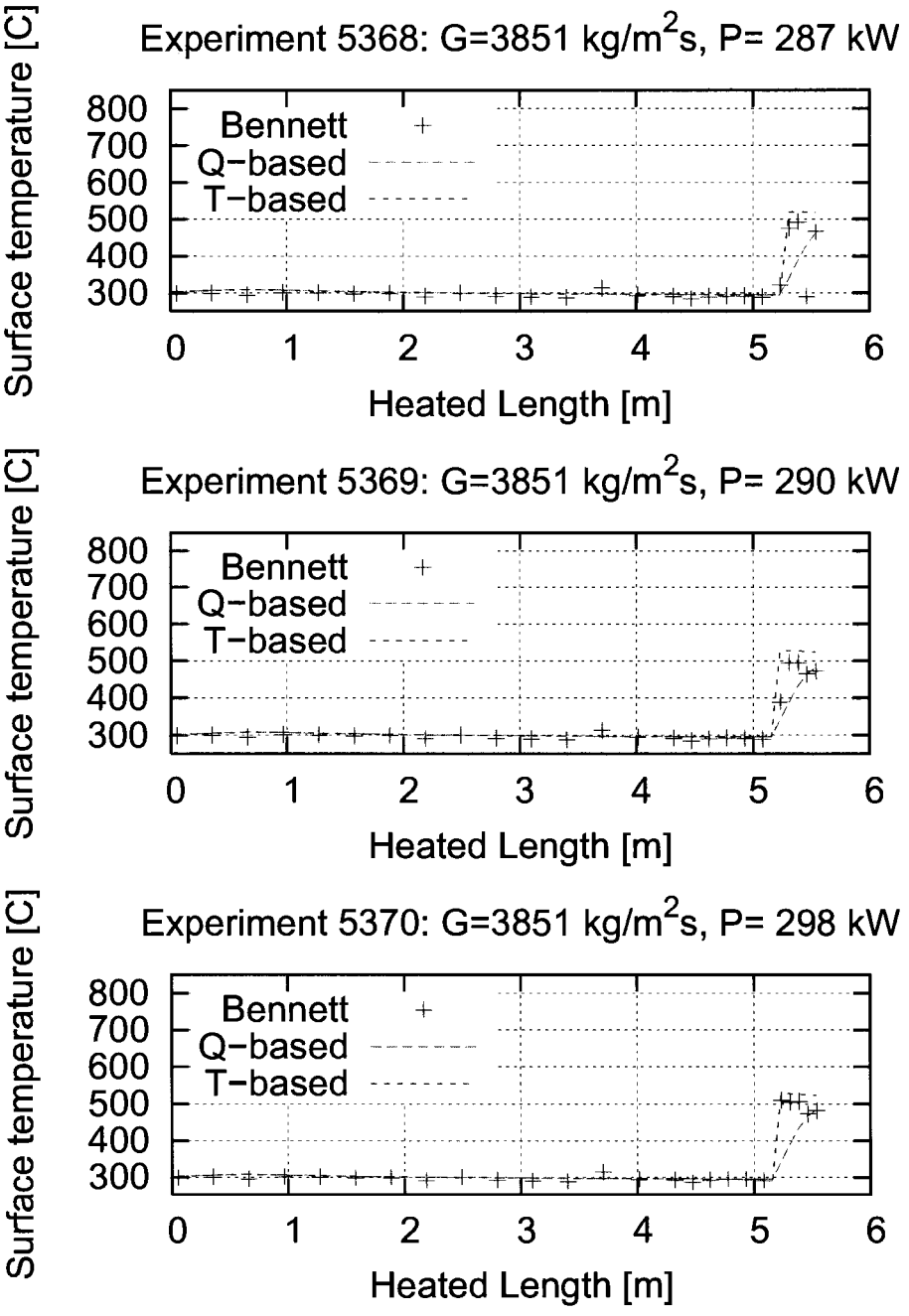

Figure IV.26 Experiments 5368, 5369 and 5370

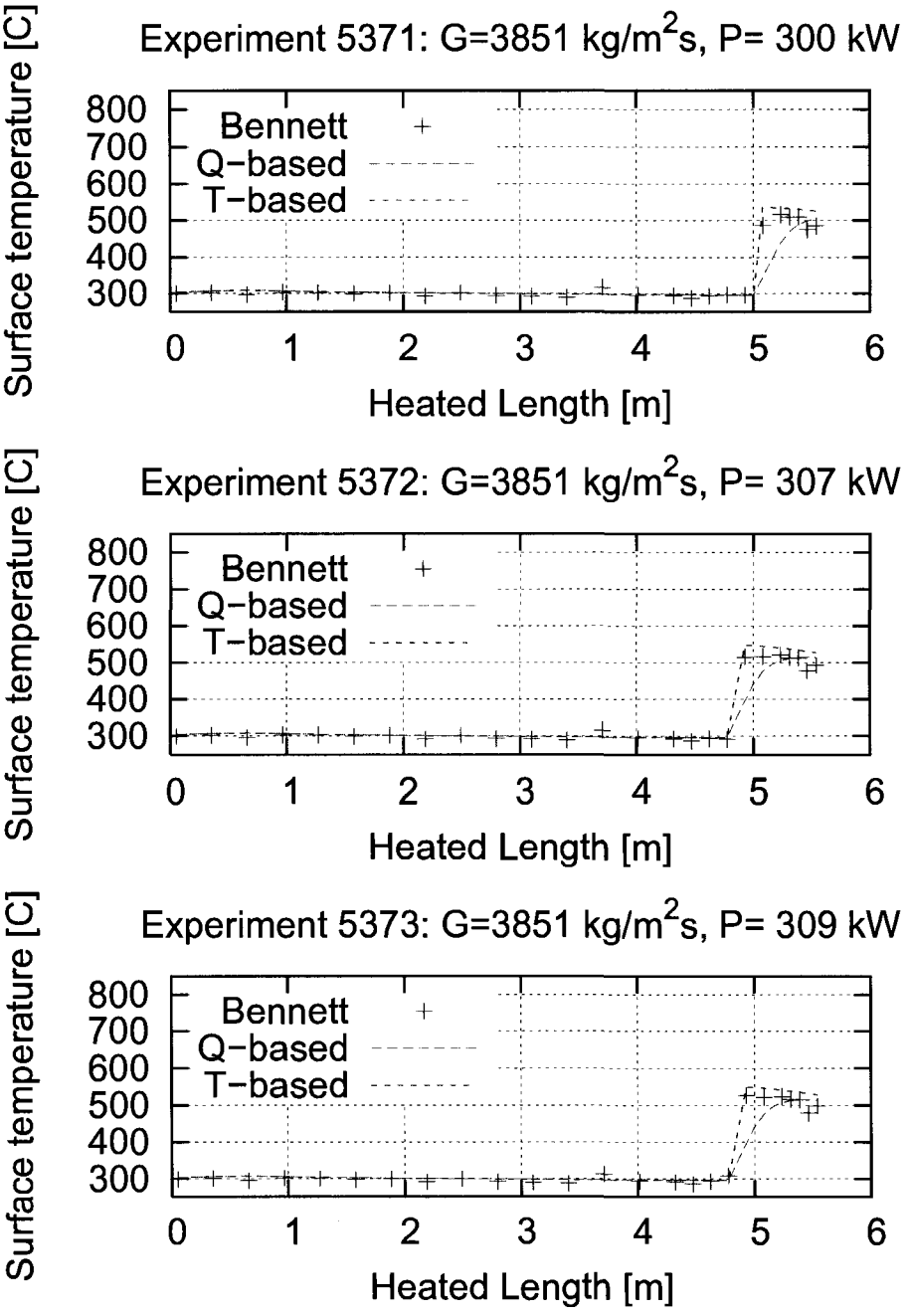

Figure IV.27 Experiments 5371, 5372 and 5373

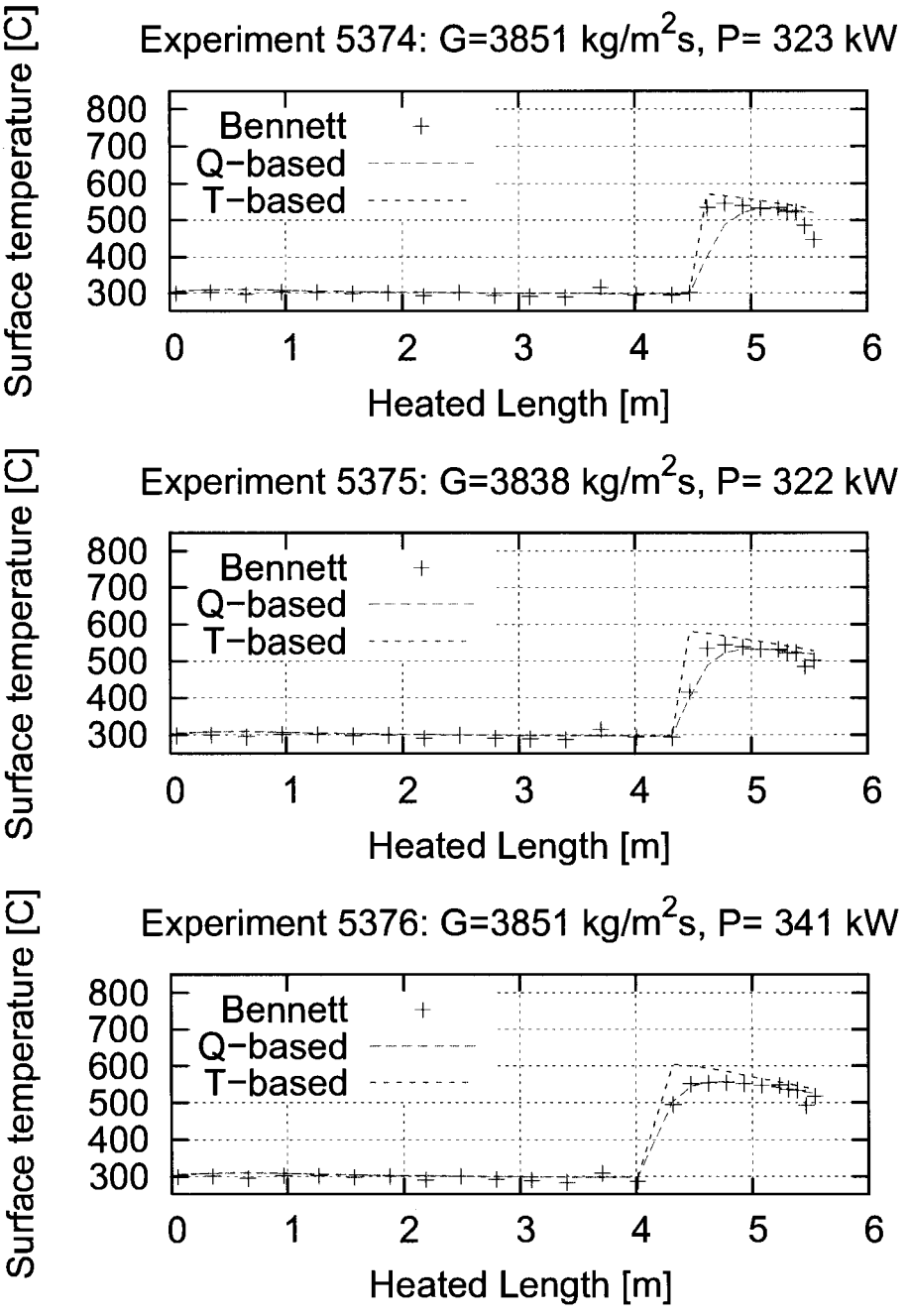

Figure IV.28 Experiments 5374, 5375 and 5376

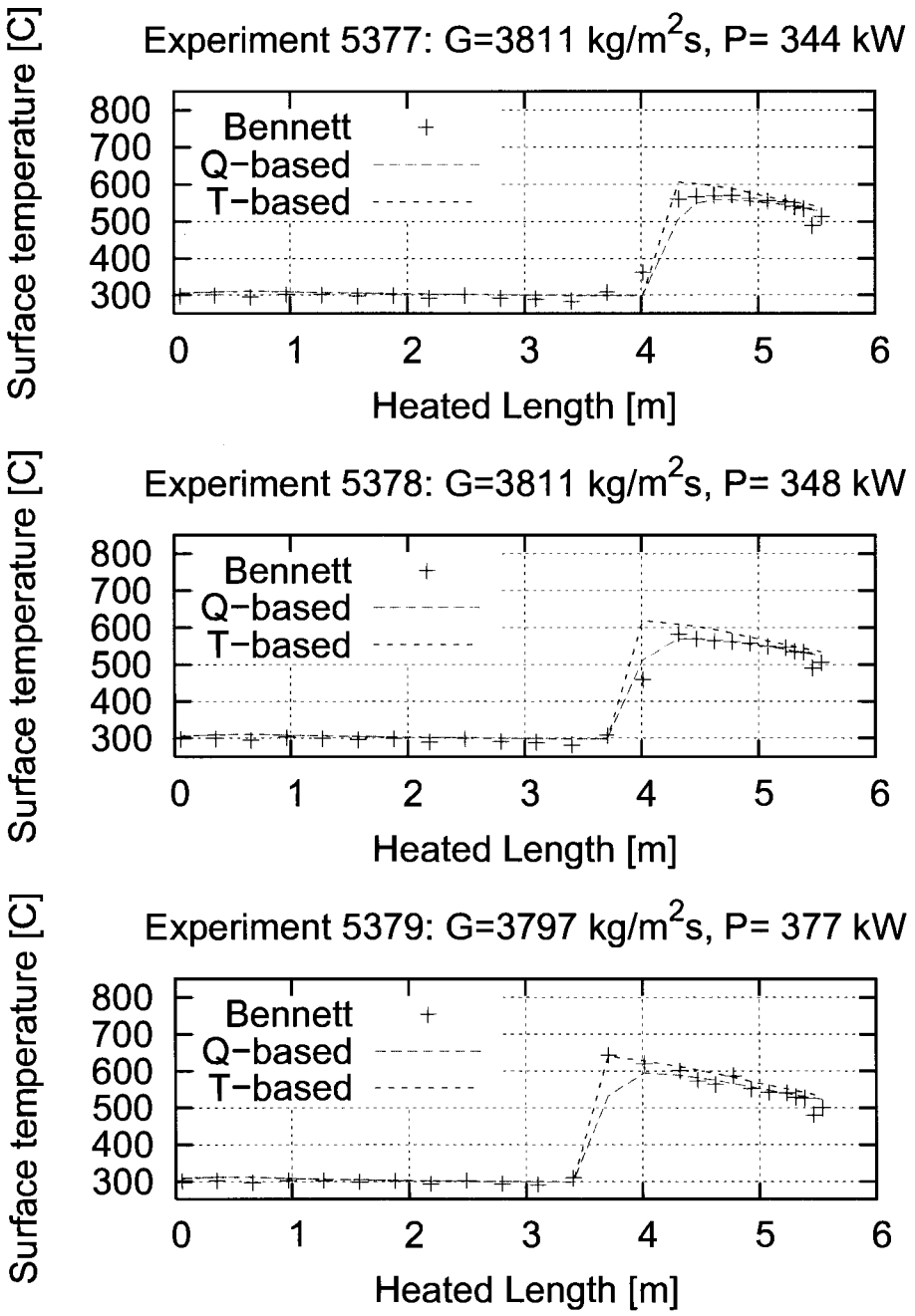

Figure IV.29 Experiments 5377, 5378 and 5379

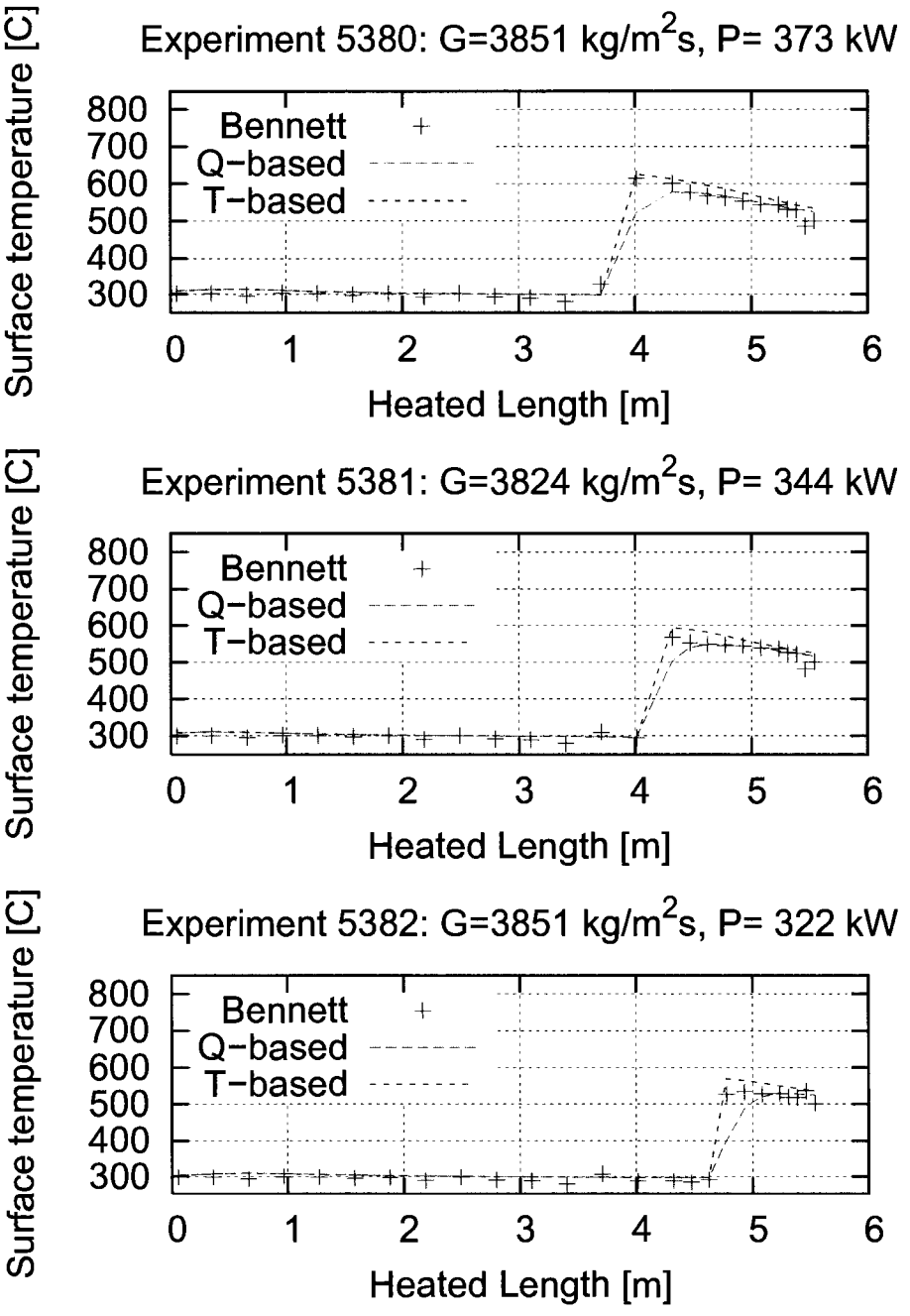

Figure IV.30 Experiments 5380, 5381 and 5382

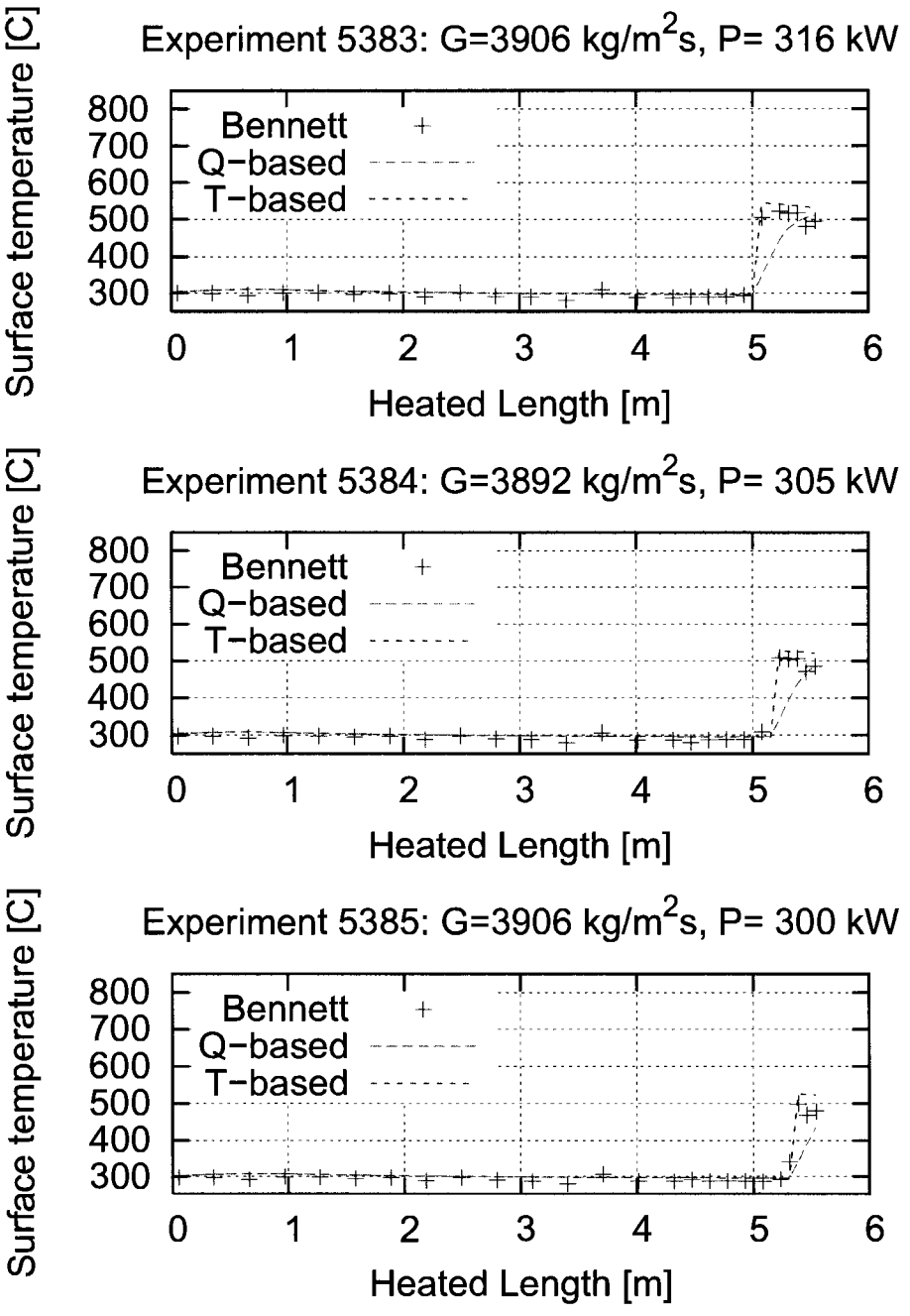

Figure IV.31 Experiments 5383, 5384 and 5385

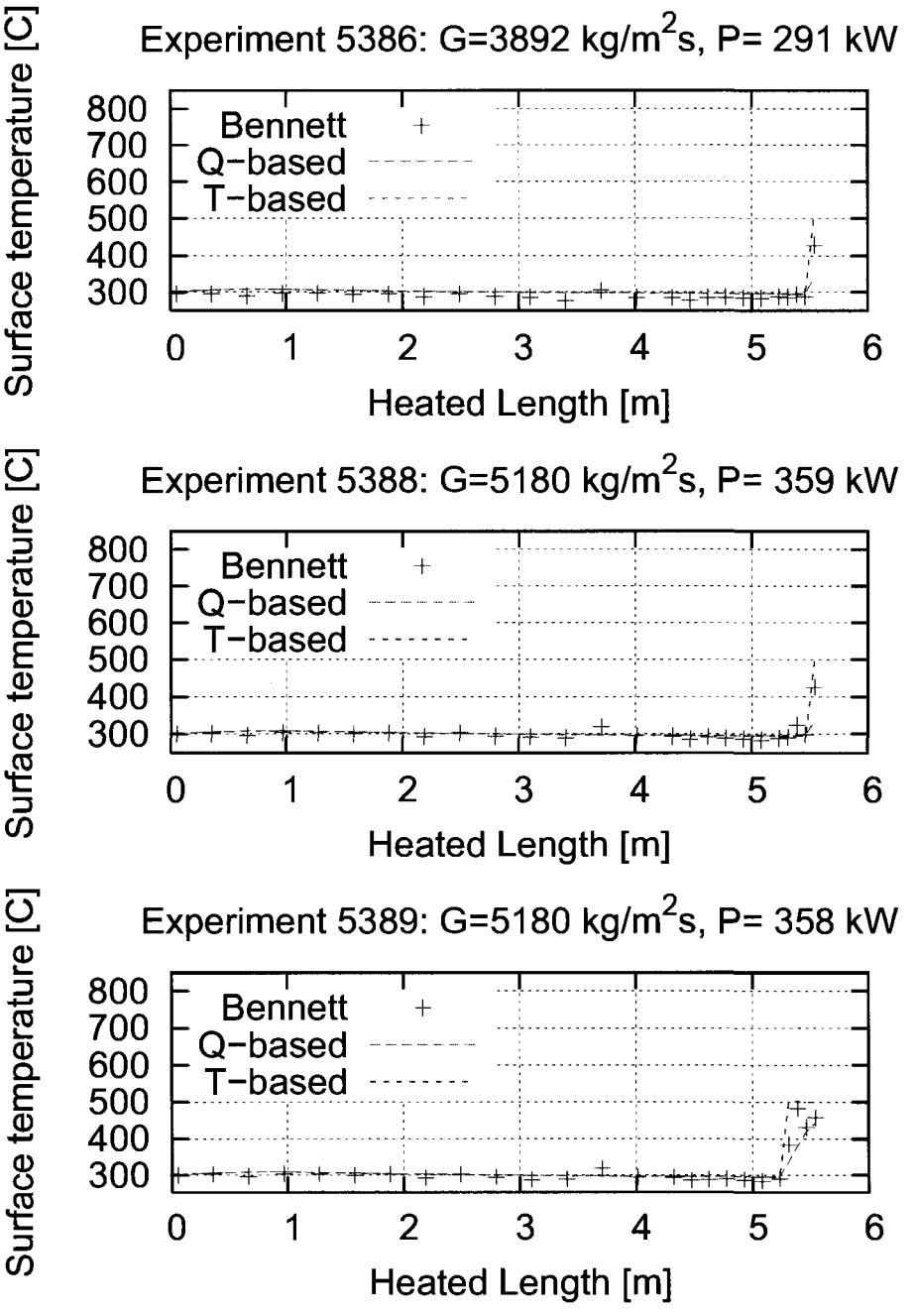

Figure IV.32 Experiments 5386, 5388 and 5389

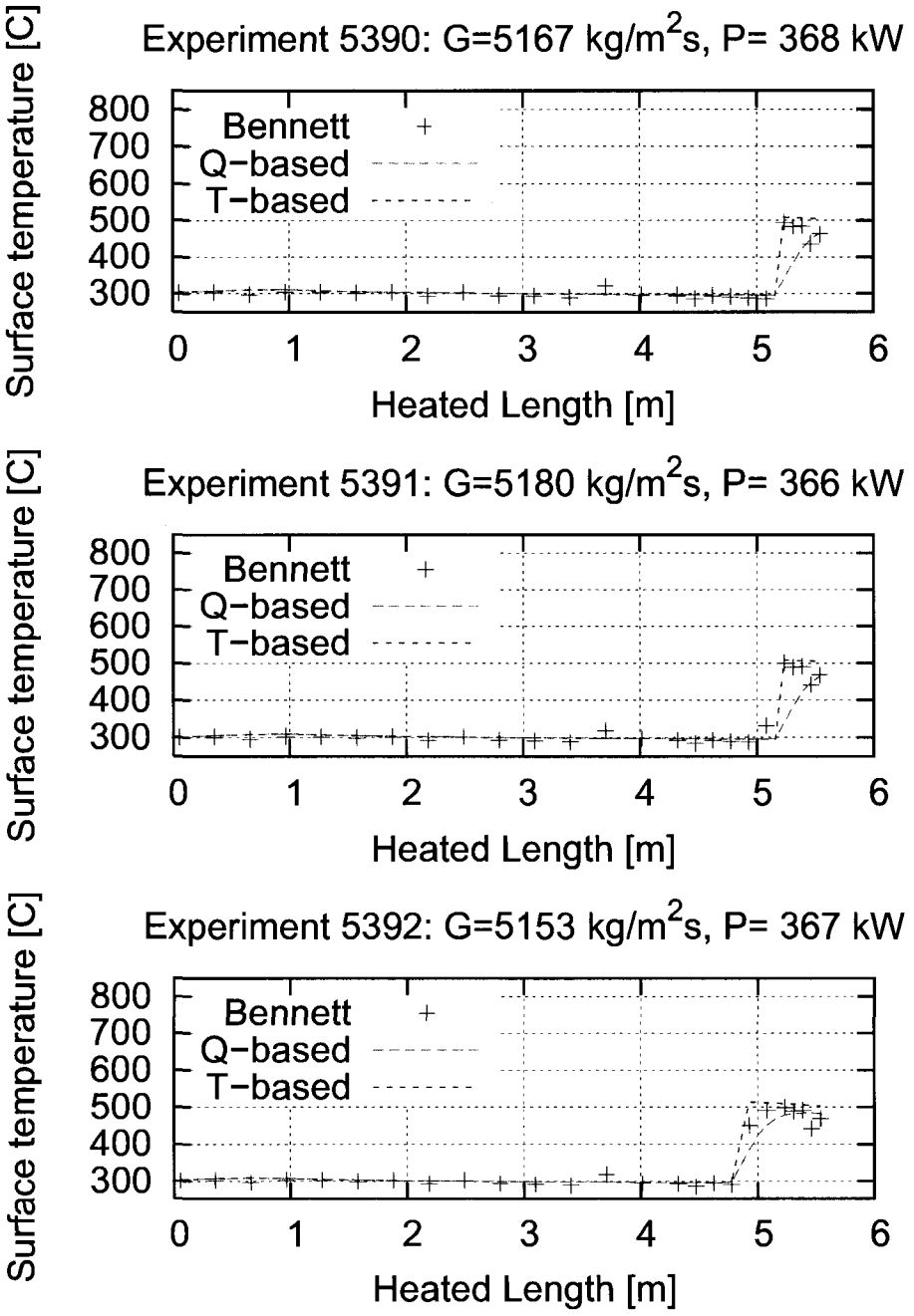

Figure IV.33 Experiments 5390, 5391 and 5392

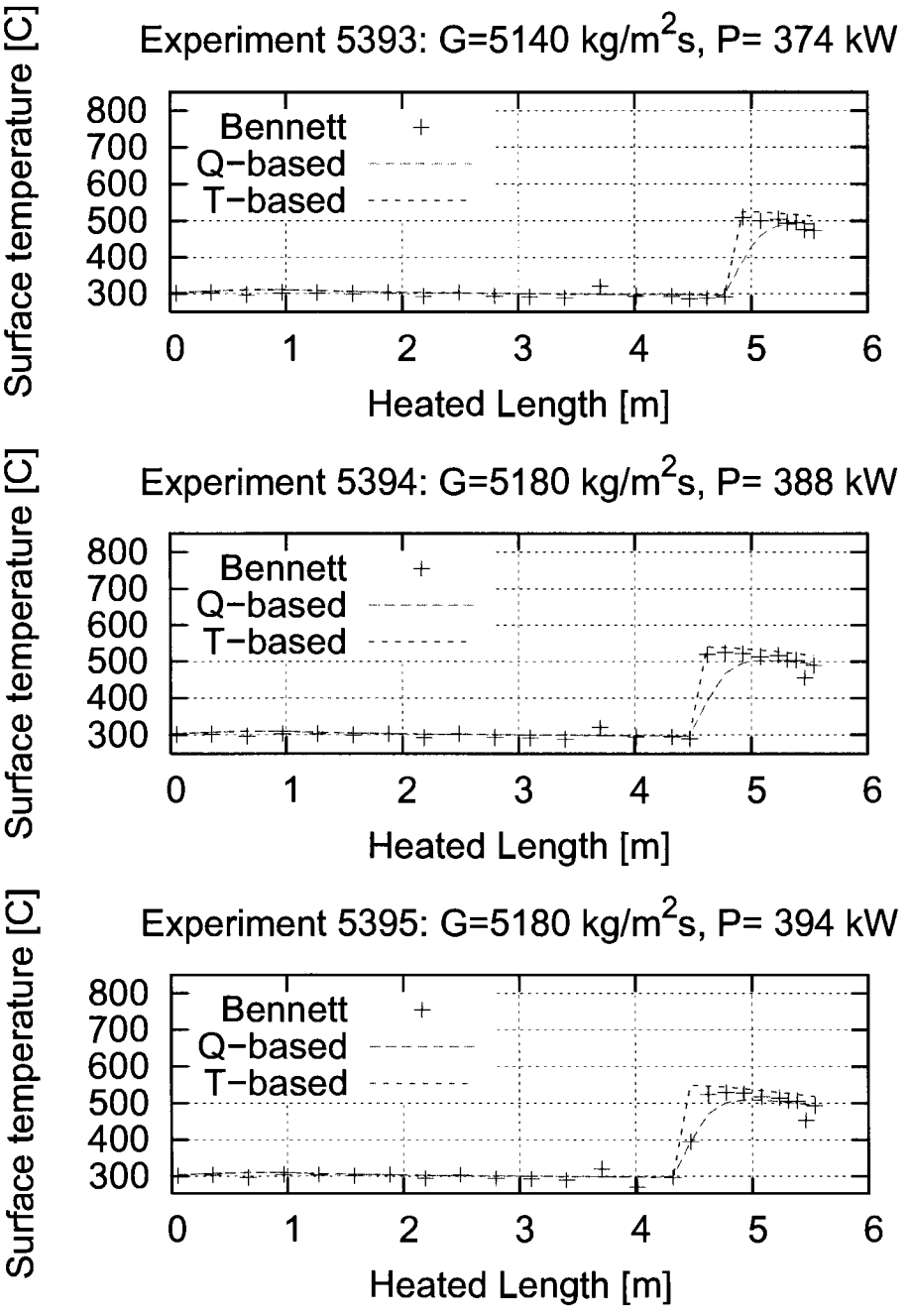

Figure IV.34 Experiments 5393, 5394 and 5395

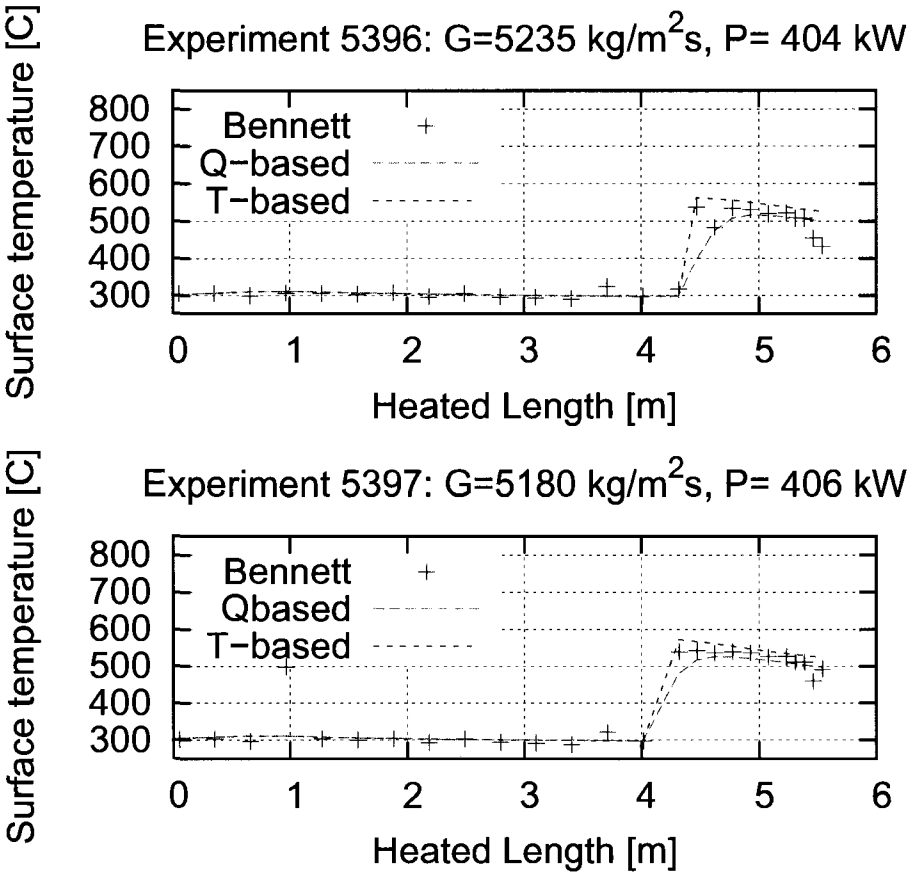

Figure IV.35 Experiments 5396 and 5397

APPENDIX V

IMPROVED CORRELATION RESULTS

V.1 Errors and Maximum Temperatures

Table V.1: Errors and Maximum Temperatures for the 5.56 m Test Section Using a Temperature-Based Methodology

Run#	G	Tin	Pwr	CHF_{cor}	T_{MaxExp}	$T_{maxCode}$	$ErrT_{max}$	Err_{PDO}	STD
	$\left[\frac{kg}{m^2 s}\right]$	$[^oC]$	$[kW]$		$[^oC]$	$[^oC]$	[%]	[%]	[%]
5239	1356	260	166	0.5780	485.8	552.1	13.64	15.97	2.33
5240	1356	260	167	0.5948	492.6	552.3	12.12	12.70	0.58
5241	1370	261	168	0.5797	507.4	554.9	9.35	10.66	1.61
5242	1356	261	170	0.5620	527.9	565.0	7.03	13.83	9.36
5243	1356	263	174	0.6519	549.3	563.8	2.64	4.96	1.93
5244	1356	262	174	0.5722	554.5	573.7	3.46	10.06	9.01
5245	1356	263	177	0.5963	566.3	577.7	2.01	6.85	5.31
5246	1356	260	180	0.5437	577.5	596.1	3.22	9.98	12.23
5247	1356	259	186	0.5579	596.1	610.9	2.49	4.96	6.76
5248	1261	261	189	0.7188	604.2	616.6	2.06	3.45	3.43
5249	1356	260	194	0.6080	616.3	624.0	1.25	1.25	4.34
5250	1356	263	202	0.5428	627.2	660.2	5.26	2.48	7.40
5251	1356	262	214	0.5452	650.8	697.0	7.10	1.83	9.06
5252	1356	263	209	0.6205	638.2	661.5	3.66	0.72	3.39
5253	1356	265	199	0.6542	610.7	629.8	3.12	2.01	4.18
5254	1343	267	185	0.6318	579.6	596.7	2.96	5.32	4.66
5255	1356	269	176	0.6509	552.7	568.5	2.86	6.79	4.20
5256	1356	270	172	0.6756	533.0	557.2	4.54	7.23	2.41
5257	1356	271	169	0.6706	512.5	551.0	7.51	10.95	3.83

...continued on next page.

Run#	G	Tin	Pwr	CHF_{cor}	T_{MaxExp}	$T_{MaxCode}$	$ErrT_{max}$	Err_{PDO}	STD
5258	1370	271	163	0.6925	453.9	527.0	16.10	16.10	0.00
5260	1044	260	147	0.5959	454.9	575.2	26.45	26.45	0.00
5261	1044	260	150	0.5705	498.6	587.9	17.90	20.97	3.69
5262	1044	261	150	0.6008	492.7	583.8	18.50	20.16	1.24
5263	1004	261	152	0.6308	520.4	598.3	14.96	18.51	3.73
5264	1017	258	153	0.6065	519.0	599.9	15.59	19.44	3.49
5265	1004	260	155	0.6158	546.9	608.9	11.34	15.28	5.50
5266	1004	261	155	0.6249	548.9	607.6	10.70	14.07	4.43
5267	1004	260	157	0.6471	558.4	610.5	9.32	12.24	3.69
5268	1004	261	160	0.6095	582.8	624.7	7.19	9.36	4.29
5269	1004	262	164	0.5111	601.0	659.9	9.80	10.66	10.18
5270	1004	262	168	0.6152	611.3	648.7	6.11	6.87	6.38
5271	1004	261	176	0.5333	631.0	686.7	8.83	6.99	9.35
5272	1004	262	184	0.5023	645.9	717.6	11.10	9.60	22.32
5273	1017	260	203	0.5421	669.6	759.9	13.49	5.12	11.43
5274	1031	264	215	0.9306	688.4	721.1	4.75	-6.89	15.02
5275	1031	261	189	0.6748	641.6	688.1	7.24	4.19	5.63
5276	1017	261	175	0.6995	613.4	651.3	6.18	7.17	6.04
5277	1031	260	155	0.6758	507.3	593.3	16.96	24.30	6.55
5278	1017	262	153	0.6735	503.4	592.0	17.60	23.13	4.37
5279	1044	261	152	0.6360	494.3	585.3	18.41	22.67	3.92
5282	1939	268	190	0.6284	581.7	530.7	-8.77	-0.89	8.98
5283	1939	268	193	0.6472	517.3	536.7	3.74	3.96	1.06
5285	1953	265	197	0.6500	514.4	542.7	5.50	15.55	14.51
5286	1953	264	203	0.6900	547.6	551.7	0.75	1.39	0.67
5287	1953	264	206	0.6662	558.5	559.2	0.12	1.65	1.49
5288	1953	264	209	0.6144	566.3	570.5	0.74	3.06	3.73
5289	1953	265	213	0.6741	574.1	572.2	-0.34	0.18	0.90
5290	1953	265	218	0.6776	582.3	582.0	-0.04	0.10	1.30
5291	1953	263	229	0.7180	602.7	601.2	-0.26	-0.42	1.94
5292	1967	266	233	0.6061	607.9	626.7	3.09	2.59	7.58

...continued on next page.

Run#	G	Tin	Pwr	CHF_{cor}	T_{MaxExp}	$T_{MaxCode}$	$ErrT_{max}$	Err_{PDO}	STD
5293	1980	265	237	0.7471	601.0	611.7	1.78	1.31	3.48
5294	1953	266	242	0.6852	618.6	635.3	2.71	0.16	2.61
5295	1980	264	230	0.8062	586.3	591.9	0.95	0.73	1.65
5296	1994	265	219	0.7318	566.7	574.5	1.38	2.55	1.93
5297	1994	266	213	0.7879	552.2	559.9	1.39	2.70	1.26
5298	1980	261	210	0.7353	535.3	558.9	4.41	10.87	9.94
5302	2577	266	223	0.7966	494.7	504.5	1.98	2.39	0.40
5303	2577	268	219	0.7819	492.0	499.2	1.47	1.25	0.58
5304	2563	267	226	0.8033	511.8	514.8	0.59	4.09	5.80
5305	2577	267	229	0.8323	517.2	516.3	-0.17	0.51	1.18
5306	2577	267	231	0.8325	531.5	521.0	-1.97	-1.38	1.49
5307	2509	266	232	0.8677	538.4	528.4	-1.86	-1.37	2.01
5308	2577	264	241	0.8419	546.7	536.8	-1.81	-0.38	1.83
5309	2550	265	243	0.9061	554.2	539.4	-2.67	-1.46	2.10
5310	2550	266	249	0.7925	565.2	559.1	-1.08	-0.23	1.70
5311	2550	263	250	0.8427	567.6	554.5	-2.32	-0.97	1.61
5312	2536	265	257	0.8122	581.9	574.7	-1.24	-0.55	1.55
5313	2536	265	265	0.8186	595.1	590.4	-0.80	-0.49	1.74
5314	2550	267	259	0.7834	579.2	584.0	0.83	0.49	2.40
5315	2523	264	246	0.8228	557.0	552.6	-0.80	0.94	1.56
5316	2523	265	239	0.8707	573.4	538.2	-6.13	-1.10	3.66
5317	2523	266	230	0.8686	519.2	521.9	0.52	1.02	1.53
5318	2523	264	229	0.8526	501.7	518.2	3.30	12.33	12.53
5319	2563	267	229	0.9400	494.1	503.9	1.99	1.48	0.51
5367	3852	274	281	1.1698	424.3	449.1	5.84	5.84	0.00
5368	3852	273	287	1.1105	493.6	500.5	1.39	3.63	2.87
5369	3852	271	290	1.0616	495.3	510.4	3.04	10.23	9.68
5370	3852	273	298	1.2303	509.6	505.5	-0.81	1.44	3.71
5371	3852	274	300	1.1730	515.5	513.3	-0.43	3.04	2.99
5372	3852	274	307	1.1281	521.7	528.7	1.34	3.50	2.75
5373	3852	273	309	1.1418	526.9	530.3	0.64	2.93	2.95

...continued on next page.

Run#	G	Tin	Pwr	CHF_{cor}	T_{MaxExp}	$T_{MaxCode}$	$ErrT_{max}$	Err_{PDO}	STD
5374	3852	274	323	1.1437	545.9	552.8	1.26	4.62	5.23
5375	3838	274	322	1.0631	545.6	564.3	3.42	6.96	9.68
5376	3852	271	341	1.0329	555.9	597.5	7.49	5.89	5.28
5377	3811	270	344	1.0522	571.8	600.5	5.02	3.72	2.79
5378	3811	272	348	0.9797	584.6	616.0	5.37	6.43	8.52
5379	3798	274	377	1.0862	644.1	636.8	-1.14	3.34	3.14
5380	3852	273	373	1.1782	614.5	617.7	0.53	3.77	2.61
5381	3825	277	344	1.1935	567.6	585.4	3.13	3.41	2.31
5382	3852	271	322	1.1653	536.0	548.6	2.35	3.29	1.67
5383	3906	271	316	1.3102	522.2	520.0	-0.42	2.34	3.03
5384	3892	274	305	1.3514	508.8	502.8	-1.18	0.59	3.79
5385	3906	271	300	1.2710	498.3	498.5	0.03	2.75	3.12
5386	3892	271	291	1.2351	428.9	468.7	9.28	9.28	0.00
5388	5181	270	359	1.3156	427.1	320.8	-24.90	-24.90	0.00
5389	5181	270	358	1.2048	482.4	453.6	-5.98	-5.43	7.38
5390	5167	271	368	1.3011	494.9	462.6	-6.52	-9.18	13.78
5391	5181	270	366	1.2394	500.0	463.8	-7.23	-9.75	13.45
5392	5154	274	367	1.1918	498.8	482.1	-3.35	-0.19	4.54
5393	5140	270	374	1.1673	509.2	491.5	-3.47	-1.66	4.16
5394	5181	271	388	1.1405	524.2	505.5	-3.58	-0.69	5.17
5395	5181	271	394	1.1219	529.4	514.1	-2.89	3.12	8.21
5396	5235	267	404	1.1024	537.8	524.7	-2.44	3.39	7.50
5397	5181	270	406	1.0745	543.4	535.2	-1.50	1.49	4.10

V.2 Figures

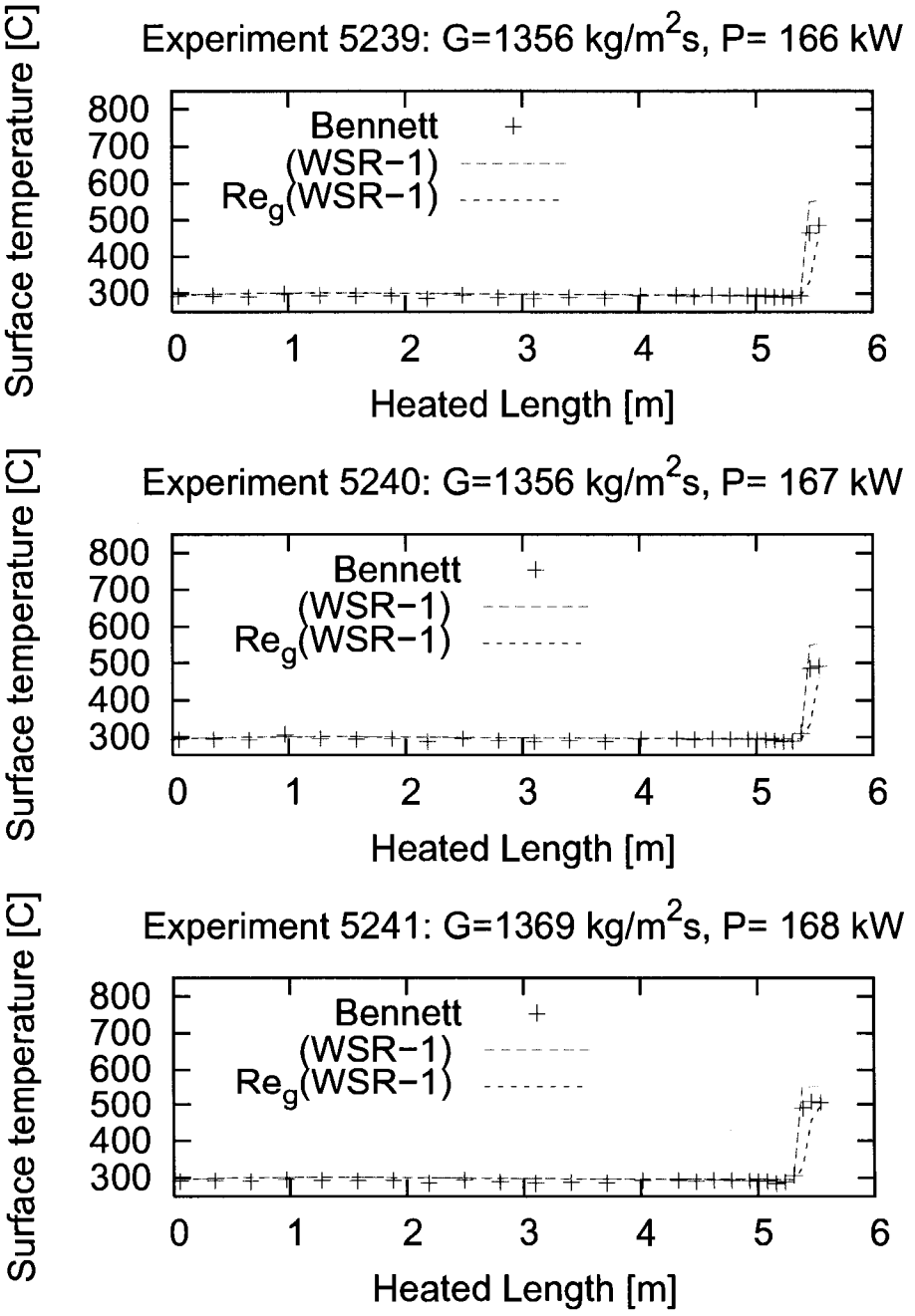

Figure V.1 Improved Correlation: Experiments 5239, 5240 and 5241

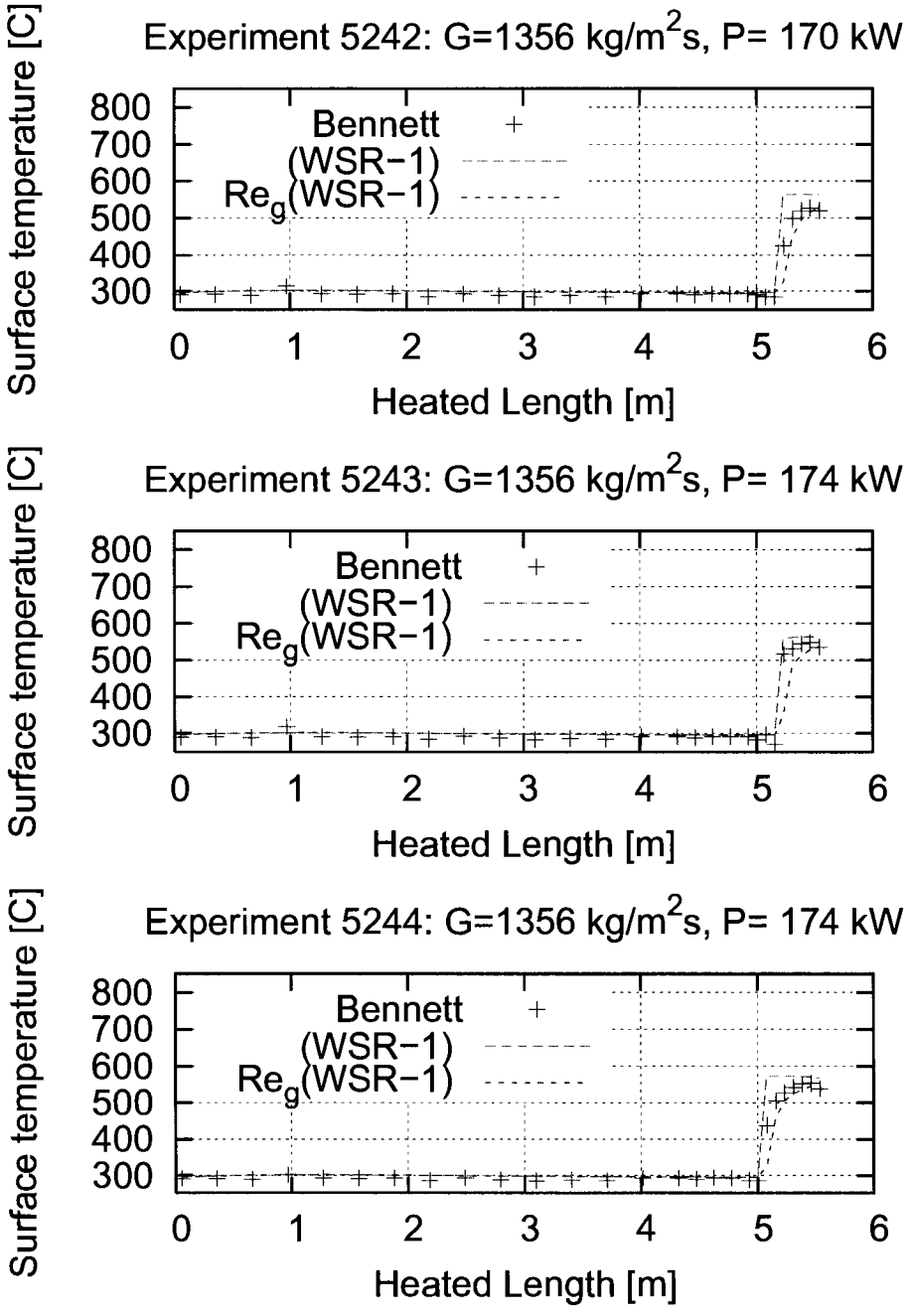

Figure V.2 Improved Correlation: Experiments 5242, 5243 and 5244

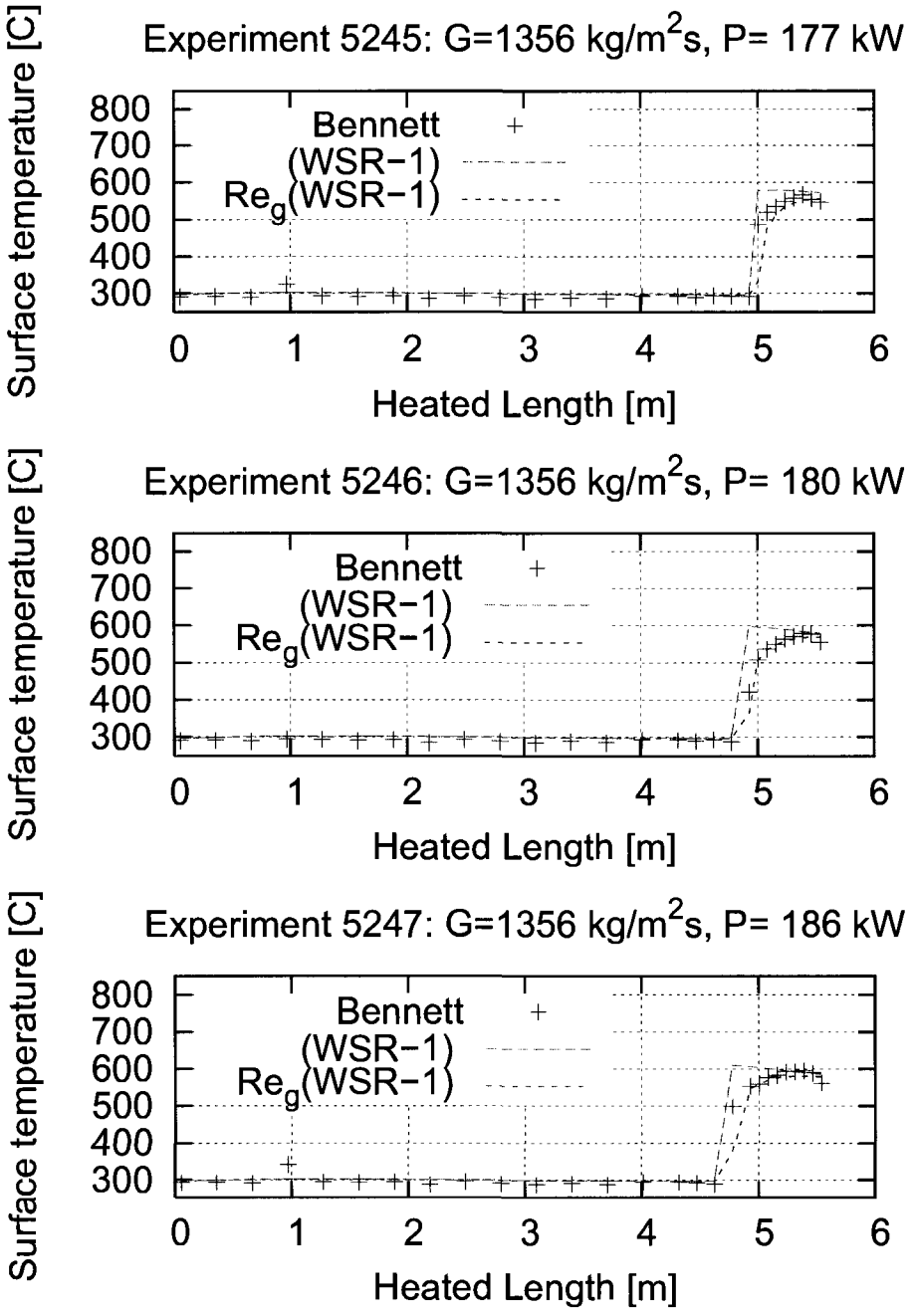

Figure V.3 Improved Correlation: Experiments 5245, 5246 and 5247

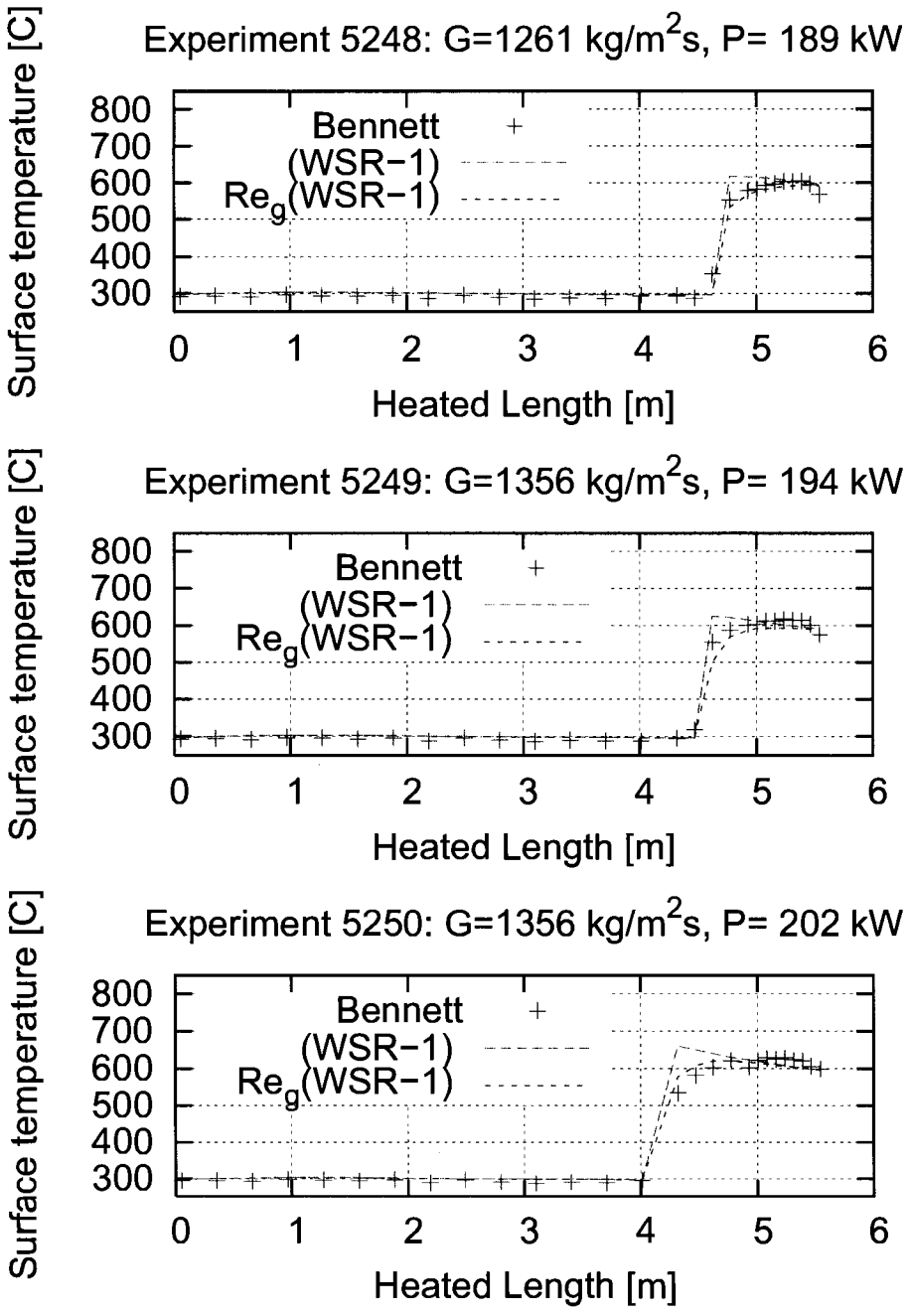

Figure V.4 Improved Correlation: Experiments 5278, 5249 and 5250

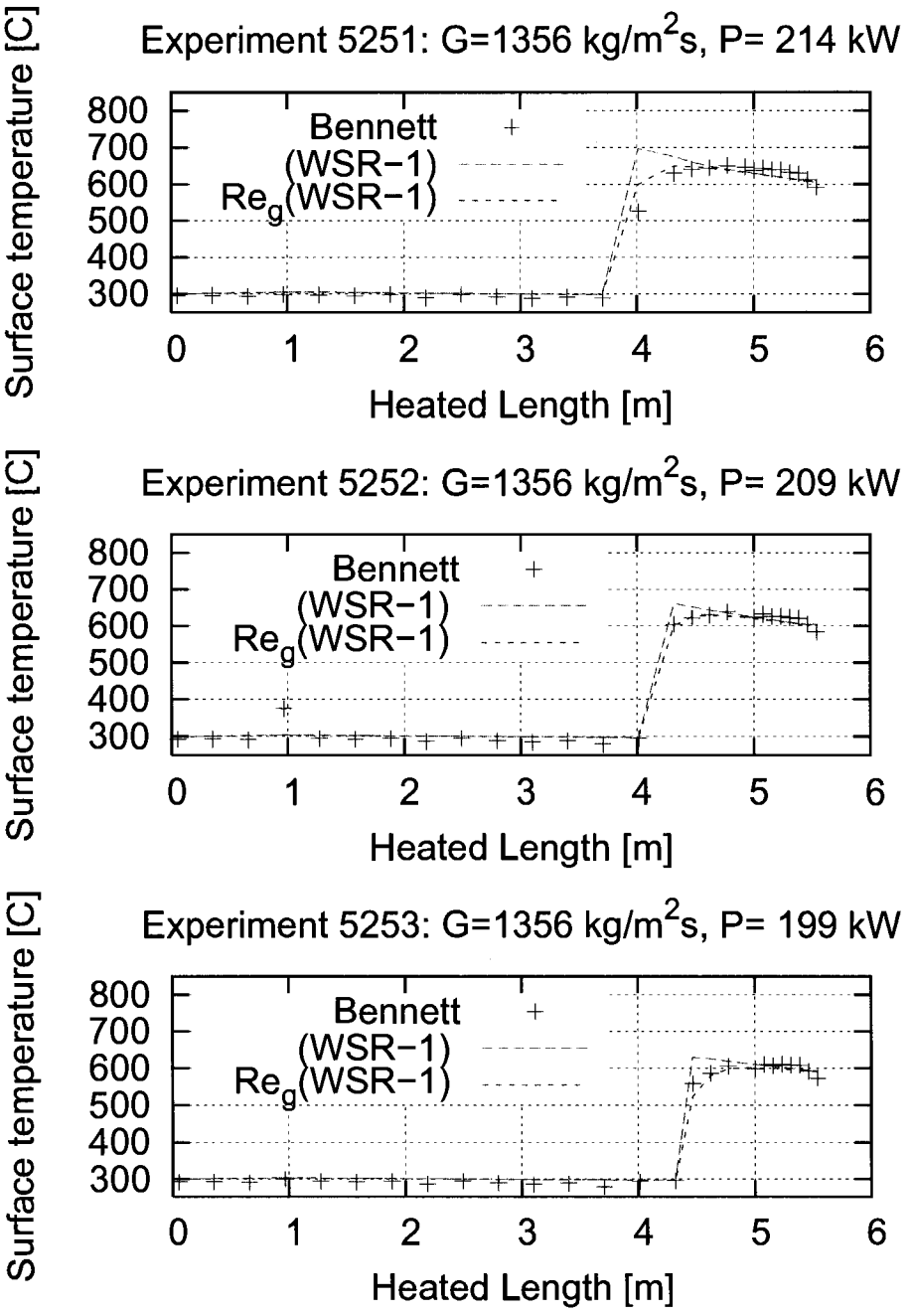

Figure V.5 Improved Correlation: Experiments 5251, 5252 and 5253

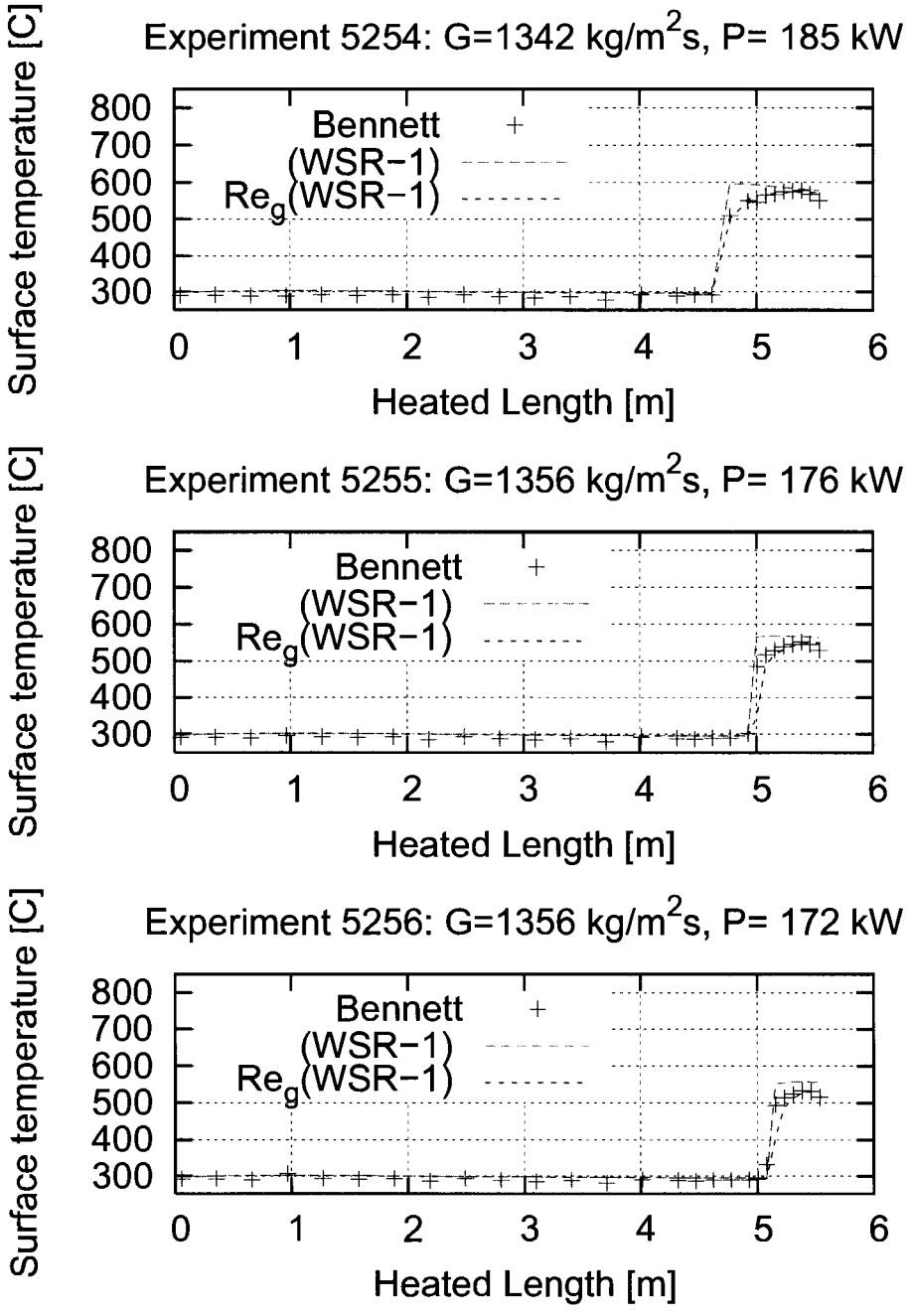

Figure V.6 Improved Correlation: Experiments 5254, 5255 and 5256

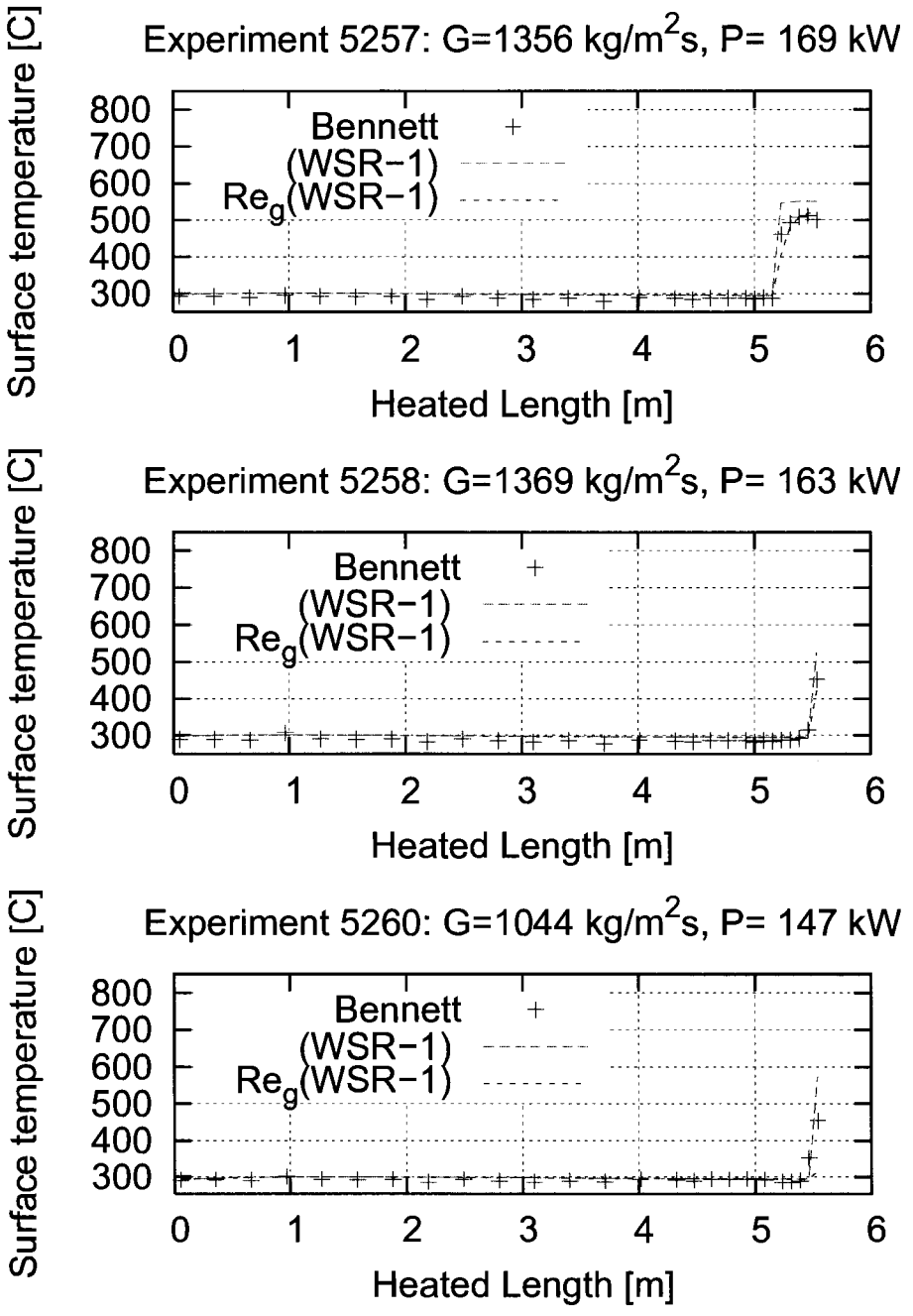

Figure V.7 Improved Correlation: Experiments 5257, 5258 and 5260

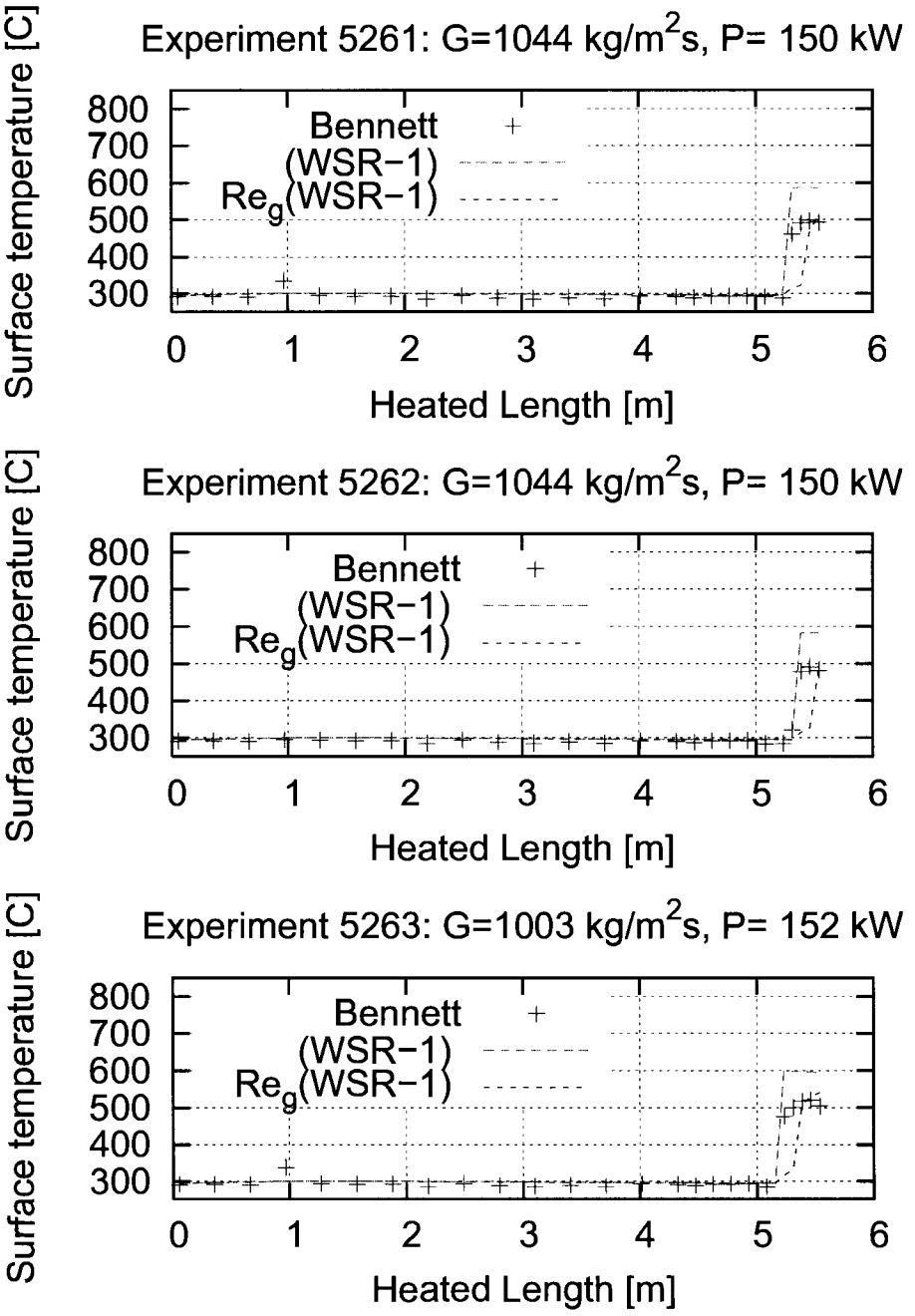

Figure V.8 Improved Correlation: Experiments 5261, 5262 and 5263

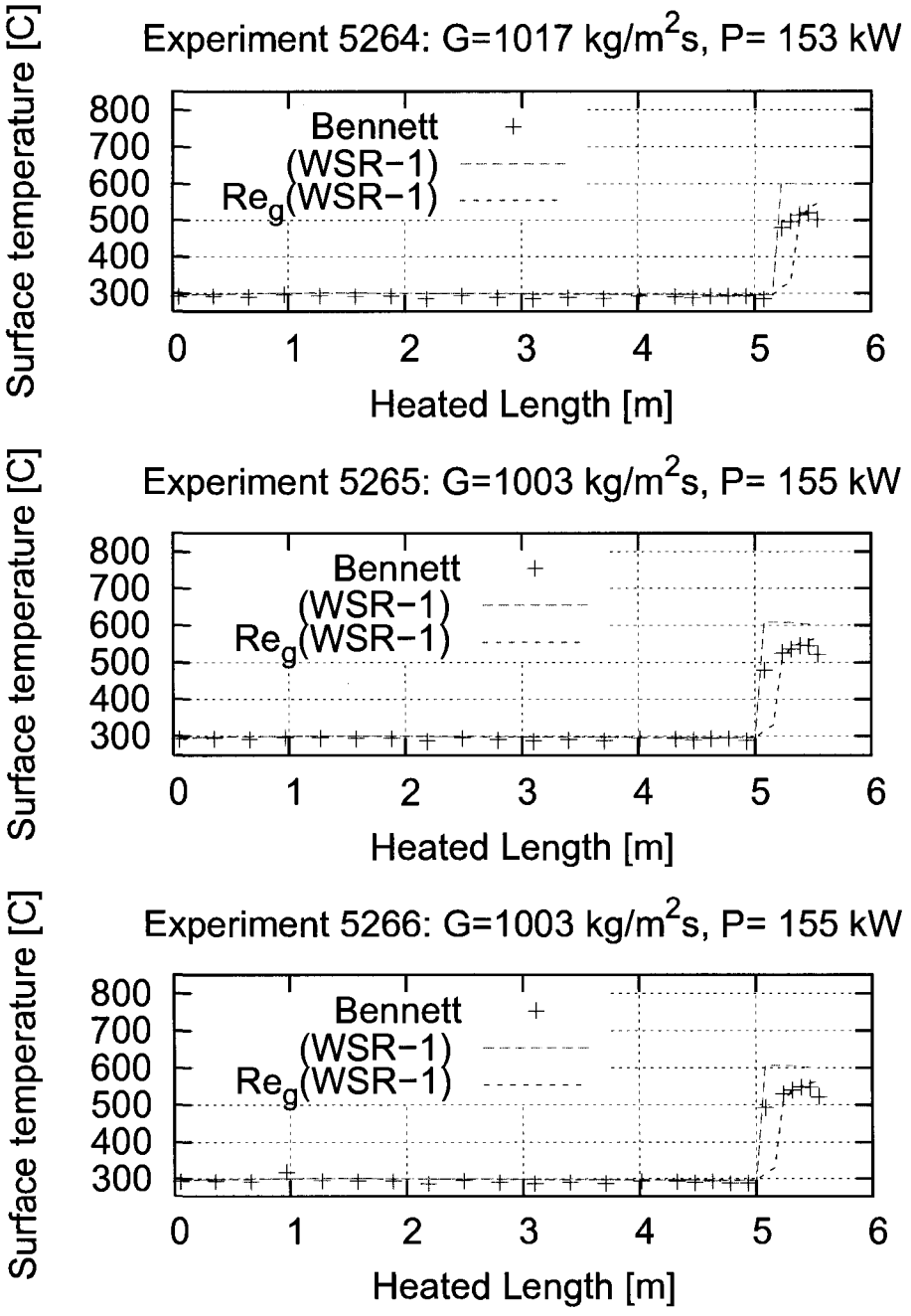

Figure V.9 Improved Correlation: Experiments 5264, 5265 and 5266

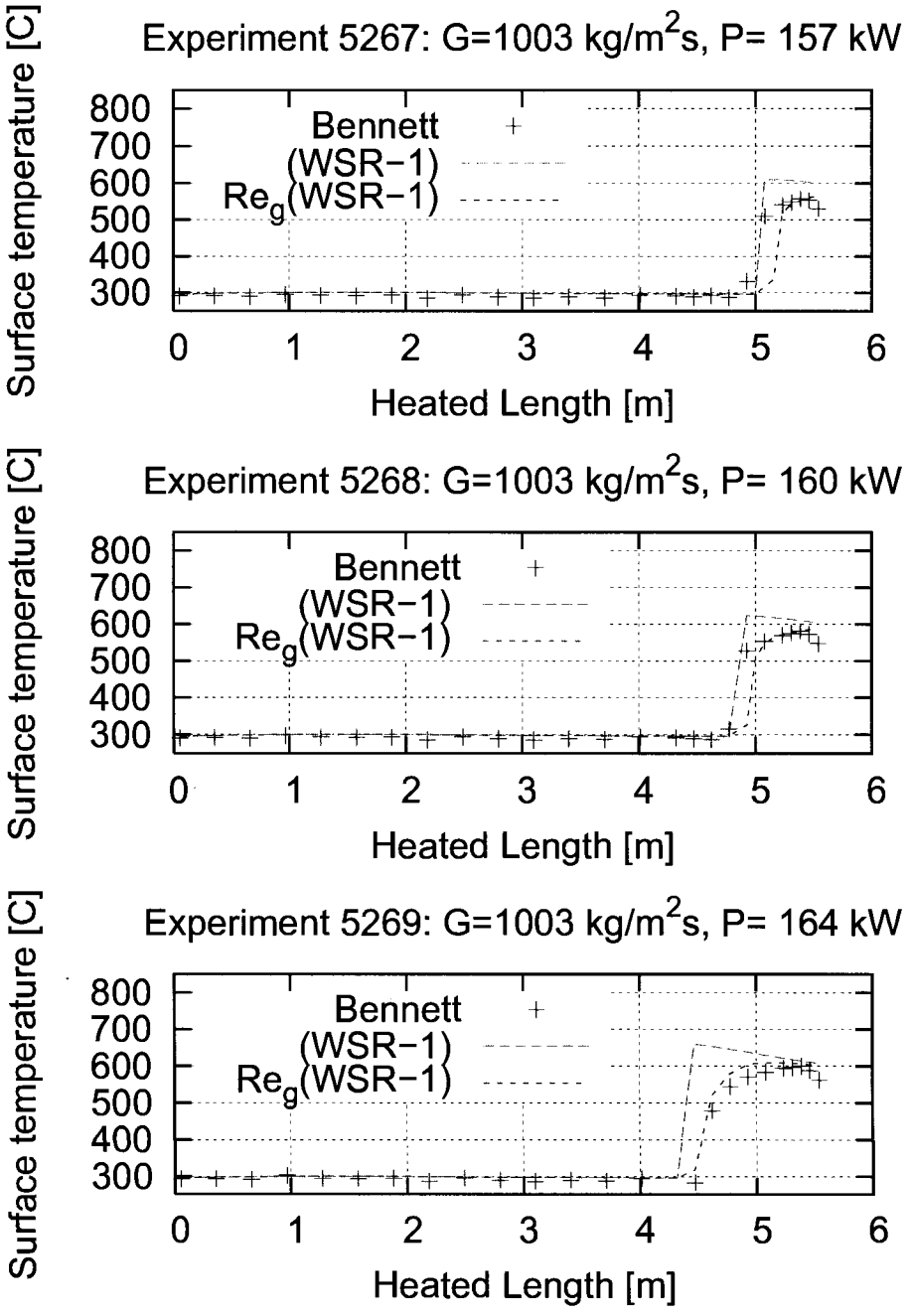

Figure V.10 Improved Correlation: Experiments 5267, 5268 and 5269

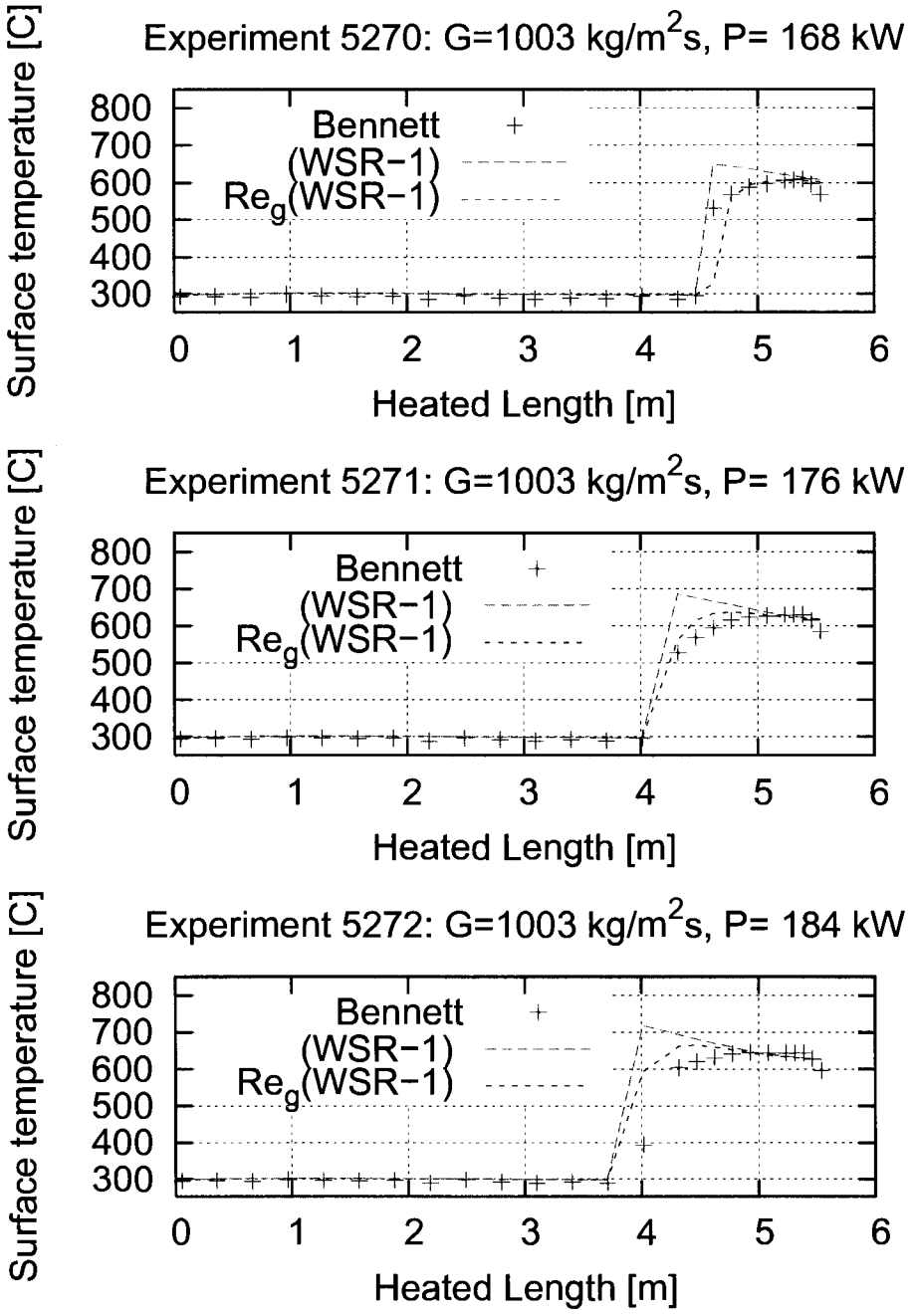

Figure V.11 Improved Correlation: Experiments 5270, 5271 and 5272

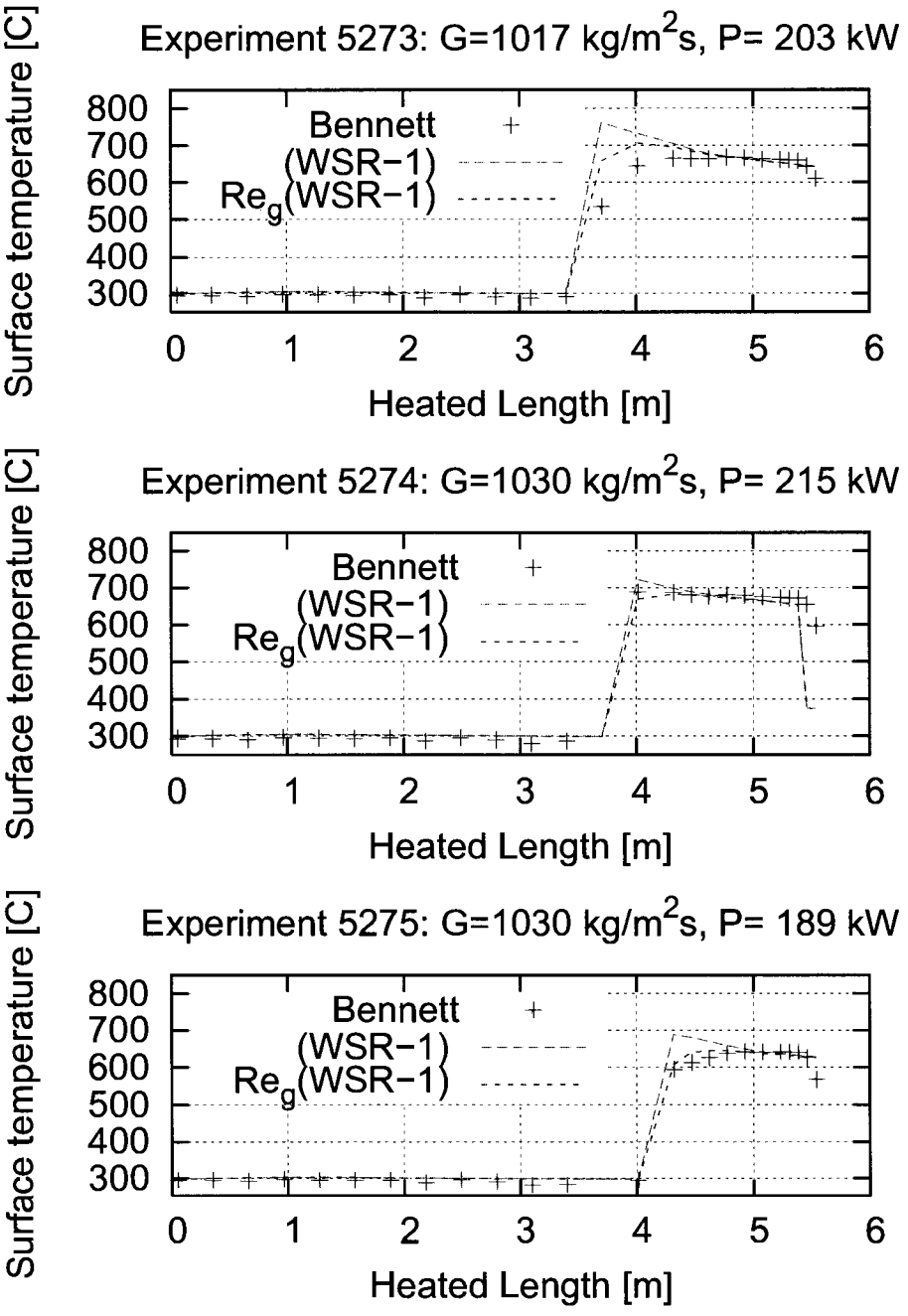

Figure V.12 Improved Correlation: Experiments 5273, 5274 and 5275

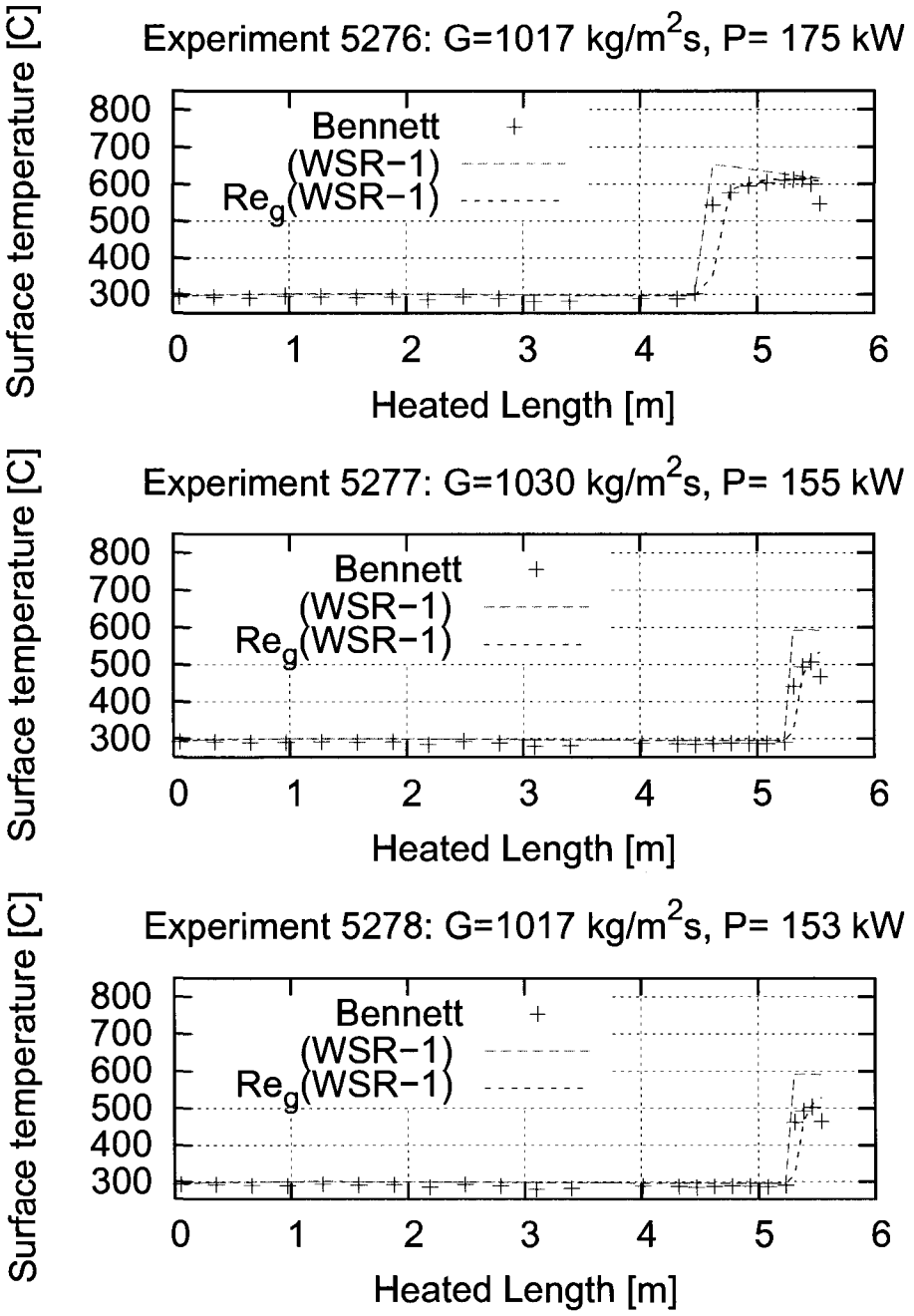

Figure V.13 Improved Correlation: Experiments 5276, 5277 and 5278

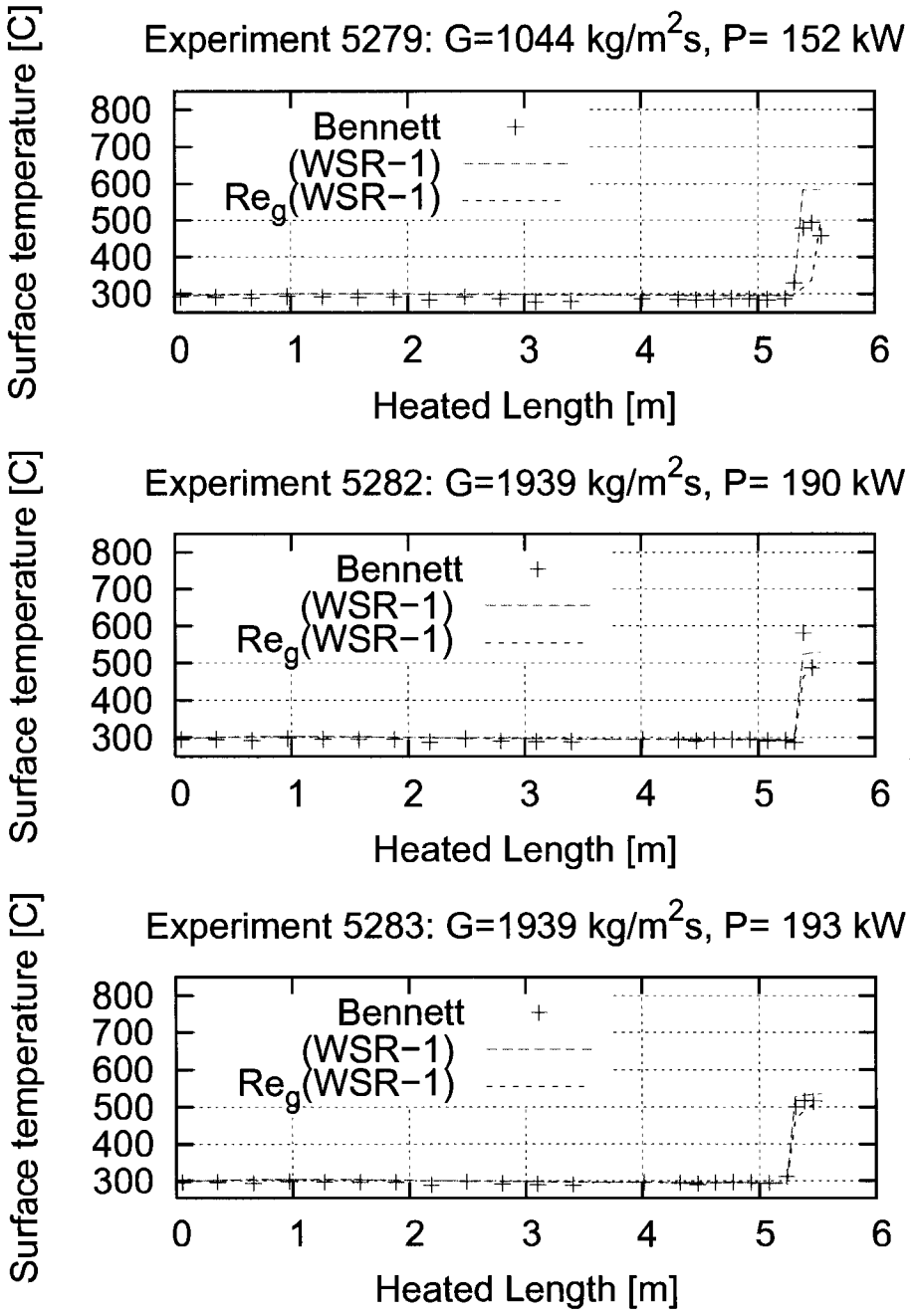

Figure V.14 Improved Correlation: Experiments 5279, 5282 and 5283

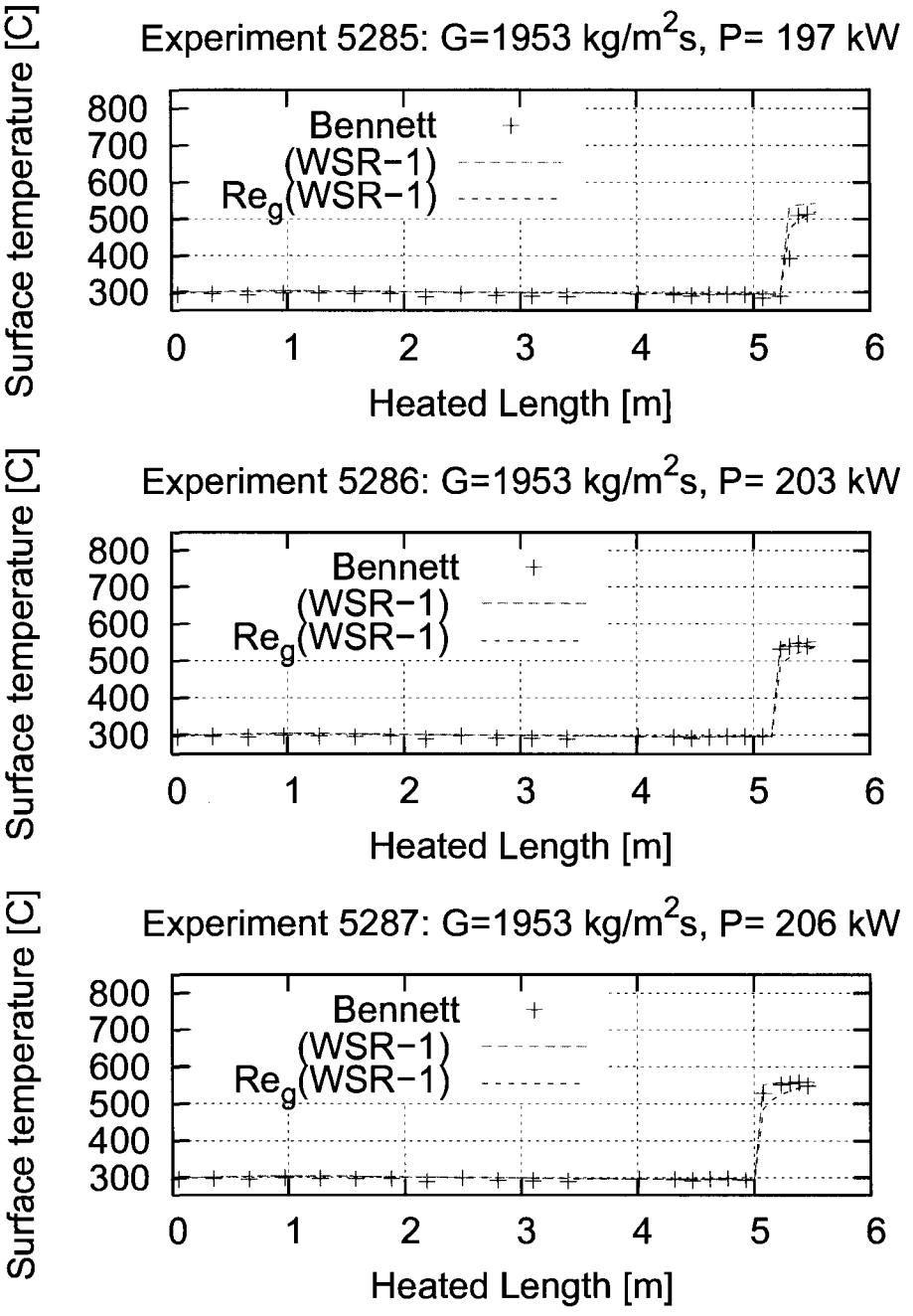

Figure V.15 Improved Correlation: Experiments 5285, 5286 and 5287

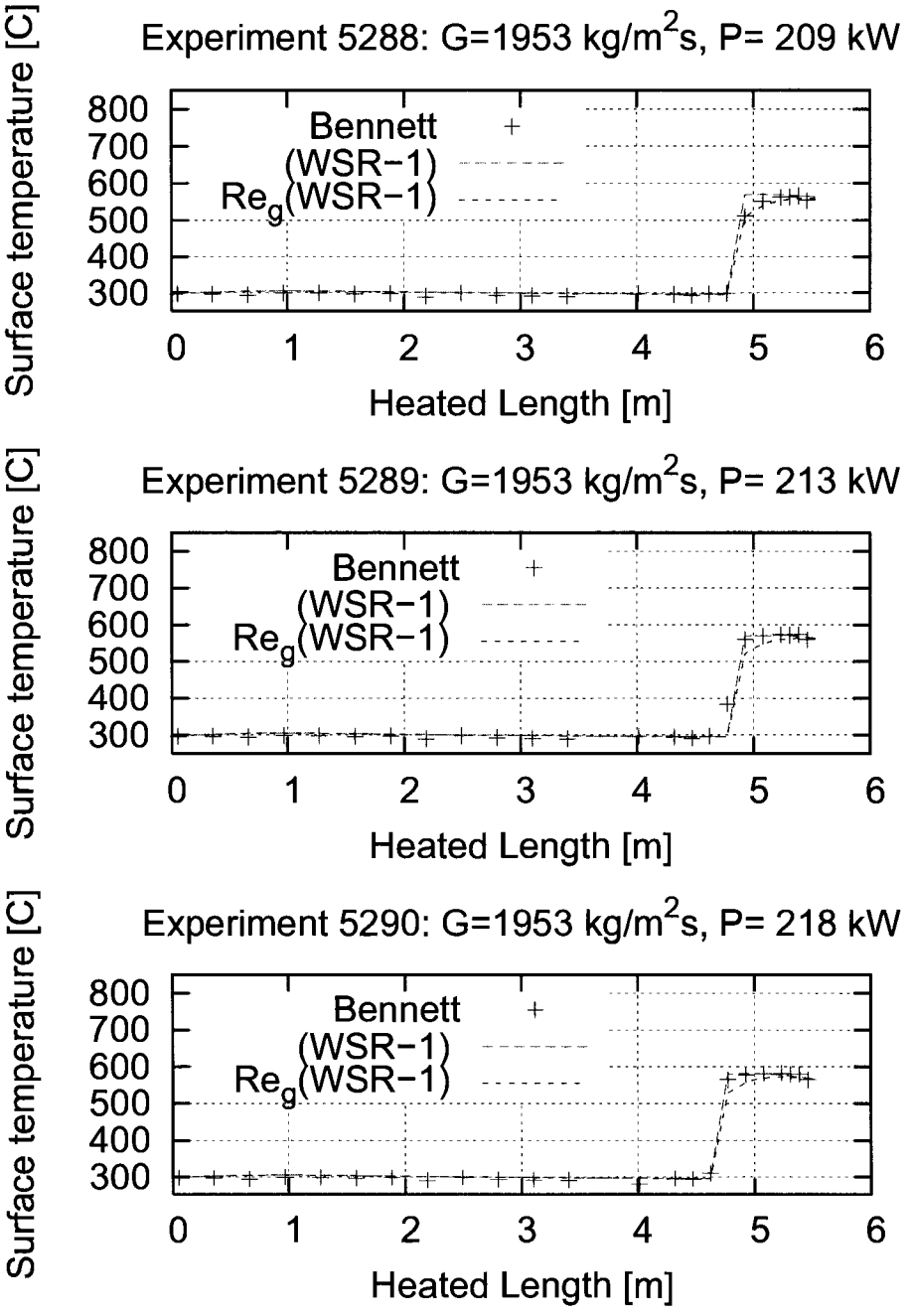

Figure V.16 Improved Correlation: Experiments 5288, 5289 and 5290

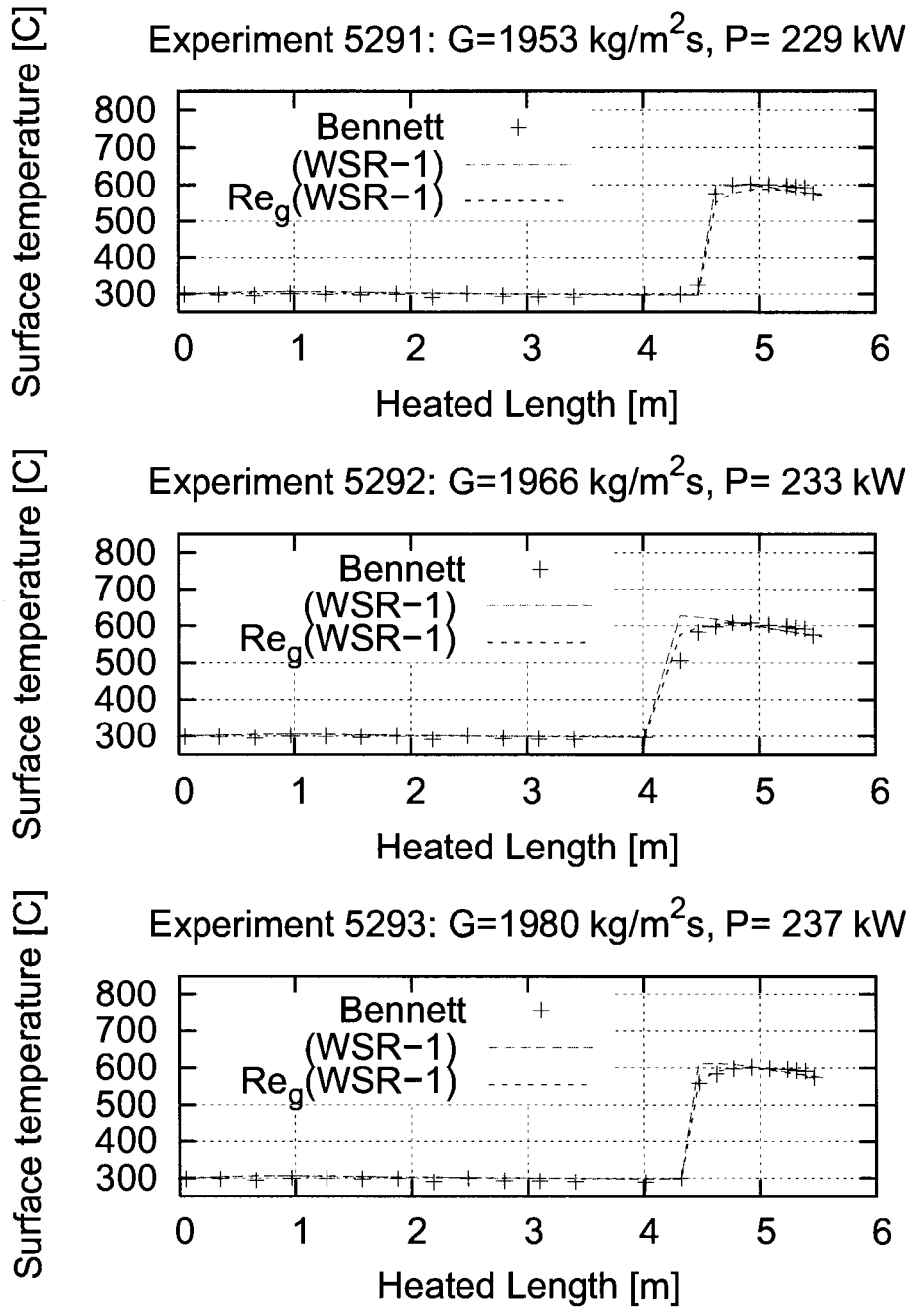

Figure V.17 Improved Correlation: Experiments 5291, 5292 and 5293

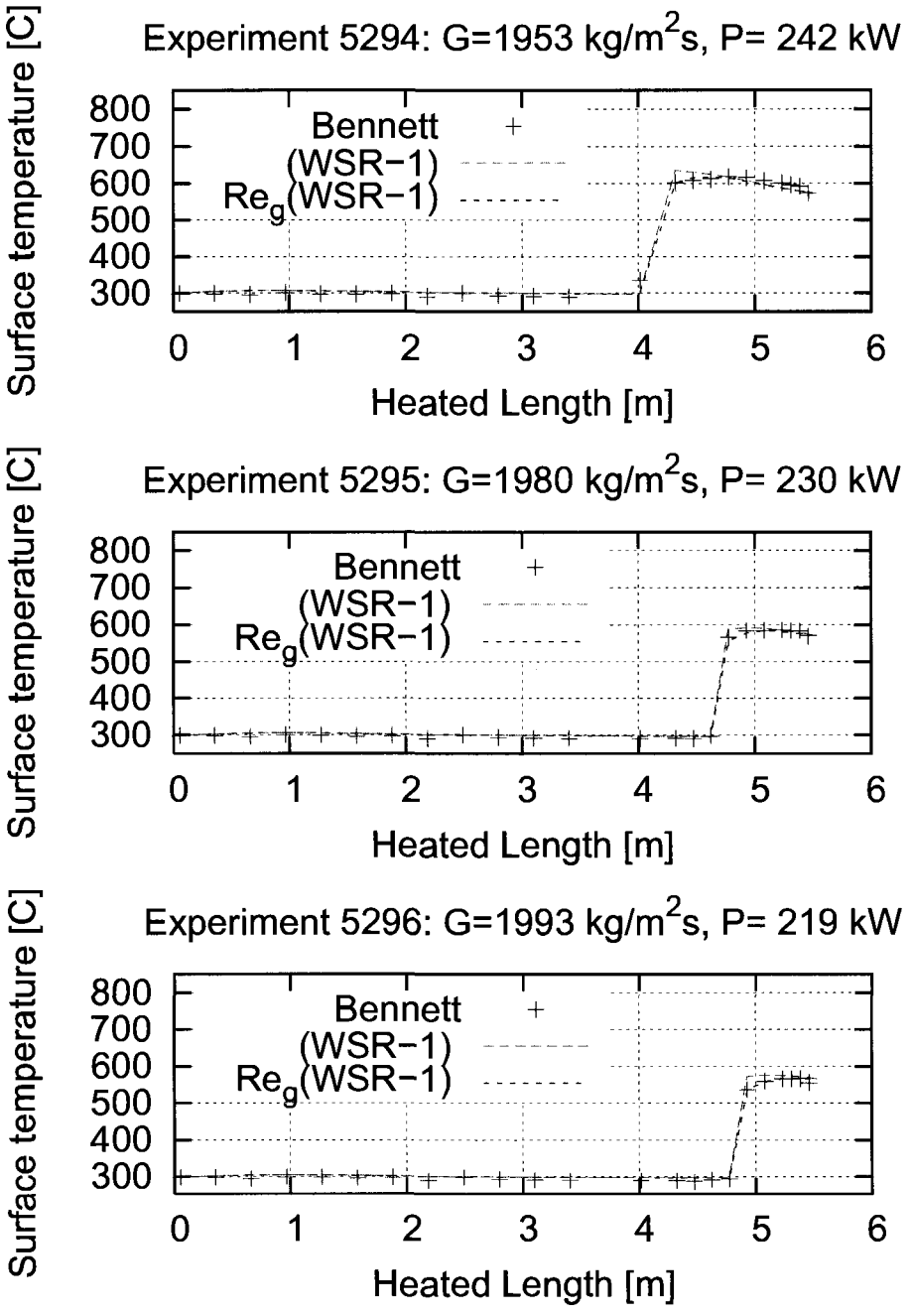

Figure V.18 Improved Correlation: Experiments 5294, 5295 and 5296

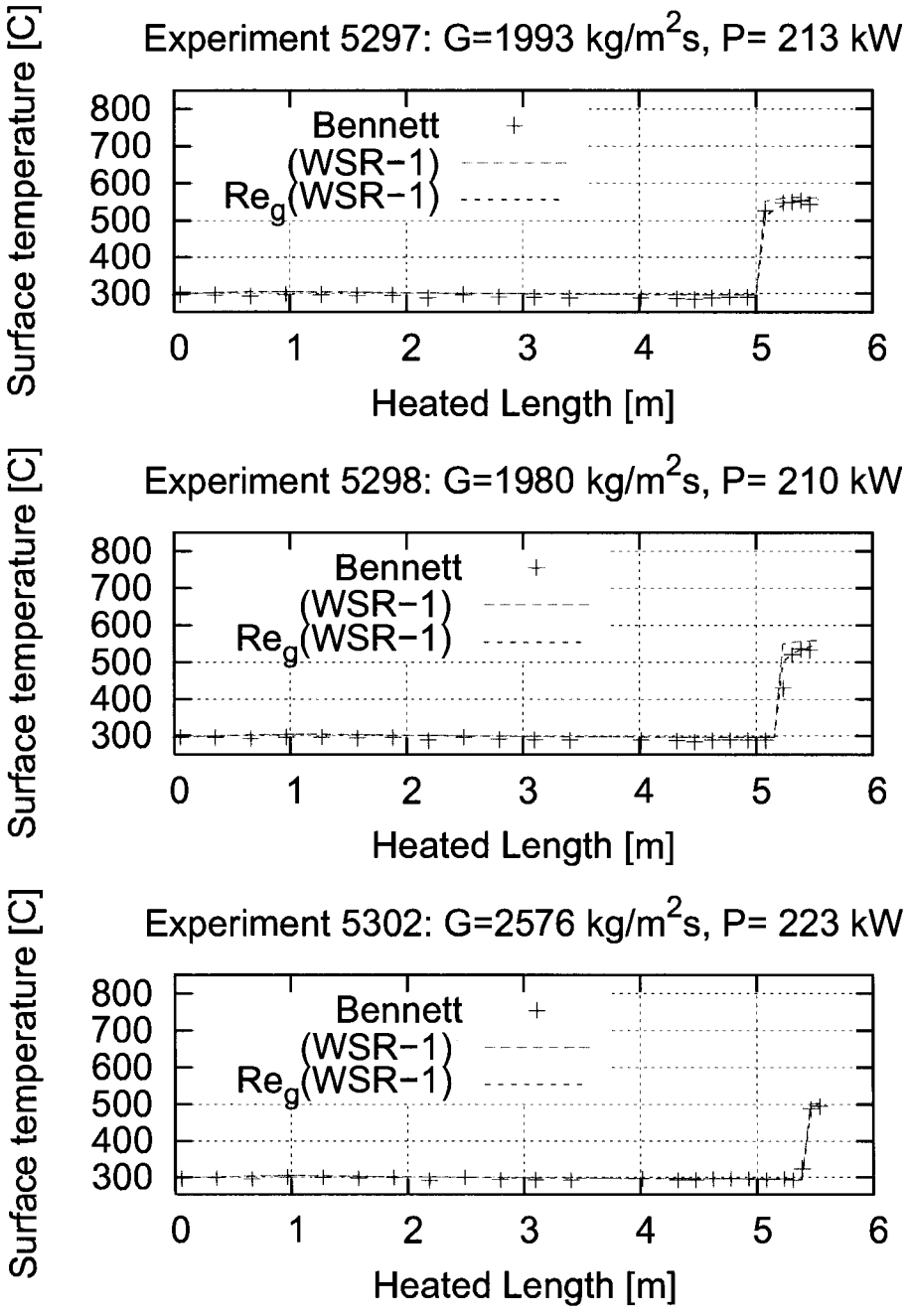

Figure V.19 Improved Correlation: Experiments 5297, 5298 and 5302

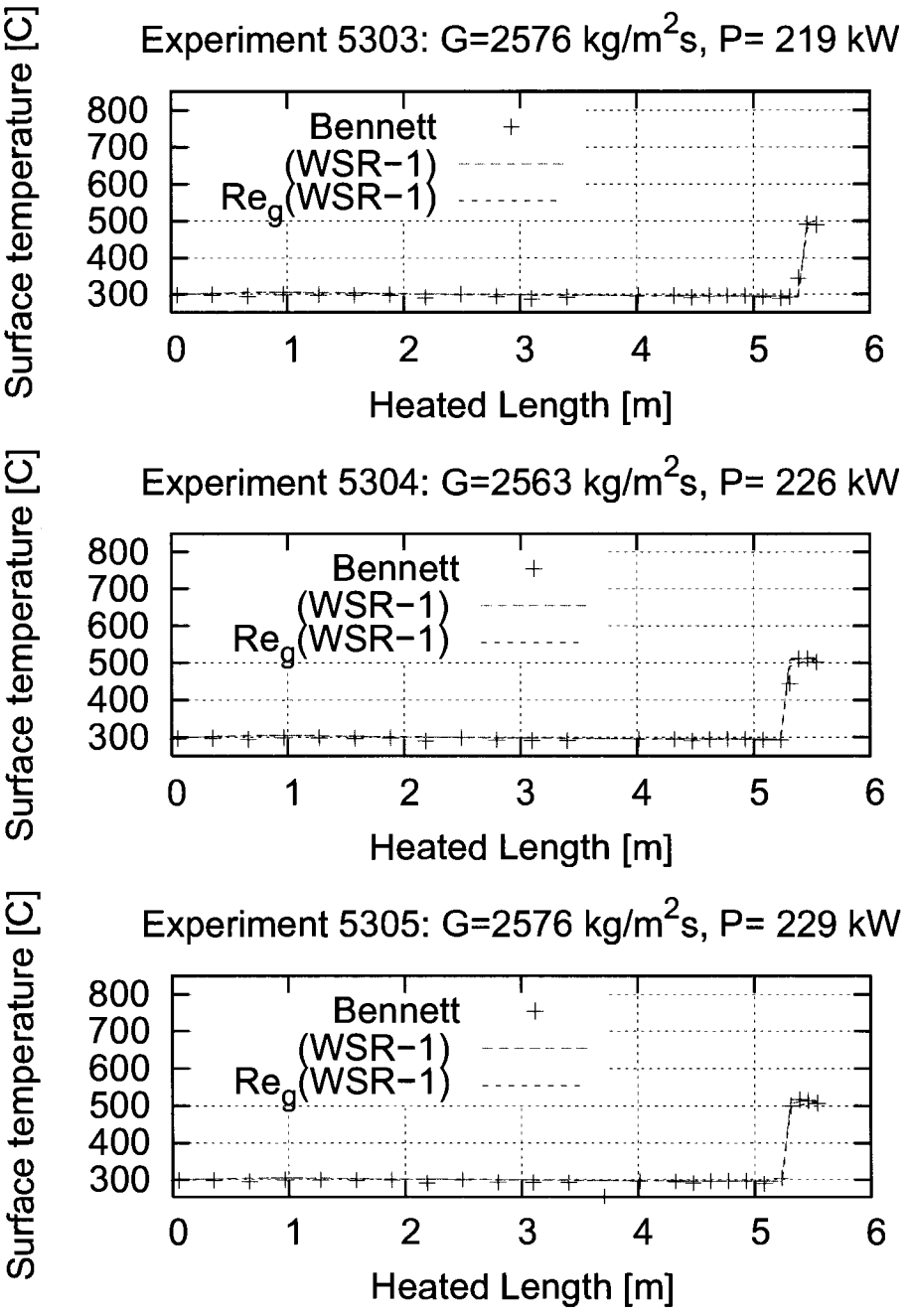

Figure V.20 Improved Correlation: Experiments 5303, 5304 and 5305

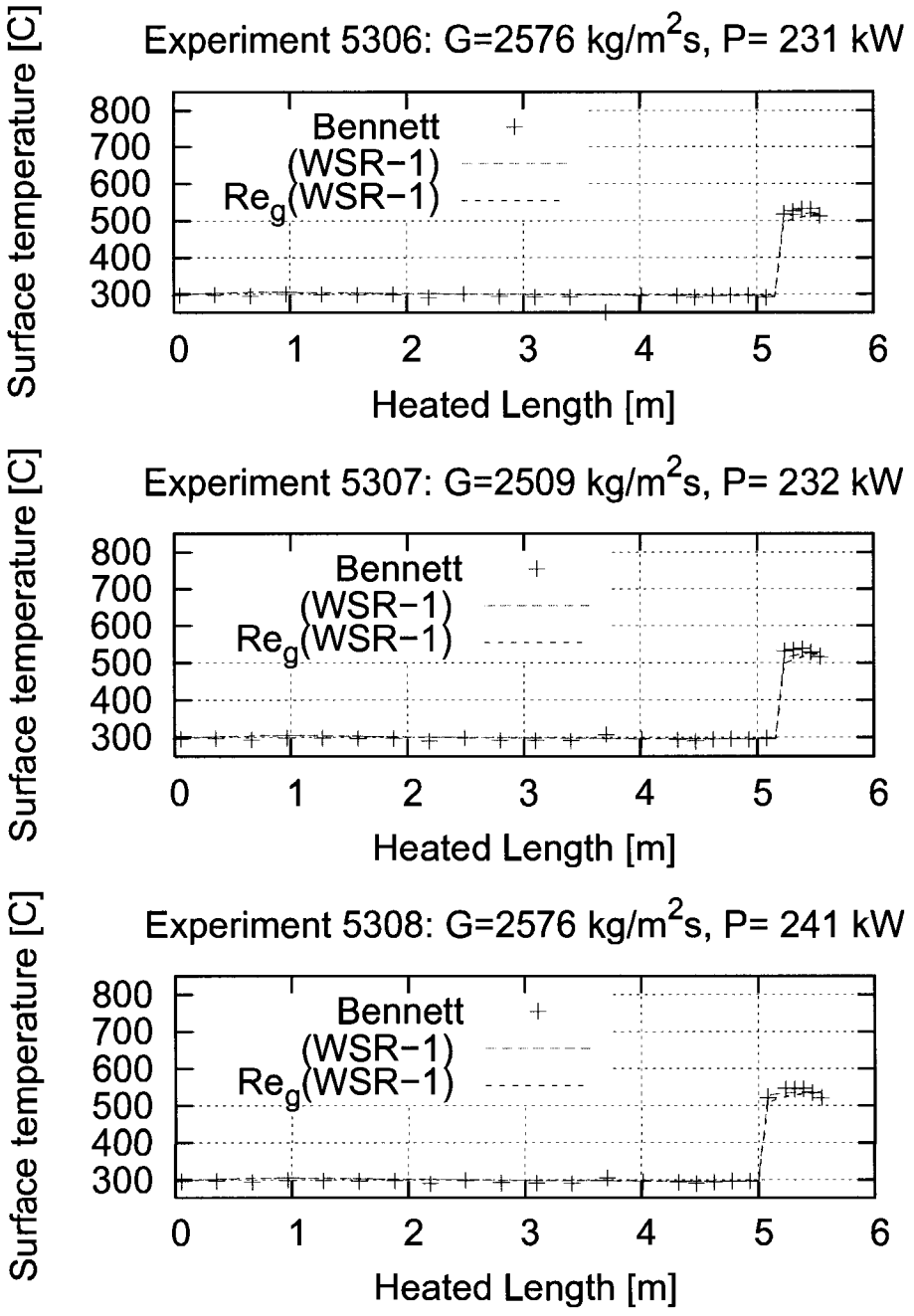

Figure V.21 Improved Correlation: Experiments 5306, 5307 and 5308

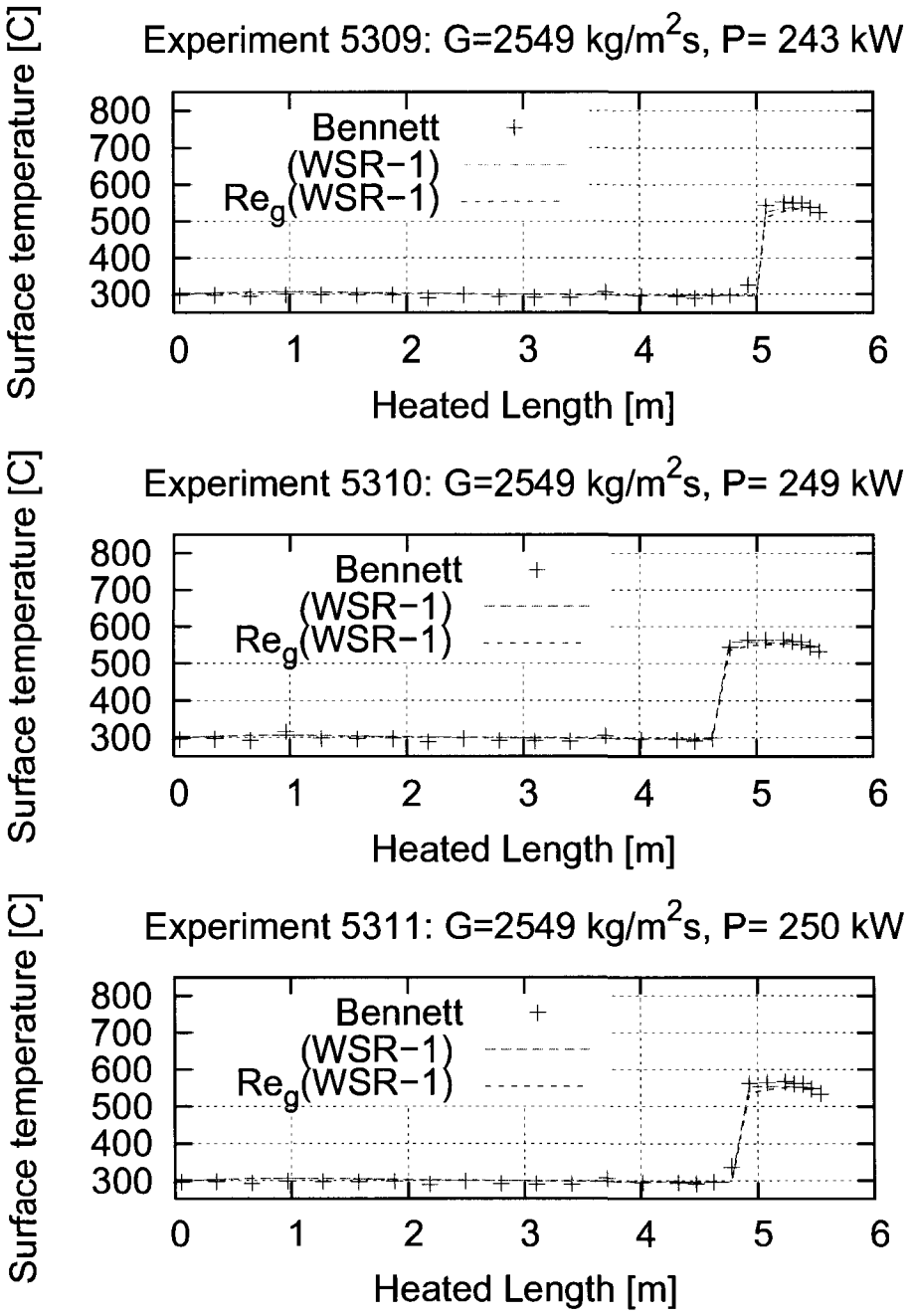

Figure V.22 Improved Correlation: Experiments 5309, 5310 and 5311

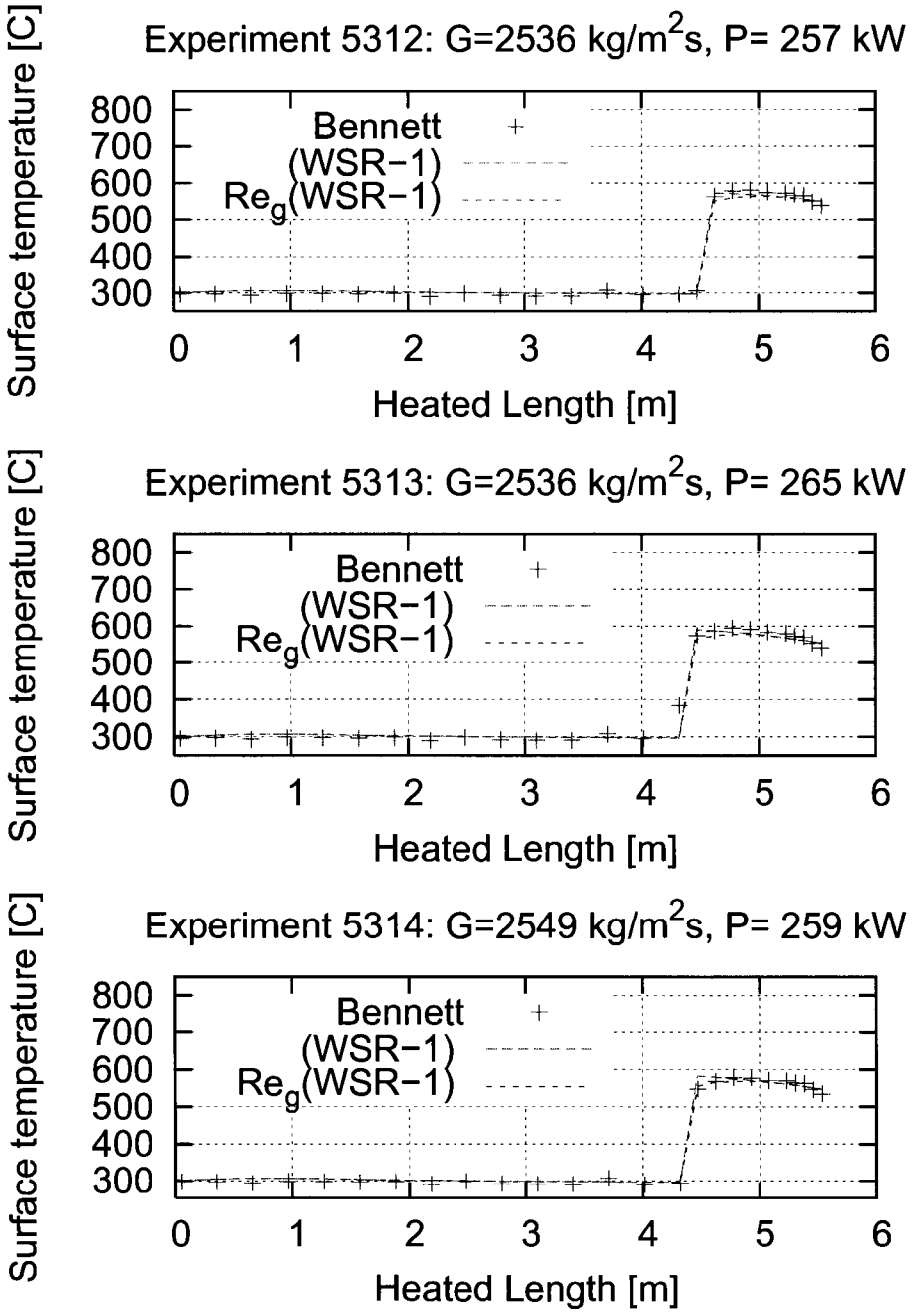

Figure V.23 Improved Correlation: Experiments 5312, 5313 and 5314

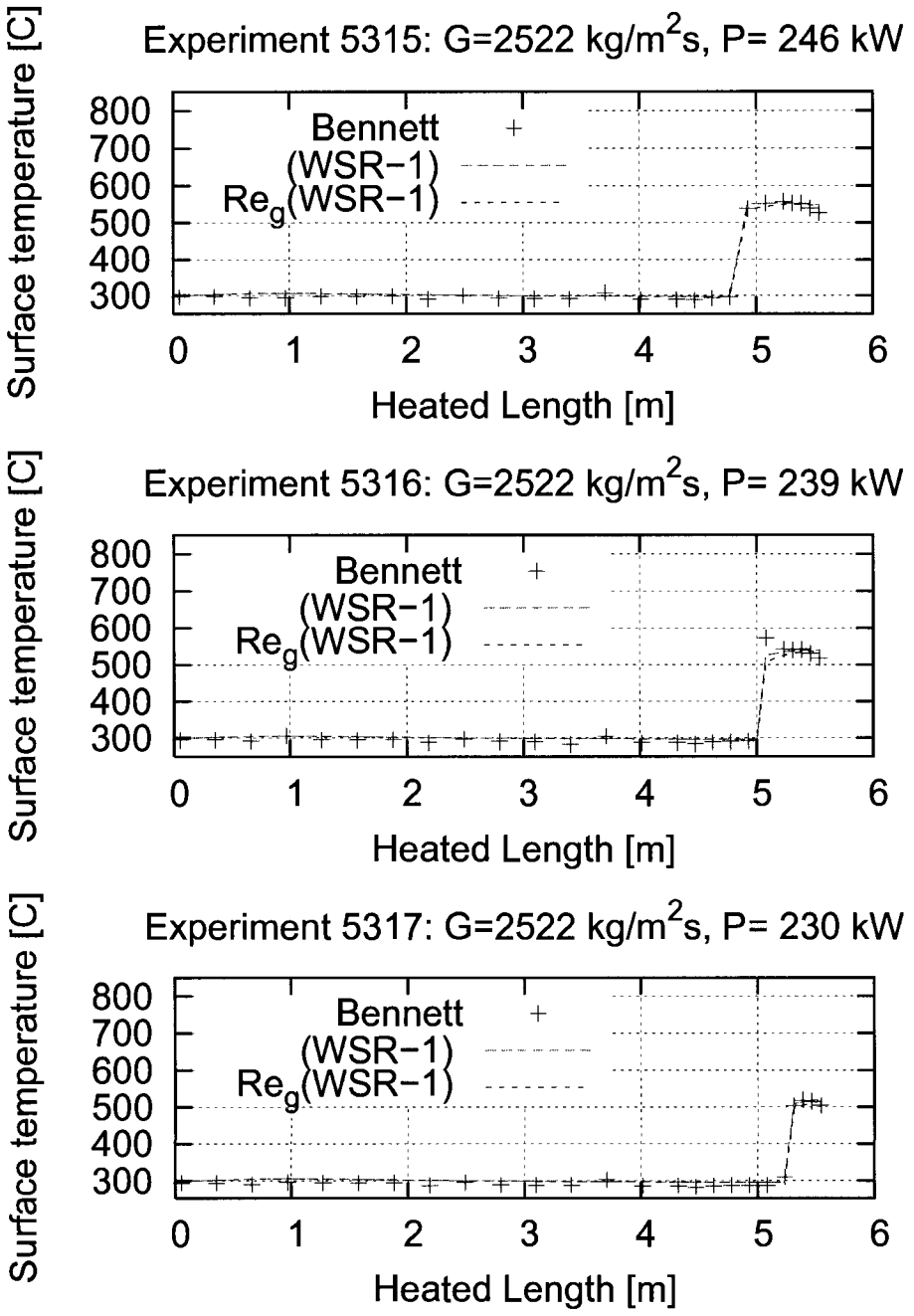

Figure V.24 Improved Correlation: Experiments 5315, 5316 and 5317

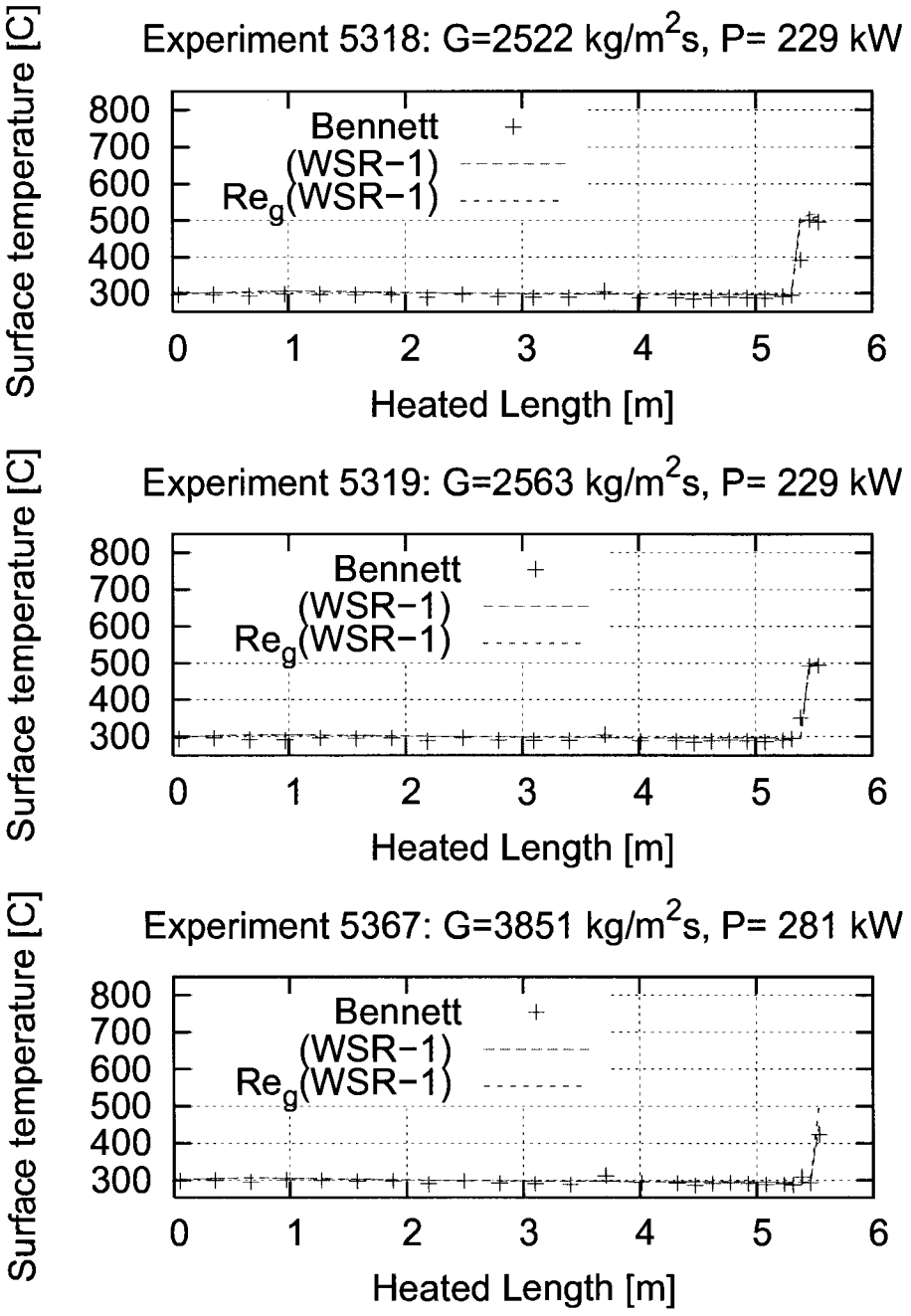

Figure V.25 Improved Correlation: Experiments 5318, 5319 and 5367

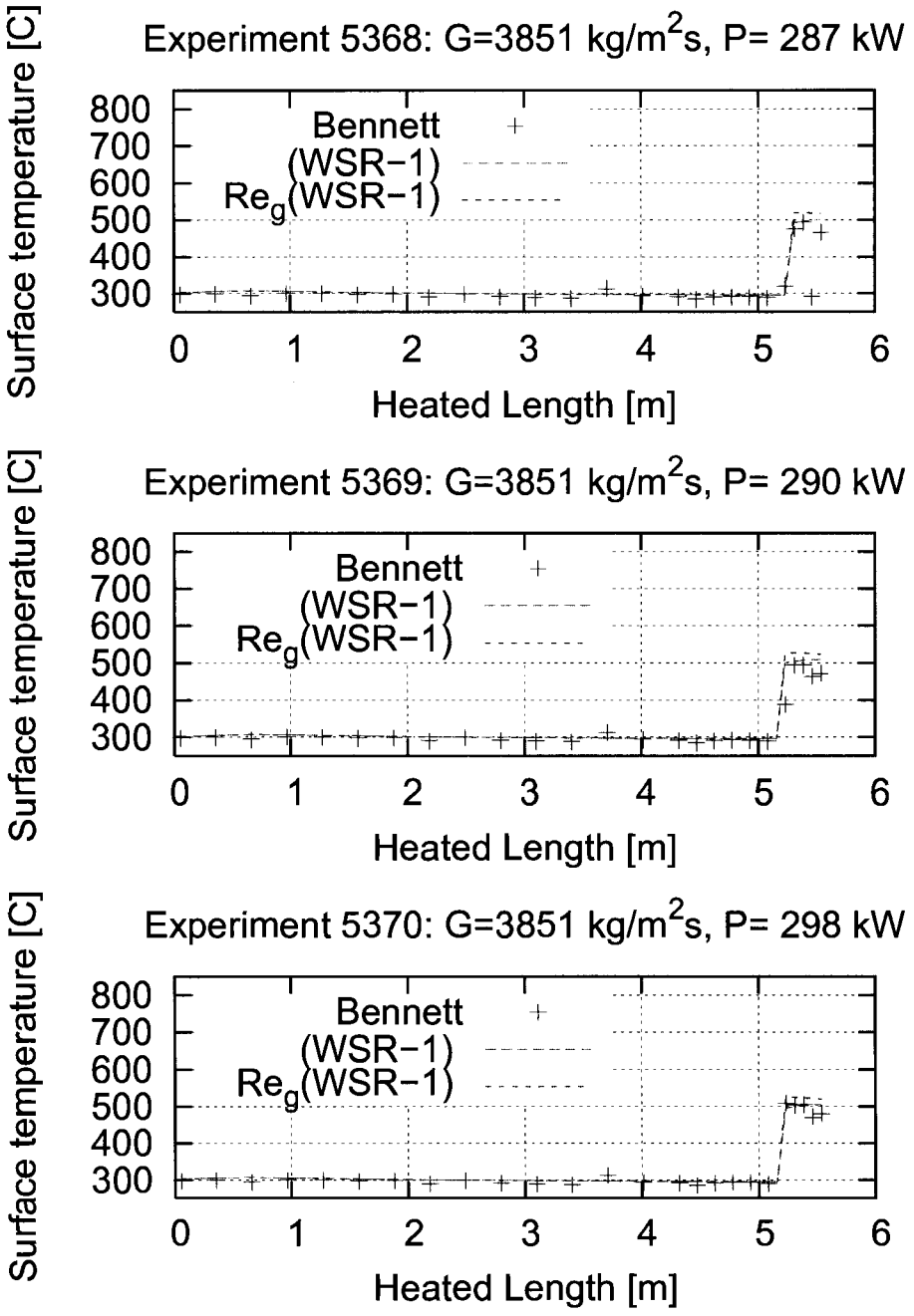

Figure V.26 Improved Correlation: Experiments 5368, 5369 and 5370

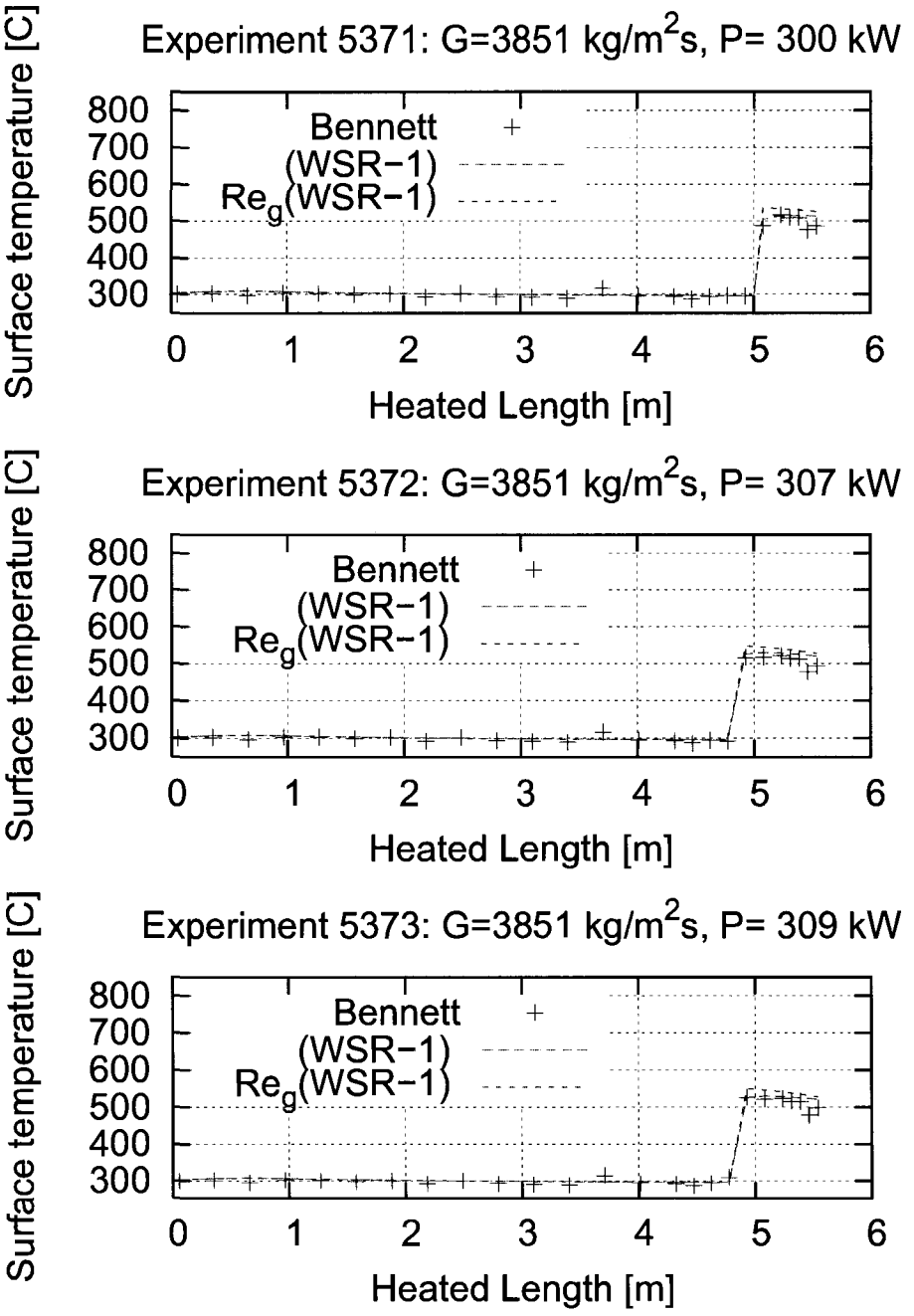

Figure V.27 Improved Correlation: Experiments 5371, 5372 and 5373

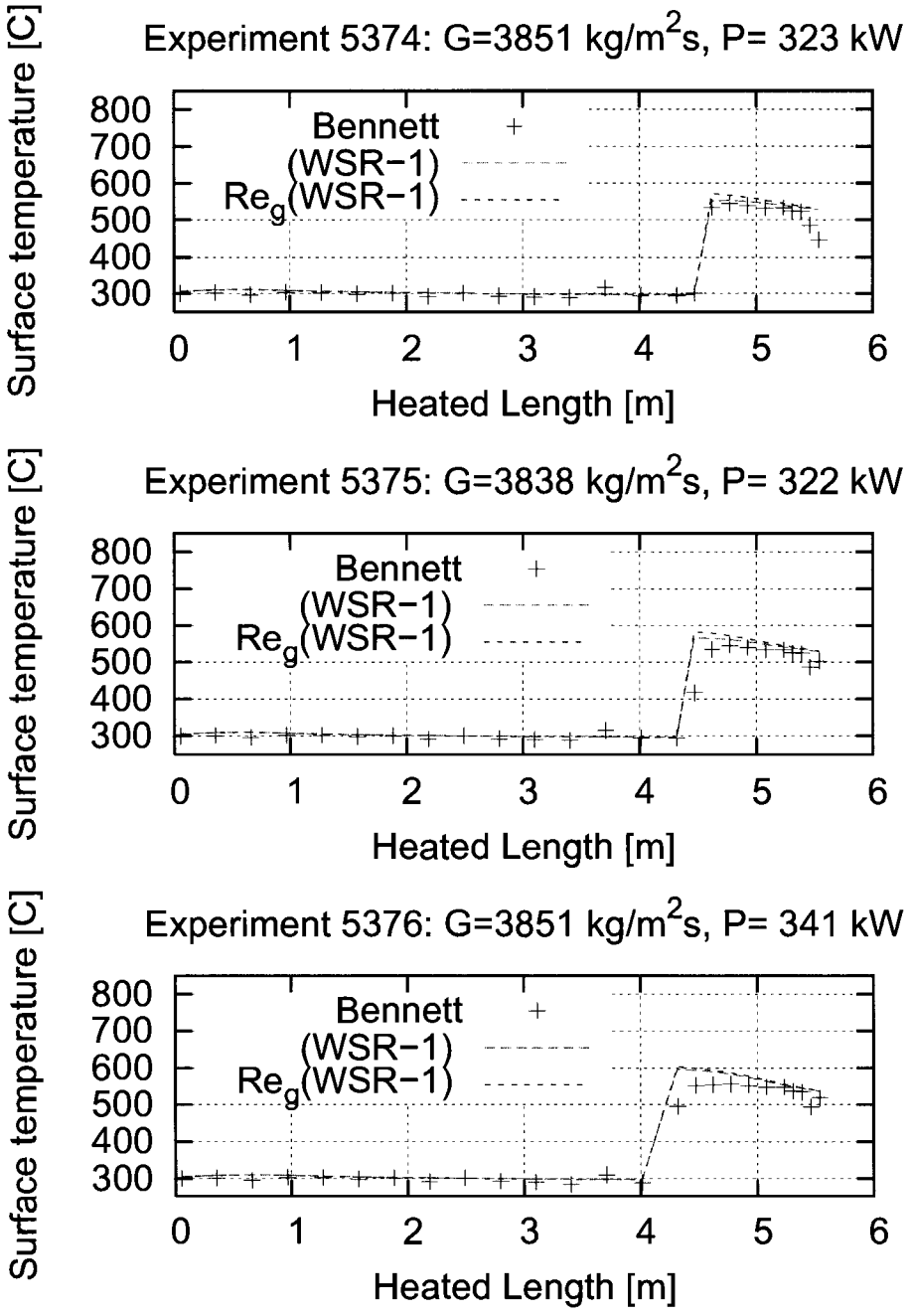

Figure V.28 Improved Correlation: Experiments 5374, 5375 and 5376

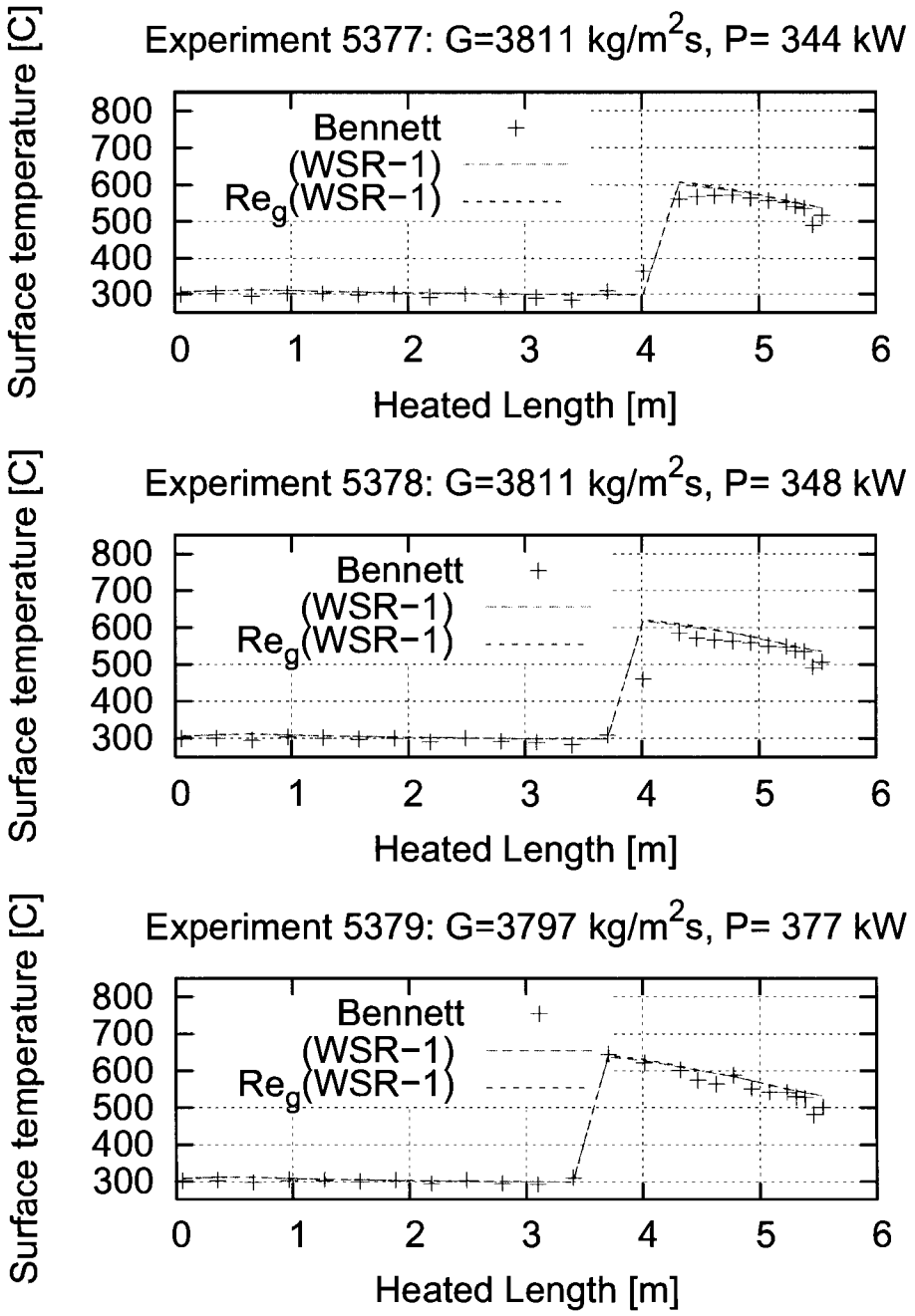

Figure V.29 Improved Correlation: Experiments 5377, 5378 and 5379

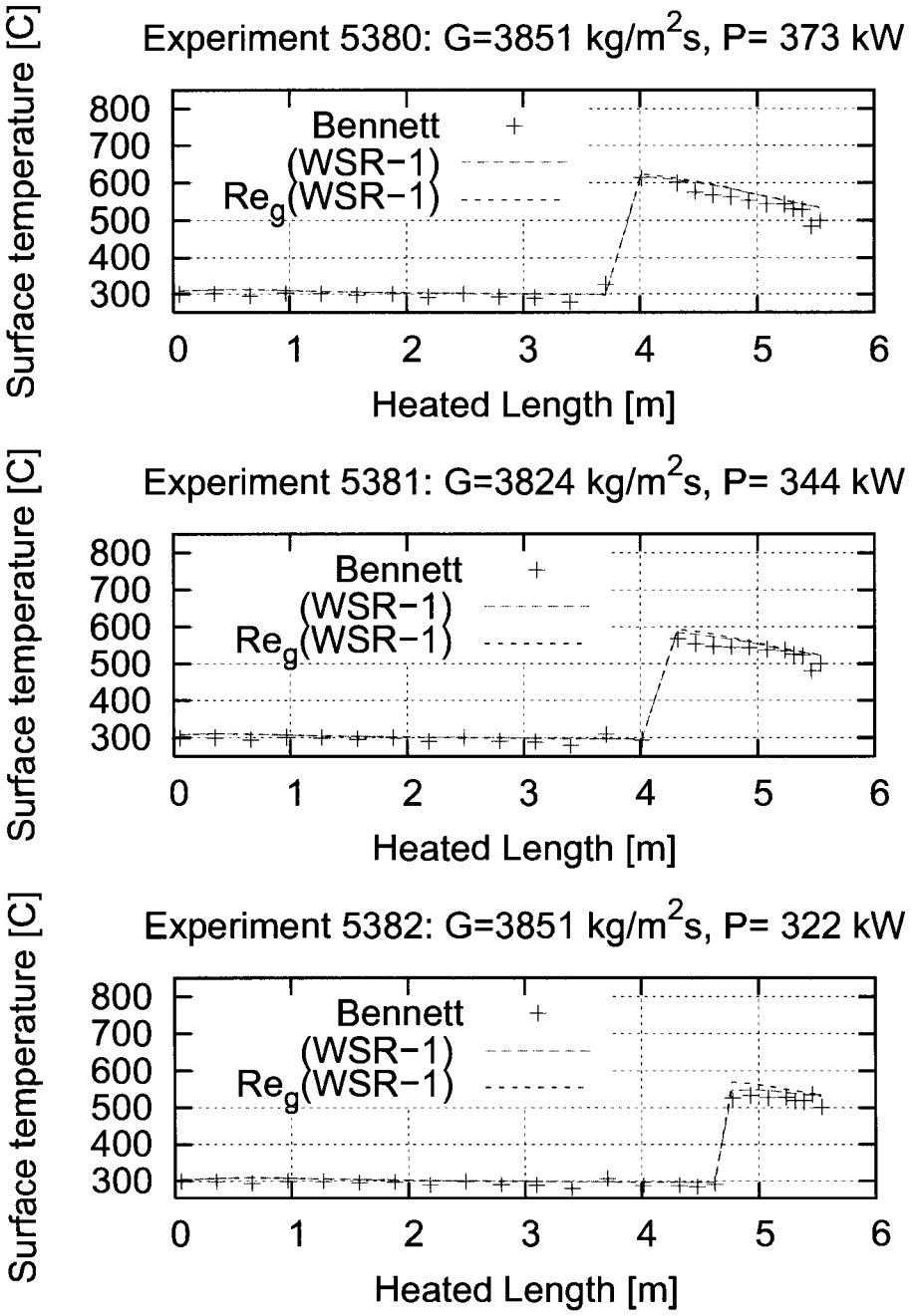

Figure V.30 Improved Correlation: Experiments 5380, 5381 and 5382

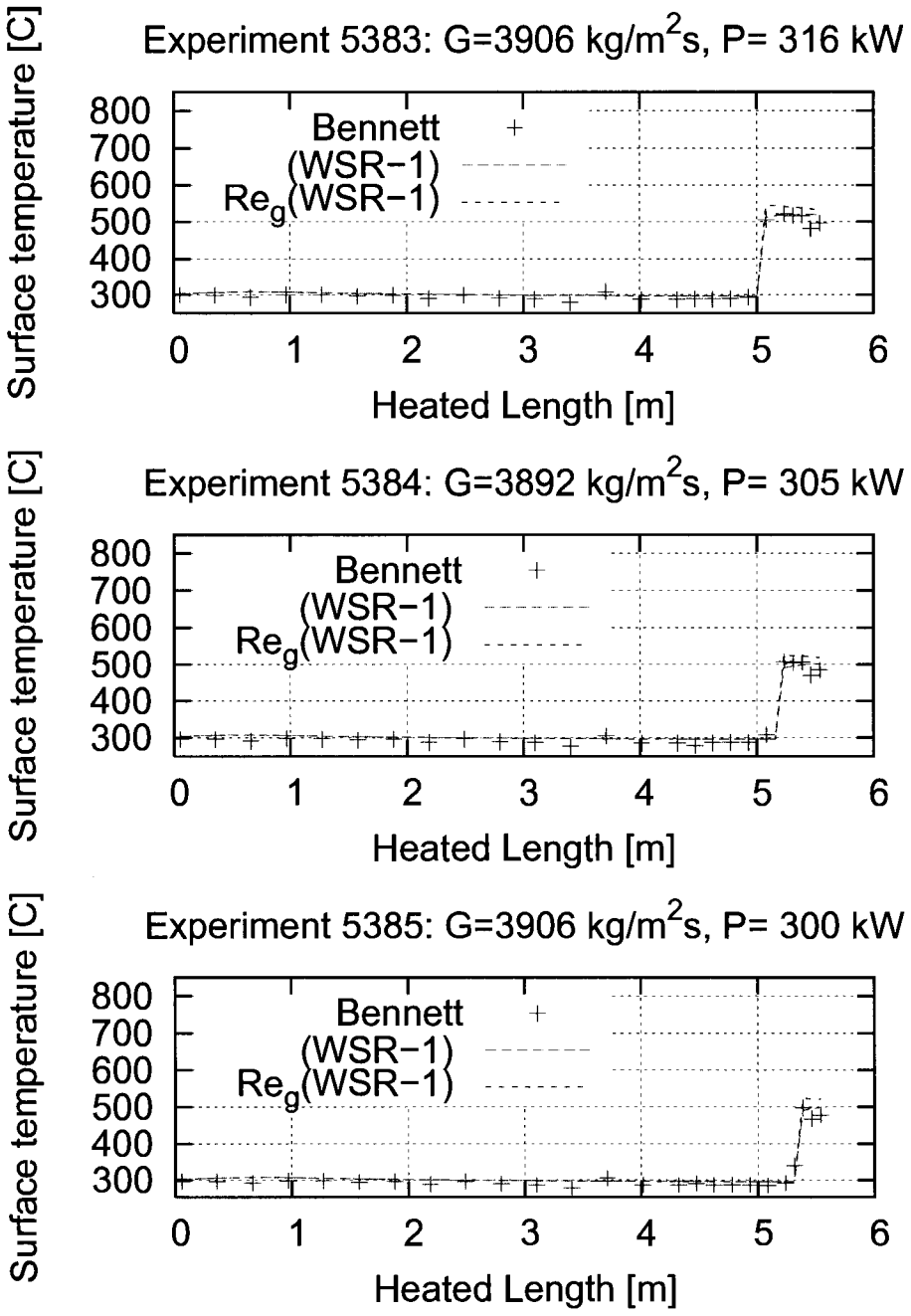

Figure V.31 Improved Correlation: Experiments 5383, 5384 and 5385

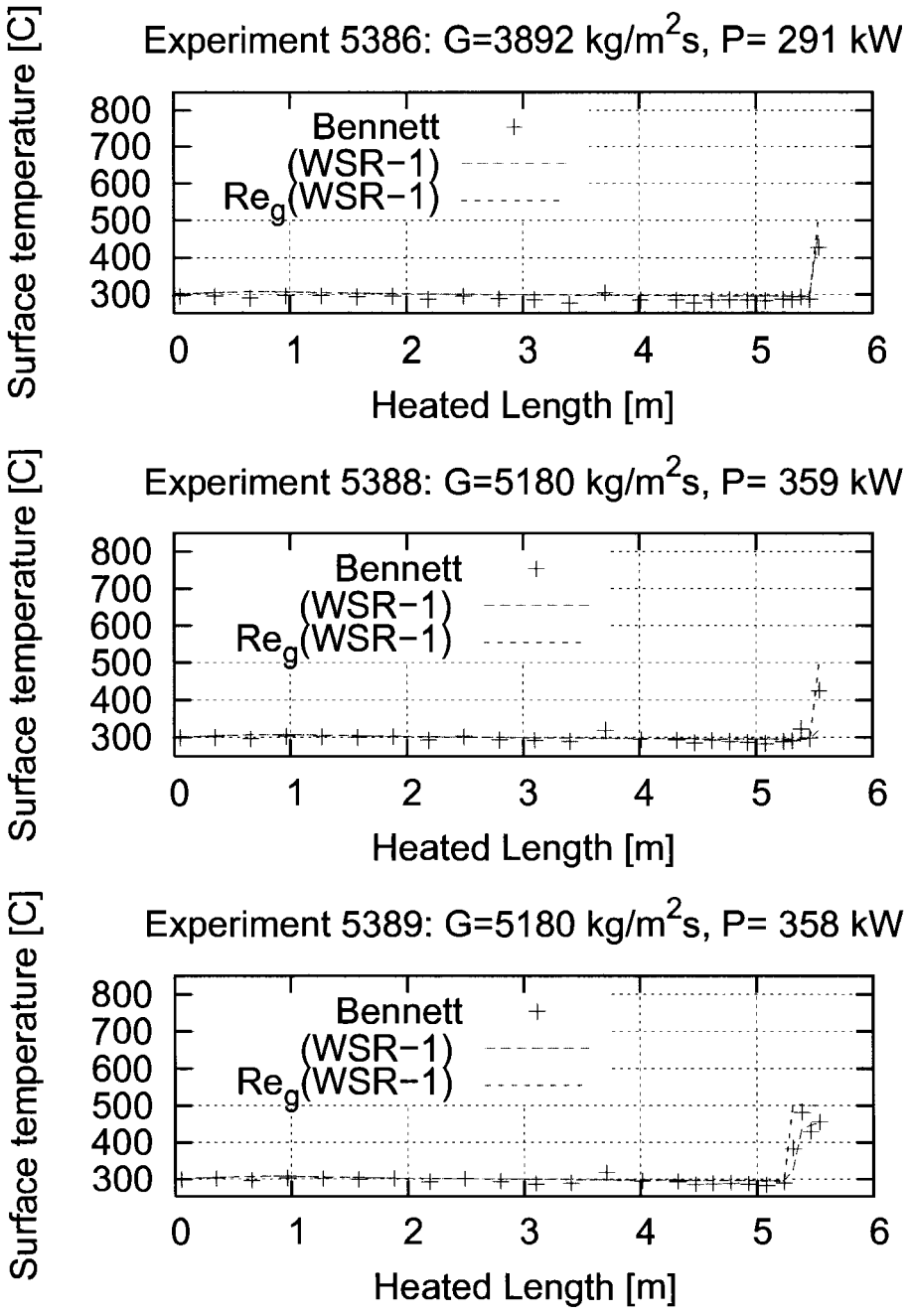

Figure V.32 Improved Correlation: Experiments 5386, 5388 and 5389

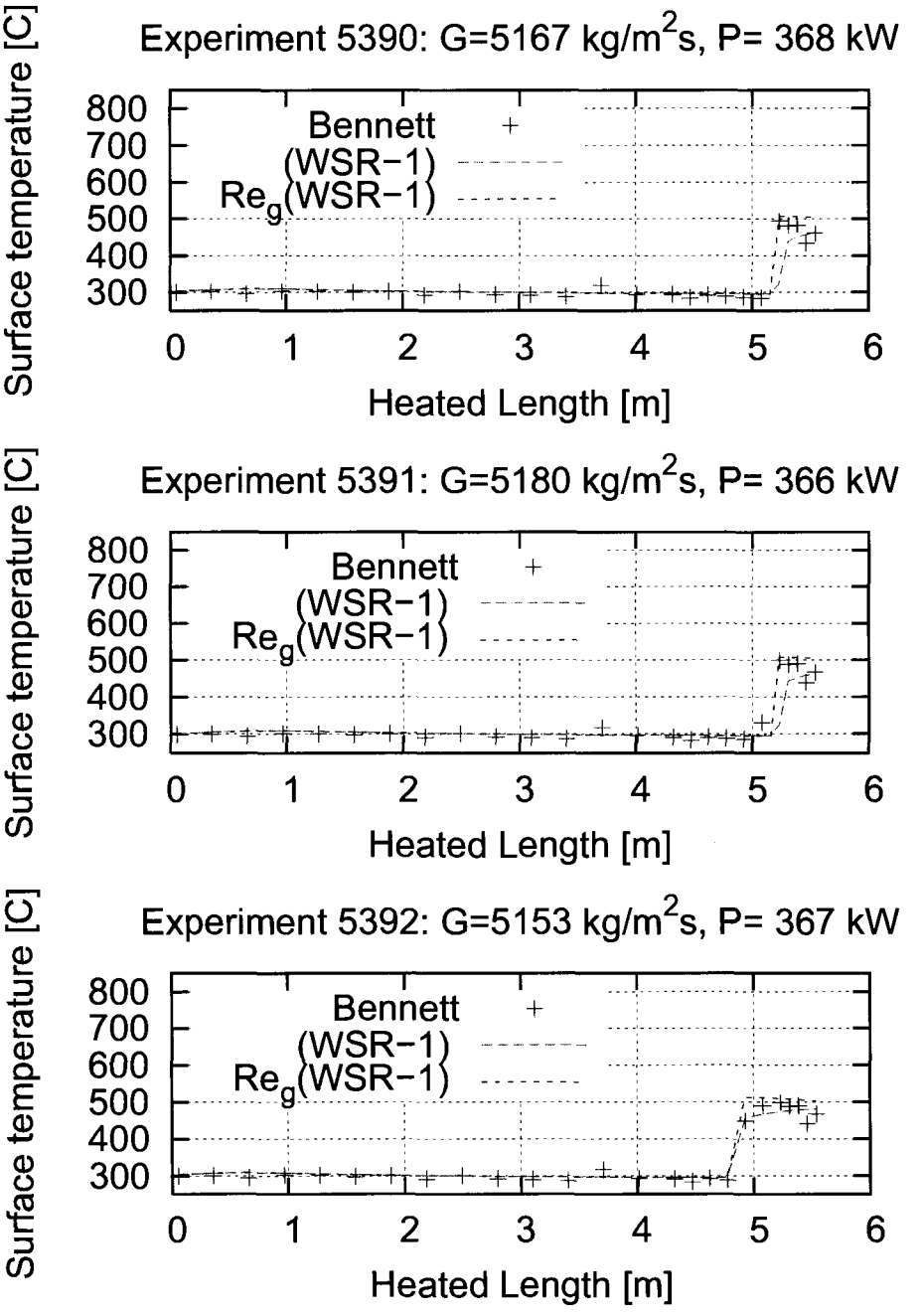

Figure V.33 Improved Correlation: Experiments 5390, 5391 and 5392

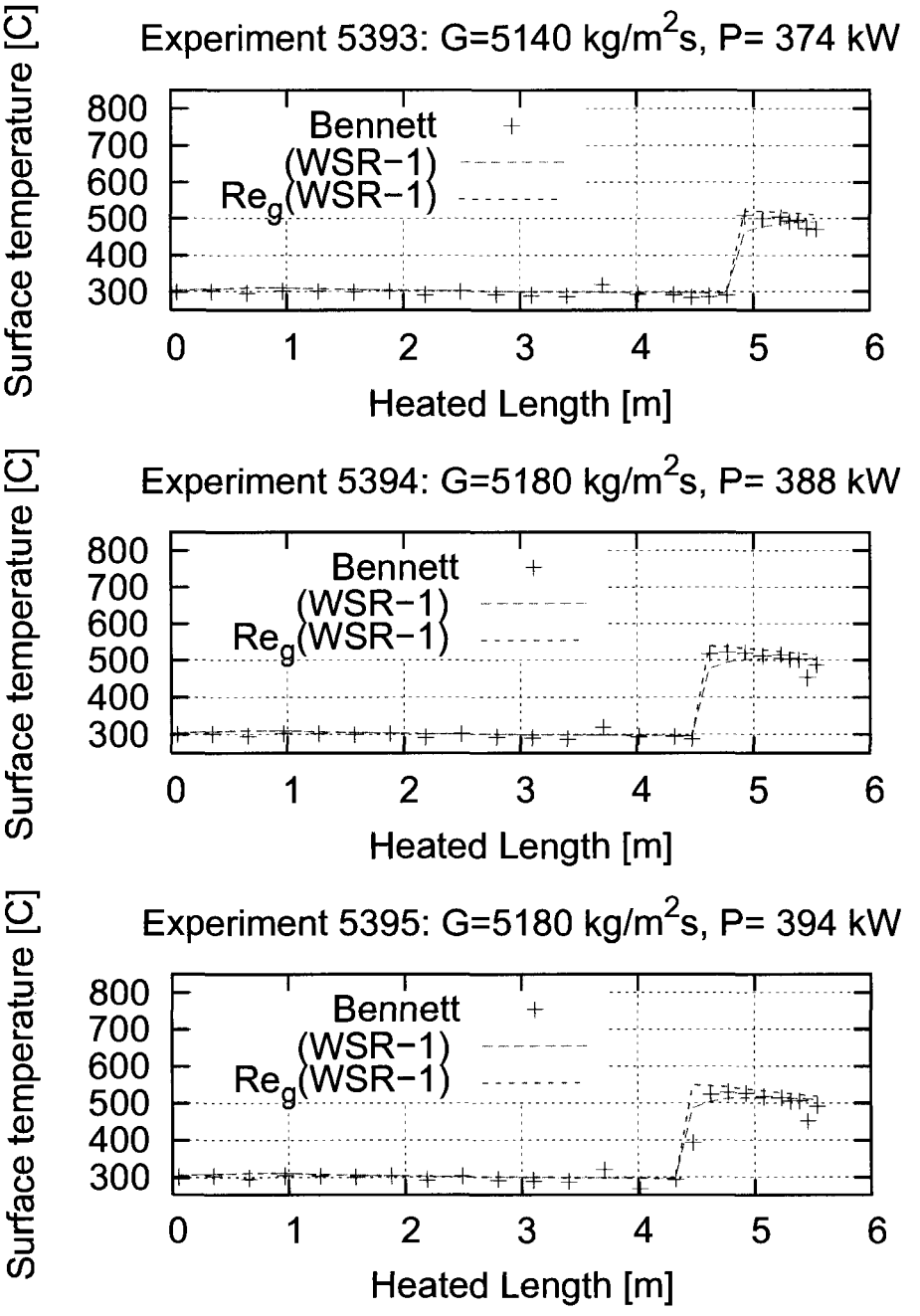

Figure V.34 Improved Correlation: Experiments 5393, 5394 and 5395

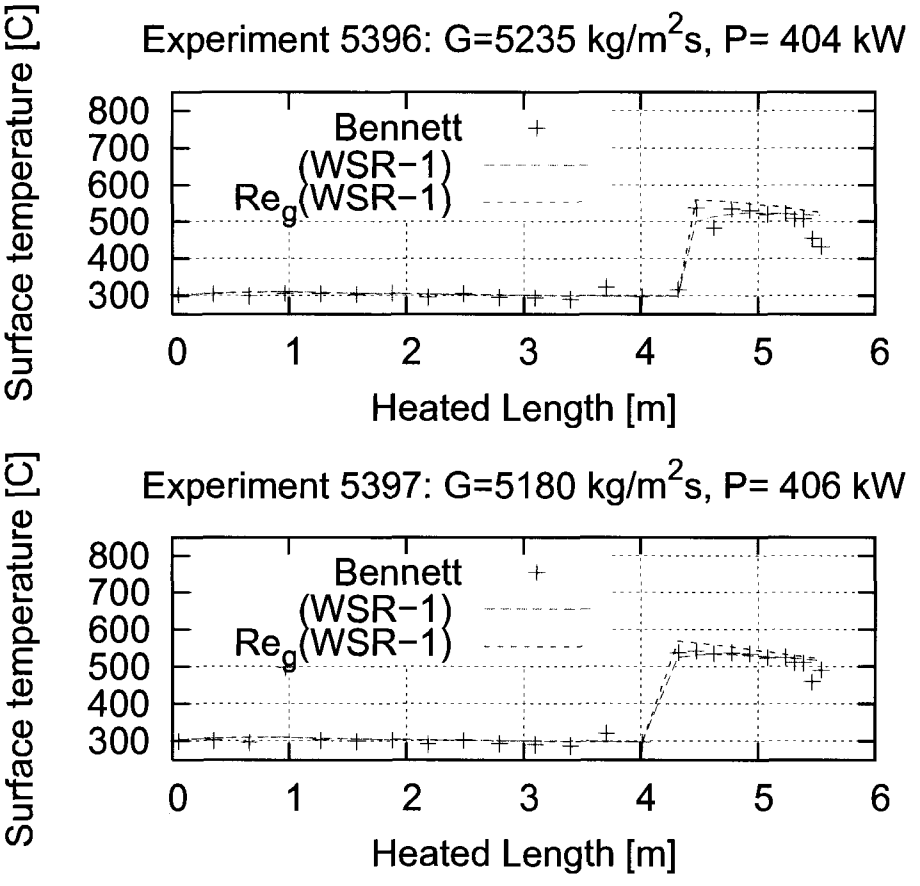

Figure V.35 Improved Correlation: Experiments 5396 and 5397